DEVELOPMENT OF UNDERACTUATED TENDON DRIVEN MANIPULATOR INCORPORATED WITH ENERGY SAVING BISTABLE ELECTROMAGNETIC COUPLING MECHANISM

by

MALAKA MIYURANGA KALUARACHCHI

Thesis submitted to the University of Nottingham for the degree of Doctor of Philosophy

May 2019

Declaration of Authorship

I, Malaka Miyuranga Kaluarachchi, hereby declare that the work presented in this thesis is solely mine and it has not been submitted elsewhere for any other degree at this University or any other institution. To the best of my knowledge, the thesis contains no materials from previously published work other than those been cited and acknowledged.

Malaka Miyuranga Kaluarachchi

25 Sep 2019

Abstract

Lightweight manipulator design is one of the diverse and rich research fields in the area of robotics. The lightweight manipulator development has become increasingly essential because of its distinctive benefits such as reduced inertia, low energy consumption and safer operation that are the key challenges in optimising a manipulator design. Various designs approaches have been proposed over the past decades in the development of lightweight manipulators. However, majority of lightweight manipulator designs from the literature were developed following the conventional design approach such as positioning the actuators at base or allocating a dedicated actuator for each degree of freedom. Reduction of number of actuators (underactuation) utilised has significant benefits such as cost reduction, compactness and reduced weight. Thus, incorporation of underactuation concept with the lightweight manipulator design will integrate the features of underactuation concept with lightweight manipulator that enhance the design. More interestingly, development of tendon driven manipulators incorporating underactuated concept has not been explored extensively in the field of lightweight manipulator design. In addition, electromagnetic clutches have been widely utilised in underactuated systems as a coupling device due to its advantages such as fast activation and electrical controllability. However, a continuously supply of electrical energy is essential to sustain the engaged state of an electromagnetic clutch during operation. Therefore, an electromagnetic clutch consumes substantial amount of electrical energy during the operation. Moreover, conventional electromagnetic clutch is not fail safe in unexpected power failure conditions. These factors have a significant impact on energy efficiency and safety of the manipulator design, that are vital design aspects of underactuated lightweight manipulators.

These elements are addressed in this research through the development of underactuated tendon driven manipulator incorporated with bistable electromagnetic coupling mechanism. A bistable electromagnetic coupling mechanism is developed initially in this research for underactuated manipulators. The developed bistable electromagnetic coupling mechanism has the capability to maintain stable mechanism states either engaged or disengaged without a continuous electrical power supply. Thus, the design is with the potential of minimising electric energy usage and providing a fail-safe coupling mechanism. Moreover, bistable electromagnetic coupling mechanism comprises the advantages of conventional electromagnetic clutch such as rapid activation and electrical controllability. The experimental results illustrated that the proposed bistable electromagnetic coupling mechanism has utilised only 1.104 J of energy throughout the entire operation of the coupling mechanism. In addition, a tendon driven manipulator is developed which utilises reduced number of motors for the actuation, adopting the underactuation concept in the design. The developed manipulator is with the capability of reducing driving joint torques required for actuation. The effectiveness of the proposed design in reducing driving joint torques is examined via theoretical and experimental studies. The experimental and theoretical results have highlighted the significance of the developed tendon driven manipulator design in reducing driving joint torques with comparison to the conventional manipulator. The energy consumption of the proposed bistable coupling mechanism based actuation is also analysed experimentally. Experimental results further illustrated that proposed coupling mechanism based approach has reduced the energy consumption by 188 J and 144 J during the actuation of manipulator joints. Experimental studies have highlighted the potential of the proposed manipulator design in reducing both driving joint torques and the energy consumption. Furthermore, in the research

study further enhancement to the developed manipulator design is introduced by utilizing a single motor for the actuation. The single motor tendon driven manipulator design proposed in the study comprises the features of lightweight manipulators and the advantages of the underactuation concept. Thus, the proposed underactuated tendon driven manipulator incorporated with bistable electromagnetic coupling mechanisms makes a promising design approach in the field of lightweight manipulator development.

List of Publications

Journals Published

1. M. M. Kaluarachchi, J. H. Ho, S. Yahya and S. H. Teh, " Design of a bistable electromagnetic coupling mechanism for underactuated manipulators," *Smart Materials and Structures*, vol. 27, no. 7, 07531, 2018.

2. M. M. Kaluarachchi, J. H. Ho and S. Yahya, " Design of a single motor, tendon driven redundant manipulator with reduced driving joint torques," *Mechanics Based Design of Structures and Machines*, vol. 46, no.5, pp. 591-614, 2018.

Conference

3. M. M. Kaluarachchi, J. H. Ho and S. Yahya, "Kinematics analysis of a lightweight tendon manipulator design (abstract)," World Congress of Robotics (WCR-2015), Shenyang, China, 2015.

Publications in Preparation

4. A journal paper with the title of "design of lightweight manipulator with energy saving actuation method" is currently in preparation.

5. A journal paper with the title of "A review on lightweight manipulator designs" is currently in preparation.

Acknowledgements

Firstly, I would like to offer my profound gratitude to my principle supervisor, Dr. Ho Jee Hou for his visionary support, unwavering guidance and motivation provided throughout this study. His experience, patience and knowledge provided immense support to my research. Also, I am very grateful for his consistent motivation, encouragement and for providing the opportunity to conduct my studies under his supervision. Secondly, I would like to thank my co-supervisor Dr. Samer Yahya for providing guidance and support throughout the project. His guidance is greatly appreciated.

Support from co-supervisor Dr. Teh Sze Hong is also highly valued and appreciated. I would also like to express my thanks to Dr. Ai Bao Chai for providing constructive comments, valuable suggestions and for the yearly review of project that help greatly throughout the research study.

I would like to thank all the staff members in the faculty of engineering who supported me during the research study. Also, I would like to acknowledge and thank all my friends at the university for their support and for their strong friendship throughout these years.

Finally, I would like to express my gratitude to my parents for encouraging me to embark on the project and for being a stalwart at all times. Their continuous support and encouragement have greatly helped me in many ways. I am forever grateful for my parents. Also, my appreciations to anyone who has supported and contributed to this work directly or indirectly.

Table of Contents

List of Figures

List of Tables

Nomenclature

a_i	Distance between z_{i-1} and z_i axes along the x_i-axis
∇ B	Gradient of the magnetic field of the electromagnet
Br	Magnetic remanence
C_1	$\cos\theta_1$
C_2	$\cos\theta_2$
C_3	$\cos\theta_3$
C_4	$\cos\theta_4$
C_{23}	$\cos(\theta_2+\theta_3)$
d_i	Joint distance between x_{i-1} and xi axes along the z_{i-1}-axis
F_{EPM}	Force generated between the permanent magnet (L) and the electromagnet
F_f	Dry friction force
F_{LPM}	Force F_{LPM} generated between the permanent magnet (L) and ferromagnetic plate
F_{SPM}	Force generated between the ferromagnetic plate and the permanent magnet (S)
g	Gravitational acceleration
${}^{i}I_i$	Inertia matrix of the link *i* about its center of mass with respect to the *i* th link frame
I_i	Inertia matrix about its center of mass with respect to the base link frame
J_i	ith link Jacobian matrix
J_{vi}	Jacobian linear velocity submatrix
J_{vi}^{j}	jth column vectors of Jacobian linear velocity submatrix
$J_{\omega i}$	Jacobian angular velocity submatrix

$J_{\omega i}^{j}$	j[th] column vectors of Jacobian angular velocity submatrix
l_1	Length of link one
l_2	Length of link two
l_3	Length of link three
l_4	Length of link four
m	Mass of the sliding disk
m_i	Mass of the *i* [th] link
M	Magnetization of the permanent magnet
$M(q)$	Mass matrix
N	Number of loops in coil
q	Joint position vector
$\dot{q}$	Joint velocity vector
$\ddot{q}$	Joint acceleration vector
R_i^0	Rotation matrix of link *i*
S_1	$\sin\theta_1$
S_2	$\sin\theta_2$
S_3	$\sin\theta_3$
S_4	$\sin\theta_4$
S_{23}	$\sin(\theta_2+\theta_3)$
${}^{i-1}\boldsymbol{T}_i$	Homogenous transformation matrix describes the position of the I frame with respective to the frame i-1
V	Volume of the permanent magnet
$V(q, \dot{q})$	Coriolis and centrifugal forces
X	Displacement of sliding disk
$\dot{X}$	Velocity of the sliding disk motion
$\ddot{X}$	Acceleration of the sliding disk motion

X_L	Distance between the permanent magnet (L) and the ferromagnetic plate
X_s	Distance between the permanent magnet (S) and the ferromagnetic plate
α_i	Rotation of the z_{i-1}-axis about the x_i axis to become parallel to the z_i-axis.
θ_1	Angle value of the joint one
θ_2	Angle value of the joint two
θ_3	Angle value of the joint three
θ_4	Angle value of the joint four
θ_i	Joint angle is the required rotation of xi−1-axis about the zi−1-axis to become parallel to the xi-axis
$\dot{\theta}_i$	Angular velocity of joint *i*
$\ddot{\theta}_i$	Angular acceleration of joint *i*
μ	Frictional coefficient
μ_m	Permeability of permanent magnet
μ_0	Permeability of free space
τ_1	Torque value of the joint one
τ_2	Torque value of the joint two
τ_3	Torque value of the joint three
τ_4	Torque value of the joint four

Chapter 1

Introduction

1.1 Background

The lightweight manipulator design has gained a significant attention of the researches and robot manufactures due to its high demand, distinct features and the significant benefits. Furthermore, lightweight manipulator design has become a growing research trend creating a novel branch of research in manipulator design.

The huge demand of lightweight robots is contributed by the requirements of working environment such as space robots [1][2][3], service robots [4][5] and medical robots [6][7]. For example, lightweight design is crucial in space applications. The cost of transporting heavy masses to the space is relatively higher that ranges from 8000 to 20000 US Dollars per kilogram. In addition, higher operational speeds which lead to higher productivity [8][9]and safer operation for human robot interaction also enhance the demand of lightweight manipulators. Safety is an essential requirement for the coexistence of robotic manipulators and humans in industrial environments and in various domains [10][11]. Lightweight manipulators have less inertia and shorter breaking distance because of reduced weight [12]. Therefore, lightweight manipulators are safer compared to the traditional manipulators [13]. In addition, Lightweight robots consume less energy as the weight reduces. Besides that, lightweight manipulators also have higher payload to weight ratio compared to conventional manipulators [14][15].

In majority of the conventional manipulator designs, motors are fixed at each joint of the manipulator with respective gearbox and other related components. The advantage of this approach is the ease in control of joint motion independently. However, the plurality of motors increases the mass and demands high power supply. When considering the present lightweight redundant manipulators, most of robotic manufactures have developed several lightweight manipulators following the conventional lightweight manipulator design approach positioning the actuators at base and allocating a dedicated actuator for each degree of freedom.

The general strategies of designing lightweight manipulators are by designing lightweight joints [16-18] or locating the actuators, heavy joint components at the base and transmitting the power to each joint through gears, tendons or special transmission mechanisms [19][20]. When considering the present lightweight manipulators, many robotic manufactures and researchers have developed several lightweight manipulators following the conventional lightweight manipulator design approach positioning the actuators at the base and allocating a dedicated actuator for each degree of freedom (DOF). Even though lightweight concept is preserved, the designs utilise dedicated actuators, which are similar to the conventional design approach. The number of actuators employed for the actuation has not been reduced in these designs. Reduction of actuators have significant benefits such as low energy consumption, compact in design, reduced weight and cost [21].

The mechanical system with reduced number of motors in comparison to the number of degrees of freedom of the system is known as underactuated system [21][22]**.** In order to achieve this goal, passive elements are used. These elements replace the motors leading to a reduction of number of actuators.

However, these passive components do not function similarly as actuators. By definition, passive element could be considered as a device that does not contribute for the positive work generation on its environment [22]. Therefore, passive components cannot generate arbitrary forces or motions though able to modify forces or motions provided by an external source such as a human user to produce passively controlled forces and motions.

As stated previously, substantial number of motors increase the mass, cost and demands more power. Therefore, underactuated systems have significant benefits over the traditional fully actuation due to the reduced use of motors. Therefore, applying underactuated concept in design of the lightweight manipulator could merge the beneficial features of underactuated system with the lightweight manipulator enhancing the manipulator design. The distinct benefits of minimising the number of actuators used advocate the implementation of the concept of reduction of motors used in lightweight manipulator design. These are the motivating factors of the current research to explore the possibility of designing lightweight manipulator merging the underactuated system concept.

1.2 Motivation

Robot technology implementation in the manufacturing field has been evolved remarkably in the recent years. As a result, robotic devices such as robot manipulators have become general manufacturing tool in the industrial operations. These devices are implemented to enhance the efficiency of the manufacturing process and to improve the quality of the manufactured product. The traditional robot manipulators are employed for the execution of scripted tasks, while operating inside a safety fence. The manipulator is isolated from the human interaction [23]. However, the concept of human and robot collaboration in manufacturing process has become a new frontier in the industrial manipulator design sector [24]. This concept utilises abilities of each member such as the intelligence, dexterity and perception of the human worker and the memory, strength and precision of the robot manipulator [25][26]. According to the "Service Innovation for Smart Industry Human-robot collaboration" report by "European commission for Internal Market, Industry, Entrepreneurship" states that, the collaborative robot manipulators will be having a significant impact on the manufacturing sector while creating new unexplored manufacturing sector known as small-medium manufacturing [27]. The report further states there is a research trend in the development of collaborative robot manipulators in manufacturing sector. Companies such as Volkswagen, BMW and Mercedes have already initiated pilot projects with robot manipulators which operate close with humans in assembly lines of the manufacturing plants [28][29]. The safety is an essential attribute to be considered in the development of human collaborative robots. Therefore, international safety standards have been implemented to enhance the safety of the workers. ISO 10218-1, 5.10.5, ISO/TS 15066 are some

of the safety standards implemented [30][31]. Lightweight design aspect is one of the important safety attributes among international safety standards for human collaboration robots in manufacturing [31][32]. This factor has greatly influenced the growth of the research in designing of lightweight manipulators for human robot collaborative manufacturing.

Plurality of motors in a system increase the mass and demands high power supply. Reduced uses of motors (underactuation) have significant benefits over the traditional actuation mechanism such as low energy consumption, cost reduction, compactness and reduced weight[33][34]. Due to the advantages of underactuated concept over the fully actuated concept, it has gained a significant attention in many robotic fields. The underactuate concept has been implemented in various robotic applications such as mobile robots, underwater robots, space robots etc [33][35][36].

In spite of this it has not been applied extensively in the design of lightweight manipulators. The general strategies of designing lightweight manipulators are by designing lightweight joints or locating the actuators, heavy joint components at the base and transmitting the power to each joint through gears, tendons or special transmission mechanisms [37][38]. When considering the present lightweight manipulators, most of robotic manufactures and researchers have developed several lightweight manipulators following the conventional lightweight manipulator design approach positioning the actuators at base and allocating a dedicated actuator for each degree of freedom (DOF).

Several lightweight manipulators have been developed over the years. However, it could be observed from the literature that the conventional actuation principle has been adopted in majority of the developed tendon driven manipulator

designs. There is a dedicated motor allocated for each joint. As such, the number of actuators employed for the manipulation has not been reduced.

Combining underactuated concept with the lightweight manipulator design will merge the features of underactuated concept with the lightweight manipulator that will enhance the design. Furthermore, reduction of cost and energy consumption is vital for the human collaborative manipulators in manufacturing apart from weight reduction [45][46]. Therefore, there is a capability of expanding the quality of lightweight robot manipulators in manufacturing by introducing a novel idea that is to develop a tendon driven manipulator comprising both lightweight and underactuated characteristics. With the initiation of concept, it will aid for the achievement of vital goals such as lowering the cost and the energy consumption in addition to the lightweight attribute.

Furthermore, over the years researchers have developed several under actuated robot designs. These underactuated robot systems replace the motors installed at each degree of freedom with coupling mechanism. A central motor is maintained for the distribution of energy to the joints through gear trains or through tendons. The coupling mechanism installed control the supply of energy to the joints. However, majority of the underactuated robot designs have incorporated electromagnetic clutches as the coupling device due to the benefits such fast activation, moderate torque density and electrical controllability [47-51]. The underactuated system motion is manoeuvred through controlling the energy supply to the passive joints by engaging and disengaging the clutches [52]. Engaging of the clutch is analogous to switch On state of the motor and similarly disengaging to the switch Off state. This leads to reduction of motors in these underactuated robot systems.

Apart from the benefits, the major drawback of the conventional electromagnetic clutch is that, power should be supplied throughout the operation. The power supply is used for the excitation of the electromagnetic coil. The electromagnet provides the holding force required to maintain the engaged state of the clutch. Therefore, power supply could only be terminated during disengaging the clutch [53-55]. As such, electromagnetic clutch consumes high amount of energy during the clutch operation. Furthermore, disengagement of the clutch due to unexpected power failure is another drawback [56] [57]. According to the EU directive 2006/42/EG clause 1.2.6 the drive must not disengage in case of a power failure [58]. The directive enhances the safety of a system in a situation where unexpected power failure occurs. However, a conventional electromagnetic clutch cannot remain in engaged state without a continuous power supply. Hence implementation of conventional electromagnetic clutch may affect the safety of the system. Moreover, dissipation of heat energy from the electromagnetic coil due to the continuous power supply is another disadvantage. Therefore, designing of energy efficient and safe mechanism is essential for the underactuated manipulators. Furthermore, it will enhance the fundamental design requirements of underactuated lightweight manipulators such as safety and efficiency. These elements are the major incentive for this research on the development of underactuated tendon driven lightweight manipulator incorporated with energy-saving and safe coupling mechanism.

1.3 Aims and Objectives

The aim of the research is to develop a tendon driven lightweight manipulator incorporating reduced number of motors with reduced driving joint torques and with the capability of independent movement of each degree of freedom using low energy consuming coupling mechanism.

The objectives of this research include:

1. To develop a coupling mechanism with low energy consumption for the independent joint motion of the underactuated lightweight manipulator.

2. To develop a working prototype of the tendon drive lightweight robot manipulator using reduced number of motors with reduced driving joint torques.

3. To implement the dynamical model of the lightweight manipulator and coupling mechanism.

4. To analyse the performance and to validate the theoretical models of the lightweight manipulator and the coupling mechanism via experimental studies.

1.4 Summary of Original Contributions

The contribution of this work is to introduce a novel design of the light weight tendon driven manipulator that incorporates underactuated concept and to introduce a coupling mechanism that consumes reduced electric energy for underactuated lightweight manipulators. A summary of original contributions is given as below.

A design of bistable electromagnetic coupling mechanism, with reduced energy consumption and with fail-safe design is introduced. The concept of the bistable electromagnetic mechanism consists of an electromagnet with two permanent magnets. The proposed bistable coupling mechanism is with the capability of maintaining stable states of the mechanism either engaged or disengaged without a continuous electrical power supply. As such the mechanism is unaffected due to sudden power failure. Thus, enhancing the fail-safety. Furthermore, the bistable coupling mechanism could function without a continuous power supply during the operation. Hence the proposed design reduces the energy consumption. Apart from that, the proposed mechanism prevents dissipation of heat energy from the electromagnetic coil due to continuous flow of current. Moreover, the design incorporates the advantages of conventional electromagnetic clutch design such as fast activation and electrical controllability. The rotor and armature sections of the proposed coupling mechanism are developed utilizing aluminium and Teflon materials respectively. These materials are used to reduce the weight of the design and to maintain the lightweight aspect. Neodymium permanent magnets are employed in the mechanism due to its distinct benefit of high magnetic power to weight ratio. Two Neodymium magnet with the holding force of 33 N and 2.9 N are employed in the mechanism that provides the holding

force to sustain engaged and the disengaged states of the design respectively. The fabricated prototype design was implemented on a lightweight underactuated manipulator to investigate the operation. The experimental results highlight the effectiveness of the proposed mechanism in reducing electric energy consumption and the functionality. The reduced electric energy consumption and fail-safe design make the bistable electromagnetic mechanism a promising concept for underactuated lightweight manipulators. Furthermore, it fulfils the fundamental design requirements of underactuated lightweight manipulators such as safety and efficiency that lack in currently used electromagnetic clutches. The proposed design eliminates the drawbacks of the traditional electromagnetic clutch and provides a safe and energy saving coupling mechanism for underactuated lightweight manipulators.

Mechanical design of a tendon driven lightweight manipulator that incorporates reduced number of motors is also introduced. The introduced design deviates from the traditional manipulator design. In conventional manipulators a dedicated motor is allocated for each degree of freedom, however in the proposed design only a single motor is allocated for the manipulation of four degrees of freedom. As such, the design has reduced the number of motors used in comparison to the conventional manipulator design. Reduction of number of motors has added advantages such as cost reduction and compact in design apart from the reduction of weight. Therefore, the proposed tendon driven manipulator incorporates these benefits in the design that lacks in conventional manipulator.

Apart from that the design does not contain any heavy components fixed at the joints. Motor, coupling mechanisms and the gear trains are fixed at the base. Thus, the lightweight characteristics and the compactness of the design further enhanced by reducing the heavy components installed at the joints. Moreover,

proposed manipulator design is capable of reducing the driving joint torque during its motion. A comparison between the driving joint torques of the proposed manipulator design, and that of the conventional (one motor for each joint) manipulator are conducted. The theoretical and experimental results have highlighted the impact and the effectiveness of the design in reducing the driving joint torques. The reduction of cost is another vital aspect required to be achieved in manipulator design. The proposed manipulator design accomplishes these aspects such as reduction of cost and space required due to the use of underactuated mechanism over traditional actuation mechanism. Therefore, the design is capable of reducing the cost and achieving a compact design apart from minimisation driving joint torque.

1.5 Thesis Overview

Chapter 1 introduces background study of lightweight manipulator design. The motivation and the contributions of the work are also presented in the chapter.

Chapter 2 presents a literature review conducted on light weight manipulator designs. The comprehensive literature study is performed focusing on three main lightweight manipulator design solutions namely tendon driven robot manipulators, gears and clutches driven manipulators and modular mechatronics approach. The mechanisms and the significance of each design approach are analysed and discussed thoroughly under this chapter. The chapter also describes the advantages and challenges of each design approach. In addition, the future research trends of lightweight manipulator design are addressed in the chapter that will shape the future of the lightweight robot manipulators.

Chapter 3 illustrates the overview of the research methodology performed during the research study. The research methodology is also presented in a flow chart to illustrate the sequence of research activities.

Chapter 4 introduces a design of an energy saving bistable coupling mechanism for underactuated manipulator. The mechanical design and the operation principle of the proposed bistable coupling mechanism are discussed in detail under this chapter. The chapter also illustrates the development of mathematical model of the bistable coupling mechanism. Developed mathematical model is validated via experimental studies in this chapter. Furthermore, to study the effectiveness of the proposed coupling mechanism in reducing electric energy usage with comparison to the conventional electromagnetic clutch, experimental investigations are conducted. The experimental studies conducted and the results obtained are also presented in this chapter.

Chapter 5 presents a design of underactuated tendon driven manipulator design incorporated with bistable coupling mechanism. The detailed mechanical design and the operation of the proposed manipulator prototype design with reduced motors are discussed in the chapter. In addition, kinematics and the dynamic model of the proposed manipulator are developed. The development of the dynamic and the kinematic model of the proposed manipulator prototype are illustrated in detail under this chapter.

Chapter 6 investigates the performance of the proposed manipulator protype design in reducing both driving joint torques and energy consumption during joint actuation. The chapter includes the experimental studies conducted to analyse the significance of the proposed manipulator design in reducing driving joint torques

and verification of the dynamic model developed. Furthermore, the energy consumption of the proposed and the conventional actuation approaches during joint actuation are investigated experimentally under this chapter. The results obtained from the experimental analysis are presented here in the chapter.

Chapter 7 proposes a further enhancement of the manipulator design prototype introducing a single motor tendon driven manipulator design. The operation and the design of the enhanced manipulator are presented in this chapter. The kinematics and the dynamic model developed for the manipulator are also shown in the chapter. The chapter further includes simulation studies performed to analyse effectiveness of the proposed enhanced manipulator.

Chapter 8 concludes the thesis and provides recommendations for the possible future research work.

Chapter 2

Literature Review

2.1 Introduction

A robot manipulator consists of a series of connection of individual links and joints. The links are the rigid members connecting the joints or axes. The manipulators execute its motion via the joints and the actuators connected with the joints. The actuators connected to each joint control the motion of each link independently and hence introduce an independent degree of freedom (DOF) to the system. Traditionally a robot's DOF is defined by the number of actuators installed. This landscape has changed in recent years as some alternative designs have been proposed [22]. The general strategies include designing lightweight joints or locating the actuators at the base and transmitting the power to each joint through tendons or special transmission mechanisms. For example, Yahya *et al* proposed a robotic manipulator architecture which uses gears instead of separate actuator on each joint [52]. Although the motion of these links is constrained by the gear ratio and should not be treated as an independent DOF, this design approach has stimulated research interests in developing robotic manipulators with less actuators. A potential advantage of such approach is the reduction of weight and the actuation components which leads to cost savings. This has created a novel branch of research in lightweight manipulator design.

The huge demand of lightweight robots is contributed by the requirements of working environment (e.g. space robots [53-56] service robots [57][58] and medical robots [59][60]). For example, lightweight design is crucial in space applications. The cost of transporting heavy masses is relatively higher. In production systems, the needs of higher operational speeds (which lead to higher productivity) [61-63] and safer operation of human robot interaction also enhance the demand of lightweight manipulators. Safety is an essential requirement for the coexistence of robotic manipulators and humans in industrial environments and other domains such as medical robots , personal care robots in home environments which is a subcategory of domestic robots [64-68]. Lightweight manipulators have less inertia and shorter breaking distance because of reduced weight [69]. Therefore, lightweight manipulators are safer compared to the traditional manipulators [69][70]. In addition, Lightweight robots consume less energy. Besides that, lightweight manipulators also have higher payload to weight ratio compared to conventional manipulators [71-74].

In recent years various design approaches have been proposed for the lightweight manipulators. Transmission of power from base actuator to each joint using tendons, gear trains or other mechanisms is a viable approach and gaining increasing attention. Tendon driven manipulators have relatively longer development history in this field. Tendon driven manipulators has evolved since 1980s with enhancement in joint torque reduction, controllability, payload to weight ratio and energy consumption. Mackori *et al* developed a 6 DOF manipulator with seven tendons in 1980 [75]. Jaccobsen *et al* developed a system to drive joints of Utah/MIT dexterous hand using antagonistically pulled tendons against each other in 1985 [76]. Other examples include Coupled Tendon drive (CT) arm 1 and CT arm 2 in 1986 [75], Whole Arm Manipulator (WAM) in 1988

[77], 7 DOF coupled tendon drive manipulator in 1993 [78] and recently Thomas Lens *et al* developed series elastic tendon driven manipulator in 2010 [79]. In commercial applications, Barret company commercialized the WAM manipulator developed by Salisbury and Townsend in 1988 [80]. The manipulator is designed with two configurations, one with 4 DOF and another one with 7 DOF. The weight of the manipulator ranges from 25.4 kg to 27.2 kg and its payload varies from 3 kg to 4.5 kg. Higher payload to weight ratio and back drivability are the main advantages of the Whole Arm Manipulator [80].

Meanwhile the development of lightweight manipulator using gear train and clutch system is relatively new. Karbasi *et al* proposed the first modular robot design with uni-drive concept using, gear train and clutch system in 2002 [81]. Karbasi *et al* implemented a modular robot design with single actuator and each joint is equipped with gear train and clutch system. Shafer *et al* proposed a single motor powered manipulator design with Magneto-Rheological clutches for safe human machine interaction in 2011 [82]. Li *et al* proposed a manipulator with single motor with multiple joints in 2011 inspired by Karbasi *et al* design approach [83]. Yahya *et al* implemented a lightweight redundant manipulator with three motors and gear train in 2012 [2]. Joint controlling mechanisms such as clutches are used in the designs reviewed except for the Yahya *et al* design. The joint control mechanisms are used in the designs at the joints instead of actuators. The actuators installed at the joint are replaced with clutch systems in the design. The usage of the motors at the joints are prevented in these design that aids for the reduction of driving joint torques.

In contrast, the modular mechatronic approach is different compared to the other approaches mentioned previously. It is a relatively new concept and first proposed by DLR German aerospace centre in 1993 with development of ROTEX

manipulator end effector [84]. Unlike reducing the number of actuators or placing the actuators at the base, the modular mechatronic approach integrates electronics to the joint while considering lightweight design structures. Another interesting feature is that Harmonic drives and structures fabricated with lightweight materials and composites are also integrated. Harmonic drive is also known as strain wave gearing. It is used for the high torque transmission by maintaining high position accuracy, repeatability and lightweight. The individual elements of the harmonic drive are fabricated with lightweight materials. Furthermore, the drive is small in size compared to traditional torque transmission system. Lightweight materials and composites such as nanocrystalline aluminium sheet metal, cellular titanium, carbon fibre composites are used in the design of miniaturized lightweight mechanical components [85-87].

DLR has developed series of lightweight manipulators after the initial design ROTEX. In particular, the Light Weight Robot I (LWRI) was developed in 1995 with carbon fiber structure maintaining 1:2 load to weight ratio. Light Weight Robot II (LWRII) was built with integration of harmonic drive and toque measuring electronic system in 2000 [88]. Meanwhile Light Weight Robot III (LWRII) was introduced in 2003 with lightweight motor drive (DLR Robo-drive), lightweight harmonic drive and lightweight structure (carbon fiber reinforced plastic). Commercial examples include DLR Micro robot and KUKA lightweight robots. DLR Micro robot is tailored for surgical applications. The manipulator weights 10 kg with a payload capacity of 30 N. The compact and lightweight modular design enables the safe human interaction and integration in crowded surgical environment [89]. KUKA lightweight manipulator weights 15 kg with a payload of 7 kg. The manipulator has additional degree of freedom apart from the seven axes, which enhance the flexibility. The compliance control of the manipulator

enables manual guidance of the manipulator. In addition, KUKA lightweight manipulator has with high performance force control. The manipulator is tailored for industrial assembly operations [90].

This chapter presents a summary of the lightweight manipulator development to date, with discussions on the actuation means, structural design, benefits and the drawbacks of current designs and as well as future research trends. The Section 2.1 provides a general overview of the lightweight manipulators and its historical development background. Section 2.2 to Section 2.4 present a detail discussion on three main classes of lightweight manipulator designs namely tendon manipulators, gear/clutch driven manipulators and modular mechatronics based manipulators. The advantages and challenges of each class are explained. The Section 2.5 of the chapter presents the future trends of lightweight manipulator design and it is discussed in generally under the title future research trends. Finally, the chapter concludes on the perspectives of current research that are shaping the future of the lightweight robot manipulators in the Section 2.6.

2.2 Lightweight Manipulators with Tendon Driven Mechanism

Tendon driven manipulators employ a mechanism inspired by the musculoskeletal systems used in the design of lightweight miniature robotic arms [76][91][92] and devices [93-95]. In tendon driven mechanism, actuators are positioned at the base of the manipulator and the energy is transmitted from the base to the joints of the manipulator using wire cables [96-98]. Therefore, it reduces the weight and joint torque of the manipulator. Light weight, reduced backlash and low friction are some of the significant advantages of tendon drive transmission systems

[19][99]100]. However high antagonistic forces and tendon slacking intervene smooth operation of the mechanism, affecting the performance and the efficiency.

The tendon driven systems are categorized as open ended and closed loop tendon drives. In the open-ended tendon mechanism one end of the tendon is attached to a movable link while the other end is connected to an actuator as shown in Figure 2.1 [101][102]. In closed loop drives, a belt is looped around two pulleys placed with constant centre distance as shown in Figure 2.2 [101][102]. The driving pulley is mounted to an actuator and the driven pulley is connected to a link to be controlled. The transmission of force is limited to unidirectional in open ended tendon mechanism. However, in the closed loop configuration, drive force can be transmitted in both directions [102].

Besides that, tendon driven mechanism can be further classified according to the system degree of freedom (DOF) *N*, *N*+1 and 2*N* [103-105]. In the first configuration (*N*) number of motors required is equal to the degree for freedom. Khalil and Liegeois developed a six-degree-of-freedom manipulator with this configuration [106]. Another example is the three-fingered hand developed by Okada [107]. As for the *N*+1 configuration, the number of actuators and tendons required to control *N* degree of freedom manipulator is *N*+1. For example, Morecki and Salisbury developed a six DOF manipulator with seven tendons and Stanford/Jet Propulsion Laboratory Hand with four cables for each three degree of freedom finger respectively [108][109]. The actuator required for the third configuration (2*N*) is twice the DOF of the manipulator. The (2*N*) configuration employs more actuators in the design compared to other design approaches. However, in the design approach motors used for the actuation are positioned at the base or near to the base of the manipulator. Therefore, the lightweight design concept of the manipulator is still justifiable [110-112]. Furthermore, 2*N*

configuration supports the generation of low contraction forces and the independent control of joints [103]. Jacobsen *et al* has implemented the 2*N* configuration in the design of Utah/MIT Dexterous manipulator [76].

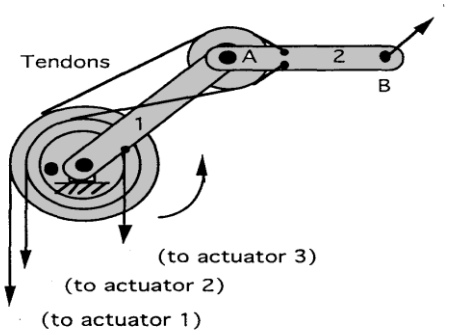

Figure 2.1: Opened ended tendon drive [101].

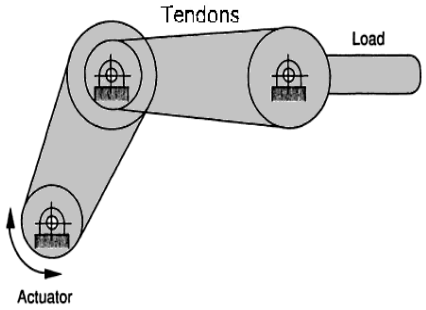

Figure 2.2: Closed loop tendon drive [101].

Tendon drive mechanisms are employed widely in various robotics designs such as lightweight spatial arms [113][114], robotic hands [91][115] and humanoid robots [116]. Tendon drive mechanisms are extensively adopted in the biomimetic robotic fingers and hand designs compared to other robotics designs. Similarly, tendon drive concepts have also been implemented considerably in the lightweight manipulator domain as well. In the following section, several examples of the lightweight articulated manipulators developed with tendon drive mechanisms are discussed.

2.2.1 Tendon Driven Manipulator Designs

CT arm 1 is a manipulator with open ended 2*N* configuration with couple tendon drive mechanism designed by Hirose [117]. Sets of pulley and tendon are used for the transmission of power from the actuators to the joints. The pulleys are fixed at each corresponding joint [118]. Pair of tendons are looped around the

pulley *i* riveted to link *i*. The other ends of the tendons are wound on the pulley *i*-1 connected at joint *i*-1 and similar on the pulley *i*-2 at the joint *i*-2 then the tendon is looped around first pulley at the first joint prior to connecting to the actuators at the base [118]. The design has also employed connected differential mechanism. During the operation, equal amount of torque is applied thought all the joints in the manipulator [118]. Therefore, coupled drive mechanism in manipulator distributes required output power among the actuators without concentrating power on one actuator. As a result, lightweight driving mechanism can be implemented without using high torque actuators. In the CT arm design, traction force supporting the payload at each joint is maintained at a constant value and the burden of the tendon traction force is also reduced [119]. The design is shown in Figure 2.3.

CT arm 2 is an improved version of CT arm 1 design developed by Hirose [118]. The fundamental structure of the mechanism remains the same to that of CT arm 1, however the only difference is a pair of tendons are looped through joint *i*-1 to joint 1 via two pulleys. The tendons are stretched on the same side of the pulleys [118]. The stretched driving tendons are positioned at upper section of the arm with respect to the gravitational field. The mechanism functions efficiently, as such the torque generated from the bias force accumulates to the joint torques 1 to *i*-1 reducing the torque to be generated by the tendons. Apart from that the generated torque also sustains the manipulator weight and payload weight [112]. The pulley and cable design is shown in Figure 2.4.

Furthermore, both CT arms have the capability of varying the joint compliance controlling the two driving actuators corresponding to each joint. The joints of CT arm 1 and 2 are driven by torque controlled 100 W DC servo motors [120]. The CT arm 1 uses 16 DC motors for the actuation of 9 DOF [120]. In the

both designs CT arm 1 and CT arm 2 velocity controlled 100W DC servo motors are positioned at the base apart from joint motors to rotate the entire manipulator. The payload capacity of the manipulators are 3 kg and 8 kg in CT arm 1 and CT arm 2 respectively [120].

The CT arm design uses couple drive mechanism that contributes to the lightweight design. The mechanism distributes the required power for the actuation of the robot joints among all actuators. This rule out the use of high power and larger actuators for the manipulator. Consequently, lightweight actuators are implemented in the design reduces the weight of the manipulator. Apart from that the actuators in the design are installed at the base of the manipulator enhancing the lightweight attribute of the design. Due to the design configuration (2N) both the designs have used more motors for the actuation. The major applications of the CT robot manipulator involve unstructured industrial environments with the interaction of soft, fragile objects and humans because of the CT arm's lightweight attribute and larger payload capacity [19].

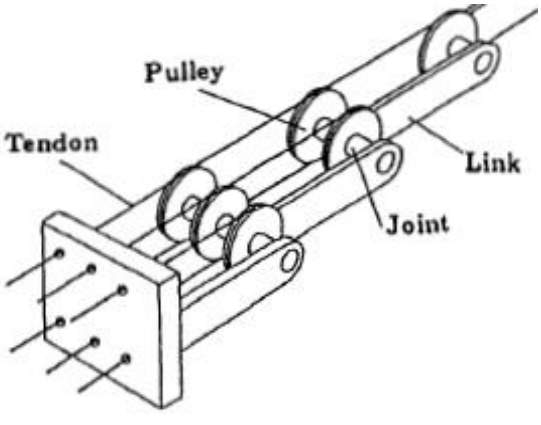

Figure 2.3: CT Arm model 1 [118].

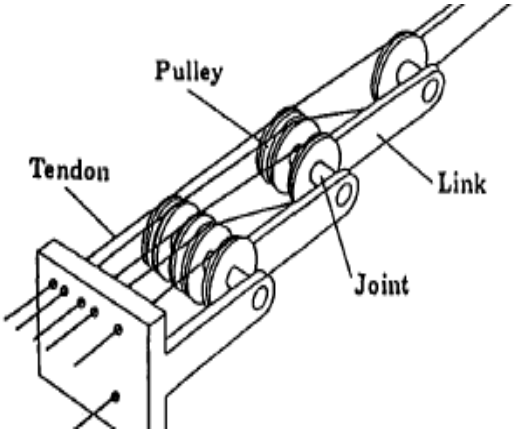

Figure 2.4: CT Arm model 2 [118].

Seven degree of freedom tendon driven manipulator developed by Yokoi *et al* is another example of opened ended (*N*+1) tendon drive robot. The design employs set of pulleys and tendons to transfer power from the actuator to the corresponding joints. Number of pulleys fixed at each joint is identified by the joint number *i*. If the joint number is *i* then the number of pulleys fixed is either 9-*i* or 10-*i*. If *i* is an odd integer then number of pulleys required is (9-*i*) otherwise it is (10-*i*) [121]. The manipulator design has seven degrees of freedom. Therefore, eight tendons are employed according to (*N*+1) configuration. The tendons are connected to a fixed link in a pattern. Where tendon 1 and 2 are connected to link 7. The tendon 3 and 4 are connected to the link 6. Similarly, tendon 5 and 6 to the link 4. The last two tendons 7 and 8 are connected to link 2. The other end of the tendon is looped around the respective pulleys and then connected to the actuators positioned at the base [121]. The maximum torque is generated at joint 1 and 2 closer to the base. Therefore, the joints 1 and 2 are actuated with eight tendons. Similarly, six, four and two tendons are used for actuation of joints 3 and 4, joints 5 and 6, and joint 7 respectively. Joint torque and tendon tension are considered at the time of designing the pulleys. Eight direct drive motors with 5 Nm maximum torque are installed as the actuators. The actuators are connected at the base, hence it reduces the weight providing a higher payload to weight ratio. The significant feature of the mechanism is that the joints with large torque requirement are driven by more tendons. Therefore, more actuators will be engaged in supply power as the more tendons are used. Because all the tendons are connected with actuators installed at the base. In this case, actuators of the same size could be installed as such the required power is distributed among the actuators. The actuators with the same size could function corporately according to the mechanism to achieve the required large power for the actuation. Therefore,

implementation of high torque large actuators is avoided, hence it reduces the weight of the manipulator design. However, in this design number of motors utilised for the actuation is greater than the degrees of freedom of the manipulator. The design is shown in Figure 2.5.

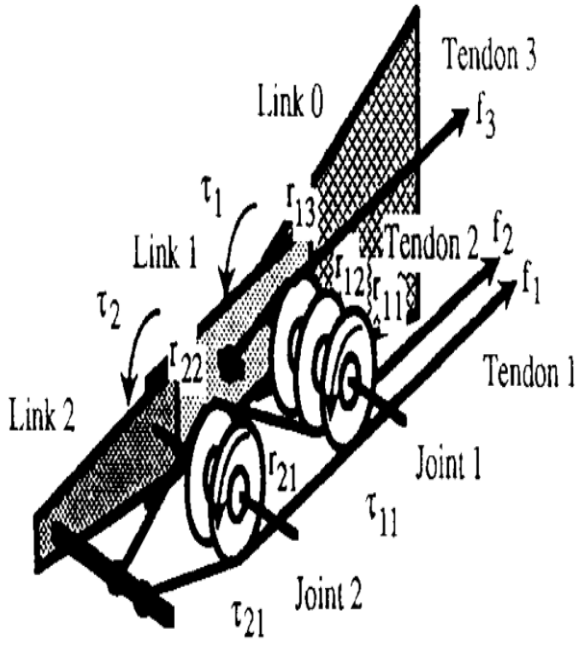

Figure 2.5: 7 DOF coupled driven manipulator mechanism for 3 joints [121].

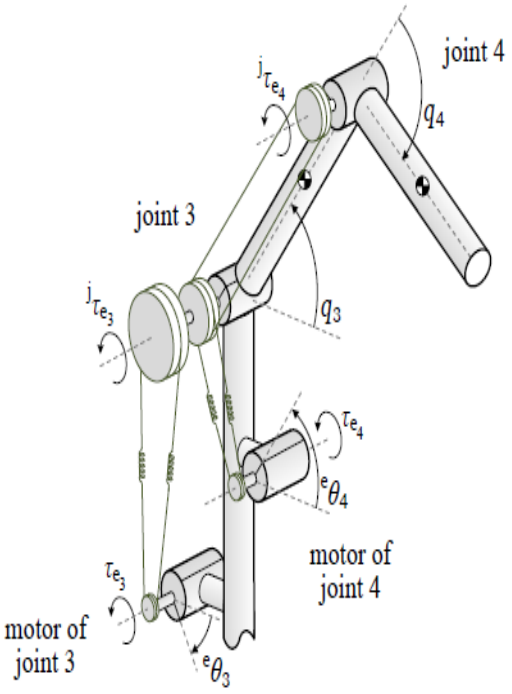

Figure 2.6: Structure Series elastically driven manipulator mechanism [122].

The BioRobo arm designed by Lens *et al* is a lightweight manipulator with the *N* tendon drive configuration [122]. The objective of the design is to implement a human robot interaction with manipulator capable of cooperating safely with humans. The manipulator has combined both tendon drive actuation mechanism and series elastic concept in the design. In the series elastic design concept springs are integrated with the tendons used for the tendon drive mechanism that contributes for the actuation as shown in Figure 2.6. The springs (elastic element) connected to the tendons restrict the slacking of cables [122]. Apart from that the

mechanism provides compliant tendon actuation enhancing the safety of the system. Furthermore, the series elastic design dynamically decouples the link and motor inertia which protects the actuators [123].

In this design joints are actuated using a DC motor drive fixed near to the base. Two motors actuating joints 1 and 2 are positioned in the first link. Similarly, the remaining two motors actuating joints 4 and 5 are placed within the second link as counterweights for the link [123]. Each joint is connected with four cables combined with springs. The cables are looped around the actuator and the other ends of cables are looped around the pulley [122]. A cable is wound to the guiding pulley and the other end of the cable is looped around the pulley fixed at joint 4. Another cable is looped around the guiding pulley and the actuator as shown in the Figure 2.7. Guiding pulley fixed at joint 3 aids for the actuation of pulley fixed at joint 4. Guiding pulley operates as power transferring device between the actuator and the pulley fixed at joint 3. The total weight of the manipulator is 3.7 kg. Figure 2.6 shows a schematic diagram of the mechanism. The actuators are installed close to the base and away from the joints, hence the weight of the manipulator is reduced significantly enhancing the lightweight attribute of the manipulator [122]. Apart from that in the design tendons are protected from fatigue or plastic stretching that occur as a result of larger strains generated on the tendons [122].

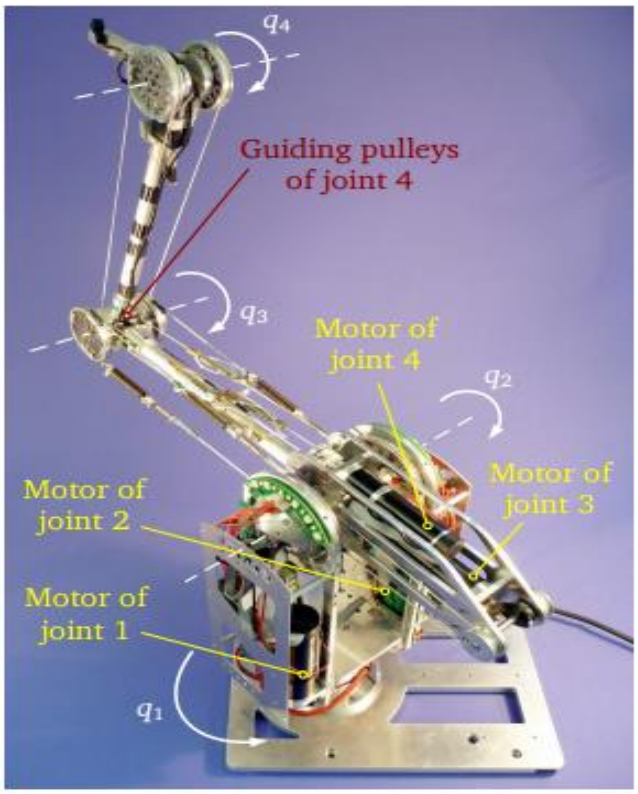

Figure 2.7: Series elastically driven manipulator [123].

Robot arm introduced by Lee *et al* with motion decoupled joints and cable drive actuation is another tendon drive manipulator model [124]. The shoulder joint of manipulator has 2 DOF: pitch and roll of the upper arm. The design consists of three pulleys with equal diameter fixed to the arm namely P1, P2 and P4 [124]. The pulley P3 performs a linear motion with respect to the forearm pitch motion. The mounted pulleys in the manipulator are shown in Figure 2.8. During the rotation of the forearm in clockwise wise direction, pulley moves towards left to compensate the overall length change in the cable [124]. Similarly, when the forearm rotates in the counter clockwise direction, pulley moves towards the right direction. The decoupling link is connected to the pitch link of the forearm in which two cables are looped in an opposite direction at both sides of the link. Figure 2.9 shows the operation of the mechanism using pulleys P5, P6, P7 and Fig. 8 shows

the diagram of the same mechanism installed with the manipulator. The pulleys P5, P7, P6 in Figure 2.9 corresponds to the pulleys P2, P3, P4 in the Figure 2.8 respectively. When the forearm rotates, the cable looped around the pulley P6 is wrapped and the cable on pulley P5 is unwrapped. These cables move pulley P7 linearly with respect to the direction of rotation of the forearm [125]. Therefore, no variation of length occurs in the cable [125]. The robot arm has 6 DOF with a motion range of 1.55 m, 1.66 m and 1.575 m in the x, y and z direction respectively. The manipulator has the capability of handling 25 kg of load [125].

This design prevents the variation of the length of the tendon during the operation [126]. A novel joint motion decoupling concept is introduced in the manipulator design. Apart from that the mechanism prevents the change in tensile forces in the cable as a result of change in the length of the cable during the operation. In addition, similar to other tendon drive designs, this design reduces the weight of the manipulator as the actuators are positioned at the base [127].

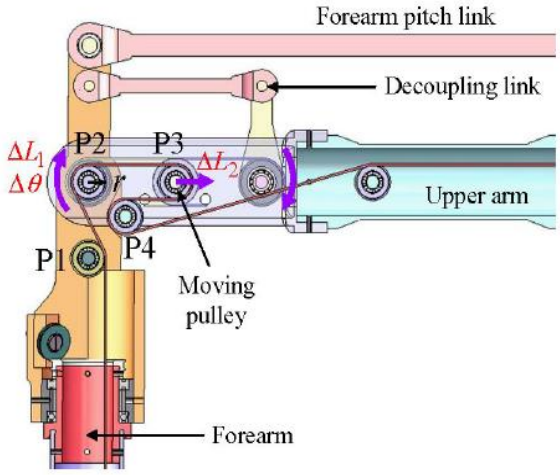

Figure 2.8: Pulley P1, P2, P4 and P3 design [124].

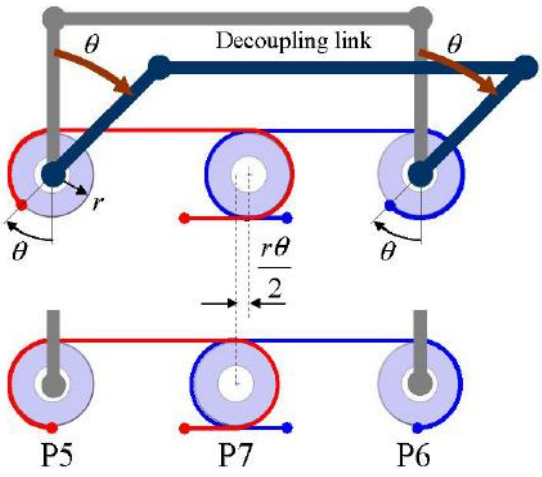

Figure 2.9: Decoupling link mechanism [124].

WAM is a commercially available tendon driven manipulator designed by Salisbury and Townsend [128] and later was commercialized by Barrett

Technology Company. WAM manipulator has gained considerable attention commercially, being employed in many global corporations such as Honda, Ford, Sony and Z-KAT Medical Inc. [129]. The manipulator has two different versions, one with 4 degrees of freedom and the other with 7 degrees of freedom. The motors are positioned at the shoulder height close to centre plane at the base, reducing the inertia of the joints [128]. The actuators for the wrists are mounted in the forearm to prevent cables connecting through the elbow joint. The manipulator adopts a novel cable differential in the design, which has zero backslash and near zero friction [129]. Apart from that the design uses a speed reduction mechanism developed using cables instead of gears, which reduces the cable compliance [129]. WAM manipulator has high back drive-ability. Motion control in the manipulator is performed through joint torque control, which enables the intrinsic sensing of forces over the whole arm and makes it inherently safe to human operation [129]. Furthermore, WAM innovation helps to overcome two barriers: axial cable compliance and absence of equivalent fully cable drive mechanism for the bevel gear differential mechanism [130]. The total weight of the 4 DOF and 7 DOF manipulators are 25.4 kg and 27.2 kg respectively.

Over the past years several tendon drive manipulator designs have been developed using tendon driven approach. Among these different tendon drive designs a common design aspect could be observed. Positioning of actuators at the base of the manipulator or near to the base is common design technique used in all the tendon drive designs to reduce the weight. In addition the tendon driven manipulator with configuration *N* also follows the traditional manipulator actuation principle "One actuator for One degree of freedom ". Therefore, each joint is allocated with dedicated actuator similar to the conventional manipulator (one actuator for each joint). However, the tendon configurations such as 2*N* and (*N*+1)

even require additional number of actuators than the number joints in the manipulator. Therefore, even though the lightweight property is maintained in 2*N* and (*N*+1) design configurations, large number of actuators are implemented for the manipulator actuation.

2.3 Lightweight Manipulators with Gear Driven Mechanism

The gear driven manipulators use gear trains, shafts and clutches to transmit mechanical power to the joints of the manipulator and permit the mechanical drives to be installed closer to the base of the manipulator [131-133]. Therefore, it reduces the joint torque and the weight of the manipulator. The gear drive transmission systems are capable of handling higher torque and higher stiffness [134]. Mechanisms with gear drive transmission frequently employ shafts to transmit power in scenarios that actuator and the driven gear are located with larger physical separation [134]. Therefore, it permits the actuators to be located remotely from the driven joint [134]. According to the literature three lightweight manipulator designs have been identified that are developed using the gear drive transmission. Therefore, it could be observed from the literature relatively few manipulator designs have been developed using gear drive transmission concept compared to other design approaches. In the following section, examples of the lightweight manipulators implemented with gear drive transmission concept are discussed.

2.3.1 Gear Driven Manipulator Designs

Single motor driven manipulator with multiple joints developed by Li *et al* adapts the uni-drive concept for the development of the manipulator [135]. The uni-drive concept uses a single actuator to drive multiple joints in a manipulator [81][136][137]. A single motor is used to control each joint of the manipulator in the design. The robot is designed to achieve two types of motion, namely joint motion and main motion. Gears and the two clutches in each joint function and perform the motion of the joint or transfer the energy to next joint. The main shaft and the gear box transfer energy to the joints of the manipulator, however the clutch controls the supply of energy to the joints by switching it off and on [135]. Each joint consists of a brake and two clutches. The main shaft of the manipulator is driven by a DC motor. The two clutches control the bidirectional motion and the brake is used for stopping the motion, while the motor is rotating uni-directionally at a constant speed [135]. The design incorporates three pivoting joints and three twisting joints. In the twisting joint, initially the main motion is transmitted to the planetary gear box through the spur gear train before transmitting to the next joint [135]. To perform the joint motion, the main shaft torque is transmitted to the harmonic drive through the clutches. Two spur gears are fixed with two clutches to control the direction of motion. The spur gear fixed with the brake is used to halt the motion.

Similarly, three spur gears in the pivoting joint perform the same functionality as in the twisting joint. Five bevel gears are mounted to the pivoting joint. These gears can be divided into two gear trains. The gear train with three bevel gears are used to transmit the motion to the next joint [135]. The gears in the gear train share the same pitch and are smaller in dimensions compared to

the gears in the second gear train. The second gear train contains two large bevel gears used to perform pivoting motion of the joint through a harmonic drive [135].

Each joint is designed to perform bidirectional motion even the main actuator rotates at constant speed in unidirectional [135]. Furthermore, the design does not contain actuators at each joint and energy is transmitted to the joints from the base motor. Therefore, the design reduces the weight of the manipulator. However, transmission gears and electromagnetic clutches are installed at the joints of the design. This is a limitation of the design that contributes for the increment of driving joint torques.

A three dimensional 6 DOF redundant manipulator designed by Yahya *et al* is an example of gear driven manipulator [138]. There are three motors in this design. The first motor is fixed at the base of the manipulator. It is used to perform the rotational motion of the entire robot manipulator around vertical axis. The second actuator controls the angle between the first link and the second link. The gear wheel is fixed to the second link, when the worm wheel driven by the actuator rotates, the gear wheel of the second link rotates correspondingly [138]. Therefore, the motion of the second link is driven by the rotation of gear wheel as shown in Figure 2.10. The torque transmission mechanism consists of a planetary gear train with two bevel gears, shaft connected to one of the bevel gears in planetary gear train and an arm. At the instance wheel gear fixed to the arm starts rotating. The rotation of the second bevel gear around the first bevel gear will start at the same angular velocity [138]. The second bevel gear is fixed to a shaft that rotates with the second bevel gear as shown in Figure 2.11. Transferring of power from the second link to the third link is performed by rotating the first bevel gear. When first bevel gear rotates, as a result the second bevel gear will start rotating. Therefore, the shaft connected to second bevel gear will rotate

transferring the power to the subsequent joint. The mechanism is as shown in Figure 2.11. The rotating shaft transfers the motion from second link to the third link as shown in Figure 2.12. The same mechanism is implemented for other links to perform the motion without an actuator.

The design uses three motors to control *N* degree of freedom in three-dimensional redundant robot arm instead of using *N* number of actuator as the traditional manipulator design approach [139]. However, according to the design the angle and speed of rotation can be controlled independently only on the first three joints of the manipulator that are connected with the actuators. All the joints in the manipulator afterwards the third joint perform motion similar to the third joint following the same angle of rotation and the speed of rotation. Therefore, only the first three joints of the manipulator could be moved independently which is a limitation of the design. The design minimises the joint torque by reducing the number of actuators used at each joint [140]. Furthermore, the weight of the manipulator is also reduced as the actuators are positioned closer to the base.

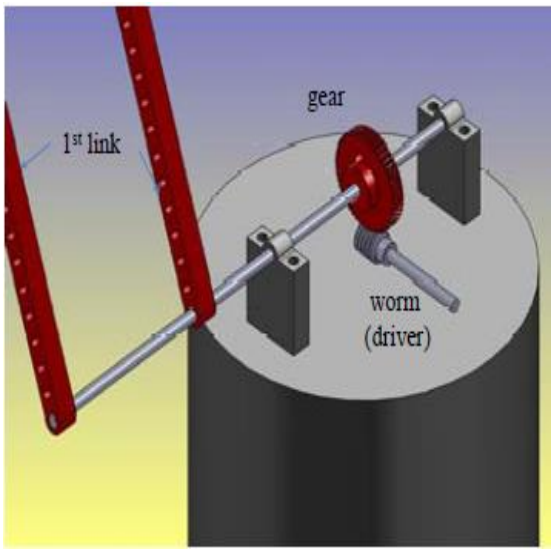

Figure 2.10: The second joint design [138].

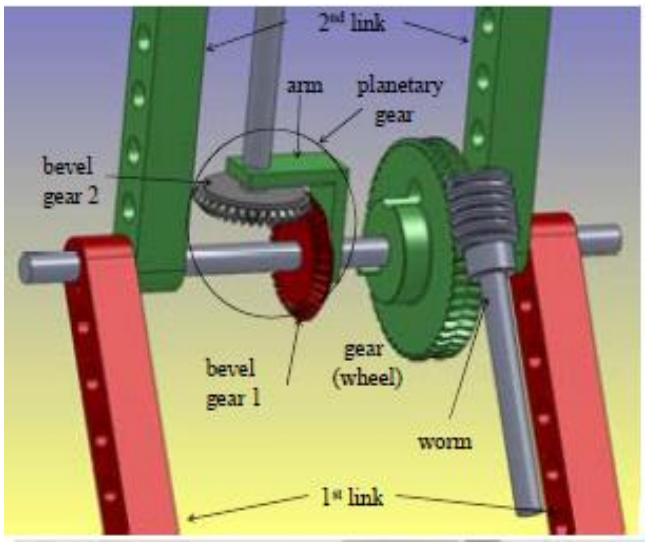

Figure 2.11: The third joint design [138].

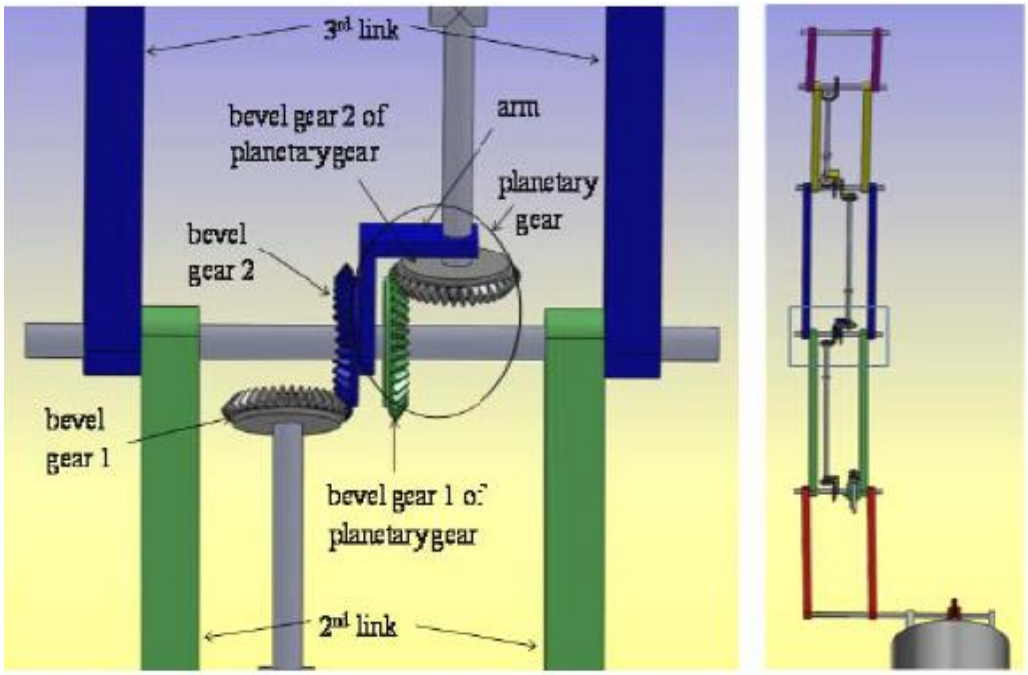

Figure 2.12: The fourth joint design and the whole manipulator [138].

In another example, Shafer and Kermani developed a robot manipulator with single motor, using Magneto-Rheological (MR) clutch and Distributed Active Semi–Active(DASA) approach [141]. It uses Magneto-Rheological (MR) clutches to distribute the torque among the joints. The MR clutch can be considered as a geared motor with series damper, which couples and decouples the input shaft from the output [82]. The MR clutch is implemented in the design due to its distinct characteristics such as higher torque capacities, higher torque to mass ratio and higher torque to inertia ratio [142][143]. Furthermore, MR clutch has the advantage of transmitting torque independent of the actuator amateur position [143]. The concept of the MR clutch is, upon establishing the magnetic field, rheological behaviour of the fluid changes and ferromagnetic particles in the fluid combine and are aligned in the direction of the field applied [143][144]. The input shaft in the design is made from a set of disks, which are aligned parallel to the output disks fixed to output shaft. The empty space between the disks is

filled with MR fluid [82]. The rotational motion of the input shaft results shearing in the fluid with the output shaft. Energizing the electromagnetic coil, the shear stress of MR fluids can be controlled by an applied magnetic field, which alters the output torque [82].

The Distributed Active Semi Active concept is proposed in the design approach of the manipulator. In DASA method the driving actuator is installed at the base and the joint of the manipulator are driven using semi active components [143]. The proposed approach helps to reduce the weight of the manipulator due to the positioning of active components (actuators) at the base of the manipulator and transferring the energy via semi active components [143]. MR clutch is used as the semi active component in DASA approach due to its distinct characteristics mentioned above. In addition to that MR clutch reduces non-linearity such as cogging torque that exists in servo motors. Antagonistic approach is achieved by connecting the output of the actuator with two clutches. Hence the direction of rotary joint could be changed by activating the corresponding clutch accordingly [145]. Similarly antagonistic MR clutch design configuration in DASA enables transmission of torque either in clockwise or anticlockwise direction independent of the active actuator output [146][147]. In addition, MR clutch employed in the design has back drive-ability, therefore it could function as an active actuator as well [148]. The transmission of torque to the manipulator joints via the actuator installed at the base is described as follows.

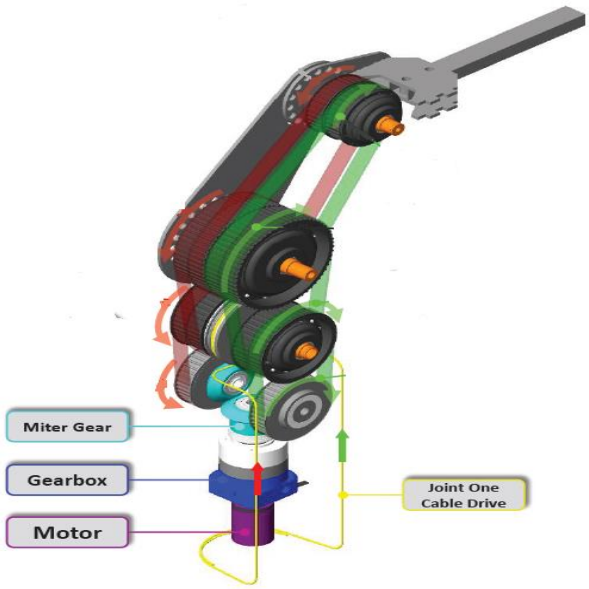

Figure. 2.13: Transmission model of the 3-DOF DASA manipulator [141].

The torque required for the robot manipulator design is provided by a single motor coupled through a gearbox. Serially coupled belt transfers the required torque to drive the three joints of the manipulator. Set of miter gears are used to generate the bidirectional rotation. The miter gears are driven by the gear box installed at the base. The clockwise (CW) and counter clockwise (CCW) rotation of joints are achieved through two sets of timing belts [98]. The rotation direction of the belt is controlled by miter gears. The CW rotation and CCW rotation are provided by green and red colour belts respectively as shown in Figure 2.13. The MR clutches perform the engaging and disengaging of the output shaft from the timing belt transmission pulleys to perform the respective motion. The clutches of joint two and three are integrated on to the shaft of the joint at the time of fabricating [141]. The mechanism implemented at joint one allows rotational motion around axis normal to the ground. A steel cable with high strength is used for the mechanism. The winch driven by the clutch wraps the cable around stationary cylinder installed at the base of the manipulator as shown in Figure

2.13 [141]. A brushless DC motor with a mass of 910 g provides the required energy for the motion of the manipulator joints [141].

In the gear drive 3-DOF DASA robot manipulator, each joint can perform bidirectional motion independent of the base actuator [141]. The drive components such as motor and the gearbox are installed at the base of manipulator therefore the inertia of the manipulator has reduced. Apart from that the design diverges from traditional robot manipulators as a result of transmission of power to the joints of the manipulator from the base motor without installing actuators at each joint. These design factors reduce the manipulator weight creating a lightweight manipulator. The weight of the clutch could be a limitation of the current design approach [141]. Another limitation of the design is that the clutches are installed at the joints of manipulator which contributes for the increment of joint torques. Furthermore, the manipulator design could be further optimised via focusing future work on reduction of the MR clutch weight and positioning the clutches at the base of the manipulator.

The general lightweight manipulator design technique, positioning the actuators at base of the manipulator or near to the base is also followed in the gear driven design approach. The technique has been employed for the reduction of weight of the manipulator similar to the tendon driven approach. However, in contrast to other lightweight manipulator design approaches in gear driven approach researchers have made an effort to decrease the number of actuators used in addition to reduction of weight of the manipulator. All three example manipulator designs reviewed have employed less actuators than the degrees of the freedom of the manipulator. The manipulator designs have not only reduced the weight of the manipulator by positioning the actuators away from the joints but also reduce the number of motors employed for the actuation. Therefore, it

could be observed that the gear driven design approach has deviated from the traditional manipulator actuation concept of "one actuator for one degree of freedom".

2.4 Lightweight Manipulator Design with Modular Mechatronic Approach

Modular mechatronic approach is a relatively new technique where it integrates miniaturized electronic and mechanical components in the design of lightweight manipulators [149-151]. Lightweight actuators, gears systems, links and joint structures are the common features in this approach [149][152]. For example, carbon fiber structures could be considered in the design of lightweight robotic links. Apart from that, technologies such as surface mounting, chipsize-packaging and flip-chip are employed in the integration of electronic components with the robot structure in the modular mechatronic design concept [149][152]. Therefore, these integrated manufacturing technologies reduces the amount of wires and cables required, facilitating the reduction of weight. These factors help to reduce the weight while maintaining the rigidity, strength, precise motion and larger weight to load ratio of lightweight manipulator.

Harmonic gear drive is a common feature in most of the modular mechatronic lightweight manipulator designs. Harmonic gear drive transmits high torque through elastically deformable component [153]. The three main components of a harmonic gear drive are circular spline, flexspline and wave generator. The diameter of the circular spline is larger than the flexspline. The wave generator of harmonic drive has an elliptical shape. The elliptical structure of wave generator causes engagement of flexspine to the circular spline at two

positions of the major axis of the ellipse. At the time of rotation of the wave generator (input), the region that gear teeth are connected will start to move in the direction of major axis of the ellipse. In harmonic drive reduction ratio depends on the number of teeth and its variance between circular spline and flexspline. Therefore the reduction ratio can be achieved with three components [153][154]. Thus, the harmonic drive is lighter than a traditional gear system as it requires less components. High positioning accuracy, repeatability, zero backlash, compactness and light weight are the main benefits of a harmonic drive [153][154]. Furthermore, harmonic drive has high torque capacity compared to a conventional drive with more weight. The weight could be reduced further by fabricating the wave generators and circular splines with aluminium alloys and titanium [153] [154].

2.4.1 Modular Mechatronic Approach Based Manipulator Designs

KUKA DLR Lightweight robots (LWR), DLR Miro, Mitsubishi PA 10 and Schunk Powerball are some of the commercial modular mechatronic lightweight manipulator designs. It could be observed based on the number of commercial lightweight manipulator designs found in the literature, modular mechatronic approach is considerably adopted in the development of commercial lightweight manipulators. In the following section, several examples of modular mechatronic approach oriented lightweight manipulators developed are discussed. The details of the some of the commercial modular mechatronic lightweight manipulator designs are presented in Table 2.1 and the Figure 2.14.

The DLR Light Weight Robot I (LWR I) is a modular mechatronic lightweight manipulator developed at DLR robotics and mechatronics lab [87]. Manipulator

link structures are fabricated with carbon fiber, which reduce the weight of the structure [87]. The electronic module integrated to the joint consists of a torque sensor, power inverter and a joint controller. The joint controller unit comprises of four circuit boards. One board consists of supply circuitry and the other two boards perform the required joint control algorithms. Apart from that the last board consists of the interface circuitry required for the joint control process [155]. The robot joint modules are integrated close to the joint controller units [155]. Therefore, only information and the electrical power are transmitted between the controller and the joint. As a result, fewer wires are required for motor connections and signal transmission. This reduces the weight, space and cost [87]. Furthermore, the power inverter is mounted directly next to the motor. Consequently, reduces the length of the high voltage wires utilised for the joint motor connection with the power adapter [155]. These seven degrees of freedom manipulator has a total weight of 18 kg [156]. The load to weight ratio of the LWR I robot is 1:2. LWR I design prevents the use of heavy wiring and electronic control cabinet in the conventional manipulators [87] [156].

The DLR Light Weight Robot II (LWR II) is an upgraded version of LWR I manipulator developed at DLR robotics and mechatronics lab [85]. The LWR II robot structure is built with aluminium, however the links between the joints 2 and 3 are fabricated with carbon fiber [157]. In designing of lightweight structure it is necessary to inspect the loaded mechanical components. The stiffness and the strength of structure should be increased while maintaining the lightweight aspect of the mechanical structure [158]. Hence Finite element method is applied for the analysis of required stiffness and strength of the structure in the manipulator design, while maintaining the lightweight aspect. The joints of the manipulator are integrated with sensors to measure the torque, link position and

the motor position [159]. The motors installed at the joints are mounted without the housing [159]. The housing of the joint is designed with aluminium to transfer the thermal energy produced from the motor to the surrounding. Apart from that 40% of the weight is reduced by this concept compared to the former design [85]. The joints are equipped with modified lightweight electromagnetic brakes that contribute for the lightweight design. The weight has reduced from 281 g to 155 g in the modified electromagnetic brake [85]. The performance of the robot can be optimized with the control of the position of the Brushless DC motor installed at each joint [85]. Therefore, two analogue hall sensors are integrated to the motor, which measure rotor magnetic field and provide the motor position. As a result of sensor integration, the additional space requirement for the installation of separate sensors has been avoided. The backplane concept is used in the design of robot. One backplane is implemented to carry the electronics required for the manipulator two joints [85]. The joints 2 and 3, joint 4 and 5, joint 6 and 7 share each electronic sector integrated to the robot structure. It is integrated to the manipulator reducing the usage of long cables and the weight. Electronics used for joint 1 is installed at the base of the robot. Apart from that aluminium crafted wave generator and circular spline of Harmonic drive further reduces the weight of the robot design [54]. LWR II manipulator has 7 DOF and the weight to payload ratio is 17 to 8 [160][161].

DLR Light Weight Robot III (LWR III) is an upgraded version of LWR II designed at DLR robotics and mechatronics lab adapting the modular mechatronic approach [162]. Even though LWR III is an improved version, several significant components developed for LWR II are implemented in the upgraded manipulator design. The torque sensor, motor positioning hall sensors and the robot electronic supply components are transferred from the former lightweight robot (LWR II)

design [161]. In LWR III manipulator, lightweight attribute is enhanced compared to the former design due to the improvement of Harmonic drive gearing. The redeveloped Harmonic drive gearing contributes for lightweight design with a reduction of weight by 60% in comparison to the former Harmonic drive gearing design [161][162]. Furthermore, lightweight motor (ROBODrive) with high energy is also introduced as an actuator for the joints of the upgraded robot manipulator [87]. ROBODrive is designed with the concept of subdividing and winding stator poles of the motor. Design increases the ratio of copper to the winding area from 40% to 60% [161][162]. Apart from that the magnetic flow computation results for the optimal positioning of poles preventing the lengthy flow paths. After further optimization of ROBODrive design, the weight and the loss of power are reduced by 50% compared to the conventional motors used in robot manipulators [88][150]162]. ROBODrive contributes significantly in the lightweight design approach of the manipulator. The improved lightweight electromagnetic breaks with a weight of 30g is also integrated with the robot [88][162]. The brake design aids the lightweight design of the robot. Apart from that, the link structure is fabricated with carbon fiber that reduces the weight of the robot structure. The links are fabricated with single direction carbon fiber rowing, which are sewed to carrier fabric [163]. The process helps for the production of lightweight links with optimally placing carrying fibres to support the expected load [164]. The total weight of LWR III is 14 kg and has the capability of handling a payload of 14 kg over its complete dynamic range [165].

Table 2.1: Details of lightweight manipulators designed with modular mechatronic approach.

	Manipulator	Total Weight (kg)	Maximum Payload (kg)	Degrees of freedom
1	DLR LWR- I (1995)	14.5	7	7
2	DLR LWR- II (2000)	18	7	7
3	DLR LWR- III (2003)	14	14	7
4	DLR Miro	3	9.8	7
5	Schunk Powerball LWA 4P	12	6	6
6	Mitshubishi PA-10	40	10	6

Figure 2.14: Lightweight manipulators designed with modular mechatronic approach.

DLR Miro is a lightweight manipulator designed to perform surgical applications using modular mechatronic approach. DLR Miro robot adopts the technologies and the components developed through the designing of DLR

Lightweight robots LWR I, LWR II and LWR III. The shell structural design is used in the DLR LWR lightweight manipulators. However, the design of Miro manipulator required a compact and a minimal design in complexity [165]. Therefore, it is developed differently to fulfil the functionality and requirements. The structure of manipulator is based on the skeletal structure with unencumbered housings [166] [167]. The design follows human bone structure and the components are designed as tubes. It imitates the human arm structure to improve the lightweight structure and flexibility [17]. The electronic components used for joints are fixed outside the structure [168]. Furthermore, the casing of the robot can be removed completely and operated while performing maintenance and repair. The robot contains hollow shafts that allows internal electronic components and cables allowing the robot to be compact and lightweight [169]. The manipulator is capable of handling a maximum payload of 30 N [170]. Micro manipulator not only uses the modular mechatronic approach in designing the robot but also uses the features in human arm to improve the design.

Apart from DLR lightweight manipulators commercial robot manufactures such as Mitsubishi company and Schunk company have also employed modular mechatronic approach in the development of lightweight manipulators such as Mitsubishi PA 10 and Powerball robot. Mitsubishi PA 10 manipulator is a 7 DOF manipulator with a payload of 10 kg [171]. The design integrates the sensors and electronic components with the joint frame structure following the modular mechatronic approach [172]. Figure 2.15 illustrates the Powerball robot joint components. Furthermore, harmonic gear drives are implemented in each joint of the manipulator to enhance the lightweight design [173]. In addition to that 'O' ring sealing structure has been adopted for all the joints of the manipulator [174].

The sealing structure prevents emitting any internally generated particles in the joints of the manipulator [174].

1 Electric control system

2 Encoder

3 Drive

4 Harmonic drive gear

5 Holding break

6 Hollow shaft for internal cabling

Figure 2.15: Powerball ERB module components [175].

Six degrees of freedom Schunk Powerball LWA 4 robot is a further example for a commercial lightweight modular manipulator [175]. The central element of the manipulator lightweight design are three ERB Powerball modules [175]. The module is integrated with two independently movable axes resulting a more compact design [176]. The design maintains the modular mechatronic approach integrating the electronic control system, encoder, electronic drive and the holding brakes to the Powerball ERB joint [176]. The integration of components enhance the lightweight design of the manipulator reducing the use of long cables and providing a compact design similar to the other modular mechatronic robot designs. In addition to that harmonic gear drives are also implemented in the joint modules. The manipulator joint contains hollow shafts that allows internal cabling allowing the manipulator to be compact and lightweight [176]. Due to the modular

mechatronic design approach the lightweight quality of the Powerball manipulator enhanced. The Powerball ERB joint module is as shown in Figure 2.15. The manipulator is capable of handling a load of 6 kg and the weight to payload ratio is 2 to 1 [177]. Position of actuators at the base of the manipulator or near to the base to reduce the weight could be observed as a common design technique in the both tendon driven and gear driven approaches. However, modular mechatronic approach adopts a different strategy compared to the first two approaches. Because in modular mechatronic approach the actuators are positioned at the joint without position at the base. Serval research investigations have been undertaken in the development of lightweight manipulators using modular mechatronic approach. Furthermore, throughout the recent years several generations of lightweight manipulator design prototypes have been developed adopting the modular mechatronic concept as well. However according to the literature in modular mechatronic approach a dedicated actuator allocated for each degree of freedom flowing the traditional actuation principle of "One actuator for One degree of freedom" [135][178]. Therefore, in modular mechatronic manipulator design a dedicated actuator is installed at each joint (DOF) for the actuation. Which is similar to the joint actuation method of the conventional manipulator. The Table 2.2 illustrates the advantages and challenges of each lightweight manipulator design approach.

Table 2.2 : Advantages and the challenges of lightweight manipulator design approaches

Manipulator Design Category	Significance of the Design	Challenges of the Design Approach
Tendon driven manipulator	Negligible backlash effect in the manipulator design.	Requirement of motor for the actuation of each joint.
	Vibration and noise effects are insignificant on the manipulator design.	Periodical retention of the tendons are required in manipulator transmission mechanism.
	Transmission component weight is less (belts and tendons) thus Lightweight aspect is preserved.	
Gear driven manipulator design	Capability of performing higher torque operations.	Higher vibration and noise effects that reduce the manipulator efficiency and position accuracy.
	Compact in design due to the requirement of less space for transmission components (gears and shafts).	Higher Transmission components weight that reduced lightweight aspect (Gears and shafts).
		Friction effect and backslash effect affect manipulator efficiency and position accuracy.
Modular mechatronic approach	Complexity of control system design is less.	Higher design cost due to the use of sophisticated electronic components and customized actuator designs .
	Higher accuracy and precision in performing motions.	Utilization of motors at each joint .
		Requirement of advanced manufacturing techniques and facilities for the development of customized components and actuators

2.5 Future Trends

The lightweight manipulators are widely engaged in human-robot interaction applications such as medical robotics and collaborative robotics in manufacturing. The Human collaborative robot applications have been increasing rapidly over the years enhancing the standards and requirement of human collaborating robots such as safety, cost and compact in design. The reduction of cost, energy consumption and compact in design are some of the aspects vital for the human collaborative manipulators in manufacturing apart from weight reduction [39]. However, not only for human collaborative robots the aspects such as reduced cost, compact design are beneficial for other lightweight manipulator applications as well such as space robots. The reduction of actuators in the design have significant benefits such as low energy consumption, compact in design, low cost due to the reduced use of actuators [33][179]. These factors have influenced researches growing research interest in developing lightweight manipulator with less actuators. Continuation of research in developing manipulators with fewer actuators will have a positive impact on the development in the lightweight manipulator design. Another growing research theme in lightweight manipulators design is designing lightweight structures. Designing of lightweight structures using composites has a potential impact because the weight of the structure also affects the lightweight concept of the manipulator. As a result of the ongoing research several lightweight manipulators have been developed over the years. Some of the examples include ROTEX manipulator, Miro manipulator and DLR LWR II *designed using* carbon fiber Reinforced Polymer structure and carbon fiber structure respectively [84][157][169]**.** Lightweight actuator with lower energy consumption and with high power are particularly desirable and vital in lightweight

manipulator design. Therefore, exploration and studies on developing and actuator with less weight, energy efficient and powerful actuator are essential. The actuator consumes greater weight of the manipulator and is one of the challenges in lightweight manipulator design. ROBODrive is an example of lightweight actuator successfully developed by DLR Company [87]. Therefore, development of lightweight actuator with higher torque and energy efficacy is a significant research area in the lightweight manipulator design. Generally, in the most of robot designs as described in the review positioning the actuators at the base or away from joints have been used as potential solution [120]. Furthermore, majority of the designs have followed the conventional actuation approach "One actuator for One degree of freedom " instead of adapting underactuation method. However, handful of research have been performed in the area of developing lightweight manipulators adapting underactuation concept. Reduction of motors has significant benefits such as compact in design, reduced cost and reduction of weight which are favourable factors in lightweight manipulator design [33][179]. Thus, development of manipulators with reduced number of actuators that enhances the lightweight aspect, energy efficiency and the compactness of the manipulator design is a blooming sector of lightweight manipulator design research. Furthermore, with the expansion of research studied on underactuated lightweight manipulator design, development of novel energy saving coupling mechanisms for the underactuated lightweight manipulators have become another growing research theme.

2.6 Chapter Conclusion

The increasing requirement of robot manipulators in space applications, manufacturing applications and medical applications foster the design and development of lightweight manipulators. It could be observed from the literature there is greater improvement in the field of lightweight manipulator design. Over the years serval manipulator designs have been developed using different approaches that have been reviewed in this chapter. The three main design approaches used for the development of lightweight manipulators are reviewed in detail discussing the design technique, significance and limitations of each approach. In addition, future research trends of the lightweight manipulator design are also addressed. In summary, the research in the lightweight manipulator design have significant amount of advantages on the future of lightweight manipulators such as higher energy efficiency, higher speed of motion, convenient in portability and higher in safety. There are potential research areas to be explored broadly such as development of lightweight manipulators with less motors, developing novel motors with less weight, higher torque capacity and with high energy efficacy and development of energy saving coupling components for the manipulators with less motors. It could be observed from literature that one of the desired design aspects of lightweight manipulator development is high energy efficient design. Furthermore, design of manipulators with energy efficiency aspect is one of the future research trends in lightweight manipulator development. Vibration, noise and the backslash effect greatly affect the energy efficiency of the manipulator that reduce the efficiency of the design. From the literature it could be observed that the tendon driven manipulator design approach has minimal vibration and noise effects as well as negligible backslash effect with

comparison to other design approaches. Moreover, development of lightweight manipulator adopting tendon driven design approach can be performed without the requirement of advanced manufacturing techniques and facilities. Furthermore, development of tendon driven manipulators utilizing reduced number of motors has not been explored in field of lightweight manipulator design. Therefore, considering these factors exploring the possibilities of desiging lightweight manipulator using tendon driven approach with underactuation concept will help to enhance the lightweight manipulator design by lowering cost and the energy consumption in addition to the lightweight attribute. In addition to that continues research in lightweight manipulator design, will enhance the standards and quality of the lightweight manipulator applications and will expand the arears of applications. Furthermore, lightweight manipulators will become a significant tool in the future of robotic manipulator applications.

Chapter 3

Methodology

3.1 Introduction

This chapter presents the research methodology performed in this study. The major segments involved in achieving the goals of this research work are shown in Section 3.2 of the chapter. The research activities performed during each stage of the study are further discussed in Section 3.2.1 to Section 3.2.3. The chapter also includes flow charts to illustrate the sequence of the research activities conducted in each segment of the research study.

3.2 Research Methodology

Figure 3.1 presents major segments of this research in the form of a flow chart. The research initiates through a comprehensive review on designs of lightweight manipulators which is presented in Chapter 2 of the thesis. From the literature, the study identifies that the designs of lightweight manipulators with reduced motors have not been widely explored. In addition, the development of energy saving coupling mechanisms for lightweight manipulator designs with reduced number of motors are found to be another research trend. Thus, as an initiation to this, present study firstly introduces the design of a bistable coupling mechanism for a lightweight manipulator as shown in Figure 3.1. Subsequently,

the development of an underactuated tendon driven manipulator incorporated with energy saving coupling mechanisms is introduced. This is followed by further enhancement of the manipulator design utilising a single motor for the actuation. Finally, as illustrated in Figure 3.1, the work is concluded with recommendations for future work. The research methodology adopted for each of the above mentioned segments are discussed in the following sections in detail.

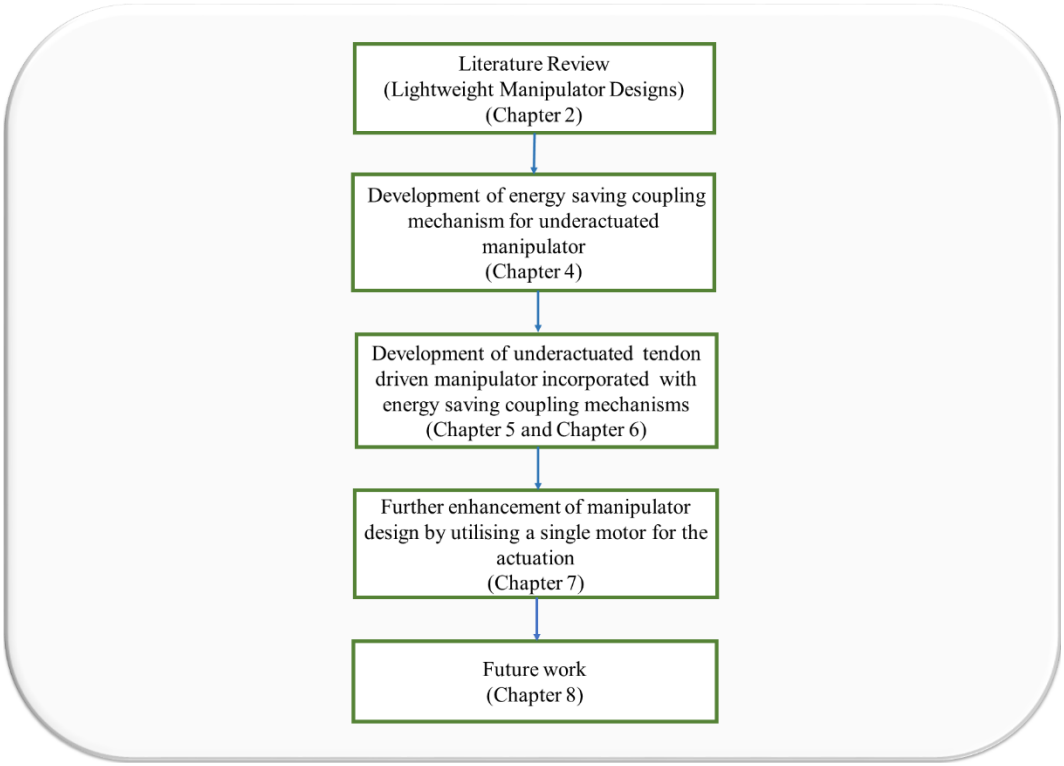

Figure 3.1: Major segments of research.

3.2.1 Development of Energy Saving Coupling Mechanism

Figure 3.2 presents the research methodology adopted in developing the energy saving coupling mechanism for a lightweight underactuated manipulator. The methodology initiates by introducing the design of a bistable coupling mechanism

for a lightweight manipulator. The design of the coupling mechanism is presented in Section 4.2. A mathematical model is developed for the proposed bistable coupling mechanism. Subsequently, simulation studies are performed using the mathematical model and the results are verified through experimental investigations. The development of the mathematical model, experimental and simulation studies performed are illustrated in Sections 4.4 and 4.6 respectively. As shown in Figure 3.2, the study further conducts experimental analysis on the energy consumption of the coupling mechanism. Lastly, the energy consumption results obtained from the experimental analysis for both conventional and the proposed coupling mechanism are compared. Sections 4.6.3 and 4.6.4 present the experimental analysis conduct on the energy consumption. This is performed for the investigation of the energy saving aspect of the mechanism.

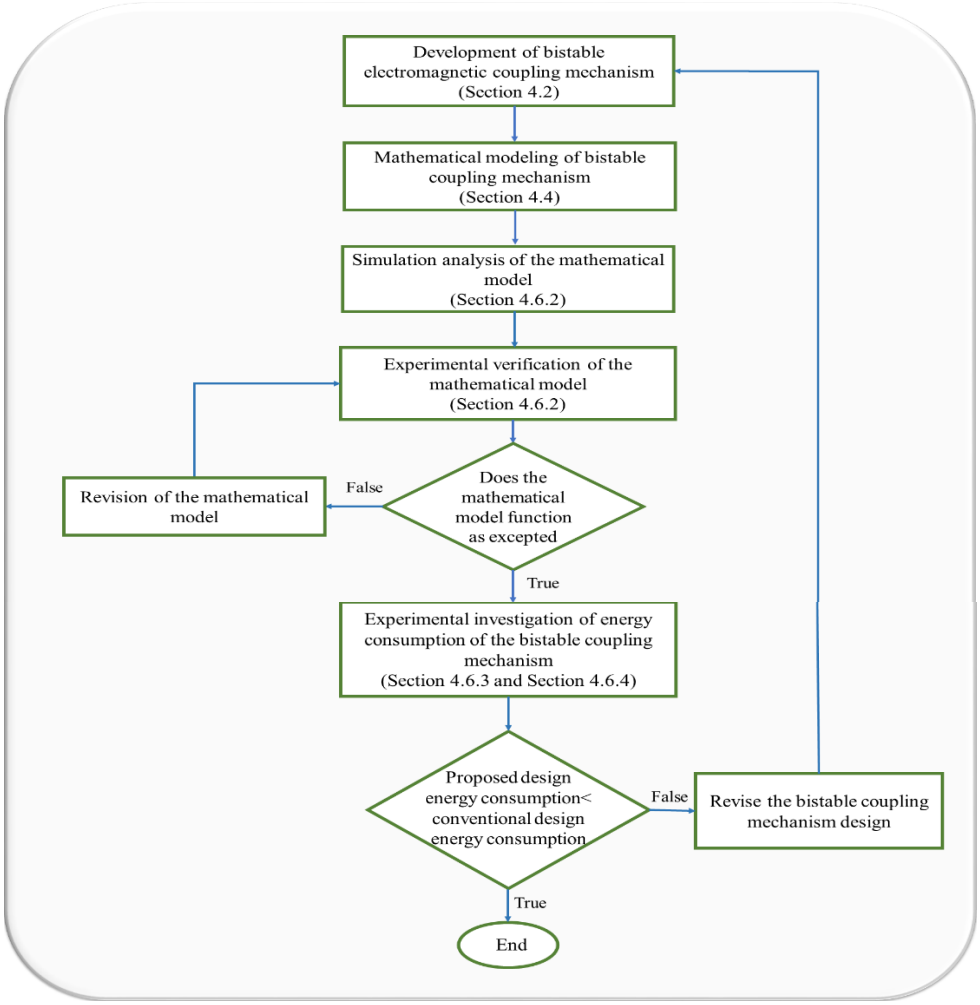

Figure 3.2: Methodology utilised for the development of bistable coupling mechanism.

3.2.2 Development of Underactuated Tendon Driven Manipulator Incorporated with Energy Saving Coupling Mechanism

The development of a lightweight manipulator model with reduced motors is introduced in the present study in addition to the development of the energy saving coupling mechanism for lightweight manipulators. The research procedure employed in the development of manipulator is presented in Figure 3.3. Initially manipulator model is developed in the study. Subsequently to the model development, a dynamic model is developed for the proposed manipulator model. This is shown in the Section 5.4. Thereafter, the simulation results obtained

through the dynamic model are compared with the conventional manipulator design for emphasizing the significance of the proposed manipulator design.

The study further introduces the prototype design of the manipulator with reduced motors incorporating the bistable coupling mechanisms as shown in Figure 3.3. The prototype design of the proposed manipulator is illustrated in Section 5.2 of the thesis. Experimental studies are conducted in this work for identifying the driving joint torques of the manipulator. In addition, the study comprises the validation of the dynamic model. The simulation and experimental studies performed are illustrated in Section 6.2. Subsequently to the above analysis, the study further investigates the energy consumption of the manipulator during joint actuation utilising both the conventional actuation approach and the proposed actuation method. The studies conducted to investigate energy consumption of the manipulator are shown in the Section 6.3.

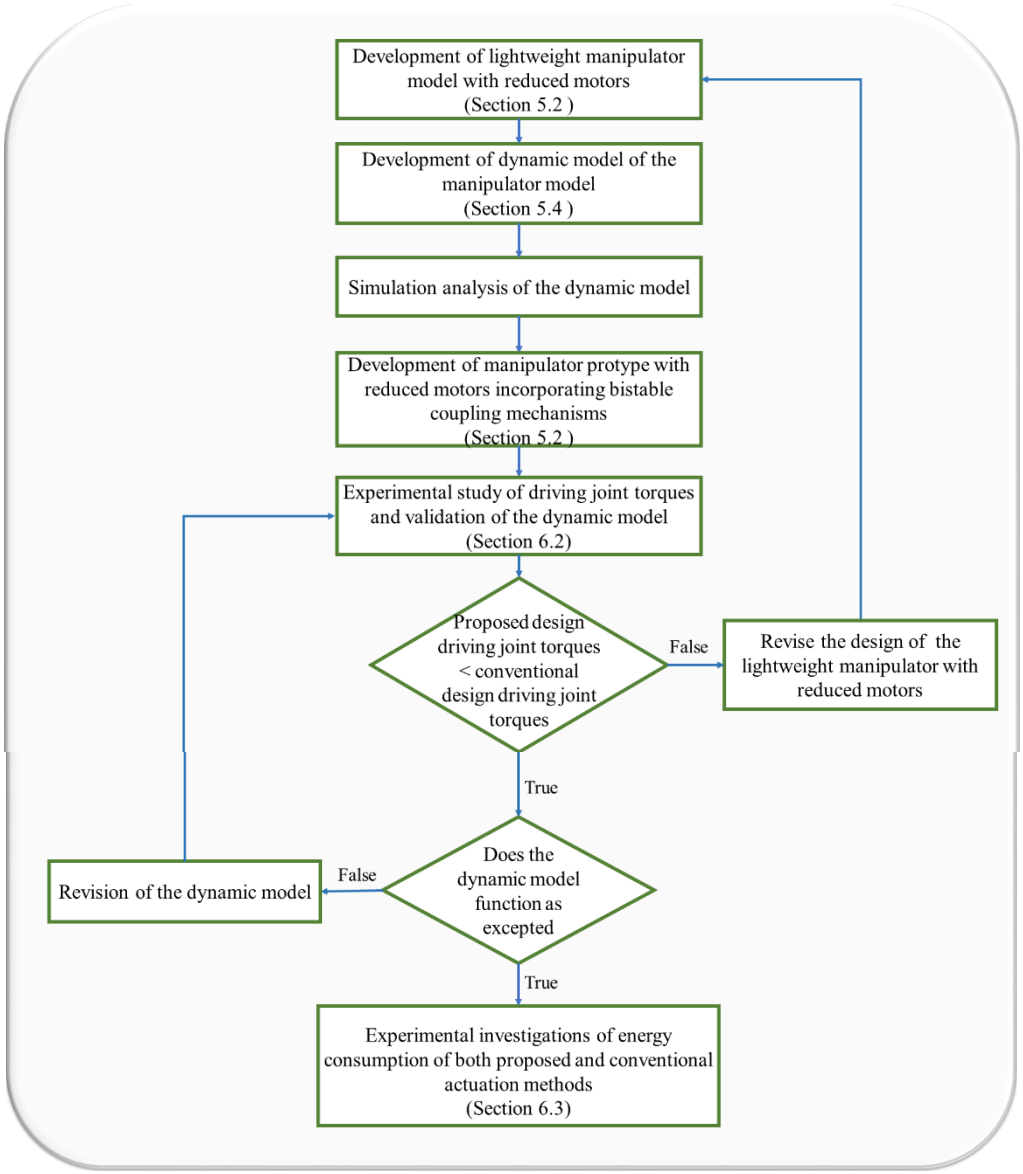

Figure 3.3: Methodology utilised for the development of tendon driven manipulator incoperated with bistable coupling mechanism.

3.2.3 Further Enhancement of Manipulator Design by Utilising a Single Motor for the Actuation

In the present work, further enhancement of the manipulator design is presented by utilising a single motor for the actuation. Figure 3.4 presents the research methodology adopted for the development of the enhanced manipulator model. Initially, manipulator model is developed and the development of the model is

discussed in Section 7.2. After the development of the modal, dynamic model is developed for the enhanced manipulator design. The dynamic model development is presented in Section 7.3.2. Thereafter, the simulation results obtained through the dynamic model are compared with the conventional manipulator design. This is performed to highlight the significance of the proposed manipulator design. The simulation analysis performed are illustrated in Section 7.4.

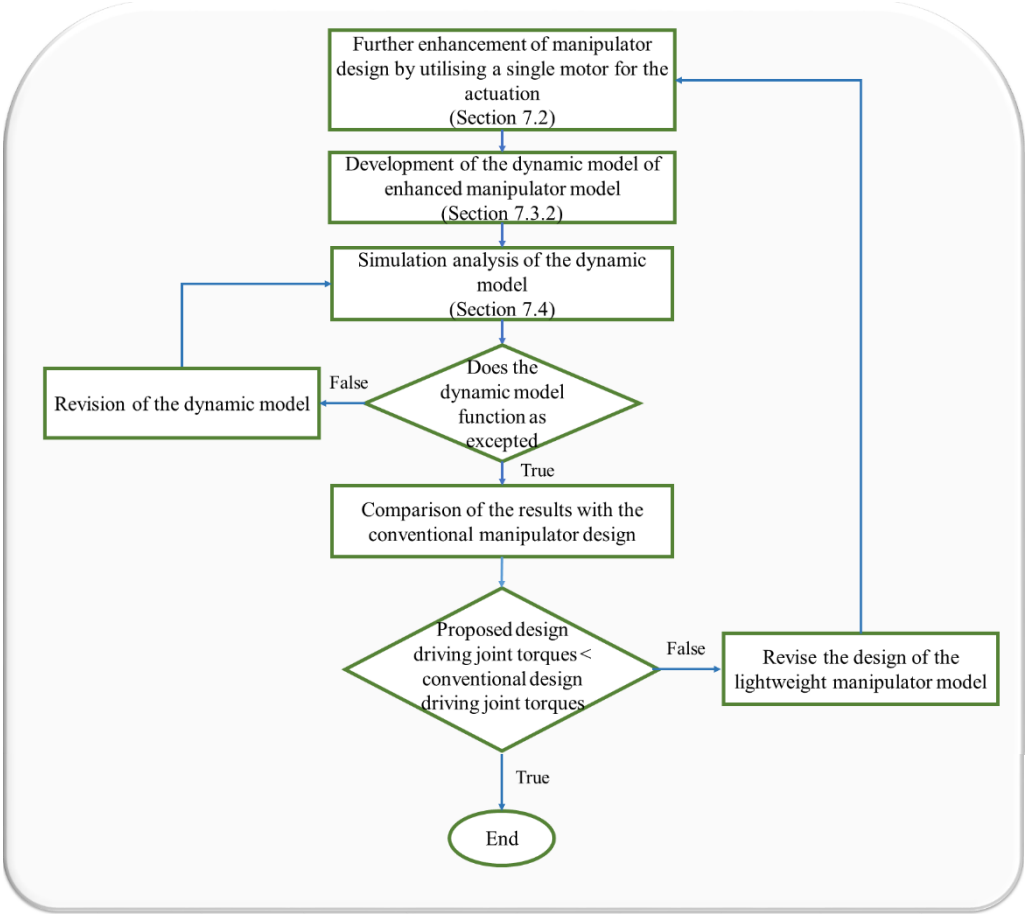

Figure 3.4: Methodology utilised for the development of enchanced manipulator model.

Chapter 4

Design of a Bistable Electromagnetic Coupling Mechanism for an Underactuated Manipulator

4.1 Introduction

The design of a bistable electromagnetic coupling mechanism used for the independent joint motion is presented in this chapter. Over the years researchers have developed systems with reduced actuator. Majority of the designs have incorporated electromagnetic clutches due to the benefits such as fast activation, moderate torque density and controlling capability via electrical signals [41-45].

Electromagnetic clutch is a device that regulates the torque transmission using an electromagnetic actuation principle [180]. However, transmission of torque is performed mechanically. Electromagnetic clutch could be categorised as a positive clutch or a friction clutch respective to its torque transmission method. In a friction clutch, torque transmission is achieved by means of friction contact between the armature and the rotor plates. The positive clutch operates through mechanical interlocking of teeth or jaws for the transmission of torque. However, the actuation mechanism for the two categories, positive clutch and friction clutch remain the same. The main components of an electromagnetic clutch are electromagnetic coil, armature, rotor and release spring as shown in Figure 4.1 [181]. The electromagnetic coil is positioned behind the rotor that generate electromagnetic field used for the controlling as shown in Figure 4.1. The operating principle of the conventional electromagnetic clutch is described as follows.

The clutch could be activated by supplying an electric current to the coil that energises the coil generating an electromagnetic field [8]. The attractive force generated by the electromagnetic field causes the armature plate to move towards the rotor overcoming the spring force. The transmission of torque begins at the instance armature plate engages with the rotor (engage state). The engaged state is maintained by providing a continuous power supply to the electromagnetic coil. This energises the coil and provides the attraction force required to maintain the engaged state. Therefore, the power supply can only be terminated during the disengaging of the clutch [183-185]. As such, electromagnetic clutches consume large amount of energy during the operation. To disengage the clutch power supply needs to be terminated. This would de-energizes electromagnetic coil eliminating the attraction force thus disengaging the clutch [182]. In the clutch design, two release springs are used to position armature away from the rotor, when power supply is switched off. At the instance electromagnet coil is de-energised spring repels the armature plate away from the rotor disengaging the clutch. Electromagnetic clutch has the advantages such as electrical controllability and rapid response time. As such electromagnetic clutches have been predominately used in various robotics applications [186].

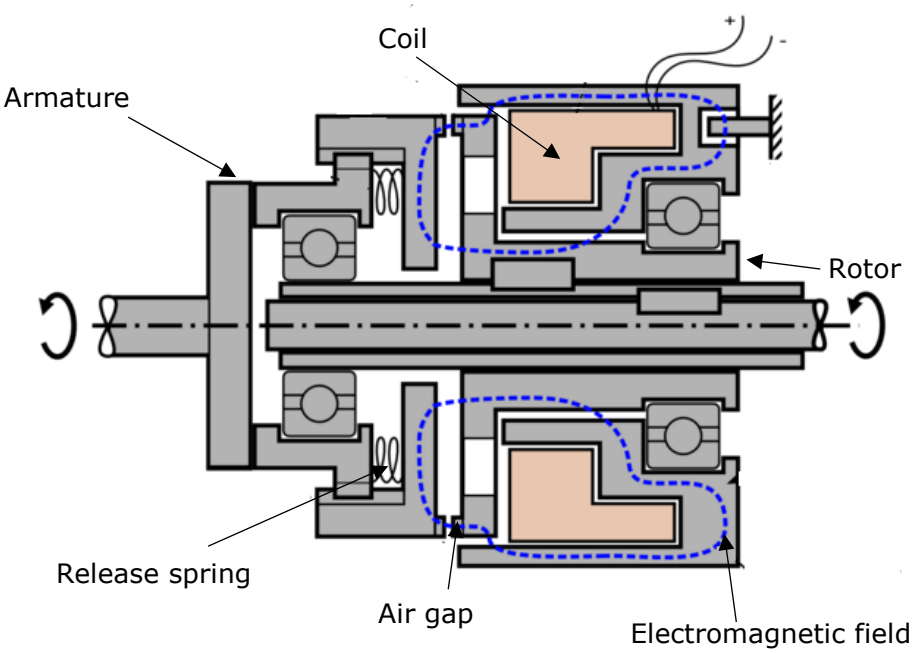

Figure 4.1: Cross sectional view of the electromagnetic clutch [180].

A conventional clutch operates in two states namely disengaged and engaged. Even though the clutch has two states the device can only sustain disengaged state without a continuous power supply [50] [187]. Therefore, a continuous current supply should be supplied during its operation (monostable) to sustain the engaged state. Thus, the traditional electromagnetic clutch is monostable. Furthermore, according to the literature few energy saving coupling mechanisms have been developed in the recent years. W. Cai et al has developed a bistable electromagnetic clutch unit for an electric vehicle to reduce the energy consumption of the electric vehicle [188][189]. However, the design is primarily developed for the wheel electric vehicle drive application [188-190]. As such, clutch is mainly developed for the function of maintaining the connection between electric vehicle wheel drive hub and the motor [189-191]. Apart from that companies such as Mönninghoff , KEB, Eletroid and EIDE have introduced bistable clutches and bistable brake designs for the applications such as air-conditioning

compressors, electric doors, wheelchairs and etc [192-195]. However, these commercial designs utilize power supply for a period of 100 ms to 1000 ms during the engaging and disengaging operations [192-195]. Energy consumption of the clutch or the brake decreases with the reduction of power supply time. Therefore, by minimising power supply time, energy consumption could be further reduced enhancing the energy efficiency. Moreover, coil springs are incorporated in the commercial bistable clutch and brake designs for the disengaging process that reduces the robustness [192][194]. Systems integrated with the coil springs have low robustness due to the wear and degrading of the springs [196-198].

The operation of the proposed coupling mechanism is similar to the conventional electromagnetic clutch. However, the proposed design overcomes the drawbacks of conventional clutch such as high power consumption during its operation. The sudden decoupling of the clutch due to unexpected power failures is another drawback of the conventional clutch design. This is also eliminated in the proposed design providing a safe coupling mechanism. Furthermore, the proposed design also incorporates the benefits of conventional clutch such as electrical controllability and rapid response time.

The proposed electromagnetic coupling mechanism is bistable. Therefore, without continuous power supply the proposed design could maintain its two states namely engage and disengage. Permanent magnets are implemented to maintain the engaged and disengaged states stable without an external power supply. The proposed design uses a current pulse for the engaging and disengaging of the coupling mechanism. The state of the coupling mechanism could be changed from one state to another by varying direction of applied current pulse. In the proposed design power is consumed only for a period of 12 ms during the engaging and disengaging operations. Therefore, in the proposed design

power consumption time period is minimised considerably with comparison to the available commercial energy saving coupling mechanisms. Hence proposed design reduces the power consumption. Moreover, Heat energy generation from the electromagnet is also reduced with the elimination of continuous current supply to the design. This improves the efficiency of the proposed mechanism. Furthermore, the proposed coupling mechanism avoids the use of mechanical elements (release spring) that is used in conventional clutch design and other energy saving coupling mechanisms. The release spring is employed for the returning of armature plate when the power supply is Off [50][187]. The designs integrated with springs have low robustness due to the wear and degrading of the springs [196][197]. Release springs are not incorporated in the proposed coupling mechanism. Magnetic force replaces the release spring function in the proposed coupling mechanism and performs the disengaging thus enhancing the robustness. The advantages of the proposed coupling mechanism are further amplified with the fail-safe design. The force generated by the permanent magnets maintains the engaged or disengaged state stable in the absence of power supply. To vary the existing state of the mechanism, current pulse with change in direction of current should be applied. Therefore, in case of power failure state of the coupling will not vary. The proposed bistable coupling mechanism state cannot be changed until a further current pulse is applied. As such, the design offers increased safety. Furthermore, the proposed design is fully compliant with EU directive 2006/42/EG clause 1.2.6 that states the drive must not disengage in the case of a power failure [51]. Thus, the directive enhances the safety of the system in a situation where unexpected power failure occurs [51]. In summary, the main features of the proposed bistable coupling mechanism can be expressed as follows. The proposed coupling mechanism is with the capability of reducing electric energy consumption during its operation.

Thus, the proposed coupling mechanism is capable of providing energy efficient coupling mechanism for underactuated manipulators. This is one of the key highlights of the proposed bistable coupling mechanism. Furthermore, fail-safe design is another highlight of the proposed mechanism. Bistable permanent magnetic design approach provides the fail safety capability to the mechanism. As such the proposed design is with the potential of providing safe coupling mechanism. Therefore, the proposed bistable design is capable of providing an energy efficient and safe coupling mechanism for underactuated manipulators.

4.2 Mechanical Design of the Bistable Electromagnetic Coupling Mechanism

The design consists of two segments. Segments are categorized as A and B as shown in the Figure 4.2. The section B contains the electromagnet used for the mechanism and section A is equipped with the permanent magnets and the sliding disk. The rotor shown in the Figure 4.2 is the rotating section of the segment B that rotates freely when engaged. Rotor transfers the rotational motion to the load when the mechanism is engaged. Load is connected to the extended segment of the rotor as shown in the Figure 4.2. Needle roller bearings are connected between the electromagnet casing and the rotor. Therefore, the rotor could rotate freely maintaining the electromagnet in a stable position.

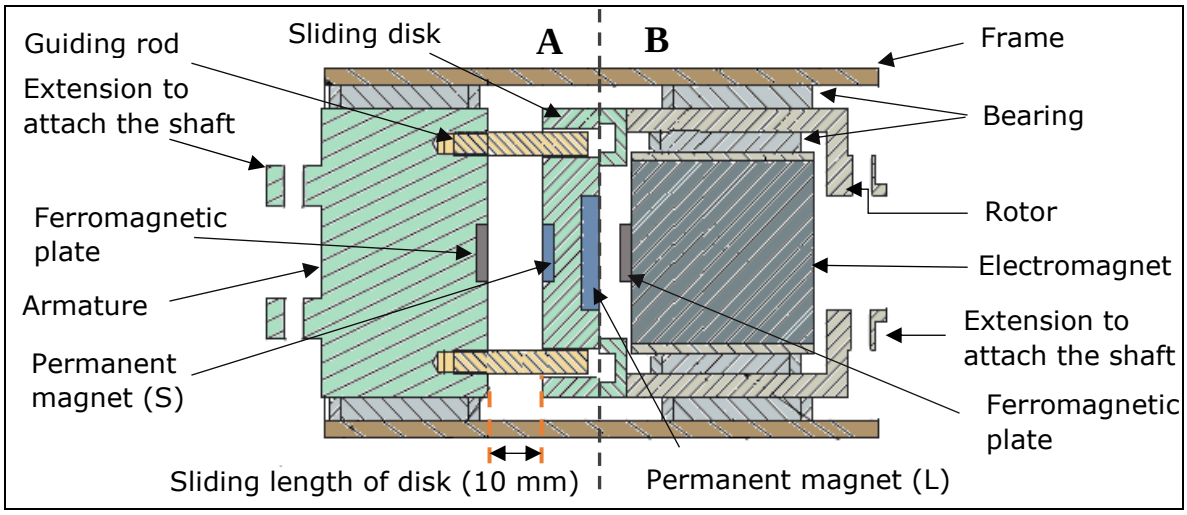

Figure 4.2: Cross sectional view of the proposed clutch design.

In the design groves are fabricated at the segment B plate to couple it with the teeth fabricated in the sliding disk. The bearings mounted between the rotor and the housing of the proposed mechanism prevent the rotation of the casing of the bistable mechanism along with the rotor. Rotor is fabricated using Aluminium.

The segment A of the proposed design consists with the sliding disk and the armature. The sliding disk is as shown in Figure 4.2. The diameter and the thickness of the fabricated sliding disk are 50 mm and 10 mm respectively. At the centre of sliding disk, a disk type NdFe35 permanent magnet (L) with a holding force of 33 N is mounted. The diameter and the thickness of the magnet are 20 mm and 3 mm respectively. The permanent magnet provides the holding force required to maintain the engaged state. Thus, the requirement of continuous power supply is eliminated. Similarly, a disk type NdFe35 permanent magnet (S) with a holding force of 2.9 N is attached to the other side of the disk, which helps to hold the disengaged state. The permanent magnet (S) is 10 mm in diameter and 5 mm in thickness.

The shafts mounted to the armature function as guide for the sliding disk's linear motion. The disk is able to slide through the shafts fixed to the armature as

shown in Figure 4.2 during mechanism engaging and disengaging process. Steel plate with 20 mm length, 20 mm width and 2 mm thickness is embedded to the armature as shown in the Figure 4.2. The purpose of the embedded steel plate is to generate an attraction force between the small permanent magnet and the steel plate. When the proposed mechanism is disengaged this attraction force functions as a holding force for the disk preventing its motion towards the rotor. Bearings are connected between the armature and the casing similar to the segment B of the bistable coupling mechanism. The two sections, section A and B are fixed inside a casing as a single component. The constructed bistable coupling mechanism external and internal view are shown in Figure 4.3(a) and Figure 4.3(b) respectively. The design parameters of the proposed mechanism are also presented in Table 4.1.

Figure 4.3(a): Constructed view of the bistable coupling mechanism.

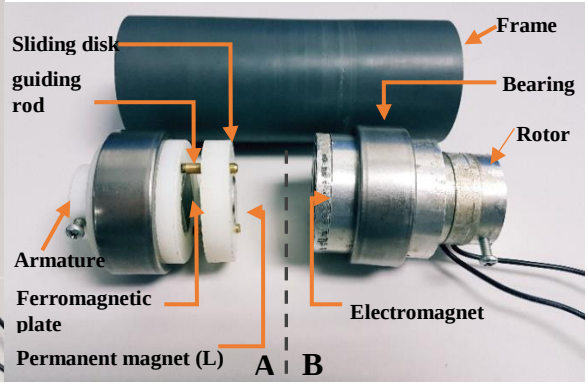

Figure 4.3(b): Internal view of the bistable coupling mechanism.

Table 4.1: Design parameters

Definition	**Value**
Permanent magnet S (NdFe35) Diameter /Thickness	20 mm/ 3 mm
Permanent magnet L (NdFe35) Diameter /Thickness	10 mm/ 5 mm
Air gap length	10 mm
Number of winding (Electromagnet)	700
Sliding disk Diameter /Thickness	50 mm/ 10 mm

4.3 Operation Principle of the Bistable Electromagnetic Coupling Mechanism

The bistable electromagnetic coupling design has two stable positions namely engage and disengage. The state varies with the movement of the sliding disk. The state of the mechanism could be changed by switching the direction of current supply to the electromagnet. The electromagnet will generate an attraction force or a repelling force on the sliding disk permanent magnet (L) with respect to the direction of supply of current. This force will result the sliding of the disk changing the state of the proposed mechanism. 10 mm gap is minimum gap that could be maintained between the sliding disk and rotor to secure the complete disengagement. Further reduction of the gap causes the sliding disk to move towards the rotor due to the attraction force between the permanent magnet (L) and ferromagnetic plate even with the absence of electromagnetic force. Identification of optimum length of gap is performed using theoretical and experimental approaches explained in detail in the results and discussion section. The Figure 4.4 (a) and (b) show the magnetic flux distribution of the coupling mechanism at the two states namely engaged and disengaged respectively. The magnetic flux distribution is simulated using Vizimag magnetic simulation software. The analysis of the magnetic field distribution related to the mechanism state change is discussed in detail under the Section 4.3.1 and Section 4.3.2 . Furthermore, operation of the mechanism at two states namely engaged and disengaged with respective forces are explained in Section 4.3.1 and Section 4.3.2 respectively.

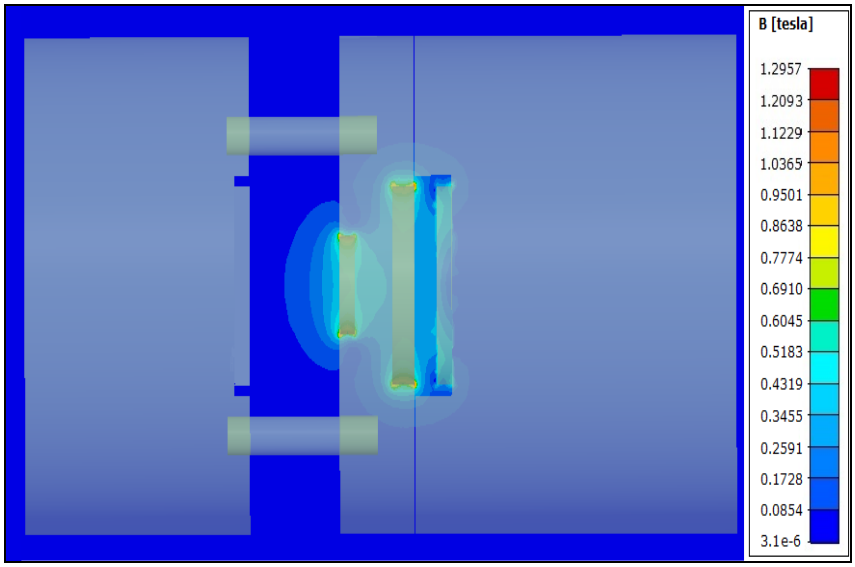

Figure 4.4(a): Magnetic flux density distribution in engaged state.

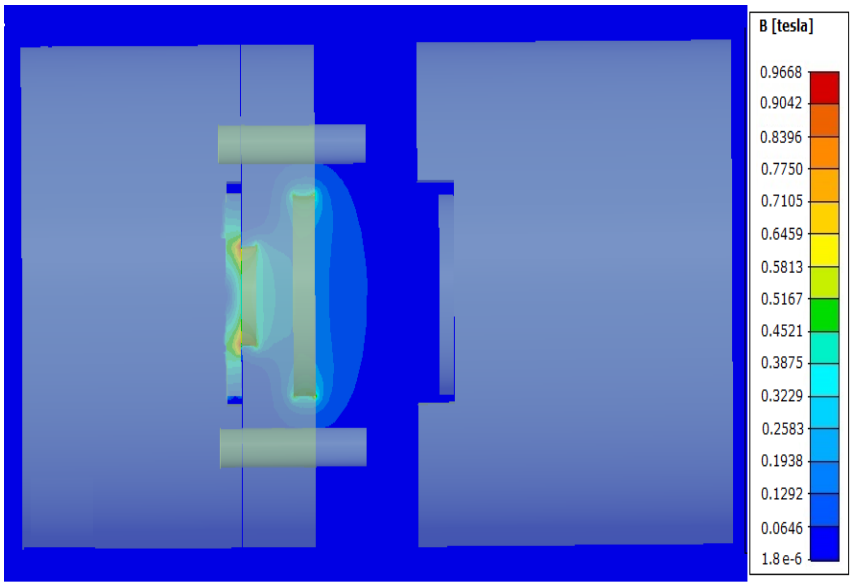

Figure 4.4(b): Magnetic flux distribution in disengaged state.

4.3.1 Engaged State

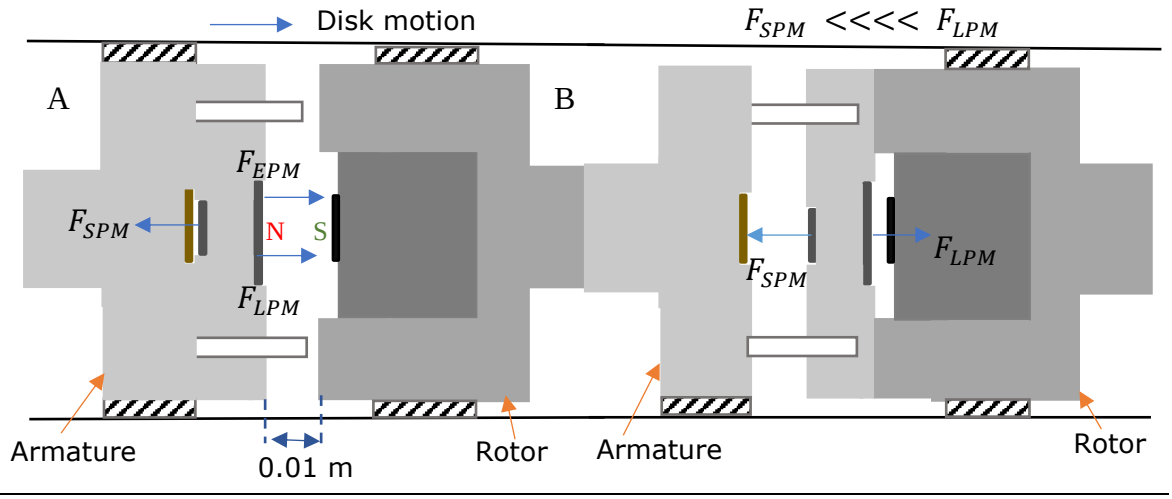

Figure 4.5(a): Instance before sliding disk moves from disengaged state to engaged when the electromagnet is energised.

Figure 4.5(b): Sliding disk after engaging and electromagnet is de-energised.

The proposed bistable mechanism remains in the disengaged state prior to varying the state to engaged. The sliding disk remains stable at the segment A of the mechanism. The force F_{SPM} generated between the ferromagnetic plate and the permanent magnet (S) prevents motion of the disk towards the rotor as shown in Figure 4.5(a). In the design, permanent magnet (L) is fixed maintaining North pole of the magnet towards the electromagnet. To move the disk towards the rotor, an additional force should be applied on the sliding disk to produce a resultant force in the direction of motion. Therefore, an attractive force should be generated between the disk permanent magnet (L) and the electromagnet. As such, the electromagnet is energised to form a South pole at the surface of the electromagnet. This creates an attractive force F_{EPM} between the permanent magnet (L) and the electromagnet, producing a resultant force on the disk. The resultant force initiates the motion of the disk towards rotor at the instance electromagnet is energised. When the disk reaches the rotor power supply could

be terminated. The force F_{LPM} generated between the permanent magnet (L) and ferromagnetic plate maintains the engaged state with the absence of an external power supply as shown in Figure 4.5(b).

There is an attraction force between the permanent magnet (S) and ferromagnetic plate. However, in the engaged state the F_{SPM} force is zero. Due to the increase of distance between the ferromagnetic plate and the permanent magnet (S), flux distribution between the permanent magnet (S) and ferromagnetic plate reduces. The flux distribution of the mechanism in the engaged state is also examined via simulation studies. As illustrated in Figure 4.4(a) zero magnetic flux density distribution is observed between the permanent magnet (S) and ferromagnetic plate in the engaged state. Therefore the F_{SPM} force becomes zero due to zero magnetic flux distribution. As such, in the engaged state the F_{SPM} force becomes zero. Similarly, magnetic flux distribution is observed between permanent magnet (L) and ferromagnetic plate as shown in Figure 4.4(a). This magnetic flux generates a force F_{LPM} between the permanent magnet (L) and ferromagnetic plate that maintains the engaged state without an external power supply. As such, the current supply could be terminated at the instance disk contacts the rotor. Therefore, disk remains engaged until the electromagnet is energised in the reverse direction.

4.3.2 Disengaged State

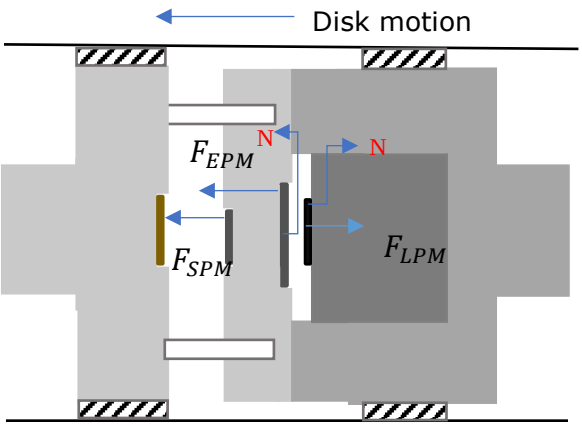

Figure 4.6(a): Instance before sliding disk moves from engaged state to disengaged when the electromagnet is energised.

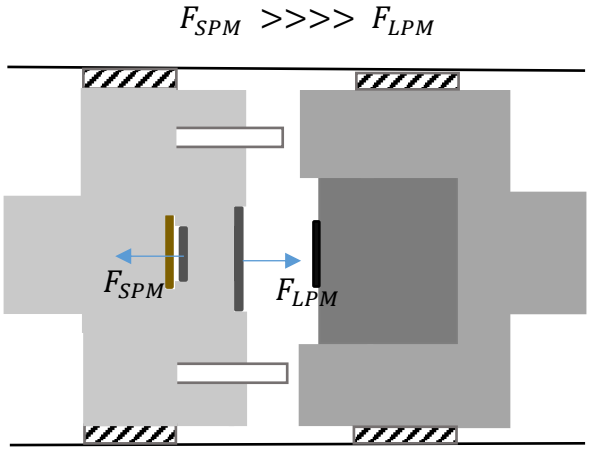

Figure 4.6(b): Sliding disk after disengaging and electromagnet is de-energised.

The proposed mechanism state could be switched from engaged to disengaged by powering the electromagnet in the reverse direction. Electromagnet polarity could be varied by switching the direction of the current supply forming a North polarity. When the current supply is reversed a repulsive force F_{EPM} will generated between the permanent magnet (L) and the electromagnet. As a result, a resultant force is generated on the disk as shown in the Figure 4.6(a). Due to the resultant force created, the disk disengages and slide towards the armature switching the state of the mechanism to disengaged. An attraction force is formed between the permanent magnet (S) and the ferromagnetic plate embedded. This attraction force F_{SPM} maintains the disengage state without an external energy supply as shown in Figure 4.6(b). Therefore, when the disk reaches the armature, current supply could be terminated. Similar to engaged state, magnetic flux distribution is examined in the disengaged state. From the Figure 4.4 (b), it could be observed that there is no flux distribution between the permanent magnet (L) and

ferromagnetic plate in the disengaged state. Therefore, at the disengaged state force F_{LPM} becomes zero due to the increment of distance between the ferromagnetic plate and the permanent magnet (L). As such, the sliding of the disk towards the rotor is prevented until an external force is applied by the electromagnet.

4.4 Mathematical Modelling of the Proposed Bistable Electromagnetic Coupling Mechanism

The mathematical model of the operation of proposed bistable mechanism is presented in this section. The engaging and disengaging operation of the coupling mechanism with the respective forces are shown in Figure 4.7 and Figure 4.8 Engaging and disengaging of the coupling mechanism is controlled by varying the direction of force F_{EPM} generated between the electromagnet and the permanent magnet (L) as described in the previous section. The magnetic force F_{EPM} represents the force generated by electromagnet on the permanent magnet (L) when energized. Magnetic force F_{EPM} can be expressed as [199-201]:

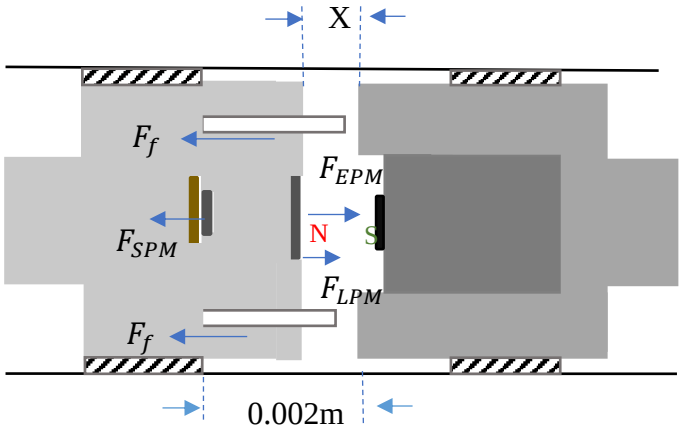

Figure 4.7: Force diagram of the sliding disk when sliding from disengaged state to engaged when electromagnet is energised.

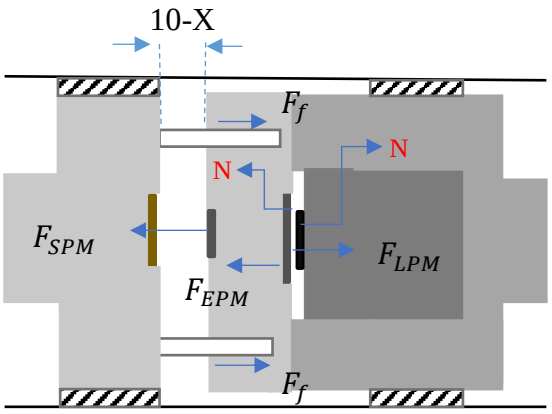

Figure 4.8: Force diagram of the sliding disk when sliding from engaged state to disengaged when electromagnet is energised in the reverse direction.

$$F_{EPM} = V.M.\nabla B \tag{4.1}$$

Where V, M and ∇ B are the volume of the permanent magnet, magnetization of the permanent magnet and the gradient of the magnetic field of the electromagnet respectively. The ∇ symbol represents the gradient operator. The computation of each component of Equation (4.1) is performed using a subset of equations. These subsets of equations used for the calculation are described as follows. The components M (Magnetization of the permanent magnet) and V (volume of the permanent magnet) are calculated as:

$$M = \frac{Br}{\mu_m} \tag{4.2}$$

$$V = \pi r^2 l \tag{4.3}$$

Where Br corresponds to the magnetic remanence and is 1.30 T. The value of μ_m is 13.811×10^{-7} that corresponds to the permeability of NdFe35 magnet. In Equation (4.1) V represents the volume of the permanent magnet. The value of V is computed using the equation of volume of a disk. The final component of Equation (4.1) is the gradient of the magnetic field of the electromagnet (∇B) [202]. The calculation of ∇B is explained in the following section.

Magnetic field generated from an electromagnet could be described by Biot-Savart's law [203]. The magnetic field generated by a single loop coil carrying a current of I at a distance X from the centre of the circular coil can be derived using the Biot-Savart law as given below [204][205]:

$$B = \frac{\mu_0 r^2 I}{2(X^2 + r^2)^{\frac{3}{2}}} \tag{4.4}$$

Where μ_0 and *r* represent the permeability of free space and the radius of a coil with single turn respectively. *X* corresponds to the distance from the centre of the coil to the point where magnetic field is computed. I is the current flowing through the coil. From Equation (4.4), the magnetic field generated from a circular coil with *N* number of loops carrying steady current I can be expressed as:

$$B = \frac{\mu_0 r^2 I N}{2(X^2 + r^2)^{\frac{3}{2}}} \tag{4.5}$$

N represents the number of turns in the coil. Finally, the gradient magnetic field is calculated by computing the first order derivative of the Equation (4.5). The first order derivative of Equation (4.5) that corresponds to the gradient magnetic field is expressed as:

$$B = -\frac{3X\mu_0 r^2 I N}{2(X^2 + r^2)^{\frac{5}{2}}} \tag{4.6}$$

Finally, the magnetic force generated on the permanent magnet by the electromagnet F_{EPM} is obtained using Equation (4.1) to Equation (4.6). The dry friction force F_f is formed on the disk could be obtained from Equation (4.7). The dry friction force is obtained as:

$$F_f = \mu mg \tag{4.7}$$

Where μ is the frictional coefficient, g is the gravitational acceleration and m is the mass of the sliding disk. Range of magnetic attraction force values with respect to the distances are obtained for each magnet from the magnet manufacturing company. These magnetic force values obtained with respect to the distance are used to plot the graphs shown in Figure (4.9(a)) and Figure (4.9(b)). The Figure (4.9(a)) and Figure (4.9(b)) illustrate the magnetic force with respect to the distance of permanent magnet (L) and permanent magnet (S) respectively.

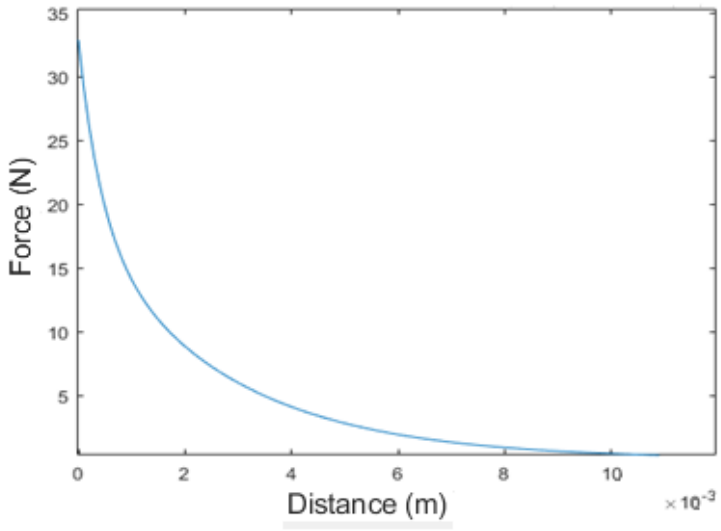

Figure 4.9(a): Permanent magnet (L) magnetic force with respect to distance.

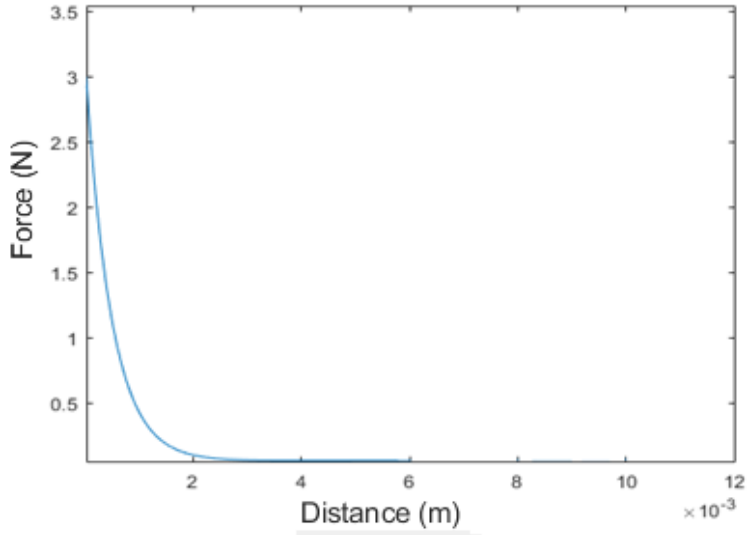

Figure 4.9(b): Permanent magnet (S) magnetic force with respect to distance.

Curve fitting application in MATLAB software is employed to obtain the mathematical equation that provides the relationship between the magnet attraction force with respect to the distance. The mathematical equations are computed by applying the magnetic attraction force and distance parameters to curve fitting application which are obtained from magnet manufacturing company. The computed mathematical equations are shown in Equation (4.8) and Equation (4.9). The relationship of the force F_{LPM} with respect to distance can be obtained using Equation (4.8). Similarly, Equation (4.9) describes the relationship of the force F_{SPM} with respect to the distance of the permanent magnet (S). The equations are as given below:

$$F_{LPM} = 18.53e^{(-377.6X_L)} + 14.34e^{(-2355X_L)} \tag{4.8}$$

$$F_{SPM} = 0.051e^{(26X_s)} + 3.1e^{(-2107X_s)} \tag{4.9}$$

In the Equation (4.9) X_s represents the distance between the permanent magnet (S) and the ferromagnetic plate. Similarly, X_L represents the distance between the permanent magnet (L) and the ferromagnetic plate.

Finally, the theoretical model of the proposed bistable mechanism for the two states engaging and disengaging are derived as:

Engaging :

$$m\ddot{X} = F_{EPM} + F_{LPM} - F_{SPM} - 2F_f \tag{4.10}$$

Disengaging :

$$m\ddot{X} = F_{EPM} + F_{SPM} - F_{LPM} - 2F_f \tag{4.11}$$

Where *m* is the total mass of the disk including the two permanent magnets embedded. F_f represents the dry friction force between the disk and the guide. $\dot{X}$ and $\ddot{X}$ represent velocity and the acceleration of the disk. Furthermore, *X* represents the distance between the surface of permanent magnet (L) and the surface of the electromagnet as shown in the Figure 4.7. Distance varies with the motion of the sliding disk. The value of *X* which is the optimum distance that sliding disk moves ranges from 0 to 0.01 m. Disk attains a maximum displacement of 0.01 m at the disengaged state and a minimum of 0 m at the engaged state.

The disk maintains stable state at the instance resultant force is zero. Thus, until a resultant force is applied, the sliding disk does not perform a motion. The total number of forces acting on the sliding disk that causes the motion are namely F_{LPM} (force generated between the permanent magnet (L) and ferromagnetic plate), F_{SPM} (force generated between the ferromagnetic plate and the permanent magnet (S)) and F_f (dry friction force between the disk and the guide). The force vs distance relationship of the forces F_{LPM} and F_{SPM} are show in Equation (4.8) and Equation (4.9) respectively. The force F_{LPM} pulls the sliding disk towards the rotor while other two forces F_{SPM} and F_f pull the disk in opposite direction towards the armature. F_r represents the resultant force of these three forces acting on the disk towards the direction of rotor. Therefore, the sliding disk performs motion until the resultant force of these three forces F_r becomes zero. Thus, the optimal theoretical distance that the disk can achieve is obtained at the instance when resultant force F_r becomes zero. The theoretical optimum distance (value of X) is obtained using the Equation (4.12) as given below. The theoretical optimum distance (value of X) is computed by continuously substituting distance values starting from zero to the Equation (4.12) until the resultant force F_r value reaches zero. The distance value that provides the resultant force F_r zero is

recorded as the theoretical optimum distance (value of X). The resultant force vs distance relationship theoretical graph is shown in the Figure 4.18 of Section 4.6.2. Furthermore, optimum distance is also validated experimentally by positioning the disk at range of distances away from the rotor. The distance in which the sliding disk remains in stable position without a motion during experimental analysis is identified as the experimental optimum distance.

$$F_r = F_{LPM} - F_{SPM} - 2F_f \quad (4.12)$$

4.5 Bistable Electromagnetic Coupling Mechanism Controlling Circuit

The bistable coupling mechanism engaging and disengaging is controlled via a control circuit. Two transistors (TIP120) and a double pole double touch (DPDT) relay are used to control the direction of current flow and to switch the power supply On and Off. Two 220Ω resistors are used to protect the microcontroller from high current. Figure 4.10 shows the schematic view of the control circuit and Figure 4.11 shows the constructed control circuit. Varying the direction of current flow to the mechanism changes the state of the mechanism. To vary the direction of current flow, base current of the transistor A is varied via microcontroller. Activating of transistor A energises the DPDT relay resulting in the engagement of the mechanism. Similarly, deactivating transistor A de-energises the DPDT relay resulting in the disengagement of proposed design. Transistor B controls the power supply to the mechanism. Transistor B switches the current supply On or Off to the DPDT relay, after the mechanism is engaged or disengaged. This results in switching the current supply On or Off to the proposed mechanism. During the

engaging process, current flows to the bistable coupling for 12 ms, whereas in the disengaging process current flows for 12 ms. Figure 4.12 presents the functionality of the circuit in a flowchart.

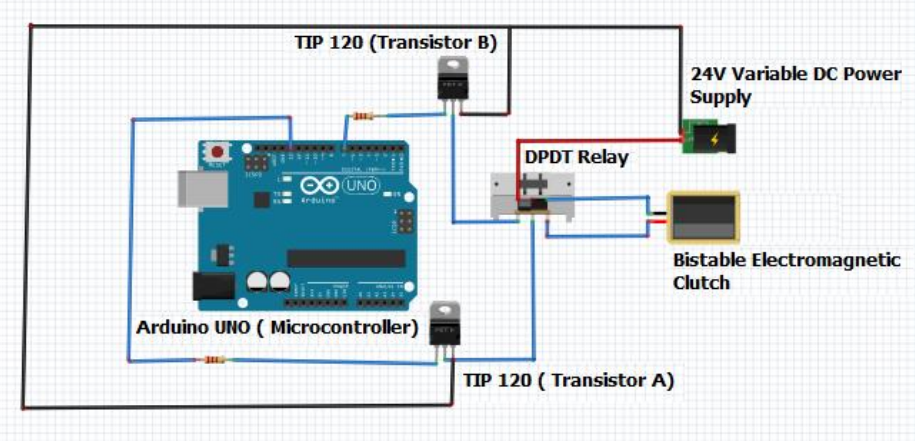

Figure 4.10: Schematic of the proposed controlling circuit design.

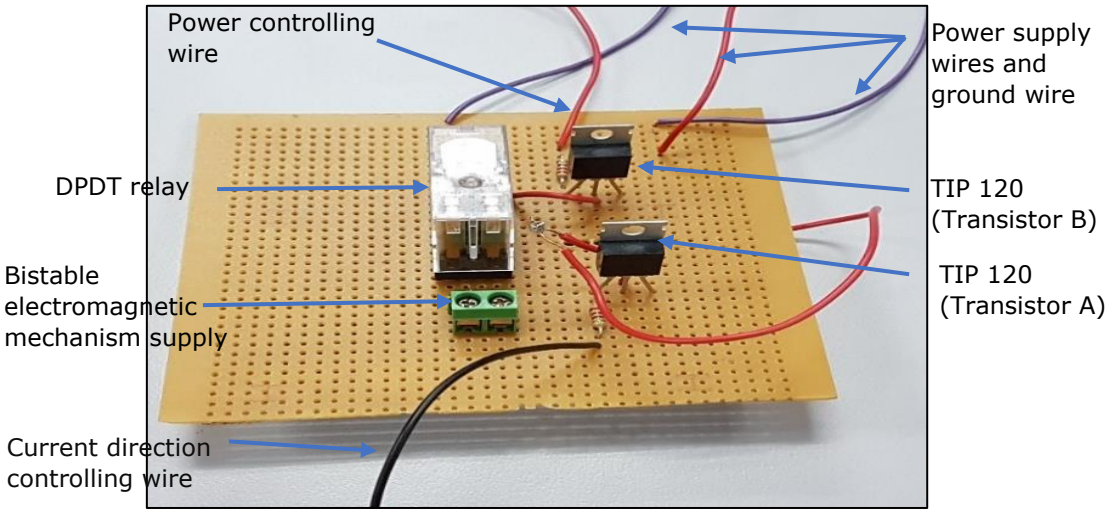

Figure 4.11: Bistable electromagnetic coupling mechanism control circuit.

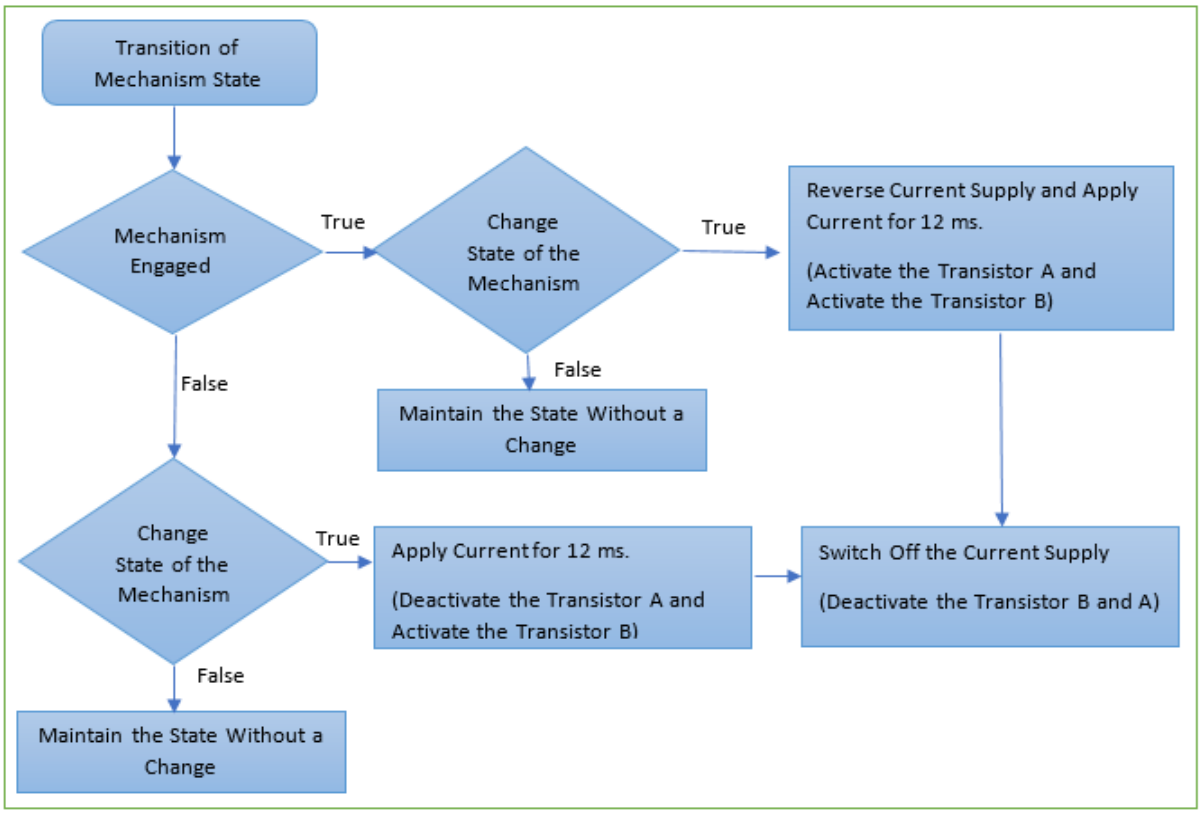

Figure 4.12: Flowchart presenting the operation of the control circuit.

4.6 Experimental Validation of Mathematical Model and Operation of the Bistable Electromagnetic Coupling Mechanism

In this section the mathematical model developed in Section 4.4 for the proposed bistable electromagnetic coupling mechanism is validated experimentally. Furthermore, the energy consumption and the operation of the proposed bistable coupling mechanism are analysed. The current and voltage usage are measured experimentally in both conventional electromagnetic clutch and the proposed bistable mechanism during the operation. The total energy consumption and power consumption are also computed for the conventional electromagnetic clutch and the proposed mechanism to examine the significance of the proposed design.

The setup used for the experimental analysis and results obtained are presented in detail under this section.

4.6.1 Experiment Methodology

The time consumed during engaging and disengaging of the mechanism are investigated experimentally and it is verified with the dynamic model developed. The schematic diagram of the experimental setup used for the time measurement of engaging and disengaging process is depicted in Figure 4.13.

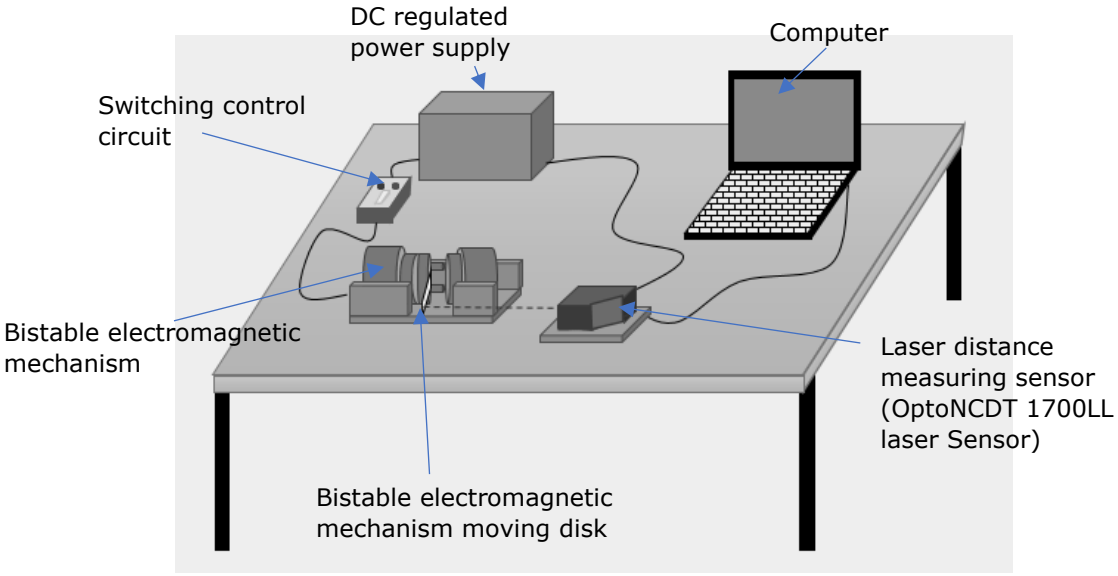

Figure 4.13: Schematic diagram of the experimental setup.

The time taken for the sliding disk motion from the armature to the rotor and from the rotor to the armature correspond to the engaging and the disengaging time respectively. Therefore, the sliding disk motion with respect to time is analysed in the engaging and disengaging scenarios. In the experimental

setup OptoNCDT 1700LL laser distance measuring sensor is used to measure the displacement of the disk with respect to time. The output of the laser sensor is connected to a laptop for the recoding and for the analysis of data. The laser beam of the sensor is positioned directly on the sliding disk, monitoring the motion of the disk. Laboratory regulated DC power supply is used to supply the power to the bistable coupling mechanism via the control circuit. Control circuit is used to move the sliding disk from the armature to the rotor and vice versa. Therefore, the states of the proposed mechanism could be varied. Thus, the time taken for both scenarios are measured namely engaging and disengaging of the proposed mechanism.

To analyse the energy consumption of the bistable coupling mechanism, current and the voltage use of the proposed design are measured. Figure 4.14 shows the experimental setups used for the current and voltage measurement respectively. ACS756 Hall effect linear current sensor was used to measure the consumption of current. The voltage was measured using a voltage divider circuit. ACS756 current sensor was connected in series with the mechanism and the control circuit as shown in Figure 4.14. Real time current measurement data were sent to a computer via Arduino microcontroller for the analysis. Current flow through the bistable coupling mechanism was measured and recorded at every millisecond. Two Arduino microcontrollers were used in the experimental setup. One was allocated for the controlling of the bistable coupling mechanism and the other for the collection of data from the sensors. Similar to the current measurement experiment, voltage measurement data were transferred to a computer via Arduino microcontroller.

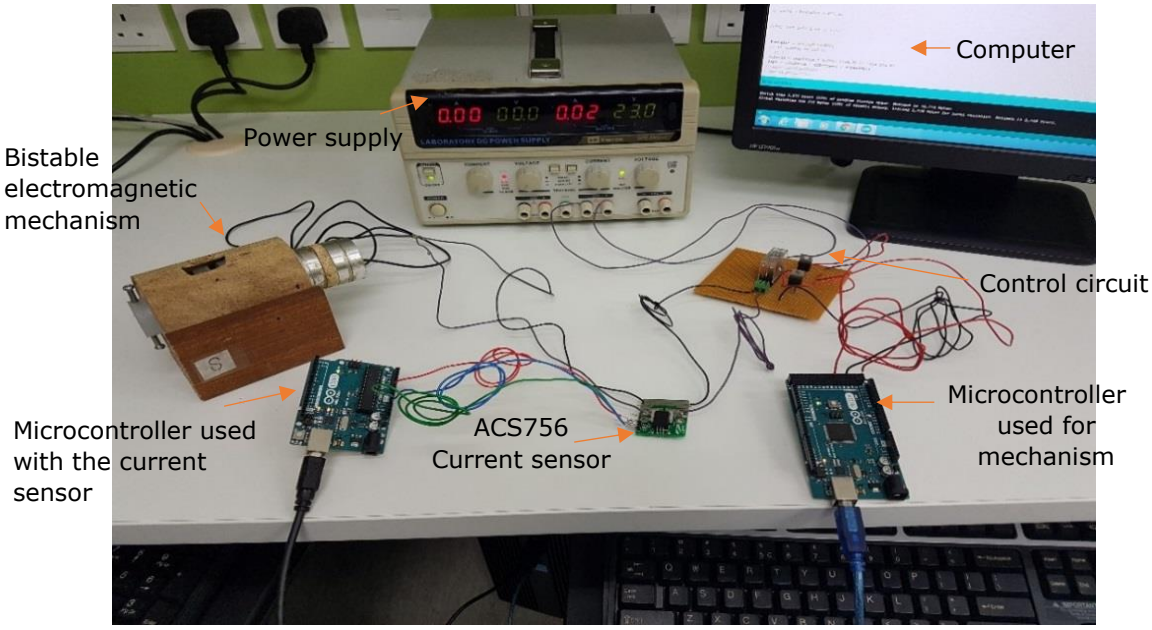

Figure 4.14: Experimental setup for the current consumption measurement of the bistable electromagnetic mechanism.

From the experimental data, energy consumption of the proposed design in engaging and disengaging operations were investigated. Initially, the current and the voltage consumption of the design during operation and engagement were investigated.

Furthermore, for the analysis of energy consumption and functionality of the design, bistable electromagnetic coupling was implemented on the developed prototype manipulator. Chapter 5 presents the design and functionality of the developed manipulator used for this analysis. Energy consumption of the design was monitored during the manipulator link motion. Figure 4.15 shows the experimental setup used for the analysis. The motion of the link was controlled by engaging and disengaging the proposed bistable coupling mechanism. During the experiment, manipulator link performs a motion of 200 degrees from the time of engagement to the disengagement of the mechanism. Current and voltage consumption of the complete system were monitored throughout the entire motion of the manipulator link. Similarly, the current and voltage utilisation of a conventional electromagnetic

clutch was also analysed by replacing the proposed mechanism with a conventional electromagnetic clutch. After replacing the proposed mechanism with an electromagnetic clutch equivalent motion scenario was conducted using the porotype manipulator. The link trajectory of the manipulator and other experimental aspects were maintained equivalent in the both the experiments.

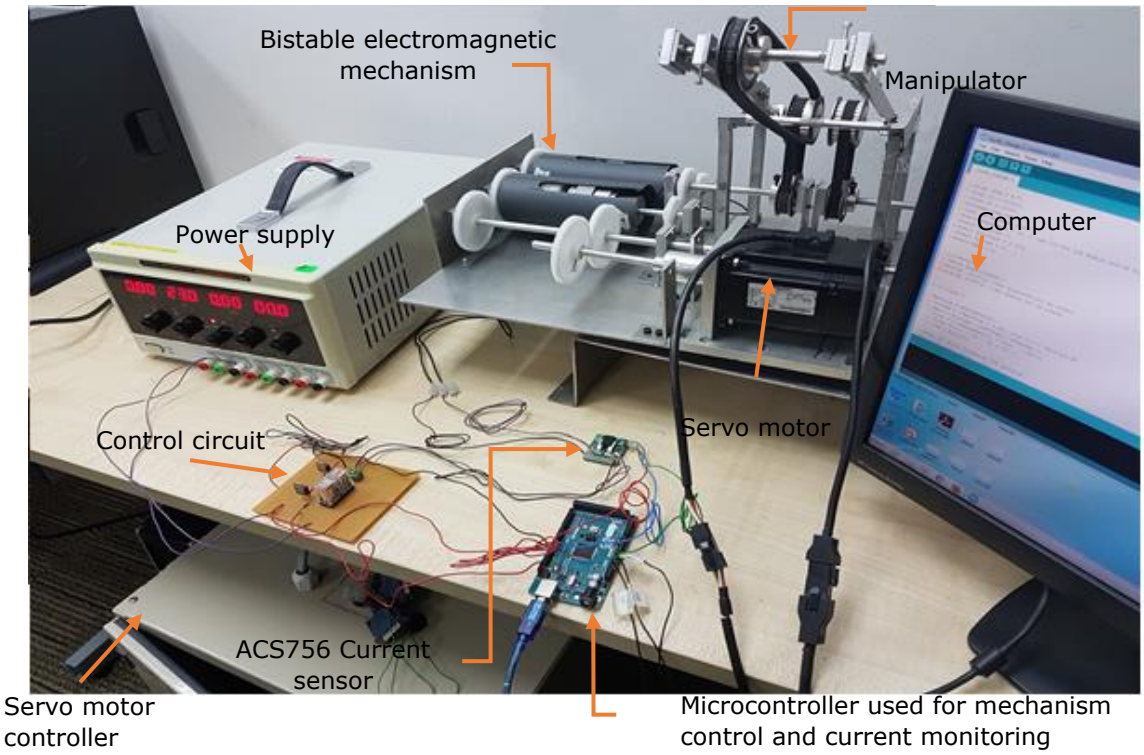

Figure 4.15: Experimental setup used for the measurement of current consumption of the single link manipulator during the actuation with bistable electromagnetic mechanism.

4.6.2 Experimental Analysis of Bistable Electromagnetic Coupling Mechanism Operation

The developed mathematical model of the bistable electromagnetic coupling mechanism in Section 4.4 is validated with the experimental analysis under this section. Theoretical results are obtained using the developed mathematical model

Equation (4.10) and Equation (4.11) for the engaging and disengaging operations of the mechanism in Section 4.4. MATLAB software is utilised for the simulation of theoretical results and the results obtained are verified with the experimental studies. The initial experiment was conducted to study two states of proposed mechanism namely engaged and disengaged. Thereafter the experiment was performed to study the energy consumption of bistable coupling mechanism. The Figure 4.16 shows the comparison of experimental and theoretical displacement of the disk during engaging process with respect to the time. Similarly, Figure 4.17 shows comparison of experimental and theoretical displacement with respect to the time during the disengaging of the mechanism.

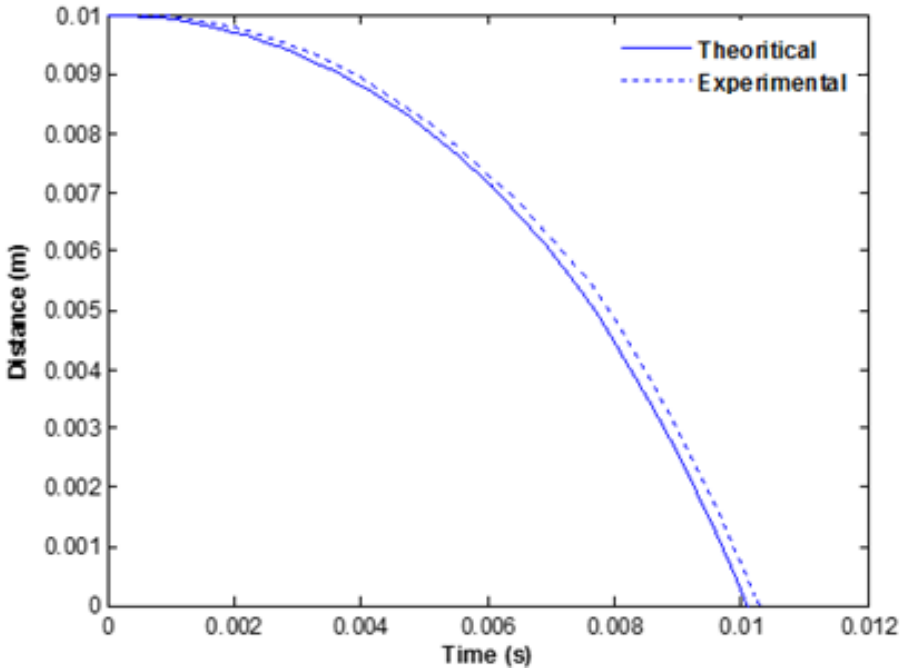

Figure 4.16: Comparison of the experimental and theoretical displacement of the disk with respect to the time during the engaging operation.

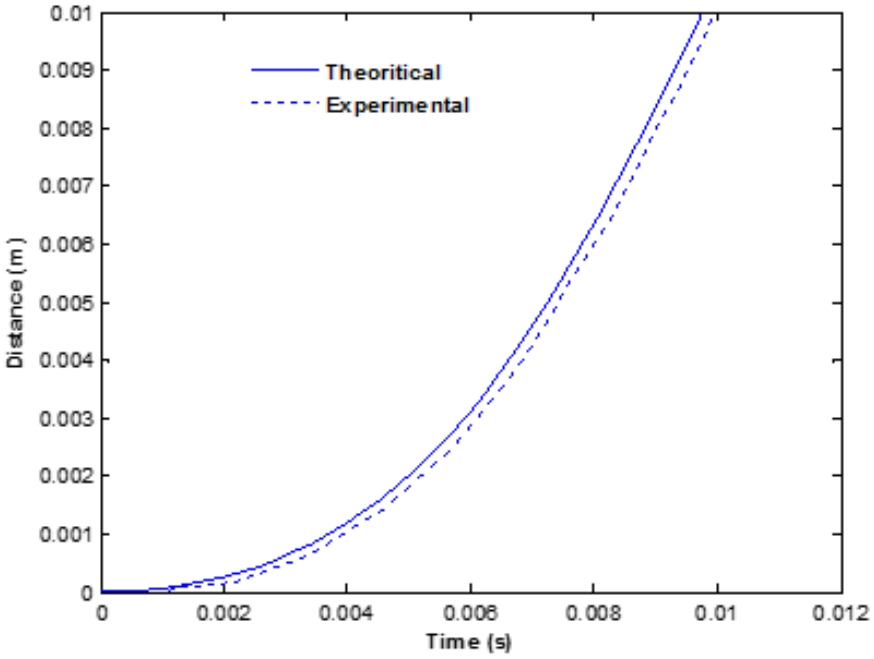

Figure 4.17: Comparison of the experimental and theoretical displacement of the disk with respect to the time during the disengaging operation.

From Figure 4.16 it could be observed that the total theoretical time and the experimental time taken for engaging of the coupling mechanism are 0.0101 s and 0.0113 s respectively. The percentage difference between the theoretical and the experimental results is about 11.8%. Therefore, in general, experimental results demonstrate a good correlation with the theoretical model. Similarly, the total time taken for disengaging in the theoretical and experimental scenarios are 0.0091 s and 0.0101 s respectively. Therefore, in both scenarios experimental and theoretical results are in good agreement.

The sliding disk maintains a gap of 0.01 m from the rotor when the bistable coupling mechanism is at disengaged state as shown in the Figure 4.5(a). The theoretical optimum distance is obtained using the Equation (4.12). Set of resultant force (F_r) values are computed for a series of gap lengths. A graph is plotted using the values obtained as shown in the Figure 4.18 to identify the optimum gap length where the resultant force is zero. There is percentage error

of 16% between the theoretical and the experimental values obtained. The theoretical distance obtained is 0.0084 m where the experimental distance is 0.01 m.

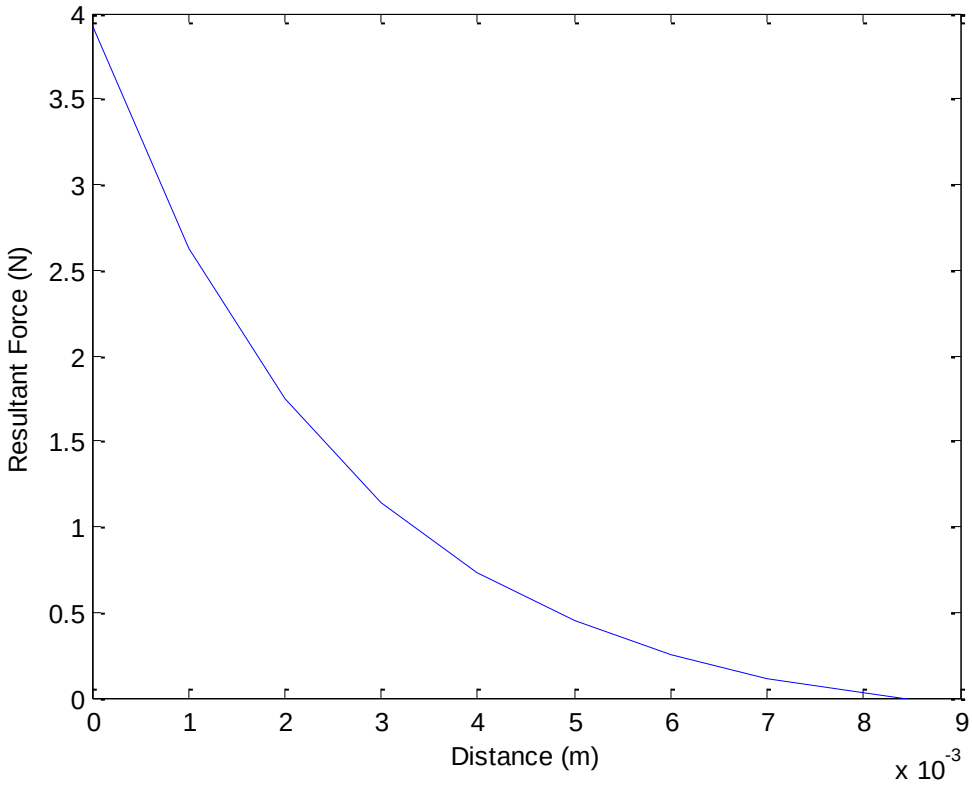

Figure 4.18: Theoretical resultant force with respect to distance at different disk positions.

4.6.3 Experimental Analysis of Bistable Electromagnetic Coupling Mechanism Energy Consumption.

After the validation of developed mathematical model of the proposed design, energy consumption of the bistable coupling mechanism in engaging, disengaging and during the operation of the mechanism were investigated. Initially, current and the voltage consumption of the design during operation and engagement were

investigated. Figure 4.19 shows the current and voltage consumption of the bistable coupling mechanism. It could be observed that 2 A of current flow through the circuit load (bistable coupling mechanism) for 12 ms. After that a current value of 0 A could be observed through the operation. Similarly, for the voltage, a positive value of 23.0 V was recorded within a time period of 12 ms. From the experimental results, it could be noted that the proposed design consumes current and voltage only for a period of 12 ms. This occurs during the engaging process of the proposed mechanism. After engagement, it could be observed that the mechanism does not consume any current or voltage for its continuous operation. The total energy and power consumed during the engaging process are 46 W and 0.552 J respectively. Figure 4.20 shows the power and energy consumption during engaging of the coupling mechanism.

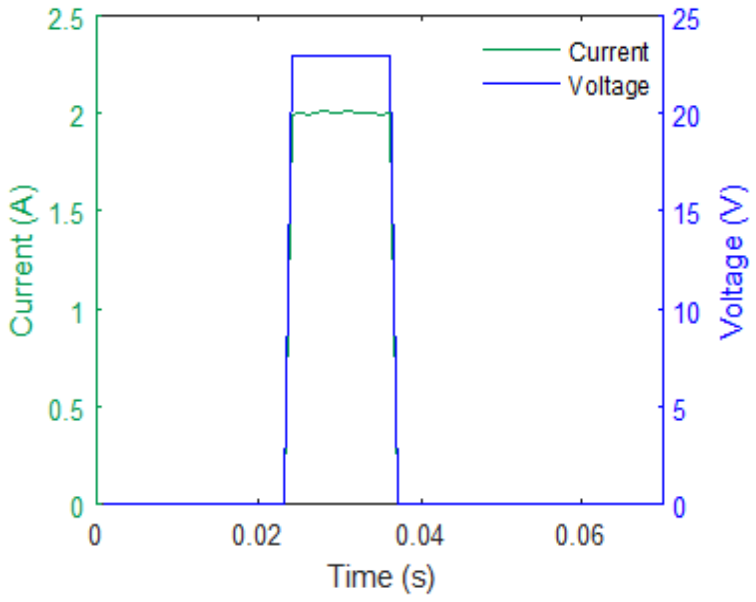

Figure 4.19: Current and voltage consumption of the bistable electromagnetic mechanism during engaging and mechanism operation.

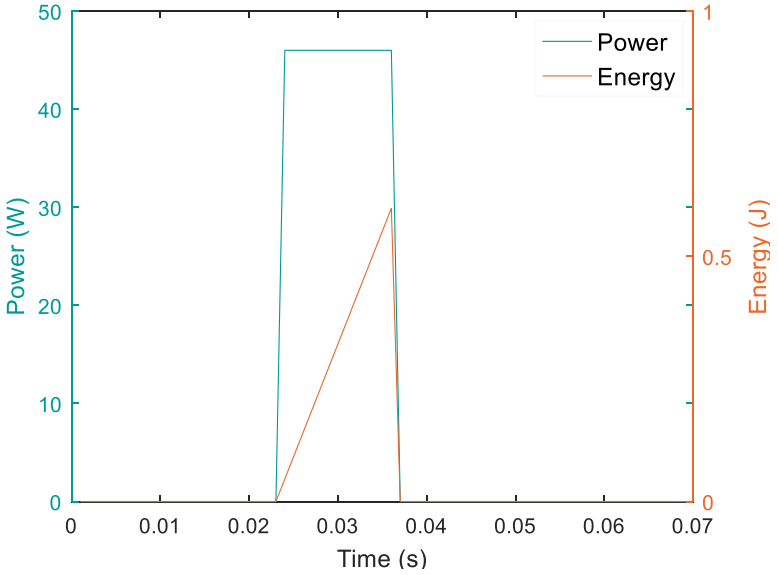

Figure 4.20: Power and energy consumption of the bistable electromagnetic mechanism during engaging and mechanism operation.

Figure 4.21 shows the current and voltage consumption of the mechanism during the disengaging process. It could be observed that current is consumed only during the time of disengaging, which is for 12 ms. The amount of current and voltage consumed during 12 ms period are -2.0 A and -23.0 V respectively. Negative values are recorded for the current and voltage readings during the disengaging process. The negative readings have been observed due to the reversing of direction of current flow in disengaging process. Figure 4.22 shows the power and energy consumption during disengaging of the coupling mechanism. 0.552 J and 46 W are the energy and power consumed during the disengaging operation respectively. In both engaging and disengaging processes equivalent amount of energy and power are utilised.

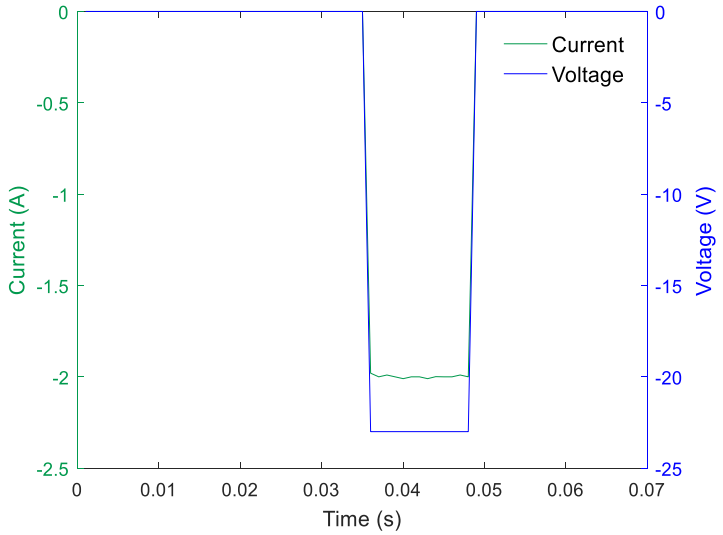

Figure 4.21: Current and voltage consumption of the bistable electromagnetic mechanism during disengaging and mechanism operation.

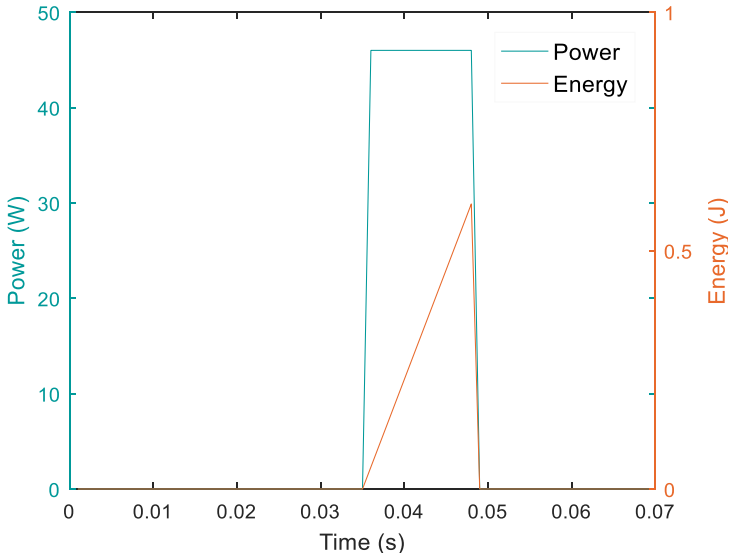

Figure 4.22: Power and energy consumption of the bistable electromagnetic mechanism during disengaging and mechanism operation.

4.6.4 Experimental Analysis of Bistable Electromagnetic Coupling Mechanism Implementing on Prototype Manipulator

The energy consumption of the proposed mechanism is further investigated by implementing the coupling mechanism on developed prototype manipulator. The

results obtained during the experimental analysis is presented as follows. Current consumption of the complete system was monitored throughout the entire motion of the link and it is shown in Figure 4.23. The negative current values recorded during the disengaging of the mechanism are considered as positive when analysing the current consumption of the complete system in Figure 4.23. Similarly, the current utilisation of a conventional electromagnetic clutch and the entire system were analysed, and it is shown in Figure 4.24. The link trajectory of the manipulator and other experimental aspects were maintained equivalent in the both experiments.

In Figure 4.23 and Figure 4.24 sections A_1 and A_2 show the consumption of current in the entire system prior to engagement of bistable electromagnetic coupling mechanism and the electromagnetic clutch respectively. Similarly, section E_1 shows the current consumption of the system after disengagement of the mechanism. Section E_2 shows the current consumption of the system after disengagement of the electromagnetic clutch in Figure 4.24. Section C_1 and C_2 in both Figures 4.23 and 4.24 indicate the usage of current during the link motion. B and D in Figure 4.23 presents the current consumption of the manipulator system during the engaging and disengaging process of the bistable coupling mechanism respectively. Apart from that utilisation of current in the motor, proposed mechanism and the electromagnetic clutch are also observed independently during the motion. Figure 4.25 displays the independent usage of current by the bistable coupling mechanism and the electromagnetic clutch.

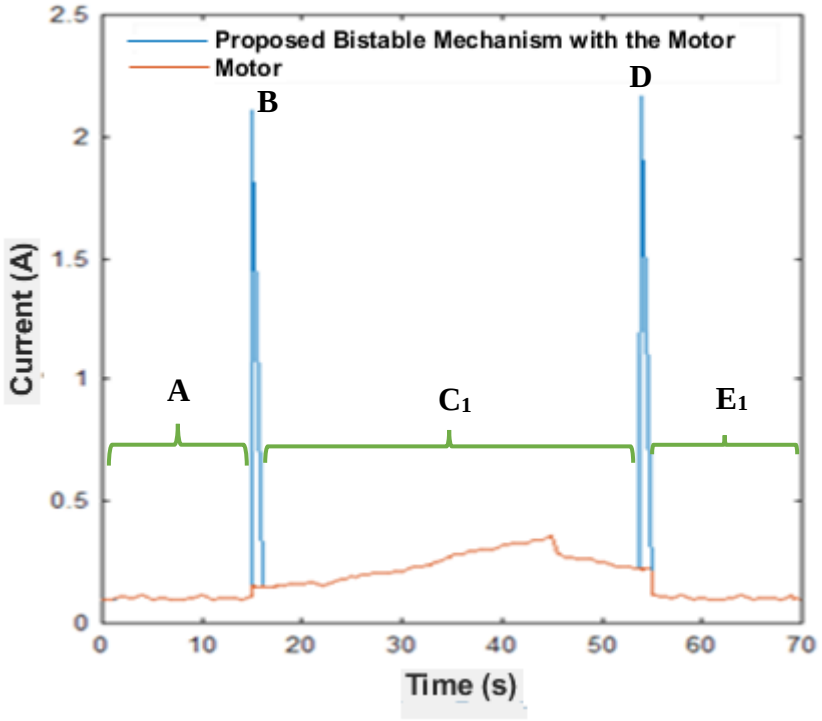

Figure 4.23: The total current consumption of the system including bistable coupling mechanism and independent current consumption of the motor during link motion.

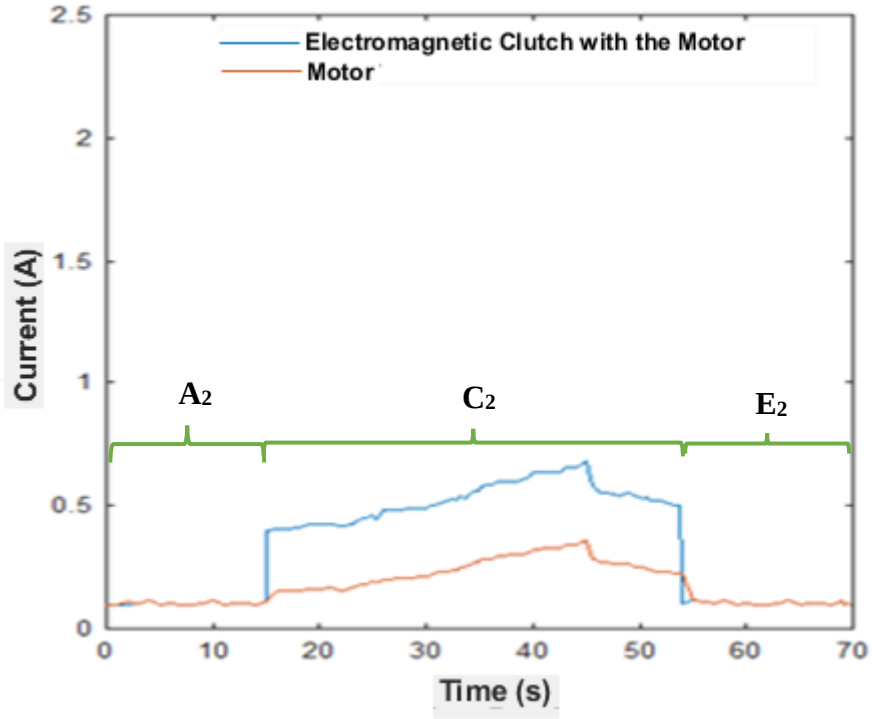

Figure 4.24: The total current consumption of the system including electromagnetic clutch and independent current consumption of the motor during link motion.

It could be observed that in Figure 4.23, current utilisation of the entire system at sections A, C and E are equivalent to the motor current consumption. Furthermore, combined current consumption of coupling mechanism and the motor in Figure 4.23 varies from motor current utilisation graph only at the points B and D. The variation is only observed at two instances, namely at the time of engaging and disengaging of the mechanism. Therefore, it is apparent that mechanism utilises power (46 W) only during the engaging and disengage of the bistable coupling design. Furthermore, Figure 4.25 also indicates that current is only consumed during two instances (engaging and disengaging) throughout the complete motion of the manipulator link. The total energy utilisation of the proposed design is computed using the area under the power graph and it is about 1.104 J. The power consumption of both electromagnetic clutch and the proposed bistable coupling design are presented in the Figure 4.26. From Figure 4.24 and Figure 4.25 it could be observed that current is supplied to the conventional electromagnetic clutch uninterruptedly throughout manipulator link motion. This is because a continuous supply of current is a vital requirement for an electromagnetic clutch to maintain its engaged state.

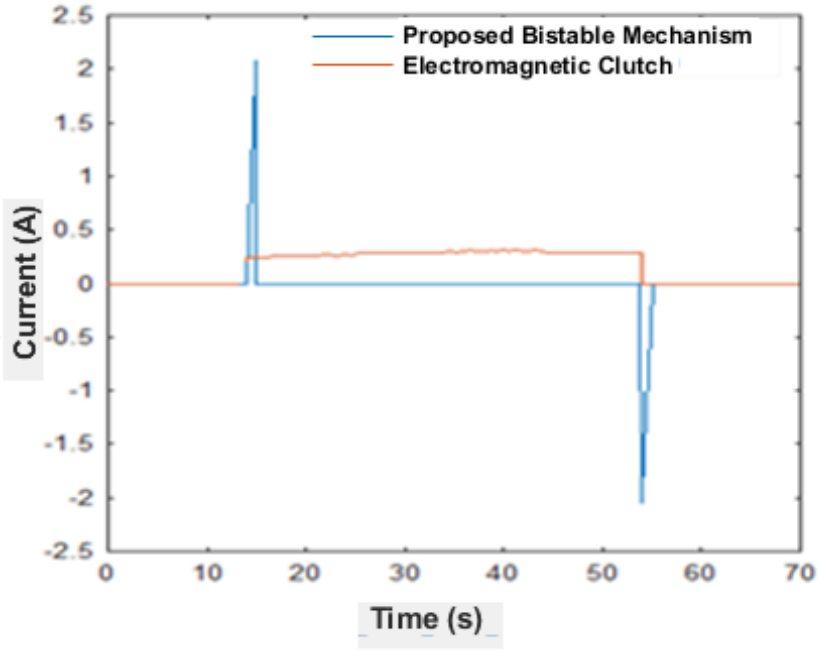

Figure 4.25: The current consumption of the bistable coupling mechanism and electromagnetic clutch during link motion.

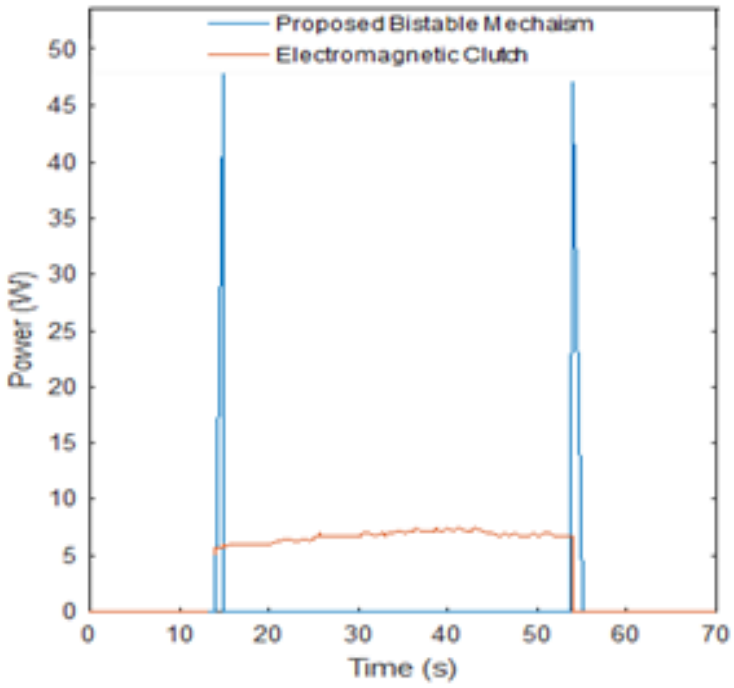

Figure 4.26: The power consumption of the bistable coupling mechanism and electromagnetic clutch during link motion.

The energy consumption of the electromagnetic clutch is computed for the entire manipulator link motion and it is about 271.445 J. Therefore, it is apparent

that in underactuated manipulators with electromagnetic clutches, the electromagnetic clutches utilise large amount of additional energy during manipulator motion apart from the motor. However, consumption of energy in the proposed design is only observed during two states namely engaging and disengaging of the mechanism. The total energy consumed by the bistable coupling mechanism during the manipulator link motion is about 1.104 J. As such, it could be observed that the conventional electromagnetic clutch has consumed 270.336 J of energy additionally during the link motion with respect to the proposed mechanism. The total energy utilised by the proposed mechanism for the entire motion is only about 0.406% with respect to the energy consumed by the conventional electromagnetic clutch for the equivalent motion scenario. Therefore, it is apparent that the proposed design is effective in reducing the consumption of electrical energy with comparison to the conventional electromagnetic clutch. Furthermore, because of continuous flow of current through the electromagnetic coil, heat energy is generated and dissipated from the coil reducing the efficiency of the clutch. The experimental results obtained indicate that the electromagnetic coil of the proposed design is energised for maximum of 12 ms. Thus, the time electromagnetic coil remains energised state has been reduced with comparison to a conventional electromagnetic clutch. As such, the proposed design is effective in reducing dissipation of heat energy as well enhancing the mechanism efficiency.

4.7 Chapter Conclusion

In this chapter, mechanical design of an energy efficient and safe bistable electromagnetic coupling mechanism is presented, that could be implemented on underactuated lightweight manipulators. To evaluate the performance of the design theoretical and experimental analysis were performed. The theoretical model developed has shown a good correlation with the experimental results.

Furthermore, the current and voltage consumption results were obtained to highlight the significance of the proposed mechanism in reducing the electric energy usage in comparison to a conventional electromagnetic clutch. Moreover, total energy consumed by both the bistable coupling mechanism and the electromagnetic clutch were analysed by implementing on prototype manipulator. The energy consumption results recorded for both proposed mechanism and the electromagnetic clutch are 1.104 J and 271.445 J respectively. Thus, the experimental results have illustrated that bistable electromagnetic coupling mechanism has reduced 270.336 J of electric energy usage. Therefore, the total energy consumption of the proposed bistable electromagnetic coupling mechanism with respect to the electromagnetic clutch is about 0.406%. Therefore, experiment results obtained indicate the effectiveness of the proposed bistable electromagnetic coupling mechanism in reducing the electric energy utilisation.

In addition, the proposed bistable electromagnetic coupling design is safe in operation compared to the traditional electromagnetic clutch due to the permanent magnetic bistable design. The design is capable of maintaining stable state of the mechanism even in the absence of electric power. Hence the mechanism is unaffected due to sudden power failure. Therefore, the proposed

bistable electromagnetic mechanism can provide an energy efficient and safe coupling mechanism for underactuated lightweight manipulators.

Chapter 5

Design of Underactuated Tendon Driven Manipulator Incorporated with Energy Saving Bistable Electromagnetic Coupling Mechanism

5.1 Introduction

The general method of designing lightweight robots are positioning the actuator at the base of the manipulator and transmit energy to the joints via tendons or gear trains [18][206]. Over the years several lightweight manipulators have been developed employing the general design concept where positioning the actuators at the base and allocating a dedicated motor for each joint actuation [20][138][206]. Thus, in general manipulator design the number of motors employed is equivalent to the number of degrees of freedom of the manipulator. In majority of the manipulators, manipulator weight is mainly contributed by the joint motors [17][206]. As such reduction of motors aids to maintain the lightweight attribute in the manipulators. Moreover, minimisation of the usage of motors (underactuation) provides additional benefits such as low cost and compact in design [33] [34]. Due to the advantages of underactuated concept, it has been widely implemented in robotics applications such as underwater robots, mobile robots, and etc [35][207]. From the literature review in Chapter 2, it could be observed only a handful of manipulators have been developed using the underactuated concept. In these designs the manipulating components such as coupling components and gear trains are installed at the joint. Thus, these components fixed at the joints contribute for the increment of driving joint torque. As mentioned earlier

lightweight characteristics and compactness of the design could be further enhanced by reducing the heavy components installed at the joints such as clutches and gears trains. Therefore, reduction of heavy components installed at the joints of the design aids the minimisation of driving joint torques. Moreover, the development of tendon drive manipulator with reduced number of motors has not been explored extensively in the field of lightweight manipulator design. Therefore, with the development of tendon driven manipulator with reduced number of actuators, the manipulator design could be enhanced incorporating the benefits of underactuated concept in addition to the joint torque reduction.

Furthermore, majority of underactuated systems developed over the years have utilised general actuation approach where electromagnetic clutches are employed as a coupling device [41][44]. Similarly, following the general approach Karbasi *et al* developed an underactuated modular robot incorporating electromagnetic clutches in the design [81]. LARM manipulator is another example of manipulator design which incorporates electromagnetic clutches [36]. It could be observed that the limited number of underactuated manipulators developed over the years have also utilised electromagnetic clutches following the general design approach [81][186]. However, there is a major drawback in electromagnetic clutch based actuation approach. It is the requirement of an uninterruptable power supply for the continues operation of an electromagnetic clutch. The power supply maintains the engaged state of the clutch by sustaining the electromagnet excitation state. Failure to maintain a continuous current supply result disengaging of the clutch [46] [47]. Therefore, continuous current supply should be provided throughout the operation [46] [47]. As such, additional energy is required for the electromagnetic clutches integrated in the underactuated system apart from the energy requirement for the motor. Hence, the underactuated manipulators incorporated with electromagnetic

clutch based conventional approach require additional energy for the joint actuation. Therefore, the energy usage of underactuated manipulators could be minimised by implementing a coupling mechanism that utilises less energy. This will optimise the energy consumption of underactuated manipulator design. As such it is worth exploring the possibility of minimising the energy consumption of underactuated manipulator during joint actuation by implementing an energy saving coupling mechanism-based actuation approach.

The design of tendon driven underactuated manipulator incorporated with energy saving coupling mechanism is presented in this chapter. The mechanical design and the operation of the proposed underactuated tendon driven manipulator are explained in detailed in Section 5.2. Furthermore, kinematics and the dynamics of the proposed manipulator are developed. The development of kinematics and dynamic model of the proposed manipulator are presented in detail under Section 5.3 and Section 5.4 respectively. Finally, the conclusion of the chapter is drawn in Section 5.5.

5.2 The Mechanical Design of the Manipulator

The manipulator design is incorporated with two motors for the actuation of three degrees of freedom. The design utilises combination of gears and tendons for the transmission of energy. The timing belts and the pulleys are used for the transmission of energy to each joint shaft from the base. In addition, series of spur gears are installed at the base of the manipulator to distribute energy to the respective joints. The first motor is fixed at the base of the manipulator that drives the base joint (θ_1). The second motor is installed on the base plate of the design

as shown in Figure 5.1. Second motors is used for the actuation of second (θ_2) and third (θ_3) joints. The design specifications of the manipulator are illustrated in Figure 5.2. Energy is transmitted from the second motor to the second and the third joint via gear trains and tendons. The manipulator is with the capability of varying the direction of joint motion independent of the direction of rotation of the motor. As such manipulator link motion could be varied independently at any instance even though a single motor is used for the actuation of two joints. Two bistable electromagnetic coupling mechanisms are allocated for the each joint with spur gears that control the direction of motion of the link. One of the bistable coupling mechanisms is allocated for the clockwise motion and the other is for anticlockwise motion. Therefore, direction of motion of the link could be varied by engaging and disengaging the respective bistable coupling mechanism. The operation principle of the manipulator is explained as follows.

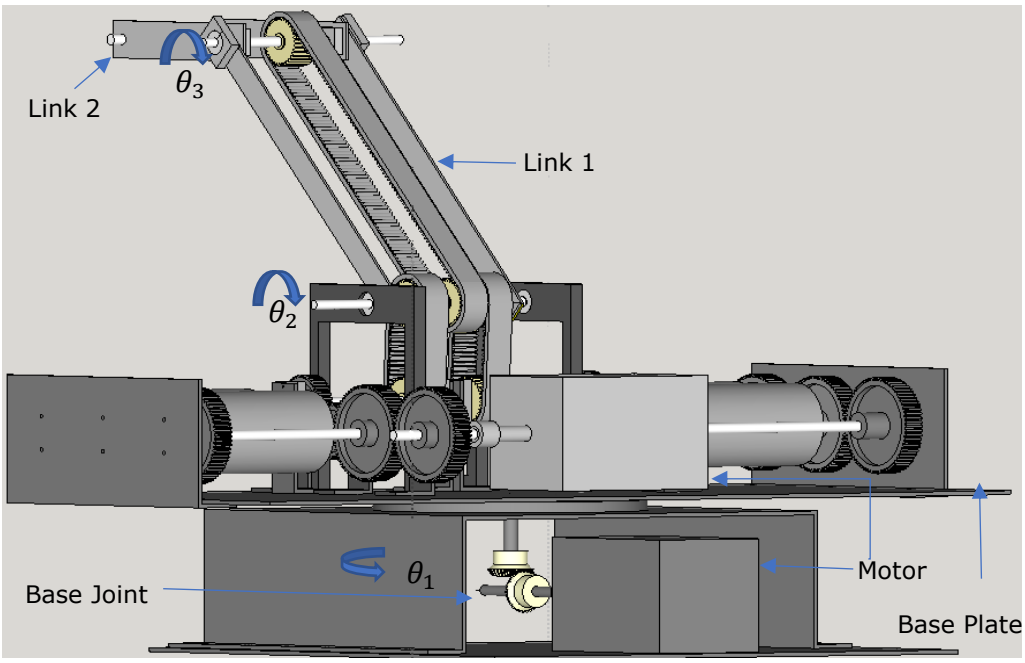

Figure 5.1: The prototype view of the proposed manipulator.

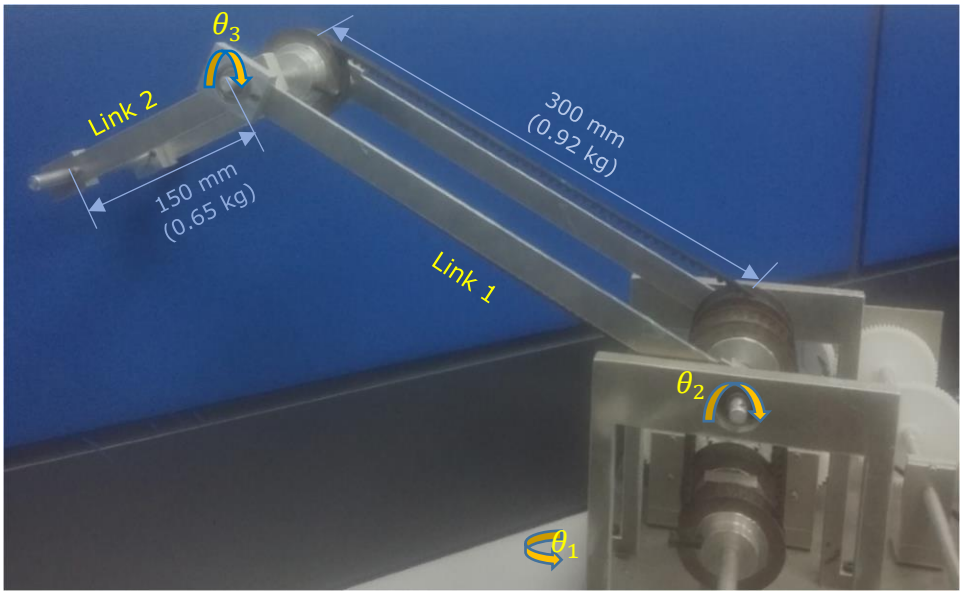

Figure 5.2: The developed manipulator design with link parameters.

Figure 5.4 shows the developed manipulator design incorporated with the bistable coupling mechanisms. The main shaft is used to transmit energy from the motor to the second (θ_2) and the third (θ_3) joints as illustrated in Figure 5.3 and Figure 5.4. The motor transmits rotational energy to the main shaft via spur gears as shown in the Figure 5.3 and Figure 5.4. Thereafter the main shaft distributes energy to the respective joints (θ_2 and θ_3). Two spur gears are connected at the end of the main shaft for the transmission of energy from the main shaft to the joints as illustrated in the Figure 5.3 and Figure 5.4. The spur gear connected with the main shaft transfer energy to the two spur gears connected in series that transfer the motion to the joint via bistable coupling mechanism. The series of arrows shown in orange colour in the Figure 5.3 indicate the energy transmission path for the actuation of second and third joint (θ_2 and θ_3) of the manipulator. The spur gears connected in series rotate in the opposite direction with respect to each other. Thus, the bistable coupling mechanism connected with the spur gears performs rotation in opposing direction. Therefore,

by engaging and disengaging the respective coupling mechanism desired direction of motion of the link could be attained. This provides the option of altering the direction of motion of joint without varying the direction of motor rotation. The driven ends of the two coupling mechanisms are connected to another set of spur gears as shown in Figure 5.3 and Figure 5.4. These spur gears transmit energy to a secondary shaft which is connected with timing pulleys. Thereafter the energy is transmitted to respective joint via timing belts and pulleys as illustrated in Figure 5.3 and Figure 5.4. Same approach has been utilised to distribute energy from the main shaft to the both joints (θ_2 and θ_3) in the manipulator design. Each joint is incorporated with two bistable coupling mechanisms as in the Figure 5.3 and Figure 5.4. As such four bistable coupling mechanisms are implemented in the design. All actuation components such as motors and the bistable coupling mechanisms are positioned at the base of the manipulator. Therefore, the design prevents installation of heavy components such as motors and gear trains at the joints. Thus, it aids the minimisation of joint torques of the manipulator.

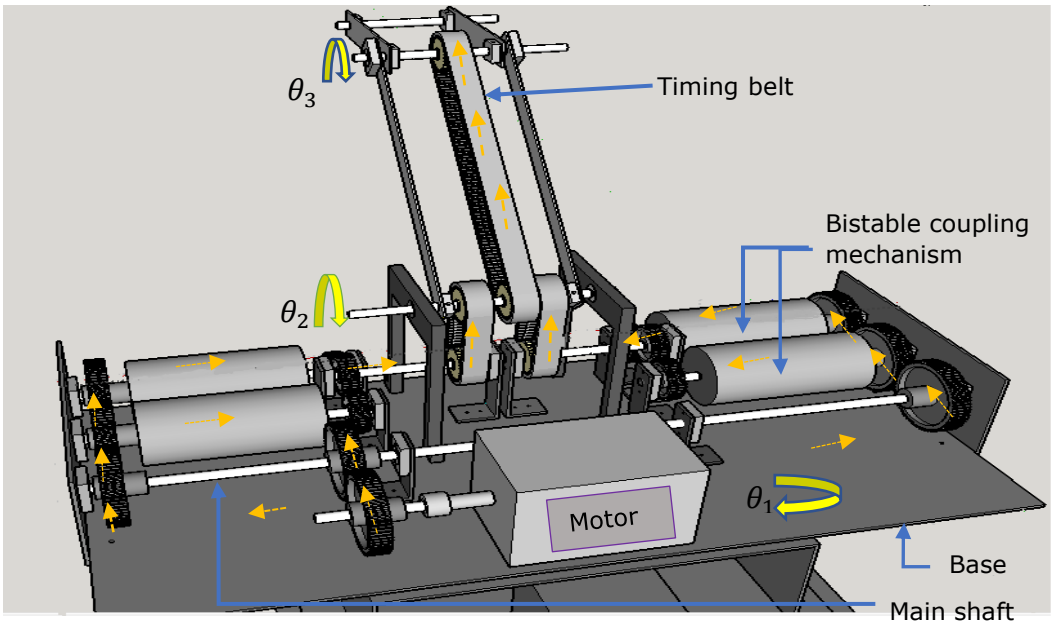

Figure 5.3: The prototype view of the proposed manipulator integrated with the energy saving coupling mechanism.

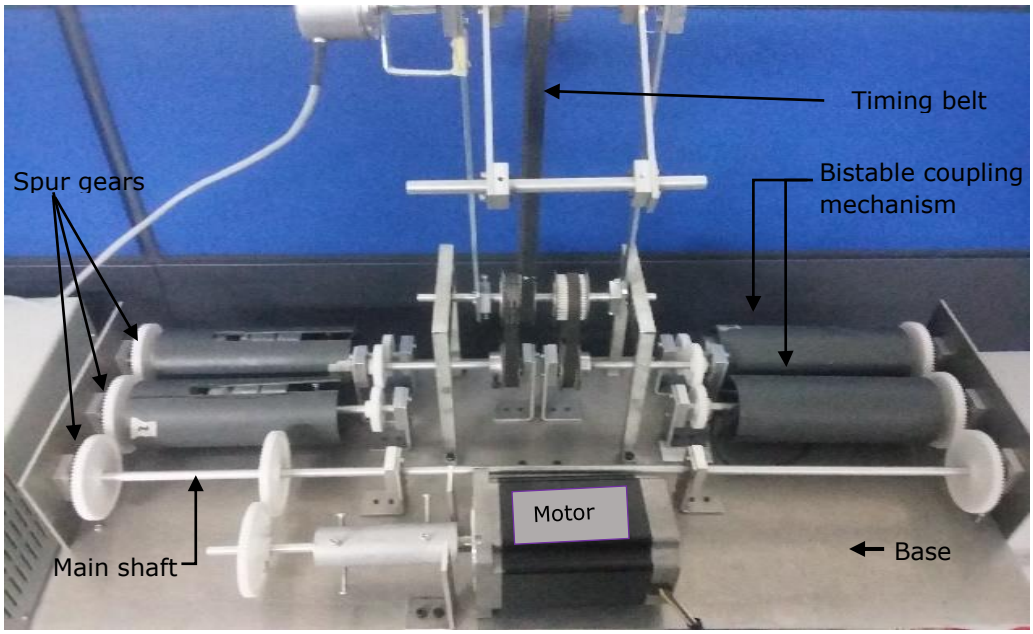

Figure 5.4: The developed manipulator design integrated with the energy saving coupling mechanisms.

5.3 Kinematic Model of the Proposed Manipulator Design

In this section, kinematic model of the proposed manipulator is derived. It is essential for a manipulator to identify the end effector (tool) position relative to the base of the manipulator in order to perform an operation. Therefore, it is essential to understand the tool position when the joint and link parameters are provided to the manipulator. The forward kinematic model provides a solution for this problem. In forward kinematics the main goal is to identify the end effector position for a given set of joint and link parameters with respect to a reference frame. The solution for the end effector position is provided as a function of joint variables and joint link constant parameters. Thus, with the forward kinematic model position of the end effector could be obtained for a given set of joint angles and link parameters with respect to a reference frame.

5.3.1 Forward Kinematics of the Proposed Manipulator

Denavit-Hartenberg proposed a systematic way of identifying forward kinematics solution of the manipulators which is employed considerably in robotics forward kinematics modelling [208][209]. In Denavit-Hartenberg (DH) method frames are allocated for each link from the base of the manipulator to the end effector. The homogenous transformation matrix associating the frames attached to links provide the relationship between the adjoining links. Combination of all the individual transformation matrixes computes the complete transformation matrix, generating the tool frame position and the orientation relative to the base. The general approach of assigning DH frames to the manipulator and the method of defining the DH parameters according to the Denavit-Hartenberg concept are described as follows. The method that should be adhered in the process of DH frames assignment according to Denavit-Hartenberg approach is given below [208].

1. Identification of the joint axes and indicate lines along them to identify the joint axes clearly.

2. Assigning the Z_i axis pointing along the i^{th} joint movement axis.

3. Assigning the X_i axis pointing along the common perpendicular away from z_{i-1} and the axis should be perpendicular to both z_{i-1} and $z_{i.}$

4. Assigning the Y_i axis according to the right-hand coordinate system after assigning Z_i and X_i.

The DH parameters could be obtained after assigning the frames to the manipulator model. Therefore, frames are assigned to the proposed manipulator and it is shown in the Figure 5.6. The parameters could be identified using definition provided for each parameter as shown in Figure 5.5.

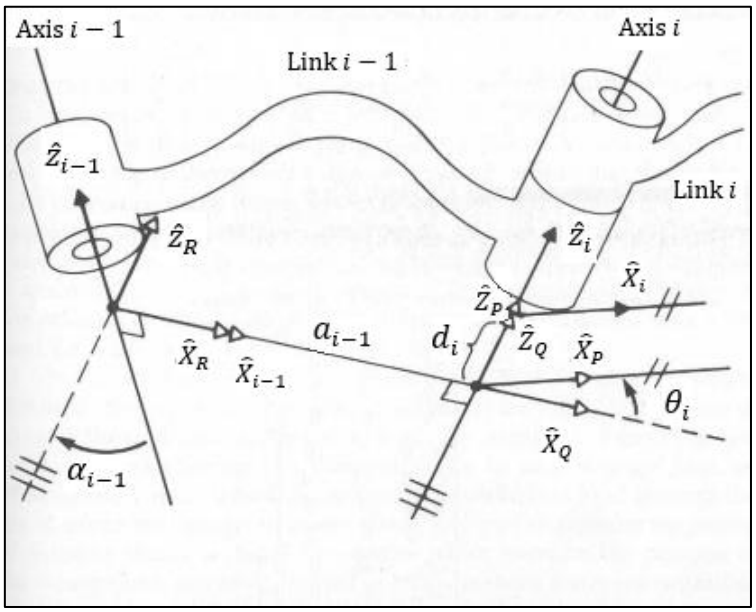

Figure 5.5: DH frame and parameter assignment [208].

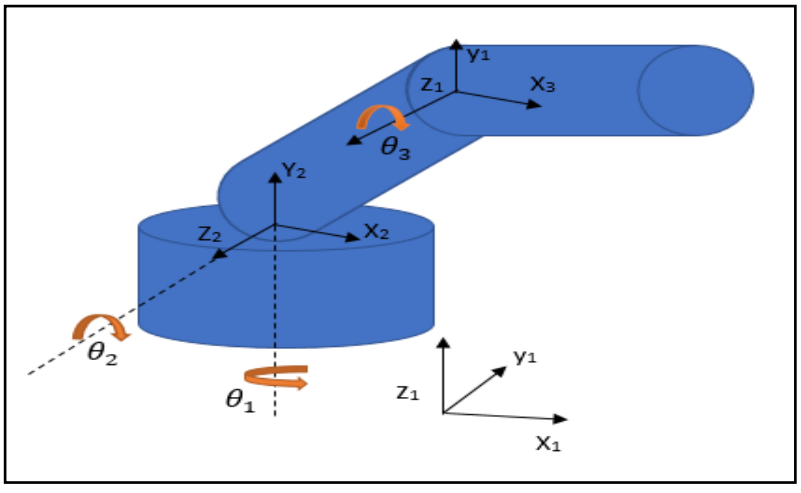

Figure 5.6: Proposed manipulator with DH frame assignment.

There are four DH parameters namely Link length (a_i), Link twist (α_i), Joint distance (d_i) and joint angle (θ_i) as defined according to Denavit-Hartenberg approach [208]. Table 5.1. presents DH parameters of the proposed manipulator. The links lengths of the manipulator link 1 and link 2 are represented by l_1 and l_2 respectively. The definition of each DH parameter is explained in detail as follows.

1. Link length a_i is the distance between z_{i-1} and z_i axes along the x_i-axis. a_i is the kinematic length of link (i).

2. Link twist α_i is the required rotation of the z_{i-1} axis about the x_i axis to become parallel to the z_i-axis.

3. Joint distance d_i is the distance between x_{i-1} and xi axes along the z_{i-1} axis. Joint distance is also called link offset.

4. Joint angle θ_i is the required rotation of x_{i-1}-axis about the z_{i-1}-axis to become parallel to the x_i-axis.

Table 5.1: The DH parameter table for the proposed manipulator.

i	α_i (degree)	a_i (m)	d_i (m)	θ_i (degree)
1	90	0	0	θ_1
2	0	l_1	0	θ_2
3	0	l_2	0	θ_3

The homogenous transformation matrix ${}^{i-1}T_i$ in Equation 5.1 maps the orientation and position of i^{th} frame with respect to i-1 frame. The matrix specifies the relationship between the links in term of DH parameters. Equation 5.1 is used

for the computation of the transformation matrix of each link. Where α_i and θ_i correspond to the Link twist angle and Joint angle respectively. Similarly, d_i represents the distance between x_{i-1} and x_i axes along the z_{i-1}-axis.

$$ {}^{i-1}T_i = \begin{bmatrix} \cos\theta_i & -\sin\theta_i \cos\alpha_i & \sin\theta_i \sin\alpha_i & a_i \cos\theta_i \\ \sin\theta_i & \cos\theta_i \cos\alpha_i & -\cos\theta_i \sin\alpha_i & a_i \sin\theta_i \\ 0 & \sin\alpha_i & \cos\alpha_i & d_i \\ 0 & 0 & 0 & 1 \end{bmatrix} \quad (5.1) $$

Thereafter the individual transformation matrixes are computed for each joint of the proposed manipulator using Equation 5.1. The computed matrices for each joint are as follows:

$$ {}^{0}T_1 = \begin{bmatrix} \mathrm{Cos}\,\theta_1 & 0 & \mathrm{Sin}\,\theta_1 & 0 \\ \mathrm{Sin}\,\theta_1 & 0 & -\mathrm{Cos}\,\theta_1 & 0 \\ 0 & 1 & 0 & 0 \\ 0 & 0 & 0 & 1 \end{bmatrix} \quad (5.2) $$

$$ {}^{1}T_2 = \begin{bmatrix} \mathrm{Cos}\,\theta_2 & \mathrm{Sin}\,\theta_2 & 0 & l_1 \mathrm{Cos}\,\theta_2 \\ \mathrm{Sin}\,\theta_2 & \mathrm{Cos}\,\theta_2 & 0 & l_1 \mathrm{Sin}\,\theta_2 \\ 0 & 0 & 1 & 0 \\ 0 & 0 & 0 & 1 \end{bmatrix} \quad (5.3) $$

$$ {}^{2}T_3 = \begin{bmatrix} \mathrm{Cos}\,\theta_3 & -\mathrm{Sin}\,\theta_3 & 0 & l_2 \mathrm{Cos}\,\theta_3 \\ \mathrm{Sin}\,\theta_3 & \mathrm{Cos}\,\theta_3 & 0 & l_2 \mathrm{Sin}\,\theta_3 \\ 0 & 0 & 1 & 0 \\ 0 & 0 & 0 & 1 \end{bmatrix} \quad (5.4) $$

The product of these three individual transformation matrixes shown in Equation (5.2), Equation (5.3) and Equation (5.4) provides the end effector frame position with respective to the base frame. The final transformation matrix for the

end effector frame position with respective to the base frame of the proposed manipulator is obtained as :

$$^{0}\mathrm{T}_{3} = {}^{0}T_{1}\ {}^{1}T_{2}\ {}^{2}T_{3} \tag{5.5}$$

The computed transformation matrix for forward kinematics model after multiplication of all the individual matrixes according to the Equation (5.5) can be expressed as :

$$^{0}\mathrm{T}_{3} = \begin{bmatrix} r_{11} & r_{12} & r_{13} & P_x \\ r_{21} & r_{22} & r_{23} & P_y \\ r_{31} & r_{32} & r_{34} & P_z \\ 0 & 0 & 0 & 1 \end{bmatrix} \tag{5.6}$$

The P_y, P_x, P_z elements in the matrix ($^{0}\mathrm{T}_{3}$) illustrated in Equation (5.6) represent x, y, z coordinates of the end effector position. Thus the corresponding x,y,z coordinate of the end effector position of the proposed manipulator could be identified for any given joint orientation. Manipulator x, y, z coordinates can be computed separately by substituting respective joint angles and link parameters in to the Equation (5.7), Equation (5.8) and Equation (5.9) as given below.

$$P_{\mathrm{x}} = l_1\mathrm{Cos}[\theta_1]\mathrm{Cos}[\theta_2] + l_2\mathrm{Cos}[\theta_1]\mathrm{Cos}[\theta_2]\mathrm{Cos}[\theta_3] + l_2\mathrm{Cos}[\theta_1]\mathrm{Sin}[\theta_2]\mathrm{Sin}[\theta_3] \tag{5.7}$$

$$P_{\mathrm{y}} = l_1\mathrm{Cos}[\theta_2]\mathrm{Sin}[\theta_1] + l_2\mathrm{Cos}[\theta_2]\mathrm{Cos}[\theta_3]\mathrm{Sin}[\theta_1] + l_2\mathrm{Sin}[\theta_1]\mathrm{Sin}[\theta_2]\mathrm{Sin}[\theta_3] \tag{5.8}$$

$$P_z = l_1\mathrm{Sin}[\theta_2] + l_2\mathrm{Cos}[\theta_3]\mathrm{Sin}[\theta_2] + l_2\mathrm{Cos}[\theta_2]\mathrm{Sin}[\theta_3] \tag{5.9}$$

5.4 Dynamic Model of the Proposed Manipulator

The development of dynamic model of the proposed manipulator design is presented under this section. Dynamic model of a manipulator provides the joint torques and forces in terms of the joint positions, velocities and accelerations [209][210]. As such the dynamic model of a manipulator enables to identify the required driving joint torque to perform a specified motion [211]. Therefore, the dynamic model is developed for the analysis of the joint torques requirement of the manipulator during the motion of the manipulator. Lagrange formulation is employed for the computation of dynamic model of the system due to its theoretical simplicity and of immediate comprehension [138][212]. The links of the manipulator are assumed to have uniform material properties and cross sectional area. Furthermore, centre of mass of the link is assumed to be located at centre of the link.

5.4.1 Development of the Dynamic Model of the Proposed Manipulator

Dynamic model equation of the manipulator could be defined using the Lagrange formulation as [102][213][214] :

$$\mathrm{M}(q)\,\ddot{q} + \mathrm{V}(q, \dot{q}) + \mathrm{G}(q) = \tau \tag{5.10}$$

Initial term of the equation $\mathrm{M}(q)$ represents the mass matrix and $\mathrm{V}(q, \dot{q})$ term represents the Coriolis and centrifugal forces. The gravitational force is

represented by the final term $\mathrm{G}(q)$ [102][215]. The terms q, $\dot{q}$ and $\ddot{q}$ represent the vector of joint position, velocity and acceleration respectively. Dynamical equations for the proposed manipulator can be expressed using Equation (5.11) as:

$$\begin{bmatrix}\tau_1\\ \tau_2\\ \tau_3\end{bmatrix} = \begin{bmatrix}M_{11} & M_{12} & M_{13}\\ M_{21} & M_{22} & M_{23}\\ M_{31} & M_{32} & M_{33}\end{bmatrix}\begin{bmatrix}\ddot{\theta}_1\\ \ddot{\theta}_2\\ \ddot{\theta}_3\end{bmatrix} + \begin{bmatrix}V_1(\theta & \dot{\theta})\\ V_2(\theta & \dot{\theta})\\ V_3(\theta & \dot{\theta})\end{bmatrix}\begin{bmatrix}\dot{\theta}_1\\ \dot{\theta}_2\\ \dot{\theta}_3\end{bmatrix} + \begin{bmatrix}G_1(\theta)\\ G_2(\theta)\\ G_3(\theta)\end{bmatrix} \tag{5.11}$$

Where:

$$\mathrm{V}(\theta,\dot{\theta}) = \sum_{j=1}^{n=3}\sum_{k=1}^{n=3}\left(\frac{\delta M_{ij}}{\delta\theta_k} - \frac{1}{2}\frac{\delta M_{jk}}{\delta\theta_i}\right)\dot{\theta}_j\dot{\theta}_k \tag{5.12}$$

$$\mathrm{G}(\theta) = \sum_{j=1}^{n=3} m_j g^T J_{vj}^i \tag{5.13}$$

The manipulator is with three degrees of freedom. Therefore, the inertia matrix is 3x3 matrix. The inertia matrix is obtained using the following Equation (5.14).

$$M(\theta) = \sum_{i=1}^{3} J_{vi}^T m_i J_{vi} + J_{\omega}^T I_i J_{\omega i} \tag{5.14}$$

Where J_i represents ith link Jacobian matrix and J_{vi} and $J_{\omega i}$ correspond to the link Jacobian submatrices. J_{vi} and $J_{\omega i}$ correspond to Jacobian submatrices namely the linear velocity and angular velocity.

Let J_{vi}^j and $J_{\omega i}^j$ be the jth column vectors of J_{vi} and $J_{\omega i}$ respectively. With the application of theory of instantaneous screw motion for j ≤ I

$$J_{vi}^{j} = \begin{cases} z_{j-1} \; x \quad P_{ci}^{j-1} & Revolute\ Joint \\ z_{j-1} & Prismatic\ Joint \end{cases} \tag{5.15}$$

$$J_{\omega i}^{j} = \begin{cases} z_{j-1} & Revolute\ Joint \\ 0 & Prismatic\ Joint \end{cases} \tag{5.16}$$

Where P_{ci}^{j-1} corresponds to the position vector defined from the origin of the j-1 link frame to the center of mass of the link i and it's expressed in the base frame. J_{vi}^{j} and $J_{\omega i}^{j}$ indicates the partial rate of change of velocity of the center of mass and angular velocity of link i with respective to the jth joint motion respectively. In the proposed manipulator all three joints are revolute joints therefore Equation (5.17) and Equation (5.18) are used for the computation of Jacobian submatrices.

$$J_{vi}^{j} = z_{j-1} \; x \quad P_{ci}^{j-1} \tag{5.17}$$

$$J_{\omega i}^{j} = z_{j-1} \tag{5.18}$$

Equations (5.17) and (5.18) are used for the computation of link Jacobian submatrices J_{vi} and $J_{\omega i}$ of the proposed manipulator. The l_1 and l_2 are the link lengths of link 1 and link 2. Similarly, θ_1, θ_2 and θ_3 corrospond to the joint 1, joint 2 and joint 3 angle values respectively. The computed Jacobian submatrices of linear velocity J_{vi} are as shown below:

$$J_{v1} = \begin{bmatrix} 0 & 0 & 0 \\ 0 & 0 & 0 \\ 0 & 0 & 0 \end{bmatrix} \tag{5.19}$$

The base joint and the base frame are on the same frame in the proposed design as such a_1 is equal to zero. This could be noted from the link parameters provided in Table 5.1 that a_1 is equal to zero. Thus J_{v1} is a zero matrix.

$$J_{v2} = \begin{bmatrix} -\frac{1}{2}l_1C_2S_1 & -\frac{1}{2}l_1C_1S_2 & 0 \\ \frac{1}{2}l_1C_1C_2 & -\frac{1}{2}l_1S_1S_2 & 0 \\ 0 & -\frac{1}{2}l_1C_2 & 0 \end{bmatrix} \tag{5.20}$$

$$J_{v3} = \begin{bmatrix} -\mathrm{S}_1\left(l_1\mathrm{C}_2 + \frac{1}{2}a_2\mathrm{C}_{23}\right) & -\mathrm{C}_1\left(l_1\mathrm{S}_2 + \frac{1}{2}l_2\mathrm{S}_{23}\right) & -\mathrm{C}_1\left(\frac{1}{2}l_2\mathrm{S}_{23}\right) \\ \mathrm{C}_1\left(l_1\mathrm{C}_2 + \frac{1}{2}l_2\mathrm{C}_{23}\right) & -\mathrm{S}_1\left(l_1\mathrm{S}_2 + \frac{1}{2}l_2\mathrm{S}_{23}\right) & -\mathrm{S}_1\left(\frac{1}{2}l_2\mathrm{S}_{23}\right) \\ 0 & \left(l_1\mathrm{C}_2 + \frac{1}{2}l_2\mathrm{C}_{23}\right) & \frac{1}{2}l_2\mathrm{C}_{23} \end{bmatrix} \tag{5.21}$$

Similarly, the computed Jacobian submatrices of angular velocity $J_{\omega i}$ of the proposed manipulator are presented as follows:

$$J_{\omega 1} = \begin{bmatrix} S_1 & 0 & 0 \\ -C_1 & 0 & 0 \\ 0 & 0 & 0 \end{bmatrix} \tag{5.22}$$

$$J_{\omega 2} = \begin{bmatrix} S_1 & S_1 & 0 \\ -C_1 & -C_1 & 0 \\ 0 & 0 & 0 \end{bmatrix} \tag{5.23}$$

$$J_{\omega 3} = \begin{bmatrix} S_1 & S_1 & S_1 \\ -C_1 & -C_1 & -C_1 \\ 0 & 0 & 0 \end{bmatrix} \tag{5.24}$$

The inertia matrix ${}^{i}I_i$ of the link *i* about its center of mass with respect to the i^{th} link frame is computed using the following equation:

$$I_i^i = \frac{1}{12} m_i a_i^2 \begin{bmatrix} 0 & 0 & 0 \\ 0 & 1 & 0 \\ 0 & 0 & 1 \end{bmatrix} \tag{5.25}$$

Where a and *m* correspond to the length and the mass of links respectively. The link inertia matrix I_i about its center of mass with respect to the base link frame is obtained using the following equation:

$$I_i = R_i^0 \, I_I^I \, (R_i^0)^T \tag{5.26}$$

R_i^0 represents the rotation matrix of link *i* which is retrieved from the transformation matrix T_i^0 obtained for the link *i* with respect to base frame. The calculation of transformation matrix for each link is shown in detail under the forward kinematics section.

The inertia matrices of link 1 and link 2 about the centre of mass of the links with reference to the base frame are computed with Equation (5.25) and Equation (5.26) as illustrated below. m_2 and m_3 correspond to the mass of link 1 and link 2 respectively.

$$I_1 = \begin{bmatrix} 0 & 0 & 0 \\ 0 & 0 & 0 \\ 0 & 0 & 0 \end{bmatrix} \tag{5.27}$$

$$I_2 = \begin{bmatrix} \frac{1}{12}({S_1}^2 + {C_1}^2{S_2}^2)l_1^2 m_2 & \frac{1}{12}(-C_1S_1 + C_1S_1{S_2}^2)l_1^2 m_2 & \frac{1}{12}(C_1C_2S_1)l_1^2 m_2 \\ \frac{1}{12}(-C_1S_1 + C_1S_1{S_2}^2)l_1^2 m_2 & \frac{1}{12}(C_1^2 + S_1^2{S_2}^2)l_1^2 m_2 & \frac{1}{12}(C_2S_1S_2)l_1^2 m_2 \\ \frac{1}{12}(C_1C_2S_2)l_1^2 m_2 & \frac{1}{12}(C_2S_1S_2)l_1^2 m_2 & \frac{1}{12}(C_2^2)l_1^2 m_2 \end{bmatrix} \quad (5.28)$$

$$I_3 = \begin{bmatrix} \frac{1}{12}(S_1^2 + C_1^2(C_3S_2 - C_2S_3)^2)l_1^2 m_2 & \frac{1}{12}(-C_1S_1 + C_1S_1(C_3S_2 - C_2S_3)^2)l_2^2 m_3 & \frac{1}{12}C_1(C_3S_2 - C_2S_3)(C_3C_2 - S_2S_3)l_2^2 m_3 \\ \frac{1}{12}(-C_1S_1 + C_1S_1(C_3S_2 - C_2S_3)^2)l_2^2 m_3 & \frac{1}{12}(C_1^2 + S_1^2(C_3S_2 - C_2S_3)^2)l_2^2 m_3 & \frac{1}{12}S_1(C_3S_2 - C_2S_3)(C_3C_2 - S_2S_3)l_2^2 m_3 \\ \frac{1}{12}C_1(C_3S_2 - C_2S_3)(C_3C_2 - S_2S_3)l_2^2 m_3 & \frac{1}{12}S_1(C_3S_2 - C_2S_3)(C_3C_2 - S_2S_3)l_2^2 m_3 & \frac{1}{12}((C_3C_2 - S_2S_3)^2)l_2^2 m_3 \end{bmatrix} \quad (5.29)$$

The finalised 3x3 inertia matrix of the proposed manipulator is obtained by substituting the Equations (5.15) through (5.29) to the above stated Equation (5.14). The elements of the computed inertia matrix of the proposed manipulator are shown as follows.

$$\mathrm{M} = \begin{bmatrix} M_{11} & M_{12} & M_{13} \\ M_{21} & M_{22} & M_{23} \\ M_{31} & M_{32} & M_{33} \end{bmatrix} \quad (5.30)$$

$$\mathrm{M}_{11} = \frac{1}{24}(24\mathrm{Cos}[\theta_2]\mathrm{Cos}[\theta_2 + \theta_3]l_1 l_2 m_3 + (5 + 3\mathrm{Cos}[2(\theta_2 + \theta_3)])l_2^2 m_3 + l_1^2((5 + 3\mathrm{Cos}[2\theta_2])m_2 + 24\mathrm{Cos}[\theta_2]^2 m_3)) \quad (5.31)$$

$$\begin{aligned}\mathrm{M}_{12} = {} & \mathrm{Sin}[\theta_1](\tfrac{1}{12}\mathrm{Sin}[\theta_1](\mathrm{Sin}[\theta_1]^2 + \mathrm{Cos}[\theta_1]^2\mathrm{Sin}[\theta_2]^2)l_1^2 m_2 - \tfrac{1}{12}\mathrm{Cos}[\theta_1](-\mathrm{Cos}[\theta_1]\mathrm{Sin}[\theta_1] + \\ & \mathrm{Cos}[\theta_1]\mathrm{Sin}[\theta_1]\mathrm{Sin}[\theta_2]^2)l_1^2 m_2) - \mathrm{Cos}[\theta_1](\tfrac{1}{12}\mathrm{Sin}[\theta_1](-\mathrm{Cos}[\theta_1]\mathrm{Sin}[\theta_1] + \\ & \mathrm{Cos}[\theta_1]\mathrm{Sin}[\theta_1]\mathrm{Sin}[\theta_2]^2)l_1^2 m_2 - \tfrac{1}{12}\mathrm{Cos}[\theta_1](\mathrm{Cos}[\theta_1]^2 + \mathrm{Sin}[\theta_1]^2\mathrm{Sin}[\theta_2]^2)l_1^2 m_2) + \\ & \mathrm{Sin}[\theta_1](\tfrac{1}{12}\mathrm{Sin}[\theta_1](\mathrm{Sin}[\theta_1]^2 + \mathrm{Cos}[\theta_1]^2(\mathrm{Cos}[\theta_3]\mathrm{Sin}[\theta_2] - \mathrm{Cos}[\theta_2]\mathrm{Sin}[\theta_3])^2)l_2^2 m_3 - \\ & \tfrac{1}{12}\mathrm{Cos}[\theta_1](-\mathrm{Cos}[\theta_1]\mathrm{Sin}[\theta_1] + \mathrm{Cos}[\theta_1]\mathrm{Sin}[\theta_1](\mathrm{Cos}[\theta_3]\mathrm{Sin}[\theta_2] - \mathrm{Cos}[\theta_2]\mathrm{Sin}[\theta_3])^2)l_2^2 m_3) - \\ & \mathrm{Cos}[\theta_1](\tfrac{1}{12}\mathrm{Sin}[\theta_1](-\mathrm{Cos}[\theta_1]\mathrm{Sin}[\theta_1] + \mathrm{Cos}[\theta_1]\mathrm{Sin}[\theta_1](\mathrm{Cos}[\theta_3]\mathrm{Sin}[\theta_2] - \mathrm{Cos}[\theta_2]\mathrm{Sin}[\theta_3])^2)l_2^2 m_3 - \\ & \tfrac{1}{12}\mathrm{Cos}[\theta_1](\mathrm{Cos}[\theta_1]^2 + \mathrm{Sin}[\theta_1]^2(\mathrm{Cos}[\theta_3]\mathrm{Sin}[\theta_2] - \mathrm{Cos}[\theta_2]\mathrm{Sin}[\theta_3])^2)l_2^2 m_3) \end{aligned} \quad (5.32)$$

$$\begin{aligned}\mathrm{M}_{13} = {} & \mathrm{Sin}[\theta_1](\tfrac{1}{12}\mathrm{Sin}[\theta_1](\mathrm{Sin}[\theta_1]^2 + \mathrm{Cos}[\theta_1]^2(\mathrm{Cos}[\theta_3]\mathrm{Sin}[\theta_2] - \mathrm{Cos}[\theta_2]\mathrm{Sin}[\theta_3])^2)l_2^2 m_3 - \\ & \tfrac{1}{12}\mathrm{Cos}[\theta_1](-\mathrm{Cos}[\theta_1]\mathrm{Sin}[\theta_1] + \mathrm{Cos}[\theta_1]\mathrm{Sin}[\theta_1](\mathrm{Cos}[\theta_3]\mathrm{Sin}[\theta_2] - \mathrm{Cos}[\theta_2]\mathrm{Sin}[\theta_3])^2)l_2^2 m_3) - \\ & \mathrm{Cos}[\theta_1](\tfrac{1}{12}\mathrm{Sin}[\theta_1](-\mathrm{Cos}[\theta_1]\mathrm{Sin}[\theta_1] + \mathrm{Cos}[\theta_1]\mathrm{Sin}[\theta_1](\mathrm{Cos}[\theta_3]\mathrm{Sin}[\theta_2] - \mathrm{Cos}[\theta_2]\mathrm{Sin}[\theta_3])^2)l_2^2 m_3 - \\ & \tfrac{1}{12}\mathrm{Cos}[\theta_1](\mathrm{Cos}[\theta_1]^2 + \mathrm{Sin}[\theta_1]^2(\mathrm{Cos}[\theta_3]\mathrm{Sin}[\theta_2] - \mathrm{Cos}[\theta_2]\mathrm{Sin}[\theta_3])^2)l_2^2 m_3) \end{aligned} \quad (5.33)$$

$$M_{21} = \text{Sin}[\theta_1](\frac{1}{12}\text{Sin}[\theta_1](\text{Sin}[\theta_1]^2 + \text{Cos}[\theta_1]^2\text{Sin}[\theta_2]^2)l_1^2 m_2 - \frac{1}{12}\text{Cos}[\theta_1](-\text{Cos}[\theta_1]\text{Sin}[\theta_1] + \text{Cos}[\theta_1]\text{Sin}[\theta_1]\text{Sin}[\theta_2]^2)l_1^2 m_2) - \text{Cos}[\theta_1](\frac{1}{12}\text{Sin}[\theta_1](-\text{Cos}[\theta_1]\text{Sin}[\theta_1] + \text{Cos}[\theta_1]\text{Sin}[\theta_1]\text{Sin}[\theta_2]^2)l_1^2 m_2 - \frac{1}{12}\text{Cos}[\theta_1](\text{Cos}[\theta_1]^2 + \text{Sin}[\theta_1]^2\text{Sin}[\theta_2]^2)l_1^2 m_2) + \text{Sin}[\theta_1](\frac{1}{12}\text{Sin}[\theta_1](\text{Sin}[\theta_1]^2 + \text{Cos}[\theta_1]^2(\text{Cos}[\theta_3]\text{Sin}[\theta_2] - \text{Cos}[\theta_2]\text{Sin}[\theta_3])^2)l_2^2 m_3 - \frac{1}{12}\text{Cos}[\theta_1](-\text{Cos}[\theta_1]\text{Sin}[\theta_1] + \text{Cos}[\theta_1]\text{Sin}[\theta_1](\text{Cos}[\theta_3]\text{Sin}[\theta_2] - \text{Cos}[\theta_2]\text{Sin}[\theta_3])^2)l_2^2 m_3) - \text{Cos}[\theta_1](\frac{1}{12}\text{Sin}[\theta_1](-\text{Cos}[\theta_1]\text{Sin}[\theta_1] + \text{Cos}[\theta_1]\text{Sin}[\theta_1](\text{Cos}[\theta_3]\text{Sin}[\theta_2] - \text{Cos}[\theta_2]\text{Sin}[\theta_3])^2)l_2^2 m_3 - \frac{1}{12}\text{Cos}[\theta_1](\text{Cos}[\theta_1]^2 + \text{Sin}[\theta_1]^2(\text{Cos}[\theta_3]\text{Sin}[\theta_2] - \text{Cos}[\theta_2]\text{Sin}[\theta_3])^2)l_2^2 m_3) \quad (5.34)$$

$$M_{22} = \frac{1}{3}(3\text{Cos}[\theta_3]l_1 l_2 m_3 + l_2^2 m_3 + l_1^2(m_2 + 3m_3)) \quad (5.35)$$

$$M_{23} = (\frac{1}{2}\text{Cos}[\theta_2 + \theta_3]l(\text{Cos}[\theta_2]l_1 + \frac{1}{2}\text{Cos}[\theta_2 + \theta_3]l_2) + \frac{1}{2}\text{Cos}[\theta_1]^2\text{Sin}[\theta_2 + \theta_3]l_2(\text{Sin}[\theta_2]l_1 + \frac{1}{2}\text{Sin}[\theta_2 + \theta_3]l_2) + \frac{1}{2}\text{Sin}[\theta_1]^2\text{Sin}[\theta_2 + \theta_3]l_2(\text{Sin}[\theta_2]l_1 + \frac{1}{2}\text{Sin}[\theta_2 + \theta_3]l_2))m_3 + \text{Sin}[\theta_1](\frac{1}{12}\text{Sin}[\theta_1](\text{Sin}[\theta_1]^2 + \text{Cos}[\theta_1]^2(\text{Cos}[\theta_3]\text{Sin}[\theta_2] - \text{Cos}[\theta_2]\text{Sin}[\theta_3])^2)l_2^2 m_3 - \frac{1}{12}\text{Cos}[\theta_1](-\text{Cos}[\theta_1]\text{Sin}[\theta_1] + \text{Cos}[\theta_1]\text{Sin}[\theta_1](\text{Cos}[\theta_3]\text{Sin}[\theta_2] - \text{Cos}[\theta_2]\text{Sin}[\theta_3])^2)l_2^2 m_3) - \text{Cos}[\theta_1](\frac{1}{12}\text{Sin}[\theta_1](-\text{Cos}[\theta_1]\text{Sin}[\theta_1] + \text{Cos}[\theta_1]\text{Sin}[\theta_1](\text{Cos}[\theta_3]\text{Sin}[\theta_2] - \text{Cos}[\theta_2]\text{Sin}[\theta_3])^2)l_2^2 m_3 - \frac{1}{12}\text{Cos}[\theta_1](\text{Cos}[\theta_1]^2 + \text{Sin}[\theta_1]^2(\text{Cos}[\theta_3]\text{Sin}[\theta_2] - \text{Cos}[\theta_2]\text{Sin}[\theta_3])^2)l_2^2 m_3) \quad (5.36)$$

$$M_{31} = \text{Sin}[\theta_1](\frac{1}{12}\text{Sin}[\theta_1](\text{Sin}[\theta_1]^2 + \text{Cos}[\theta_1]^2(\text{Cos}[\theta_3]\text{Sin}[\theta_2] - \text{Cos}[\theta_2]\text{Sin}[\theta_3])^2)l_2^2 m_3 - \frac{1}{12}\text{Cos}[\theta_1](-\text{Cos}[\theta_1]\text{Sin}[\theta_1] + \text{Cos}[\theta_1]\text{Sin}[\theta_1](\text{Cos}[\theta_3]\text{Sin}[\theta_2] - \text{Cos}[\theta_2]\text{Sin}[\theta_3])^2)l_2^2 m_3) - \text{Cos}[\theta_1](\frac{1}{12}\text{Sin}[\theta_1](-\text{Cos}[\theta_1]\text{Sin}[\theta_1] + \text{Cos}[\theta_1]\text{Sin}[\theta_1](\text{Cos}[\theta_3]\text{Sin}[\theta_2] - \text{Cos}[\theta_2]\text{Sin}[\theta_3])^2)l_2^2 m_3 - \frac{1}{12}\text{Cos}[\theta_1](\text{Cos}[\theta_1]^2 + \text{Sin}[\theta_1]^2(\text{Cos}[\theta_3]\text{Sin}[\theta_2] - \text{Cos}[\theta_2]\text{Sin}[\theta_3])^2)l_2^2 m_3) \quad (5.37)$$

$$M_{32} = (\frac{1}{2}\text{Cos}[\theta_2 + \theta_3]l_2(\text{Cos}[\theta_2]l_1 + \frac{1}{2}\text{Cos}[\theta_2 + \theta_3]l_2) + \frac{1}{2}\text{Cos}[\theta_1]^2\text{Sin}[\theta_2 + \theta_3]l_2(\text{Sin}[\theta_2]l_1 + \frac{1}{2}\text{Sin}[\theta_2 + \theta_3]l_2) + \frac{1}{2}\text{Sin}[\theta_1]^2\text{Sin}[\theta_2 + \theta_3]l_2(\text{Sin}[\theta_2]l_1 + \frac{1}{2}\text{Sin}[\theta_2 + \theta_3]l_2))m_3 + \text{Sin}[\theta_1](\frac{1}{12}\text{Sin}[\theta_1](\text{Sin}[\theta_1]^2 + \text{Cos}[\theta_1]^2(\text{Cos}[\theta_3]\text{Sin}[\theta_2] - \text{Cos}[\theta_2]\text{Sin}[\theta_3])^2)l_2^2 m_3 - \frac{1}{12}\text{Cos}[\theta_1](-\text{Cos}[\theta_1]\text{Sin}[\theta_1] + \text{Cos}[\theta_1]\text{Sin}[\theta_1](\text{Cos}[\theta_3]\text{Sin}[\theta_2] - \text{Cos}[\theta_2]\text{Sin}[\theta_3])^2)l_2^2 m_3) - \text{Cos}[\theta_1](\frac{1}{12}\text{Sin}[\theta_1](-\text{Cos}[\theta_1]\text{Sin}[\theta_1] + \text{Cos}[\theta_1]\text{Sin}[\theta_1](\text{Cos}[\theta_3]\text{Sin}[\theta_2] - \text{Cos}[\theta_2]\text{Sin}[\theta_3])^2)l_2^2 m_3 - \frac{1}{12}\text{Cos}[\theta_1](\text{Cos}[\theta_1]^2 + \text{Sin}[\theta_1]^2(\text{Cos}[\theta_3]\text{Sin}[\theta_2] - \text{Cos}[\theta_2]\text{Sin}[\theta_3])^2)l_2^2 m_3) \quad (5.38)$$

$$M_{33} = \frac{1}{3}l_2^2 m_3 \quad (5.39)$$

The velocity coupling vector is obtained using the Equation (5.12). The velocity coupling vector is computed by obtaining partial derivatives of the inertia matrix presented in Equation (5.30). The computed velocity coupling vector terms are shown from Equation (5.40) to Equation (5.42).

$$V_1 = -\frac{1}{4}\dot{\theta}_1(\text{Sin}[2\theta_2]l_1^2(m_2+4m_3)\dot{\theta}_2 + \text{Sin}[2(\theta_2+\theta_3)]l_2^2m_3(\dot{\theta}_2+\dot{\theta}_3) + 4l_1l_2m_3(\text{Sin}[2\theta_2+\theta_3]\dot{\theta}_2 + \text{Cos}[\theta_2]\text{Sin}[\theta_2+\theta_3]\dot{\theta}_3)) \quad (5.40)$$

$$V_2 = \frac{1}{8}(\text{Sin}[2(\theta_2+\theta_3)]l_2^2m_3\dot{\theta}_1^2 + \text{Sin}[2\theta_2]l_1^2(m_2+4m_3)\dot{\theta}_1^2 + 4l_1l_2m_3(\text{Sin}[2\theta_2+\theta_3]\dot{\theta}_1^2 - \text{Sin}[\theta_3]\dot{\theta}_3(2\dot{\theta}_2+\dot{\theta}_3))) \quad (5.41)$$

$$V_3 = \frac{1}{8}l_2m_3(\text{Sin}[2(\theta_2+\theta_3)]a_2\dot{\theta}_1^2 + 4l_1(\text{Cos}[\theta_2]\text{Sin}[\theta_2+\theta_3]\dot{\theta}_1^2 + \text{Sin}[\theta_3]\dot{\theta}_2^2)) \quad (5.42)$$

The corresponding gravitational vectors are obtained using the Equation (5.13) and the computed gravitational vectors are as shown below:

$$G_1 = 0 \quad (5.43)$$

$$G_2 = g \times 1/2 \times m_3 \times l_2 \times \text{Cos}[\theta_2+\theta_3] + g(m_3 + 1/2 \times m_2)l_1 \times \text{Cos}[\theta_2] \quad (5.44)$$

$$G_3 = g \times 1/2 \times m_3 \times l_2 \times \text{Cos}[\theta_2+\theta_3] \quad (5.45)$$

Finally, the torque equations for the proposed manipulator are computed by compiling the computed inertia matrix, velocity coupling vector and the gravitational vector. The developed torque equations for each joint of the proposed manipulator are presented in Equation (5.46), Equation (5.47) and Equation (5.48).

$$\tau_1 = (\frac{1}{24}(24\text{Cos}[\theta_2]\text{Cos}[\theta_2+\theta_3]l_1l_2m_3 + (5+3\text{Cos}[2(\theta_2+\theta_3)])l_2^2m_3 + l_1^2((5+3\text{Cos}[2\theta_2])m_2 + 24\text{Cos}[\theta_2]^2m_3)))\ddot{\theta}_1 + (\text{Sin}[\theta_1](\frac{1}{12}\text{Sin}[\theta_1](\text{Sin}[\theta_1]^2 + \text{Cos}[\theta_1]^2\text{Sin}[\theta_2]^2)l_1^2m_2 - \frac{1}{12}\text{Cos}[\theta_1](-\text{Cos}[\theta_1]\text{Sin}[\theta_1] + \text{Cos}[\theta_1]\text{Sin}[\theta_1]\text{Sin}[\theta_2]^2)l_1^2m_2) - \text{Cos}[\theta_1](\frac{1}{12}\text{Sin}[\theta_1](-\text{Cos}[\theta_1]\text{Sin}[\theta_1] + \text{Cos}[\theta_1]\text{Sin}[\theta_1]\text{Sin}[\theta_2]^2)l_1^2m_2 - \frac{1}{12}\text{Cos}[\theta_1](\text{Cos}[\theta_1]^2 + \text{Sin}[\theta_1]^2\text{Sin}[\theta_2]^2)l_1^2m_2) + \text{Sin}[\theta_1](\frac{1}{12}\text{Sin}[\theta_1](\text{Sin}[\theta_1]^2 + \text{Cos}[\theta_1]^2(\text{Cos}[\theta_3]\text{Sin}[\theta_2] - \text{Cos}[\theta_2]\text{Sin}[\theta_3])^2)l_2^2m_3 - \frac{1}{12}\text{Cos}[\theta_1](-\text{Cos}[\theta_1]\text{Sin}[\theta_1] + \text{Cos}[\theta_1]\text{Sin}[\theta_1](\text{Cos}[\theta_3]\text{Sin}[\theta_2] - \text{Cos}[\theta_2]\text{Sin}[\theta_3])^2)l_2^2m_3) - \text{Cos}[\theta_1](\frac{1}{12}\text{Sin}[\theta_1](-\text{Cos}[\theta_1]\text{Sin}[\theta_1] + \text{Cos}[\theta_1]\text{Sin}[\theta_1](\text{Cos}[\theta_3]\text{Sin}[\theta_2] -$$

$$\text{Cos}[\theta_2]\text{Sin}[\theta_3])^2)l_2^2m_3 - \frac{1}{12}\text{Cos}[\theta_1](\text{Cos}[\theta_1]^2 + \text{Sin}[\theta_1]^2(\text{Cos}[\theta_3]\text{Sin}[\theta_2] - \text{Cos}[\theta_2]\text{Sin}[\theta_3])^2)l_2^2m_3))\ddot{\theta_2} + (\text{Sin}[\theta_1](\frac{1}{12}\text{Sin}[\theta_1](\text{Sin}[\theta_1]^2 + \text{Cos}[\theta_1]^2(\text{Cos}[\theta_3]\text{Sin}[\theta_2] - \text{Cos}[\theta_2]\text{Sin}[\theta_3])^2)l_2^2m_3 - \frac{1}{12}\text{Cos}[\theta_1](-\text{Cos}[\theta_1]\text{Sin}[\theta_1] + \text{Cos}[\theta_1]\text{Sin}[\theta_1](\text{Cos}[\theta_3]\text{Sin}[\theta_2] - \text{Cos}[\theta_2]\text{Sin}[\theta_3])^2)l_2^2m_3) - \text{Cos}[\theta_1](\frac{1}{12}\text{Sin}[\theta_1](-\text{Cos}[\theta_1]\text{Sin}[\theta_1] + \text{Cos}[\theta_1]\text{Sin}[\theta_1](\text{Cos}[\theta_3]\text{Sin}[\theta_2] - \text{Cos}[\theta_2]\text{Sin}[\theta_3])^2)l_2^2m_3 - \frac{1}{12}\text{Cos}[\theta_1](\text{Cos}[\theta_1]^2 + \text{Sin}[\theta_1]^2(\text{Cos}[\theta_3]\text{Sin}[\theta_2] - \text{Cos}[\theta_2]\text{Sin}[\theta_3])^2)l_2^2m_3))\ddot{\theta_3} - \frac{1}{4}\dot{\theta}_1(\text{Sin}[2\theta_2]l_1^2(m_2 + 4m_3)\dot{\theta}_2 + \text{Sin}[2(\theta_2 + \theta_3)]l_2^2m_3(\dot{\theta}_2 + \dot{\theta}_3) + 4l_1l_2m_3(\text{Sin}[2\theta_2 + \theta_3]\dot{\theta}_2 + \text{Cos}[\theta_2]\text{Sin}[\theta_2 + \theta_3]\dot{\theta}_3))$$

(5.46)

$$\tau_2 = (\text{Sin}[\theta_1](\frac{1}{12}\text{Sin}[\theta_1](\text{Sin}[\theta_1]^2 + \text{Cos}[\theta_1]^2\text{Sin}[\theta_2]^2)l_1^2m_2 - \frac{1}{12}\text{Cos}[\theta_1](-\text{Cos}[\theta_1]\text{Sin}[\theta_1] + \text{Cos}[\theta_1]\text{Sin}[\theta_1]\text{Sin}[\theta_2]^2)l_1^2m_2) - \text{Cos}[\theta_1](\frac{1}{12}\text{Sin}[\theta_1](-\text{Cos}[\theta_1]\text{Sin}[\theta_1] + \text{Cos}[\theta_1]\text{Sin}[\theta_1]\text{Sin}[\theta_2]^2)l_1^2m_2 - \frac{1}{12}\text{Cos}[\theta_1](\text{Cos}[\theta_1]^2 + \text{Sin}[\theta_1]^2\text{Sin}[\theta_2]^2)l_1^2m_2) + \text{Sin}[\theta_1](\frac{1}{12}\text{Sin}[\theta_1](\text{Sin}[\theta_1]^2 + \text{Cos}[\theta_1]^2(\text{Cos}[\theta_3]\text{Sin}[\theta_2] - \text{Cos}[\theta_2]\text{Sin}[\theta_3])^2)l_2^2m_3 - \frac{1}{12}\text{Cos}[\theta_1](-\text{Cos}[\theta_1]\text{Sin}[\theta_1] + \text{Cos}[\theta_1]\text{Sin}[\theta_1](\text{Cos}[\theta_3]\text{Sin}[\theta_2] - \text{Cos}[\theta_2]\text{Sin}[\theta_3])^2)l_2^2m_3) - \text{Cos}[\theta_1](\frac{1}{12}\text{Sin}[\theta_1](-\text{Cos}[\theta_1]\text{Sin}[\theta_1] + \text{Cos}[\theta_1]\text{Sin}[\theta_1](\text{Cos}[\theta_3]\text{Sin}[\theta_2] - \text{Cos}[\theta_2]\text{Sin}[\theta_3])^2)l_2^2m_3 - \frac{1}{12}\text{Cos}[\theta_1](\text{Cos}[\theta_1]^2 + \text{Sin}[\theta_1]^2(\text{Cos}[\theta_3]\text{Sin}[\theta_2] - \text{Cos}[\theta_2]\text{Sin}[\theta_3])^2)l_2^2m_3))\ddot{\theta_1} + (\frac{1}{3}(3\text{Cos}[\theta_3]l_1l_2m_3 + l_2^2m_3 + l_1^2(m_2 + 3m_3)))\ddot{\theta_2} + ((\frac{1}{2}\text{Cos}[\theta_2 + \theta_3]l_2(\text{Cos}[\theta_2]l_1 + \frac{1}{2}\text{Cos}[\theta_2 + \theta_3]l_2) + \frac{1}{2}\text{Cos}[\theta_1]^2\text{Sin}[\theta_2 + \theta_3]l_2(\text{Sin}[\theta_2]l_1 + \frac{1}{2}\text{Sin}[\theta_2 + \theta_3]l_2) + \frac{1}{2}\text{Sin}[\theta_1]^2\text{Sin}[\theta_2 + \theta_3]l_2(\text{Sin}[\theta_2]l_1 + \frac{1}{2}\text{Sin}[\theta_2 + \theta_3]l_2))m_3 + \text{Sin}[\theta_1](\frac{1}{12}\text{Sin}[\theta_1](\text{Sin}[\theta_1]^2 + \text{Cos}[\theta_1]^2(\text{Cos}[\theta_3]\text{Sin}[\theta_2] - \text{Cos}[\theta_2]\text{Sin}[\theta_3])^2)l_2^2m_3 - \frac{1}{12}\text{Cos}[\theta_1](-\text{Cos}[\theta_1]\text{Sin}[\theta_1] + \text{Cos}[\theta_1]\text{Sin}[\theta_1](\text{Cos}[\theta_3]\text{Sin}[\theta_2] - \text{Cos}[\theta_2]\text{Sin}[\theta_3])^2)l_2^2m_3) - \text{Cos}[\theta_1](\frac{1}{12}\text{Sin}[\theta_1](-\text{Cos}[\theta_1]\text{Sin}[\theta_1] + \text{Cos}[\theta_1]\text{Sin}[\theta_1](\text{Cos}[\theta_3]\text{Sin}[\theta_2] - \text{Cos}[\theta_2]\text{Sin}[\theta_3])^2)a_2^2k_3 - \frac{1}{12}\text{Cos}[\theta_1](\text{Cos}[\theta_1]^2 + \text{Sin}[\theta_1]^2(\text{Cos}[\theta_3]\text{Sin}[\theta_2] - \text{Cos}[\theta_2]\text{Sin}[\theta_3])^2)a_2^2k_3))\ddot{\theta_3} + \frac{1}{8}(\text{Sin}[2(\theta_2 + \theta_3)]l_2^2m_3\dot{\theta}_1^2 + \text{Sin}[2\theta_2]l_1^2(m_2 + 4m_3)\dot{\theta}_1^2 + 4l_1l_2m_3(\text{Sin}[2\theta_2 + \theta_3]\dot{\theta}_1^2 - \text{Sin}[\theta_3]\dot{\theta}_3(2\dot{\theta}_2 + \dot{\theta}_3))) + (g * 1/2 * m_3 * l_2 * \text{Cos}[\theta_2 + \theta_3] + g(m_3 + 1/2 * m_2)l_1 * \text{Cos}[\theta_2])$$

(5.47)

$$\tau_3 = (\text{Sin}[\theta_1](\frac{1}{12}\text{Sin}[\theta_1](\text{Sin}[\theta_1]^2 + \text{Cos}[\theta_1]^2(\text{Cos}[\theta_3]\text{Sin}[\theta_2] - \text{Cos}[\theta_2]\text{Sin}[\theta_3])^2)l_2^2m_3 - \frac{1}{12}\text{Cos}[\theta_1](-\text{Cos}[\theta_1]\text{Sin}[\theta_1] + \text{Cos}[\theta_1]\text{Sin}[\theta_1](\text{Cos}[\theta_3]\text{Sin}[\theta_2] - \text{Cos}[\theta_2]\text{Sin}[\theta_3])^2)l_2^2m_3) - \text{Cos}[\theta_1](\frac{1}{12}\text{Sin}[\theta_1](-\text{Cos}[\theta_1]\text{Sin}[\theta_1] + \text{Cos}[\theta_1]\text{Sin}[\theta_1](\text{Cos}[\theta_3]\text{Sin}[\theta_2] - \text{Cos}[\theta_2]\text{Sin}[\theta_3])^2)l_2^2m_3 - \frac{1}{12}\text{Cos}[\theta_1](\text{Cos}[\theta_1]^2 + \text{Sin}[\theta_1]^2(\text{Cos}[\theta_3]\text{Sin}[\theta_2] - \text{Cos}[\theta_2]\text{Sin}[\theta_3])^2)l_2^2m_3))\ddot{\theta_1} + ((\frac{1}{2}\text{Cos}[\theta_2 + \theta_3]l_2(\text{Cos}[\theta_2]l_1 + \frac{1}{2}\text{Cos}[\theta_2 + \theta_3]l_2) + \frac{1}{2}\text{Cos}[\theta_1]^2\text{Sin}[\theta_2 + \theta_3]l_2(\text{Sin}[\theta_2]l_1 + \frac{1}{2}\text{Sin}[\theta_2 + \theta_3]l_2) + \frac{1}{2}\text{Sin}[\theta_1]^2\text{Sin}[\theta_2 + \theta_3]l_2(\text{Sin}[\theta_2]l_1 + \frac{1}{2}\text{Sin}[\theta_2 + \theta_3]l_2))m_3 + \text{Sin}[\theta_1](\frac{1}{12}\text{Sin}[\theta_1](\text{Sin}[\theta_1]^2 + \text{Cos}[\theta_1]^2(\text{Cos}[\theta_3]\text{Sin}[\theta_2] - \text{Cos}[\theta_2]\text{Sin}[\theta_3])^2)l_2^2m_3 - \frac{1}{12}\text{Cos}[\theta_1](-\text{Cos}[\theta_1]\text{Sin}[\theta_1] + \text{Cos}[\theta_1]\text{Sin}[\theta_1](\text{Cos}[\theta_3]\text{Sin}[\theta_2] - \text{Cos}[\theta_2]\text{Sin}[\theta_3])^2)l_2^2m_3) - \text{Cos}[\theta_1](\frac{1}{12}\text{Sin}[\theta_1](-\text{Cos}[\theta_1]\text{Sin}[\theta_1] + \text{Cos}[\theta_1]\text{Sin}[\theta_1](\text{Cos}[\theta_3]\text{Sin}[\theta_2] - \text{Cos}[\theta_2]\text{Sin}[\theta_3])^2)a_2^2k_3 - \frac{1}{12}\text{Cos}[\theta_1](\text{Cos}[\theta_1]^2 + \text{Sin}[\theta_1]^2(\text{Cos}[\theta_3]\text{Sin}[\theta_2] - \text{Cos}[\theta_2]\text{Sin}[\theta_3])^2)a_2^2k_3))\ddot{\theta_2} + (\frac{1}{3}l_2^2m_3)\ddot{\theta_3} + (\frac{1}{8}l_2m_3(\text{Sin}[2(\theta_2 + \theta_3)]l_2\dot{\theta}_1^2 + 4l_1(\text{Cos}[\theta_2]\text{Sin}[\theta_2 + \theta_3]\dot{\theta}_1^2 + \text{Sin}[\theta_3]\dot{\theta}_2^2))) + (g * 1/2 * l_2 * \text{Cos}[\theta_2 + \theta_3])$$

(5.48)

5.5 Chapter Conclusion

In this chapter an underactuated tendon driven manipulator design incorporated with energy saving bistable coupling mechanism based actuation approach is presented. The manipulator design is with the capability of reducing the driving joint torques. All the heavy components used for the joint actuation such as motors, coupling mechanisms and gear trains are installed at the base of proposed design. This aids the reduction of driving joint torques of the proposed manipulator. The design also utilises reduced number of motors for the actuation incorporating the underactuation concept in the manipulator. In addition, the proposed manipulator design incorporates bistable coupling mechanism based actuation approach that minimises energy consumption during joint actuation. The significance of the design in minimising joint torques and energy consumption during joint actuation are analysed experimentally. The experimental studies conducted to analyse the performances of manipulator in reducing driving joints torques and the energy consumption are presented in the Chapter 6.

Furthermore, detailed derivation of dynamic model and the kinematics of the manipulator design are presented in this chapter. The forward kinematics of the manipulator is computed using the Denavit-Hartenberg convention. Similarly, for the development of the dynamic model of the manipulator Lagrange approach is used. The dynamic model is developed to facilitate the study of torque requirement of the proposed manipulator design. The developed dynamic model is with the capability of predicting torque requirement of individual joints during the manipulator motion.

Chapter 6

Performance Analysis of Underactuated Tendon Driven Manipulator in Reducing Driving Joint Torques and Energy Consumption

6.1 Introduction

In Chapter 5, underactuated tendon driven manipulator design incorporated with bistable coupling mechanisms is presented. The operation principle and development of dynamic model of the proposed manipulator are also discussed in detail under Chapter 5. The purpose of this chapter is to study the driving joint torques and energy consumption of the manipulator design introduced in Chapter 5. Experimental investigations are performed to examine the driving joint torques at each joint to illustrate the significance of the manipulator design in reducing driving joint torques. Section 6.2 includes the results obtained for the driving joint torques and the validation of the dynamic model developed.

Furthermore, experimental studies are conducted to analyse the energy consumption of the proposed manipulator during joint actuation using both conventional and the proposed bistable coupling mechanism based actuation approaches. The experimental investigations performed to analyse the significance of the proposed actuation approach are discussed under Section 6.3. The results obtained for the energy consumption analysis are presented in Section 6.3.2. Finally, Section 6.5 presents the conclusion of the chapter.

6.2 Experimental Study of Driving Joint Torques of the Proposed Manipulator

In this section the driving joint torques of the proposed manipulator are analysed. Validation of the dynamic model developed for the proposed manipulator is also performed under this section. The analysis was conducted to examine the driving joint torques of the proposed manipulator while performing its motion. In this study, joint motions are performed according to the joint trajectories provided via the two motors incorporated in the design. During joint motion, the real time angular position data of the joints are obtained from incremental rotary encoders (Kubler incremental rotary encoder) fixed at each joint. The angular position data acquired from encoders are transmitted to a computer via an Arduino microcontroller for the analysis. Thereafter, angular velocity and angular acceleration of each joint motion are computed using the respective angular position data. Finally, utilising the experimental data driving joint torques are obtained in the proposed manipulator. Furthermore, the driving joint torques are also computed for the conventional manipulator design (motors are installed at each degree of freedom for the actuation) with equivalent design parameters. The dimensions, material properties, degrees of freedom and the structure aspects of the conventional manipulator design used for the comparison are equivalent to the proposed design. In the conventional design driving joint torques are obtained considering the conventional industrial manipulator joint motor weight and motor torque capacity. Specification of motors used for the actuation of conventional manipulator design with equivalent design parameters as the proposed manipulator are obtained from the motor specification datasheets of conventional industrial manipulator. Utilizing these real motor specification details of the conventional

manipulator, driving joint torque values of the conventional manipulator design are computed via simulation. The driving joint torques values of both proposed and the conventional manipulator designs are analysed in the study to highlight the effectiveness of the proposed design in minimising driving joint torques. The results obtained are presented in the following Section 6.2.1.

6.2.1 Results and Discussion

The experimental results obtained for the driving joint torques of the proposed manipulator are illustrated under this section. Furthermore, the theoretical results obtained from the dynamic model developed in Section 5.4.1 are also presented. Theoretical results are computed utilising the Mathematica software. The joint torque values obtained for the proposed manipulator and for the conventional manipulator are shown in Figures 6.4 - 6.6. The joint angle trajectories followed by first joint is defined as shown in Equation (6.1). Similarly Equation (6.2) presents the joint angle trajectory followed by joint two and joint three .

$$Trajectory_{1} = \frac{e^{0.2t}}{10} \tag{6.1}$$

$$Trajectory_{2} = \frac{e^{0.3t}}{140} \tag{6.2}$$

Figure 6.1 shows joint trajectory followed during the motion of first joint of the manipulator. Similarly Figure 6.2 illustrates the joint trajectory followed by both second and the third joint of the manipulator.

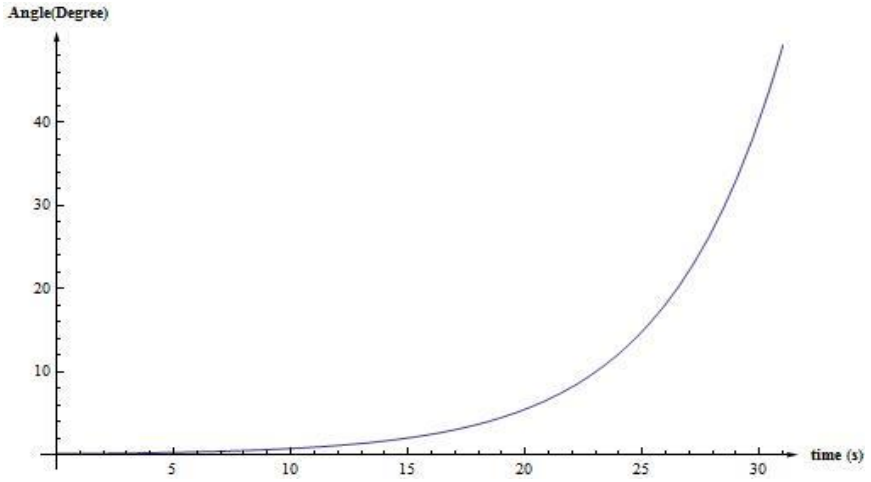

Figure 6.1: Joint angle trajectory of joint one (θ_1) of the manipulator.

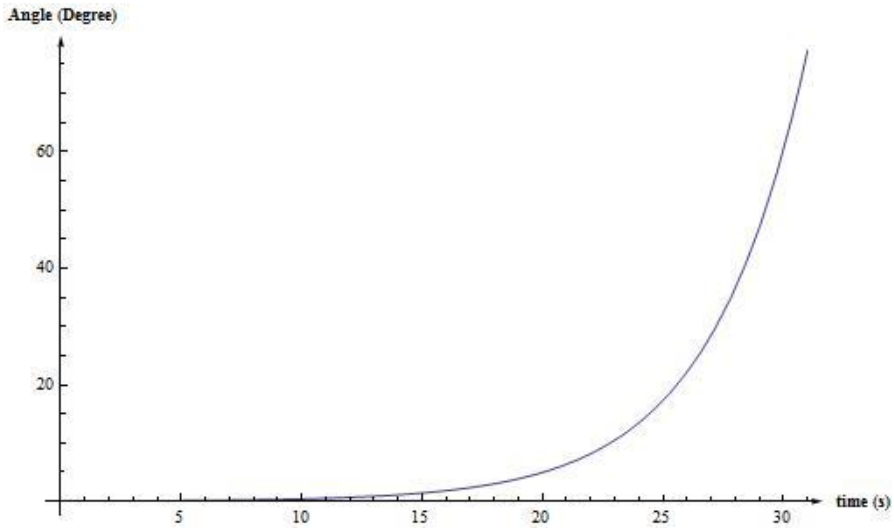

Figure 6.2: Joint angle trajectory of the second and third joints (θ_2 and θ_3) of the manipulator.

Figure 6.3 presents the theoretical and experimental torque (τ_1) of the first joint of the proposed manipulator. Similarly, Figure 6.4 shows the torque (τ_2) requirement for the actuation of second joint of the proposed design. Finally, Figure 6.5 represents the theoretical and experimental torque (τ_3) required for the motion of the third joint. Moreover, the driving joint torques of the first joint, second joint and third joint of conventional manipulator design with equivalent

design parameters are also presented in Figure 6.3, Figure 6.4 and Figure 6.5 respectively.

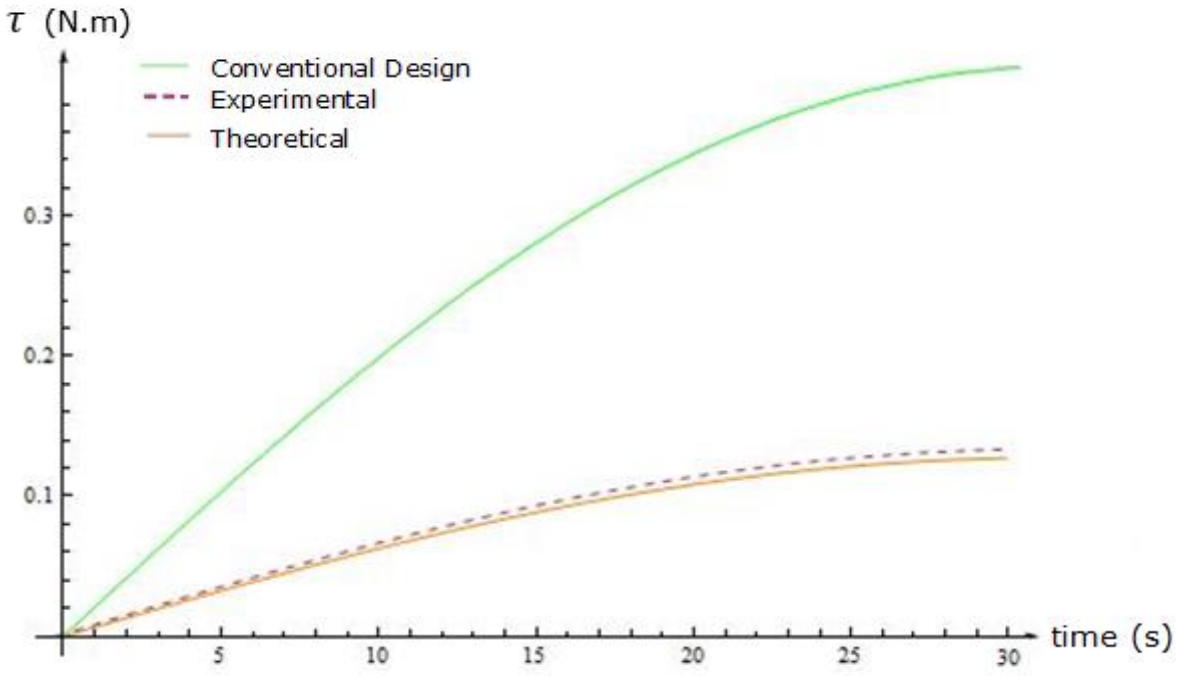

Figure 6.3: Driving joint torque values of joint one (τ_1) in both conventional and proposed manipulator.

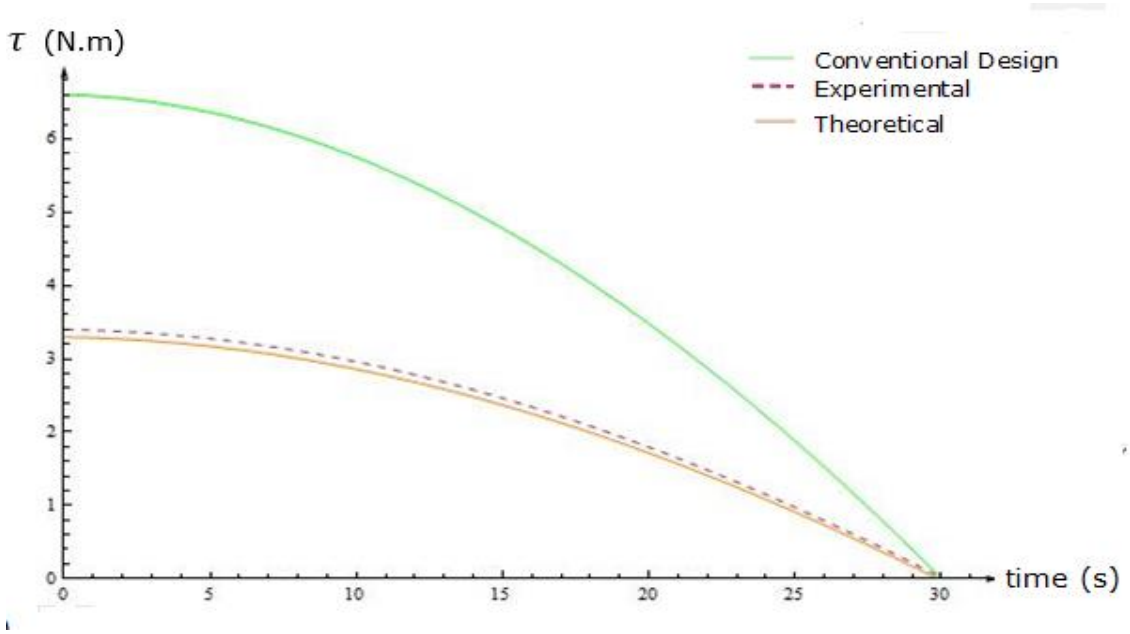

Figure 6.4: Driving joint torque values of the second joint (τ_2) in both conventional and proposed manipulator.

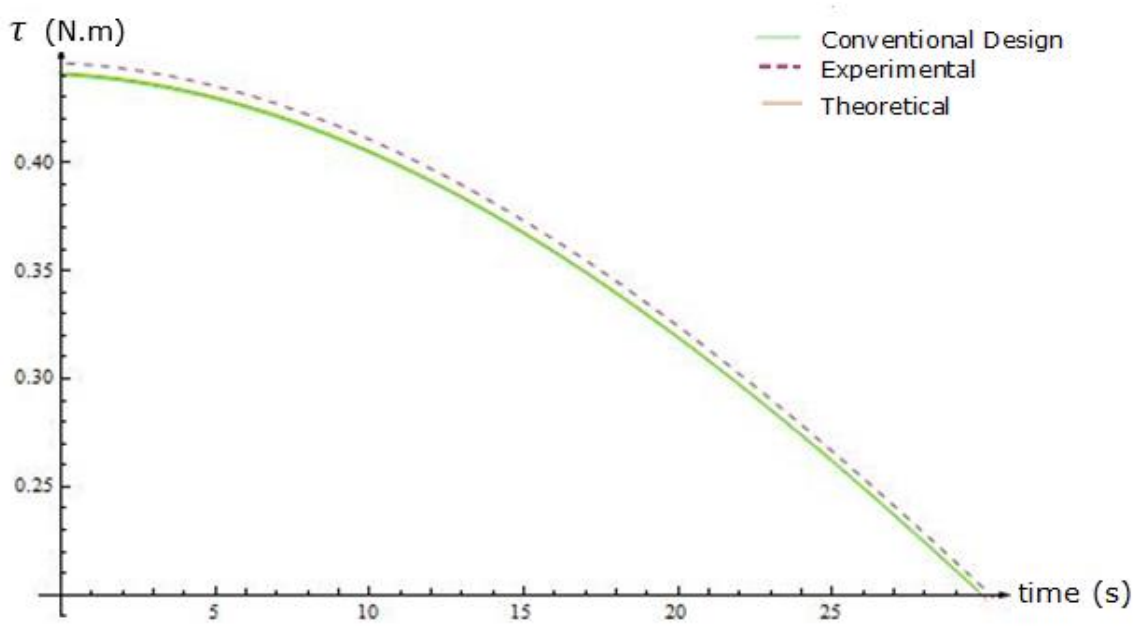

Figure 6.5: Driving joint torque values of the third joint (τ_3) in both conventional and proposed manipulator.

The manipulator joint motion was performed for a period of 30 seconds during the experimental analysis. From Figure 6.4, it could be observed that the maximum theoretical joint torque and the maximum experimental joint torque recorded during analysis are 0.1225 Nm and 0.1366 Nm respectively. The percentage difference between the theoretical and experimental results is about 10.3%. Similarly, the percentage difference between the experimental to theoretical joint torque values of the second and the third joint of the proposed manipulator are 12% and 11.6%. Therefore, the theoretical model illustrates a good correlation with the experimental results.

Conventional manipulator design contains motors at each joint and in the proposed design motors are located at the base of the manipulator. Conventional design is with equivalent design parameter as the proposed design. However traditional manipulator design incorporates servo motors at each joint, where these servo motor mass ranges from 2.5 kg to 5.5 kg [216]. Thus, conventional

manipulator contains additional mass at each link apart from its link mass with comparison to the proposed manipulator. As such conventional design has an additional weight (weight of motor) at each joint apart from its link weight that contributes for the increment of joint torque. Therefore, the driving joint torques required are reduced in the proposed design as no motors are installed at the manipulator joints. The results shown in Figures 6.3 – 6.5 also demonstrate that the proposed design has reduced the driving joint torque values with comparison to the conventional manipulator design (motors are installed at each degree of freedom for the actuation).

From Figure 6.5 it could be observed that driving torques at the third joint are equivalent in both conventional and proposed design. A conventional 3 DOF manipulator design with similar design parameter as the proposed manipulator utilises three motors for the joint actuation. These three motors are installed at the first, second and third joints of the conventional manipulator. Thus, no motors are installed beyond the third joint which contributes for the increment of driving joint torque. As such, driving joint torque at the third joint is only contributed by the mass of second link, which is analogues to the proposed manipulator design. Therefore, in both conventional and proposed manipulator designs equivalent joint torques could be observed at the third joint. From the torque results obtained, it is apparent that the proposed design is with the capability of reducing driving joint torques.

6.3 Experimental Investigation on the Energy Consumption of the Proposed Manipulator Incorporating Energy Saving Actuation Approach

Initially in Section 6.2 significance of the proposed design in minimising driving joint torques are analysed. Thereafter effectiveness of the design in reducing the energy consumption during the join actuation is investigated experimentally under this section. As stated previously, proposed manipulator design incorporates a bistable coupling mechanism for the actuation of the joints. The detailed design and the operation principle of the bistable coupling mechanism is discussed in the Chapter 4. Electromagnetic clutches have been widely employed in underactuated systems. However, electromagnetic clutch uses electrical energy throughout the operation to maintain the engaged state of the clutch. As such, additional energy is required for the electromagnetic clutches integrated in the design apart from the energy required for the motors. The proposed manipulator utilises bistable coupling mechanism based actuation approach in the design, as the bistable mechanism can sustain the engaged state during operation without the consumption of electric energy. Therefore, no additional energy is utilised by the coupling mechanism during the actuation of the manipulator link. Thus, the energy usage of manipulator could be minimised by implementing a coupling mechanism that uses less energy. The significances of the actuation approach implemented in the proposed manipulator design in reducing the energy consumption is examined experimentally. The setup used for the experimental analysis and results obtained are presented in detail under this Section 6.3.1 and Section 6.4.2 respectively.

6.3.1 Experiment Methodology

The energy utilisation of the proposed design during joint motion was investigated to identify effectiveness of the actuation method implemented in proposed manipulator. For the analysis, current and voltage usage of the motor and the bistable coupling mechanism were monitored independently throughout link motion. The experimental setup used for the analysis is shown in the Figure 6.6. Current usage is measured using an ACS756 Hall effect sensor as presented in Figure 6.6. The real time current measurement data obtained through sensor was transmitted to a computer for the analysis via an Arduino microcontroller. In the experimental analysis current consumption was monitored during the actuation of the second and third joint of the manipulator, where bistable coupling mechanism are used for the joint motion. Link motion was controlled by engaging and disengaging of the bistable mechanism. The manipulator initiates link motion with the engaging of the mechanism. Similarly, the link movement is stopped by disengaging the bistable coupling mechanism. An angle of 130 degrees and 150 degrees of motion were performed by the first and the second link of the manipulator during the experimental analysis respectively. The current and voltage usage of the motor and the bistable coupling mechanism were monitored independently, while performing link motion in a provided joint trajectory. Furthermore, energy consumption of the proposed manipulator design was also examined integrating the conventional actuation approach. As stated previously, electromagnetic clutches are utilised as the coupling device in the conventional actuation approach. Therefore, the analysis was performed replacing the bistable coupling mechanism with the electromagnetic clutch (Warner Electric electromagnetic clutch). The experimental conditions and other factors such as link motion

trajectories remained the same in the analysis of comparing the energy consumption of both bistable coupling mechanism and conventional electromagnetic clutch.

.

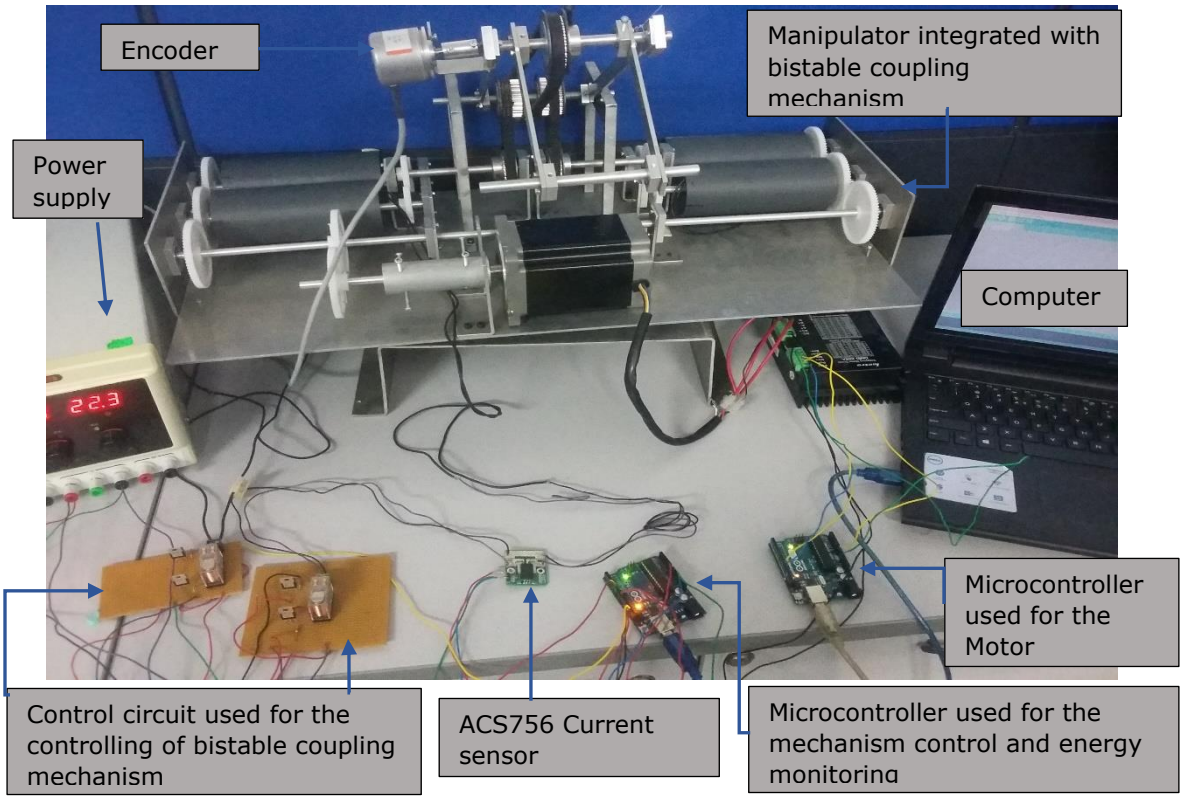

Figure 6.6: The experimental setup used for the measurement of current cosumption of the proposed actuation approach implimented on the manipulator.

6.3.2 Results and Discussion

The energy consumption results obtained during the actuation of the proposed manipulator with implementation of both actuation methods namely bistable coupling mechanism base actuation method and the conventional electromagnetic clutch base actuation approach are presented in this section. The current utilisation of each component used for the actuation is monitored during the motion of the manipulator links and is presented as follows. Initially, current

consumption of the bistable coupling mechanism and the motor were measured during the motion of first link from time of engagement to the disengagement of the coupling mechanism. The current consumption results obtained are shown in Figure 6.7. Similarly, current utilisation of bistable coupling mechanism and the motor were also measured during the motion of second link and the results are presented in Figure 6.8. Sections indicated as A_1 and A_2 in the Figure 6.7 and Figure 6.8 illustrate the current consumption of the motor and the bistable coupling mechanism during the motion of the manipulator link 1 and link 2 respectively.

After monitoring the current consumption of the manipulator integrating bistable coupling mechanism current usage of manipulator integrating conventional actuation method (electromagnetic clutch) was monitored. In this analysis commercial electromagnetic clutch (Warner company Electric electromagnetic clutch) with equivalent specifications as the proposed bistable coupling mechanism is used for the experimental studies. The current consumption results are obtained experimentally in the study for the conventional actuation approach installing a commercial electromagnetic clutch (Warner Electric electromagnetic clutch) to the proposed manipulator design. The current usage of the motor and the electromagnetic clutch were measured from the time of engagement to the disengagement of the clutch during the motion of first link. The results are shown in the Figure 6.9. Correspondingly, current consumption of electromagnetic clutch and the motor were measured independently during the motion of second link and it is illustrated in Figure 6.10. Sections specified as B_1 and B_2 in the Figure 6.9 and Figure 6.10 illustrate the current consumption of the motor and the electromagnetic clutch during the motion of the manipulator link one and link two respectively.

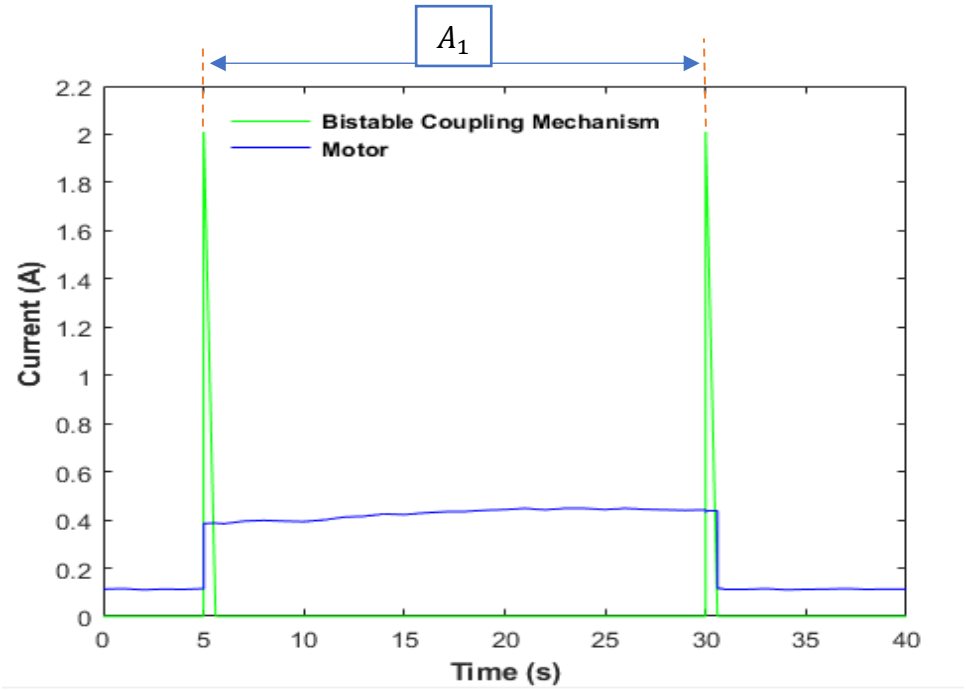

Figure 6.7: Current consumption in the motor and the bistable coupling mechanism during motion of Link 1.

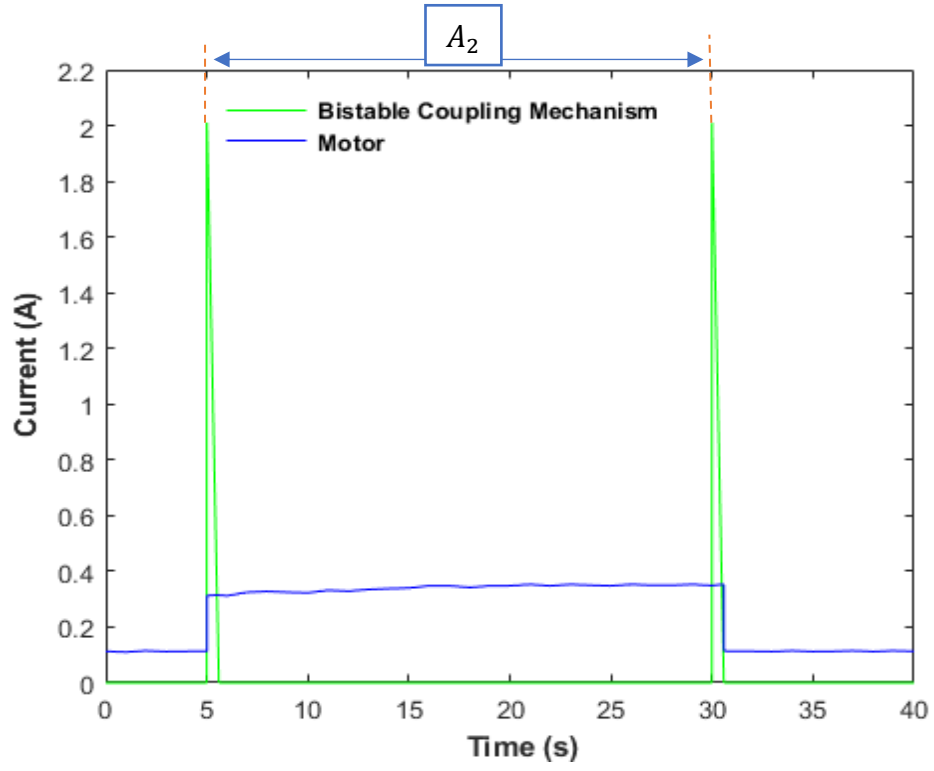

Figure 6.8: Current consumption in the motor and the bistable coupling mechanism during motion of link 2.

Moreover, the combined current usage of the motor and the respective actuation approach during the motion of the links were examined. Initially the total current consumed by the motor and the proposed actuation approach during the motion of link one were obtained. Thereafter, the total current consumed by the motor and the conventional actuation approach were also obtained performing an equivalent link motion. Similar analysis was conducted during the motion of the second link using both proposed and the conventional actuation approaches. The total current consumption results obtained for the link one and link two are as shown in Figure 6.11 and Figure 6.12 respectively.

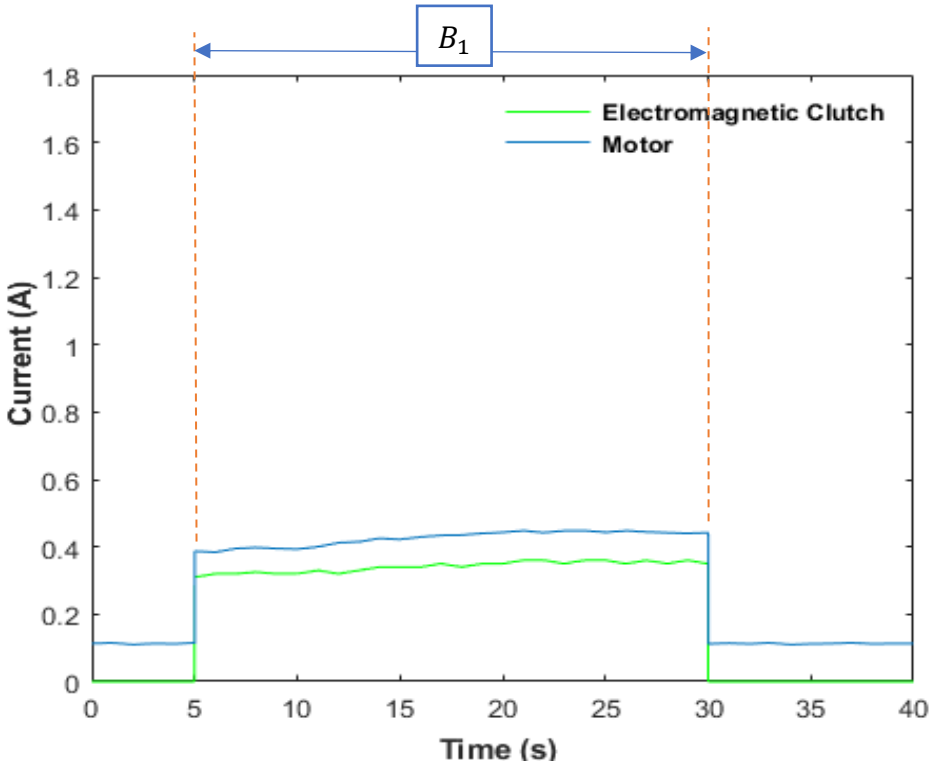

Figure 6.9: Current consumption in the motor and the electromagnetic clutch during motion of link 1.

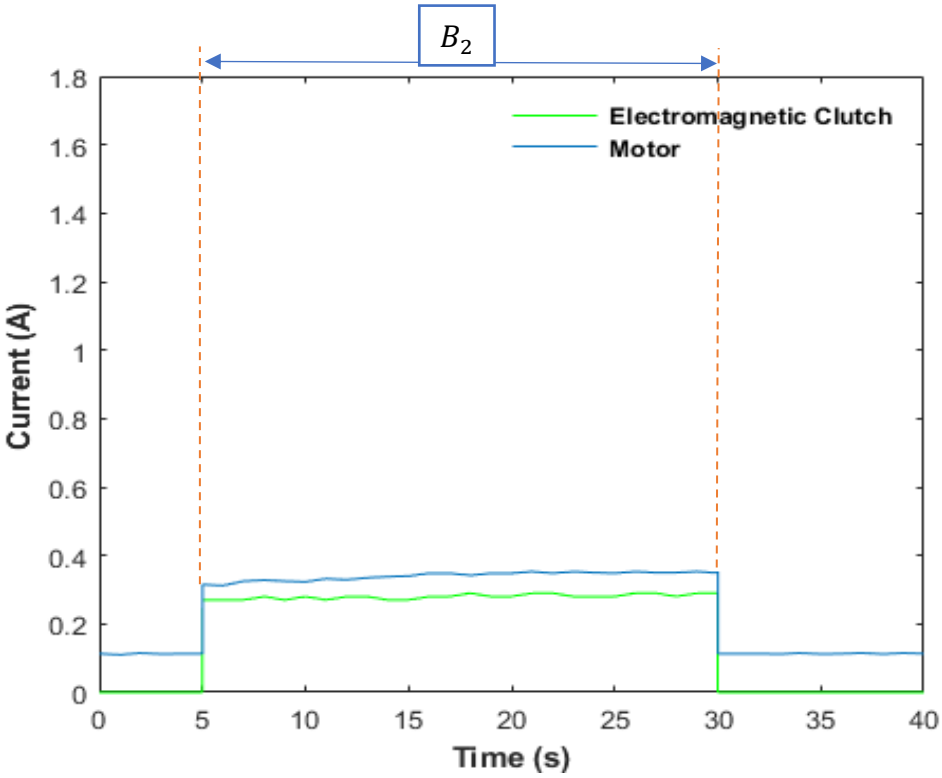

Figure 6.10: Current consumption in the motor and the electromagnetic clutch during motion of link 2.

The experiment analysis was conducted on both actuation approaches namely the conventional method which incorporates electromagnetic clutches with the motor and the bistable mechanism based actuation to compare the energy saving aspect during the motion of the manipulator. The results obtained using proposed actuation approach implemented in manipulator design shows that there was no additional current utilisation observed during the motion of the manipulator link apart from the motor current. It could be noted from Figure 6.7 and Figure 6.8, additional current was recorded only during two instances namely engaging and disengaging of the bistable coupling mechanism during the actuation of manipulator link.

Figure 6.11 and Figure 6.12 illustrate the total current utilised by motor and the respective actuation components. These graphs are obtained by combining

the motor current consumption results and respective coupling mechanism consumption results acquired independently during the motion of the manipulator. From the Figure 6.11 and Figure 6.12 it could be observed that the combined current consumption of motor and the coupling mechanism during the motion of the manipulator are equivalent to the current consumption results of the motor shown in Figures 6.7 and Figure 6.8. Therefore, it is apparent that the actuation method incorporated in the manipulator design has utilised additional energy only during the engaging and disengaging of the mechanism. Thus, in the bistable coupling mechanism based actuation method no energy is consumed during the motion of the manipulator link.

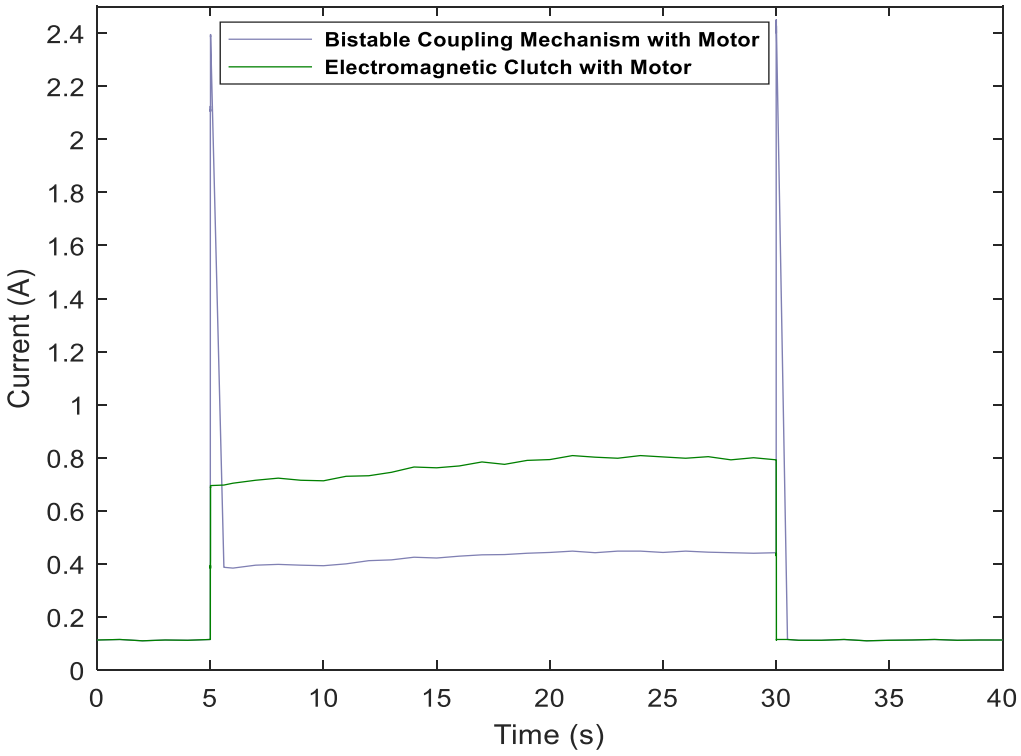

Figure 6.11: Total current consumption in proposed actuation approach and the conventional actuation approach during motion of link 1.

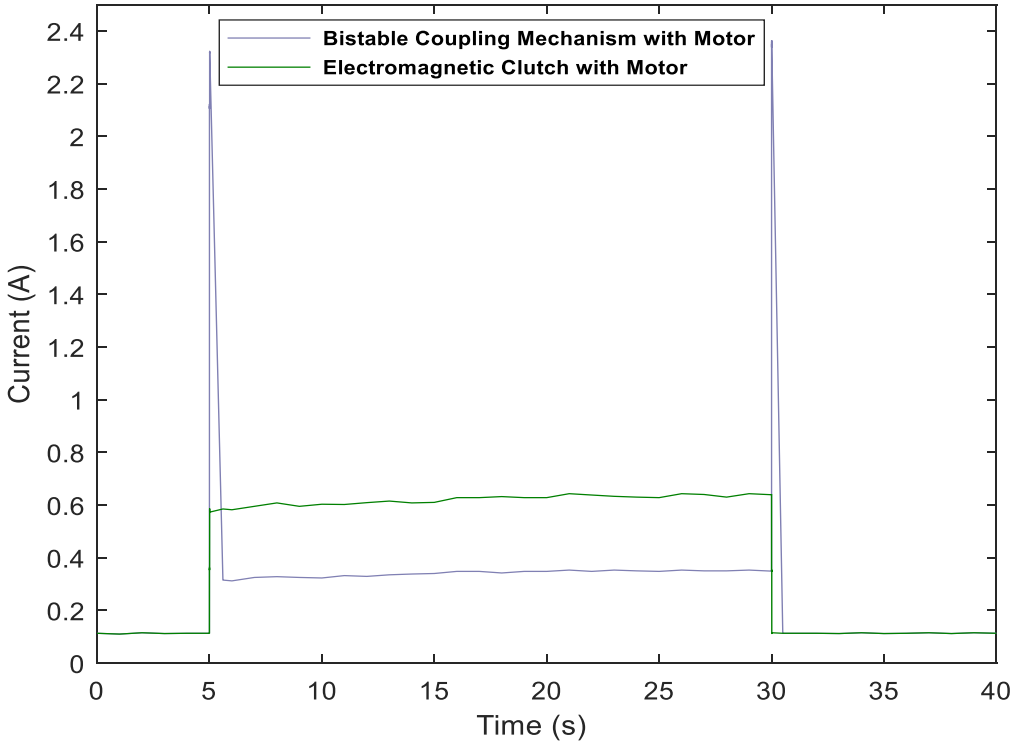

Figure 6.12: Total current consumption in proposed actuation approach and the conventional actuation approach during motion of link 2.

Referring to the experimental results of the electromagnetic clutch based conventional actuation approach shown in the Figure 6.9 and Figure 6.10, it could be noted electromagnetic clutch utilises current during the motion of the manipulator. Therefore, an additional amount of current is utilised by the electromagnetic clutch during the motion of the manipulator apart from the motor current. Furthermore, Figure 6.11 and Figure 6.12 also show that the combined current consumption of motor and the electromagnetic clutch during the motion of the manipulator is greater than the current consumption results of the motor shown in Figure 6.9 and Figure 6.10. Therefore, from the experimental investigations it is apparent that the conventional electromagnetic clutch based actuation approach requires additional electrical energy apart from the energy provided to the motor to drive the manipulator link.

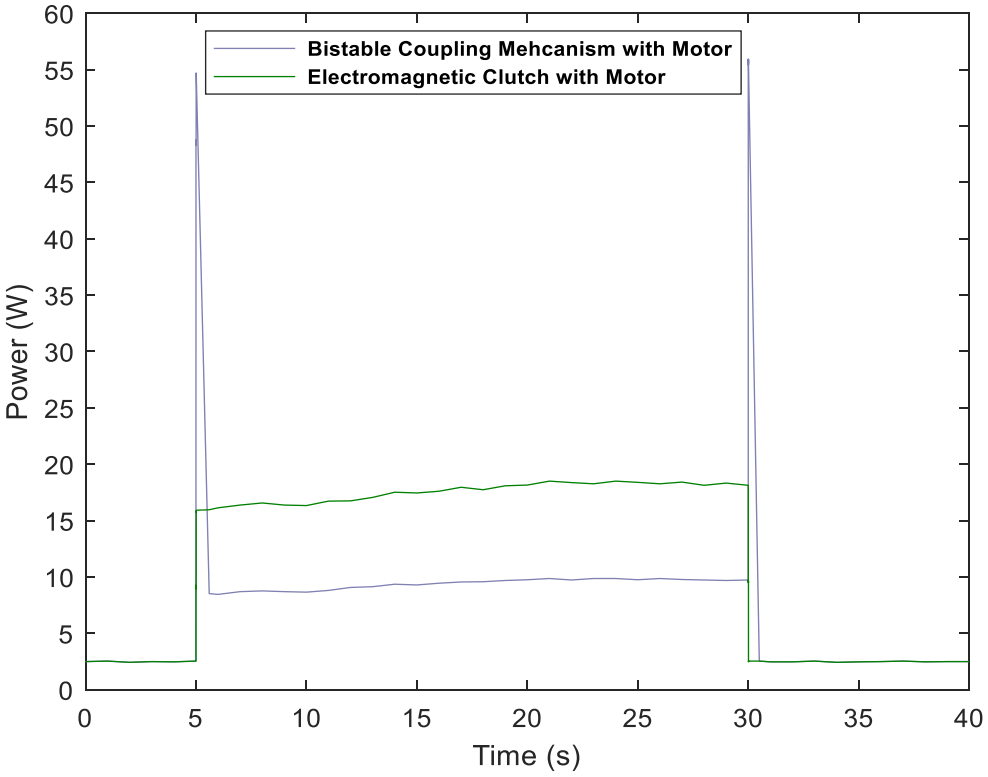

Figure 6.13: Total power consumption in proposed actuation approach and the conventional actuation approach during motion of link 1.

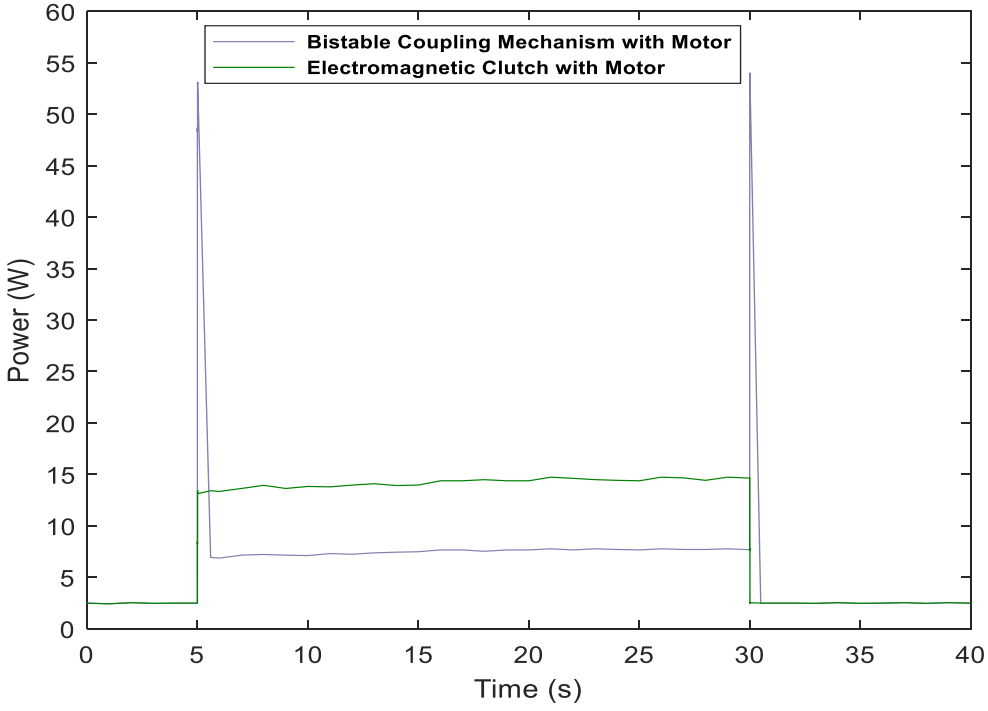

Figure 6.14: Total power consumption in proposed actuation approach and the conventional actuation approach during motion of link 2.

The total power consumption is computed during the actuation of each manipulator link using both electromagnetic clutch based conventional method and the proposed actuation approach. The results obtained for the total power utilisation during the actuation of link one and link two are illustrated in Figure 6.13 and Figure 6.14 respectively.

Furthermore, the total energy consumption during the actuation of each manipulator link is also computed with the numerical integration of electric power as follows:

$$E = \int_0^t P \, dt \tag{6}$$

Where P is the total power consumed during the motion of the links by both motor and the respective actuation component either bistable coupling mechanism or the electromagnetic clutch according to the respective approach.

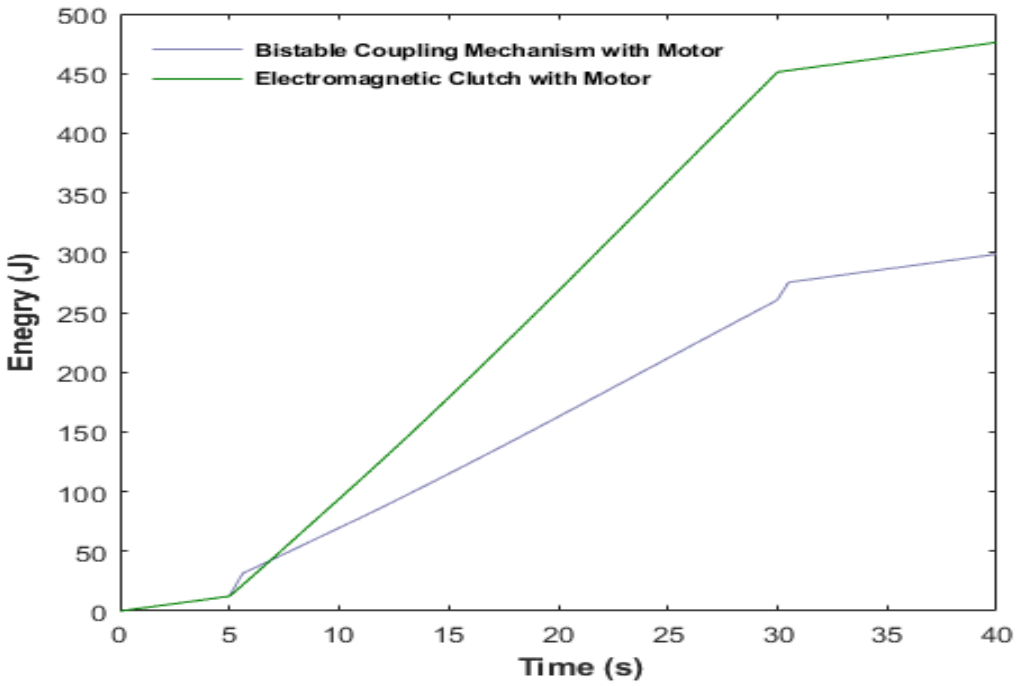

Figure 6.15: Total energy consumption in proposed actuation approach and the conventional actuation approach during motion of link 1.

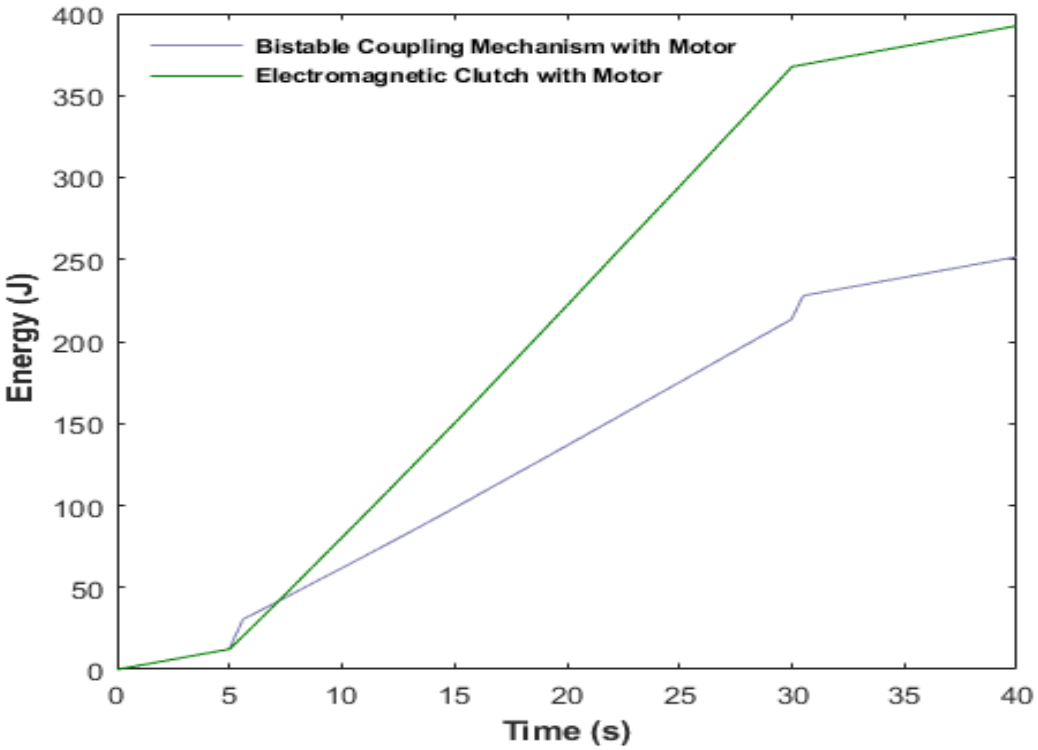

Figure 6.16: Total energy consumption in proposed actuation approach and the conventional actuation approach during motion of link 2.

The Figure 6.15 and Figure 6.16 illustrate the total energy consumption of the system during the motion of the manipulator link one and two using both actuation approaches respectively. It could be observed from the Figure 6.15 that the utilisation of energy during the motion of link one using bistable coupling mechanism based actuation approach and the conventional approach are about 298 J and 486 J respectively. Similarly, the energy usage during the actuation of second link are 251 J and 395 J using the bistable coupling mechanism based actuation approach and the electromagnetic clutch based conventional actuation approach respectively. From the Figure 6.15 and Figure 6.16 it could be noted that the bistable coupling mechanism based actuation approach has consumed about 188 J and 144 J less energy during the actuation of first and the second link with comparison to the conventional actuation approach. Therefore, its apparent from the experimental results, the actuation approach implemented in the manipulator

design is with the capability of reducing energy consumption during the joint actuation. This results due to the bistable coupling mechanism not utilising any electrical energy during the operation.

However, in the electromagnetic clutch based conventional actuation approach electrical energy is utilised to sustain the engaged state of the electromagnetic clutch throughout the operation. Thus, conventional actuation approach utilises additional energy apart from the motor energy. Therefore, even though both actuation approaches could be employed in underactuated manipulator designs, the bistable coupling mechanics based actuation approach is with the potential of minimising the energy consumption of manipulator greatly with comparison to the electromagnetic clutch based conventional actuation approach.

The studies conducted for the analysis of driving joint torques and the energy consumption of the manipulator during actuation have highlighted the significance of the proposed manipulator design in minimising both the driving joint torques and the usage of energy during joint motion. Thus, it is apparent that the proposed manipulator design is not only effective in reducing the driving joint torques but also with the capability of minimising energy consumption.

6.4 Analysation of Positioning Accuracy Performance of the Proposed Manipulator Incorporated with Energy Saving Bistable Coupling Mechanism with Reduced Motors.

In this section positioning accuracy of the proposed manipulator is analysed via simulation studies. The proposed manipulator utilizes reduced amount of motors incorporating bistable electromagnetic coupling mechanisms for the joint actuation. Simulation study is performed to examine the position accuracy of the

two actuation approaches namely motor based direct actuation and the bistable electromagnetic coupling mechanism based actuation approach. Joint motions are performed independently in provided trajectories and the end effector motion of the manipulator is analysed accordingly. The analysis performed and the results obtained are presented as follows in Section 6.4.1.

6.4.1 Results and Discussion

The accuracy of the proposed manipulator performing motion is examined and the results obtained are presented under this section. The desired position of the manipulator end effector is achieved with the movement of each joint to specific joint angles. In the simulation study manipulator joints are provided with set of joint trajectories and the motion of the end effector is analysed. The study focuses on examining the performance of the manipulator using motor based direct actuation approach and the proposed bistable coupling mechanism based underactuation approach. kinematic model developed in Section 5.3.1 is utilised in the study to identify the end effector position of the manipulator. The performance of the proposed design is examined employing two types of joint motions. Joint trajectory that increases joint angle linearly and exponentially are utilised in the study to analyse the performance. Joint angle paths used in the study are shown in Equations (6.3) to (6.8).

Linear joint trajectory equations :

$\theta_1 = 5t$ (6.3) $\theta_2 = 4t$ (6.4) $\theta_2 = 4t$ (6.5)

Exponential joint trajectory equations :

$\theta_1 = (e^{0.3t}) - 1$ (6.6) $\theta_2 = (e^{0.2t}) - 1$ (6.7) $\theta_3 = (e^{0.2t}) - 1$ (6.8)

Initially, performance of the proposed manipulator is examined performing joint motion using linear joint trajectory. Figure (6.18) and Figure (6.19) illustrate the joint motion of the manipulator using both motor based direct actuation and the bistable coupling mechanism based actuation for the two joints (θ_2 and θ_3). Joint two and joint three of the manipulator are provided with same joint trajectory. Motor based direct actuation is used for the actuation of joint one (Base joint θ_1) of the manipulator as stated in Section 5.2. Thus, no difference is observed during the actuation of joint one . Similarly, Figure (6.20) to Figure (6.22) show the manipulator end effector motion in x, y and z planes using both motor based direct actuation and bistable coupling mechanism based actuation.

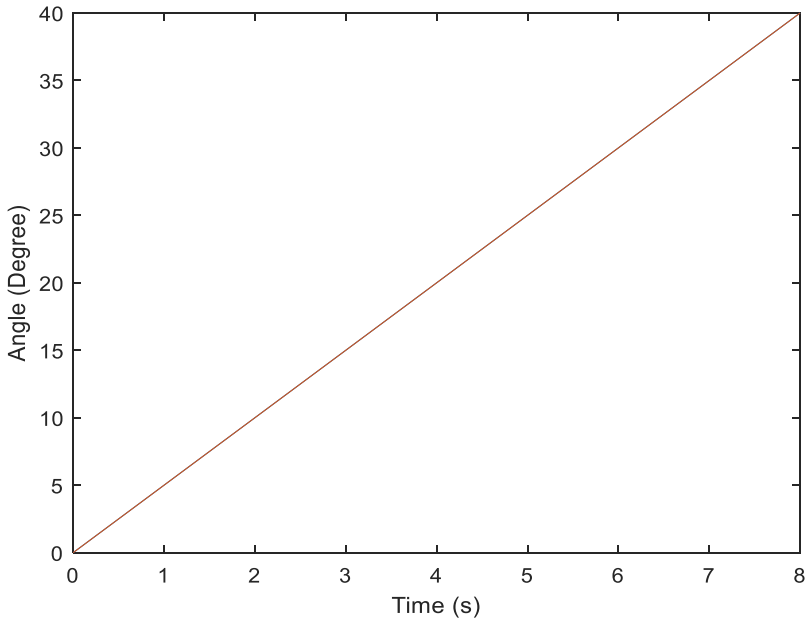

Figure 6.17: Joint one (θ_1) motion performing linear joint trajectory motion.

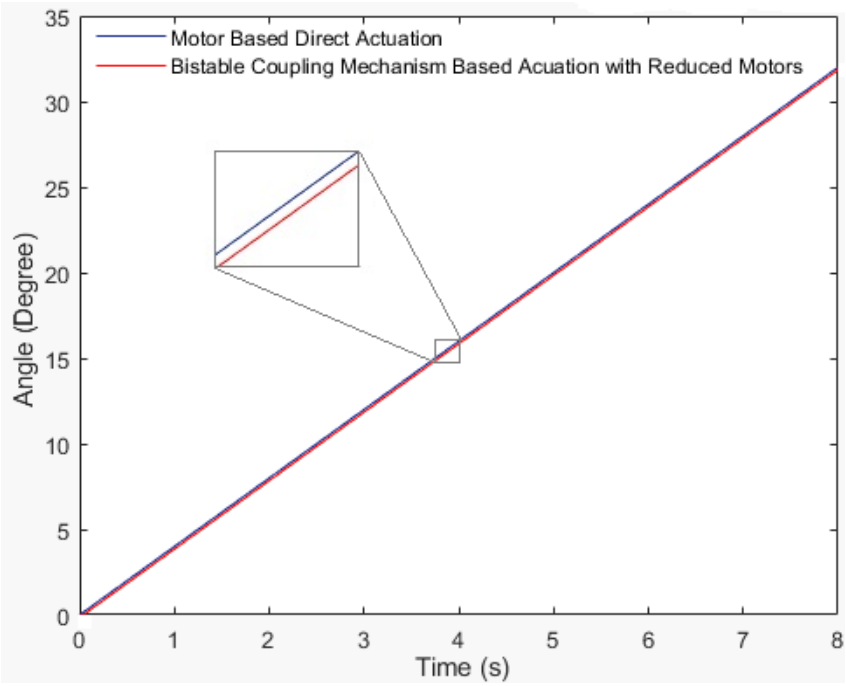

Figure 6.18: Joint two (θ_2) motion performing linear joint trajectory. using bistable coupling mechanism based actuation approach and conventional motor based direct actuation approach.

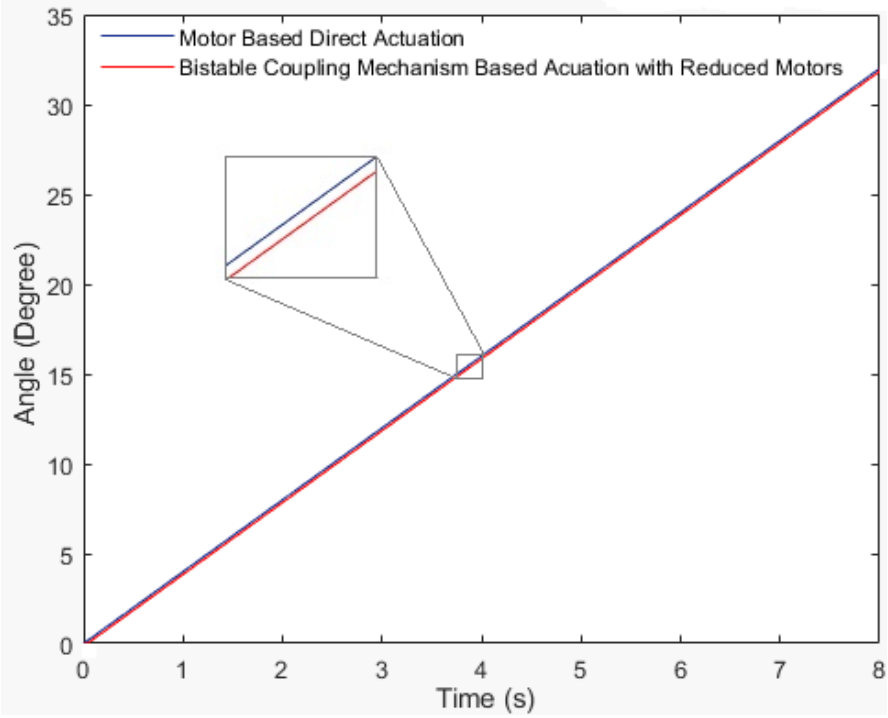

Figure 6.19: Joint two (θ_3) motion performing linear joint trajectory using bistable coupling mechanism based actuation approach and conventional motor based direct actuation approach.

It could be observed from the Figure (6.18) and Figure (6.19) that there is a difference between the motor based direct actuation and bistable coupling

mechanism based actuation in joint angle motion. In the proposed mechanism based actuation approach 0.5% of error is observed in the joint angle motion for the joint two and joint three with comparison to the conventional motor based direct actuation. This error is generated due to 12 ms time period taken for the engaging process of the bistable coupling mechanism during joint actuation. Thereafter the end effector positioning performance is analysed using bistable coupling mechanism based approach and the conventional motor based direct actuation approach. The end effector x, y and z position results obtained for the conventional motor based direct actuation are 0.2440, 0.2299 and 0.2938 respectively. The end effector x, y and z position results obtained for the bistable coupling mechanism based actuation are 0.2453, 0.2287 and 0.2923 respectively. The error recorded for positioning the end effector is about 0.5% using the bistable coupling mechanism based approach with comparison to the motor based actuation approach.

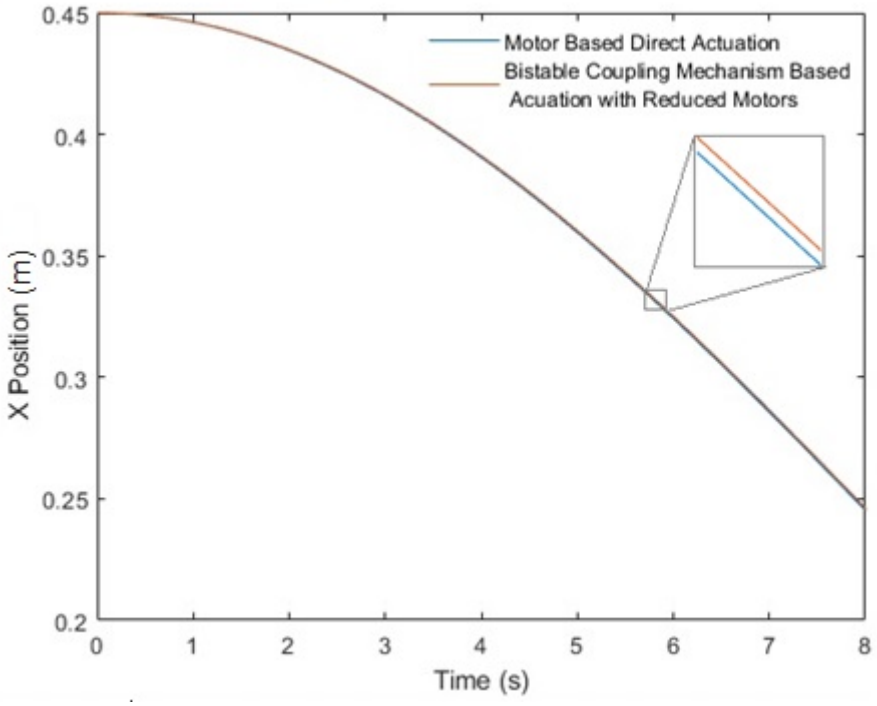

Figure 6.20: Manipulator end effector motion in x plane performing linear joint trajectory motion using bistable coupling mechanism based actuation approach and conventional motor based direct actuation approach.

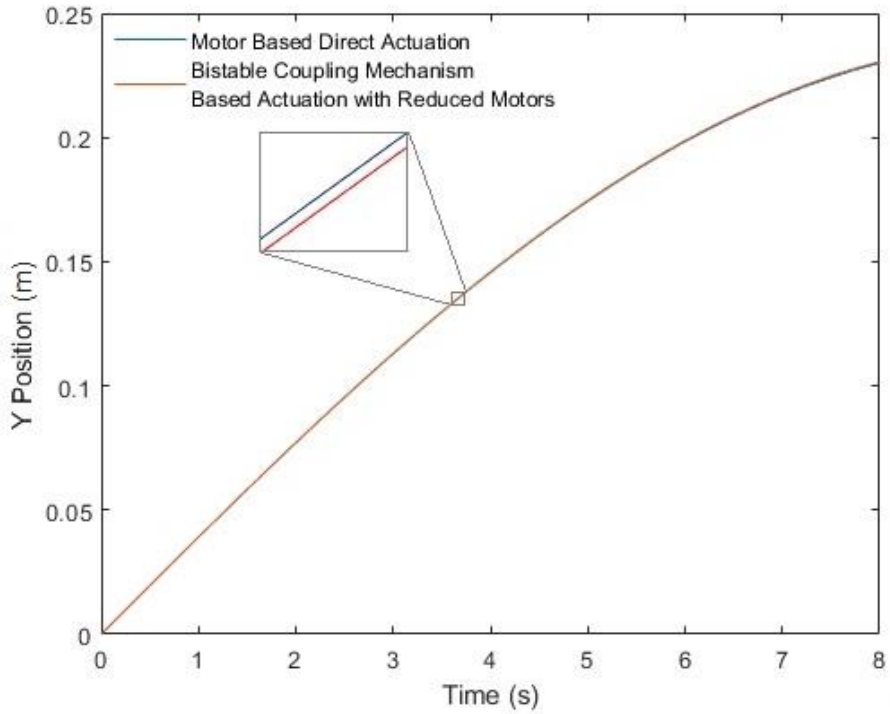

Figure 6.21: Manipulator end effector motion in y plane performing linear joint trajectory motion using bistable coupling mechanism based actuation approach and conventional motor based direct actuation approach.

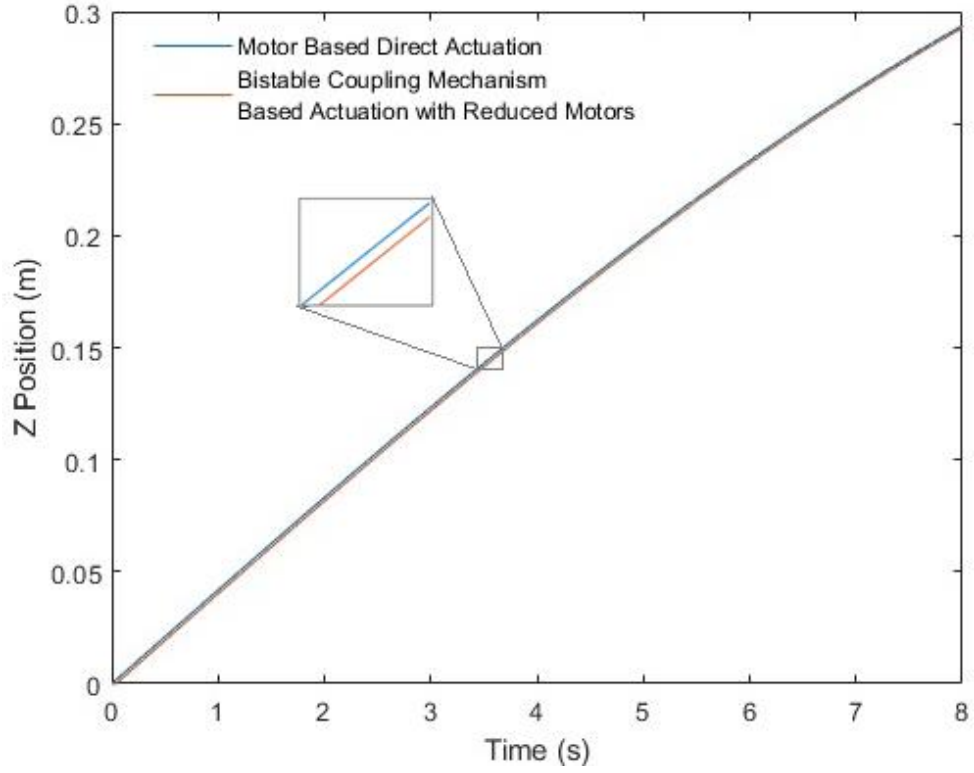

Figure 6.22: Manipulator end effector motion in z plane performing linear joint trajectory motion using bistable coupling mechanism based actuation approach and conventional motor based direct actuation approach.

Secondly, performance of the manipulator is analysed performing joint motion using exponential joint trajectory. The results obtained for the joint motion of the manipulator utilizing motor based direct actuation and the bistable coupling mechanism based actuation are illustrated in Figure (6.23) to Figure (6.25). In the proposed mechanism based actuation approach 0.6% of error is observed in joint angle motion with comparison to motor based direct actuation for the joint two and joint three.

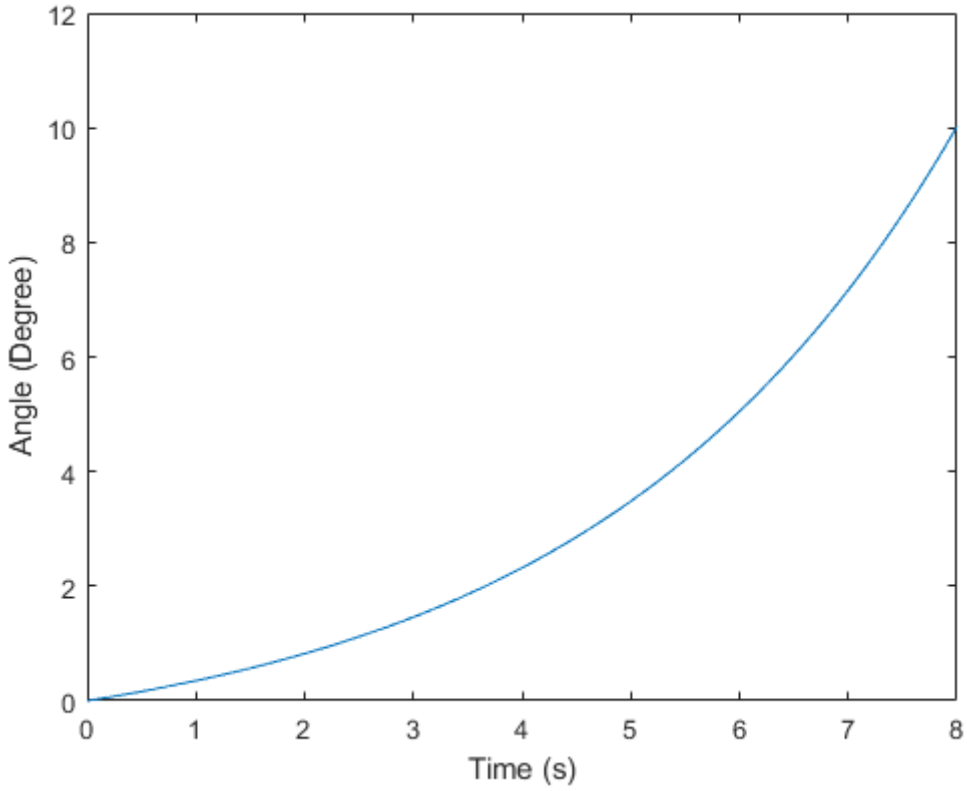

Figure 6.23: Joint one (θ_1) motion performing exponential joint trajectory.

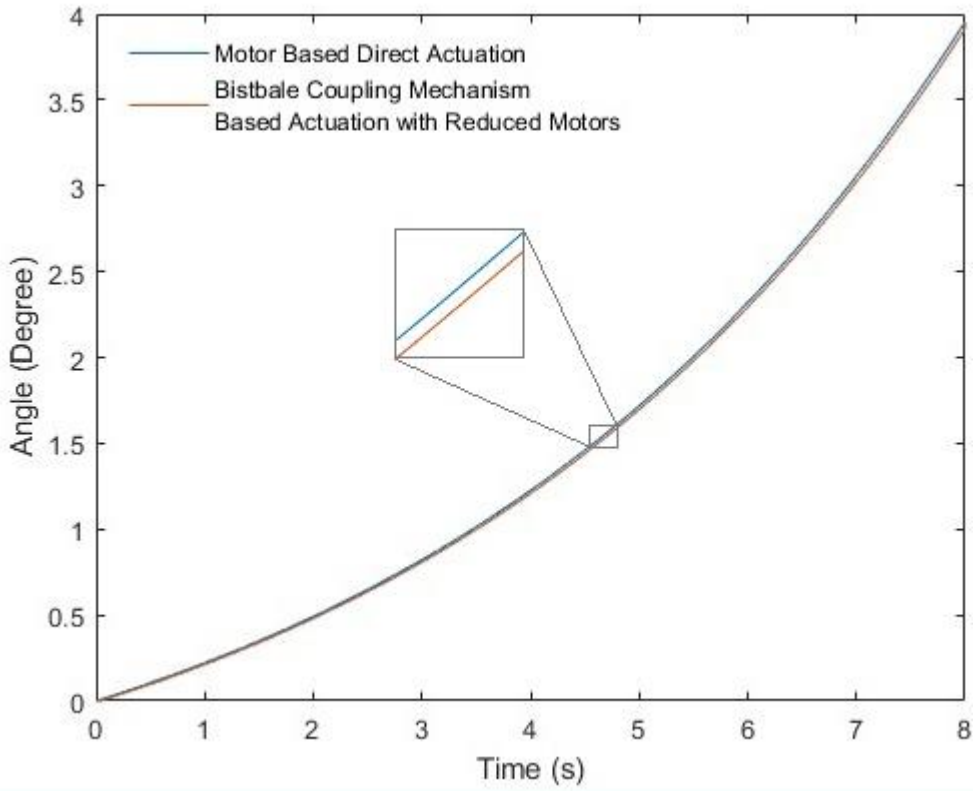

Figure 6.24: Joint two (θ_2) motion performing exponential joint trajectory using bistable coupling mechanism based actuation approach and conventional motor based direct actuation approach.

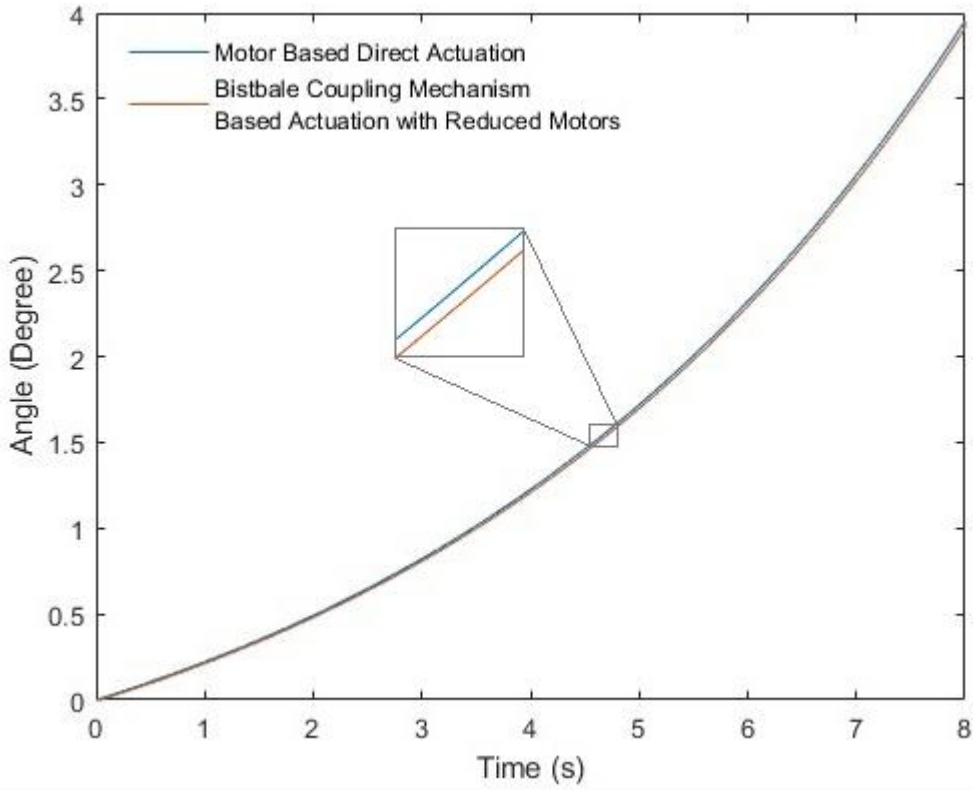

Figure 6.25: Joint two (θ_3) motion performing exponential joint trajectory using bistable coupling mechanism based actuation approach and conventional motor based direct actuation approach.

Figure (6.26) to Figure (6.28) illustrate the results obtained for the end effector positioning using both actuation approaches applying exponential joint trajectory. The end effector x, y and z position results obtained for the conventional actuation method applying exponential trajectories are 0.4383, 0.0781 and 0.0413 respectively. The end effector x, y and z position results obtained for the bistable coupling mechanism based actuation method applying exponential trajectories are 0.4410, 0.0776 and 0.0410 respectively. Results revealed that there is 0.6% error in performing end effector motion using bistable coupling mechanism based actuation approach with comparison to motor based direct actuation approach.

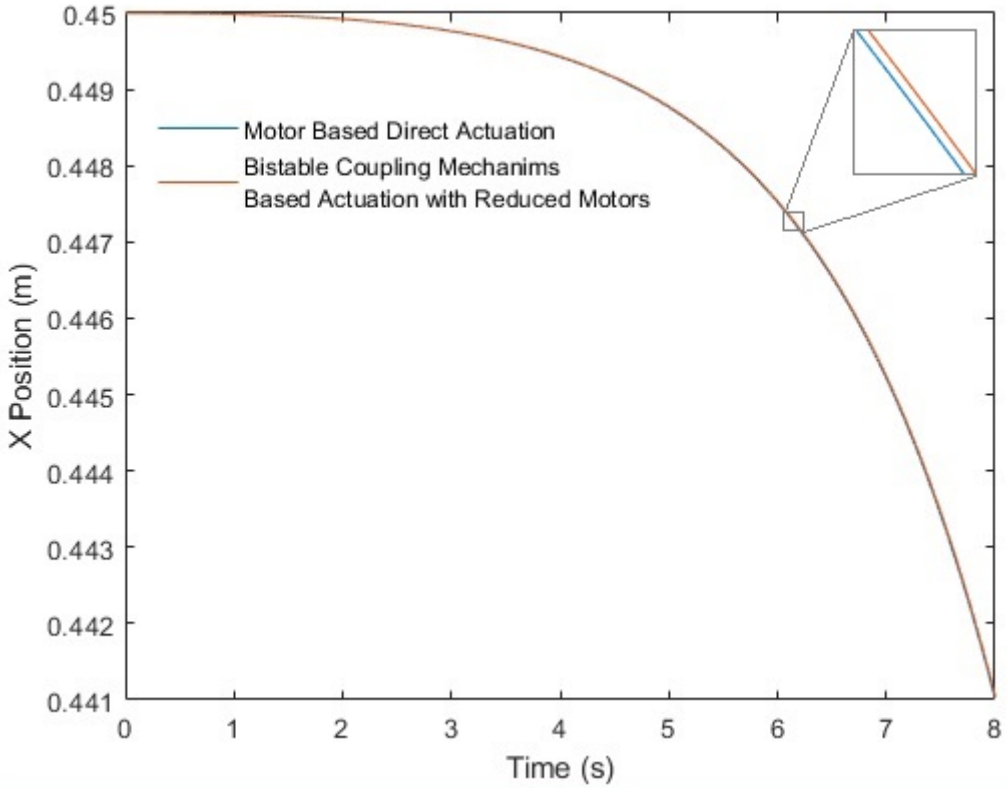

Figure 6.26: Manipulator end effector motion in x plane performing exponential joint trajectory motion using bistable coupling mechanism based actuation approach and conventional motor based direct actuation approach.

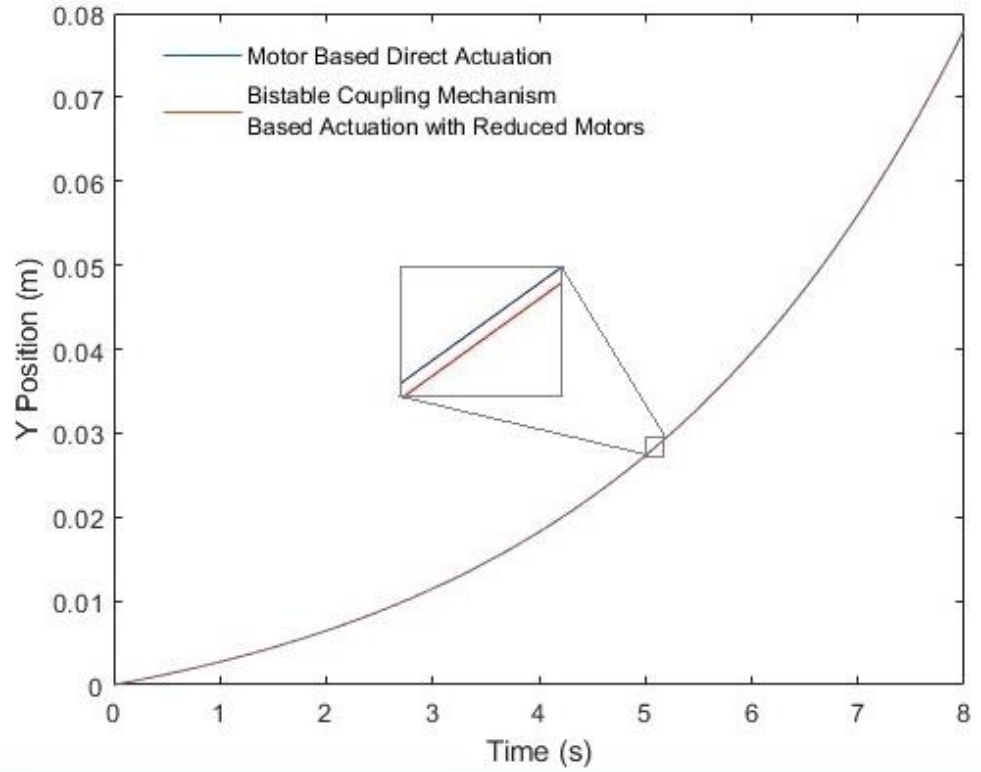

Figure 6.27: Manipulator end effector motion in y plane performing exponential joint trajectory motion using bistable coupling mechanism based actuation approach and conventional motor based direct actuation approach.

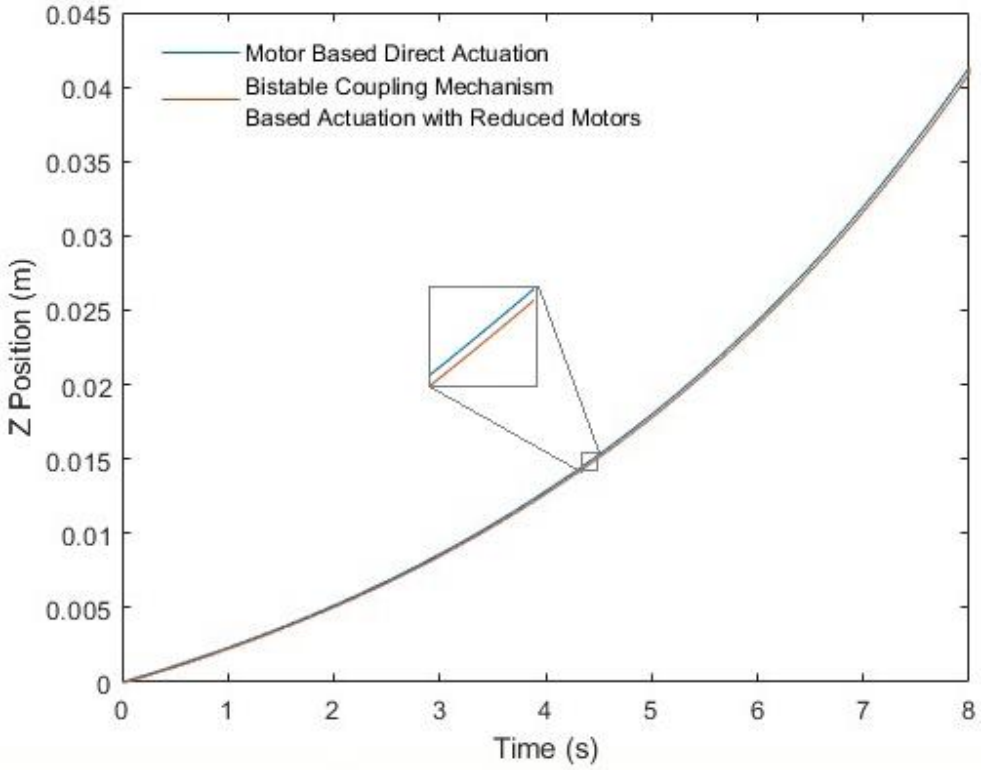

Figure 6.28: Manipulator end effector motion in z plane performing exponential joint trajectory motion using bistable coupling mechanism based actuation approach and conventional motor based direct actuation approach.

The simulation study illustrated that there is an error in positioning end effector using bistable coupling mechanism based approach with comparison to motor based direct actuation approach. However, significantly low error values are observed for the both motion scenarios examined. The error values recorded for the first and the second motion scenarios are 0.5% and 0.6% respectively. These error values recorded are less than 1% . Thus, from the simulation studies it could be observed that there is no significant effect on the accuracy of the manipulator with the implementation of bistable coupling mechanisms based actuation approach with reduced motors with comparison to the conventional motor based direct actuation.

6.5 Chapter Conclusion

In this chapter driving joint torques and the energy consumption of the proposed manipulator design are studied during the joint actuation. The effectiveness of the proposed design in reducing driving joint torques is examined via theoretical and experimental studies. Theoretical results obtained are in good agreement with the experimental results. The experimental results have highlighted the potential of the proposed manipulator design in reducing the driving joint torques with comparison to the conventional manipulator design approach.

Energy consumption during the joint actuation was examined to analyse the significance of the proposed actuation approach integrated in the manipulator. In the experimental analysis, energy usage of both conventional and proposed actuation approaches is monitored independently. The experimental results illustrate that the bistable coupling mechanism based actuation approach incorporated

in the manipulator have minimised the energy consumption by 188 J and 144 J with comparison to traditional electromagnetic clutch based actuation approach. The experimental results have highlighted the significance of the proposed actuation approach in minimising the energy consumption with comparison to the conventional actuation approach which is generally implemented in underactuated designs. Thus, due to the actuation approach implemented, proposed manipulator design is also effective in reducing energy consumption. It is apparent form the experimental studies conducted that the proposed manipulator design is not only effective in reducing the driving joint torques but also with the capability of minimising energy consumption during joint actuation.

Chapter 7

Further Enhancement of the Manipulator Design by Utilising a Single Motor for the Actuation

7.1 Introduction

In Chapter 5 a manipulator design incorporated with two motors for the joint actuation is introduced. One motor is allocated for the motion of the base joint and the other motor is used for the actuation of remaining two joints. The manipulator design presented in Chapter 5 could be further enhanced by reducing the number of motors utilised. In this chapter improved novel tendon driven manipulator model that incorporates a single motor for the joint actuation is presented. The improved model is developed following the main design concepts of the proposed developed manipulator prototype. The operation principle and detail design of the model are discussed in Section 7.2. kinematics and the dynamic model of the enhanced manipulator model are developed. The development of kinematics and dynamic model of the manipulator model are shown in Section 7.3. Furthermore, simulation studies are performed on the proposed manipulator model to highlight the effectiveness of the model in minimising driving joint torques. Section 7.4 illustrates the results obtained from the studies conducted. Finally, the chapter conclusion is drawn in Section 7.5.

7.2 Design of the Enhanced Manipulator Model

The manipulator model has four joints and a single motor is allocated for the actuation. Similar to the developed manipulator, the design uses combination of gears and tendons to transmit energy. Following the same design concept of the manipulator proposed in previous chapters, the enhanced manipulator design uses two bistable coupling mechanisms connected with gears to control the direction of motion of each link independently. One of the coupling mechanisms is dedicated for the clockwise motion of the link and the other for the anticlockwise motion. The link lengths of the proposed manipulator from link 1 to link 3 are 0.30 m, 0.20 m and 0.1 m respectively. The proposed model of the manipulator is as shown in Figure 7.1.

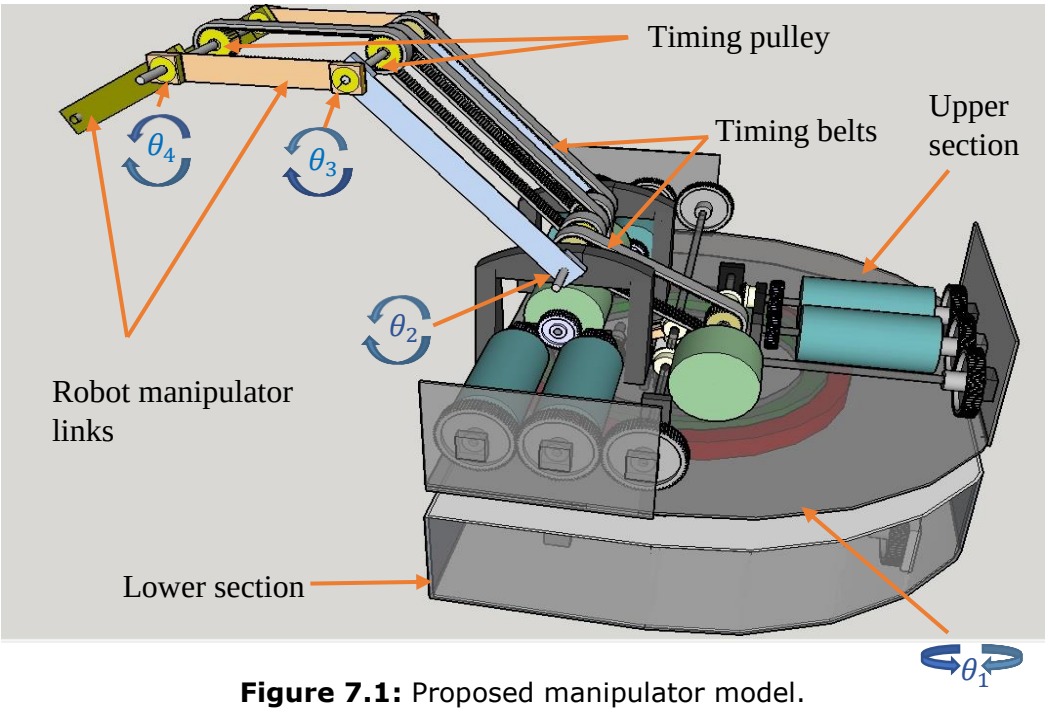

Figure 7.1: Proposed manipulator model.

The manipulator base consists of two sections, the upper section accommodates the robot structure, bistable coupling mechanisms and the gear trains. The Motor is fixed at the lower section of the basement as shown in Figure 7.1 and Figure 7.2. Apart from the motor lower section contains gear trains that distribute energy from the motor to the upper segment of the robot. The motor is connected with the main shaft and the energy is distributed from the main shaft via a series of bevel gears connected to the main shaft. Bevel gear set B is connected to the main shaft to transmit energy required for the rotation of base joint (θ_1) via secondary shaft as shown in Figure 7.2. The spur gear connected to the other end of the secondary shaft drives the two other spur gears connected with the bistable mechanism. Thereafter, bistable mechanisms transmit the energy to spur gear set A as shown in Figure 7.2 and Figure 7.3. Finally, the spur gear set A transmits energy to the spur gear C via two bevel gears and a spur gear as illustrated in Figures 7.2 and 7.3. The energy transmission path from the base motor to the joint 1 is illustrated using red colour arrows as shown in the Figure 7.3. The spur gear C is fixed to the base joint(θ_1) rotating section. Transmission of energy to the base joint is controlled by two bistable couplings. By engaging one of the bistable coupling mechanism at any instant provides the energy for the rotation of the base. The other end of the bistable coupling mechanism are connected to another set of spur gears (spur gear set A) prior to connecting to the base joint. Furthermore, the direction of rotation could be varied by coupling and decoupling the respective bistable coupling mechanisms. Moreover, same mechanism has been implemented in the remaining joints $(\theta_2, \theta_3, \theta_4)$ as well for the controlling of joint motion. The method is explained in detail as follows.

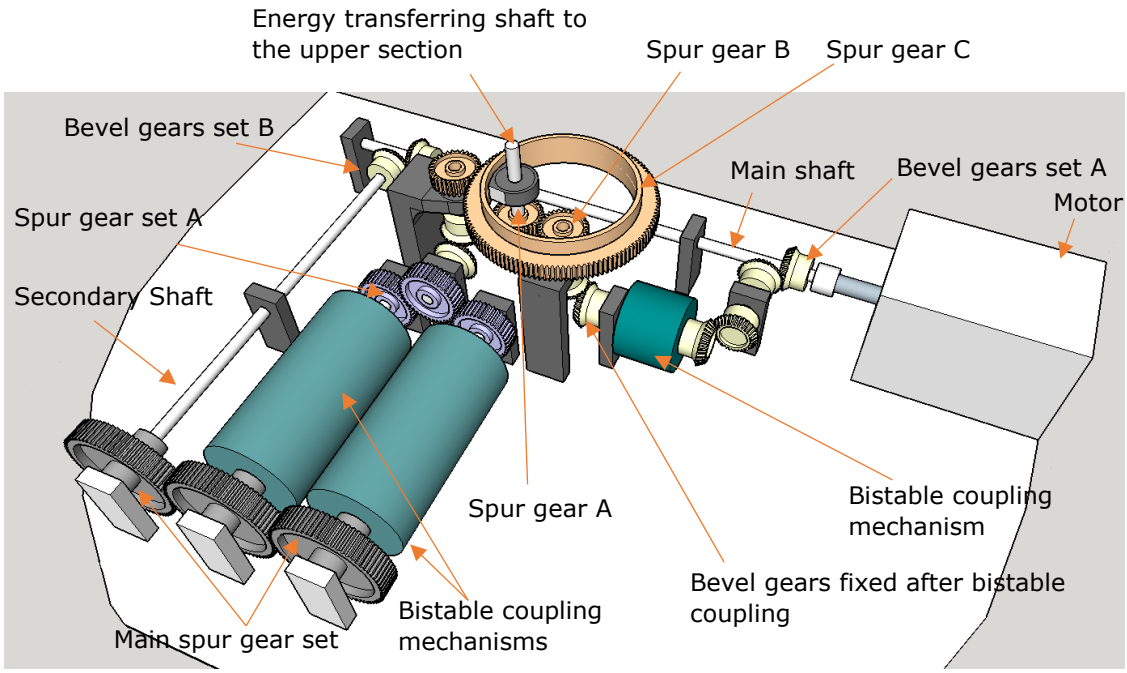

Figure 7.2: Lower section of the proposed manipulator model.

The main shaft provides energy required for the actuation of remaining joints ($\theta_2, \theta_3, \theta_4$). Using the series of connected bevel gears and spur gears energy is transmitted to the upper section of the manipulator as shown in Figure 7.4. The bevel gears set A connected with the main shaft transmit energy to the following set of bevel gears and afterwards energy is transmitted to the bistable coupling mechanism. The bistable coupling mechanism is used to control the energy transmission to the upper section. The Figure 7.4 shows the energy flow from the main shaft to the upper section. The energy transmission path from the base motor to the upper section is illustrated using red colour dash arrows similar to the Figure 7.3. The two bevel gears connected to the other end of the bistable coupling mechanism transmits energy to the spur gear B. Finally, the shaft connected with the spur gear A transmits energy to the upper segment as shown in the Figure 7.2 and Figure 7.4. The bistable mechanism is disengaged at the time base (Joint θ_1) is rotating. Therefore, when bistable mechanism is disengaged spur gear "A" connected to the shaft can rotate around spur gear "B" freely as

shown in the Figure 7.2. When bistable mechanism is engaged spur gear "B" drives the spur gear "A" so that energy will be transmitted to the upper section via the shaft. Furthermore, the bistable mechanism maintains the engage state when there is no base joint rotation.

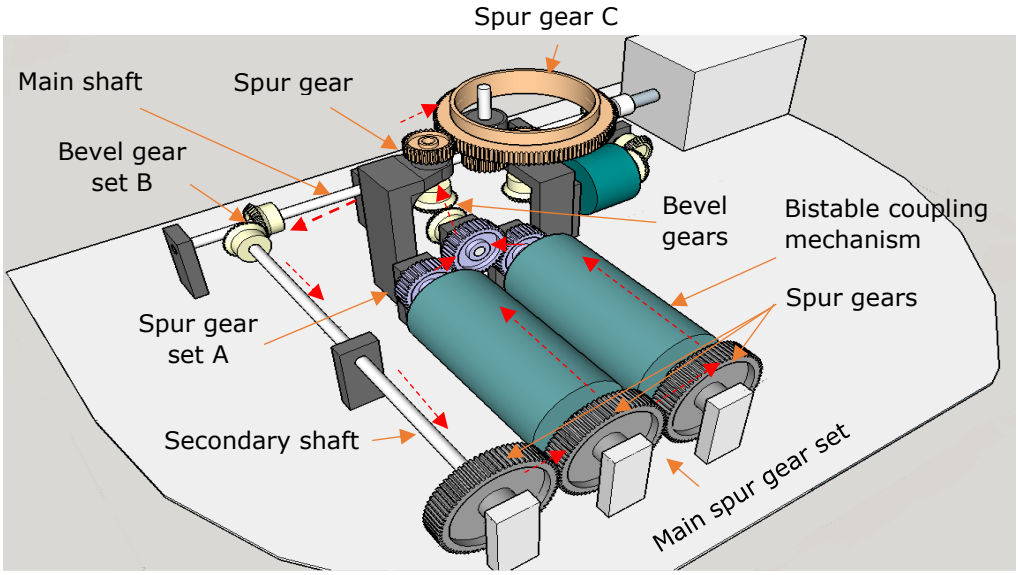

Figure 7.3: Layout of the flow of energy from the base main shaft to the joint 1 rotation.

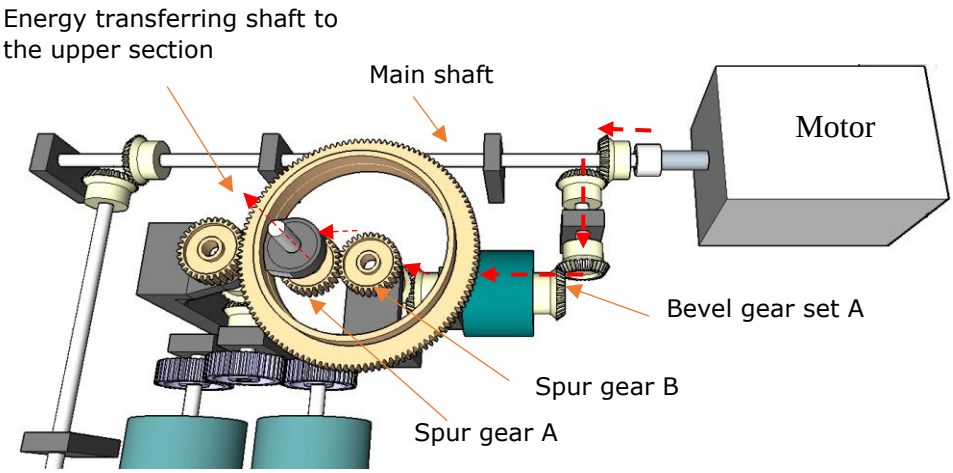

Figure 7.4: Layout of the flow of energy from the base main shaft to upper section.

The upper section of the design is described as follows. The central shaft fixed at the upper section of the base distributes energy for remaining three joints

($\theta_2, \theta_{3,} \theta_4$). Energy distribution for the link motion control is achieved by the combination of gear and bistable coupling mechanism. Furthermore, the same approach is implemented for all the three joints ($\theta_2, \theta_{3,} \theta_4$). Where each joint transmission mechanism consists of three spur gears connected in series. The spur gear connected with the central shaft transfers the motion to the other two spur gears connected with the bistable coupling mechanisms as shown in the Figure 7.5 and Figure 7.6. The motion is transmitted to two secondary shafts connected via bistable coupling mechanisms. The two driving gears (spur gears) rotates in the opposite direction to each other. Therefore, the two driven shafts connected with the also rotate in the opposite direction when the bistable coupling mechanisms are engaged. Motion of the driven shafts are controlled by coupling and decoupling the bistable coupling mechanisms. In addition, gear 1 and gear 2 are connected to the other end of the driven shafts. Finally, the gear 3 is fixed to a shaft that contains timing pulley, which transmits energy to the respective link via a time belt as shown in the Figure 7.5 and 7.6. At any instance of time one driven shaft transmits energy while other driven shaft remains stable. Hence gear 3 will be driven either by gear 2 or gear 1. Therefore, by engaging and disengaging the bistable coupling mechanism direction of rotation of gear 3 could be varied. This results the change of direction of rotation of the manipulator link.

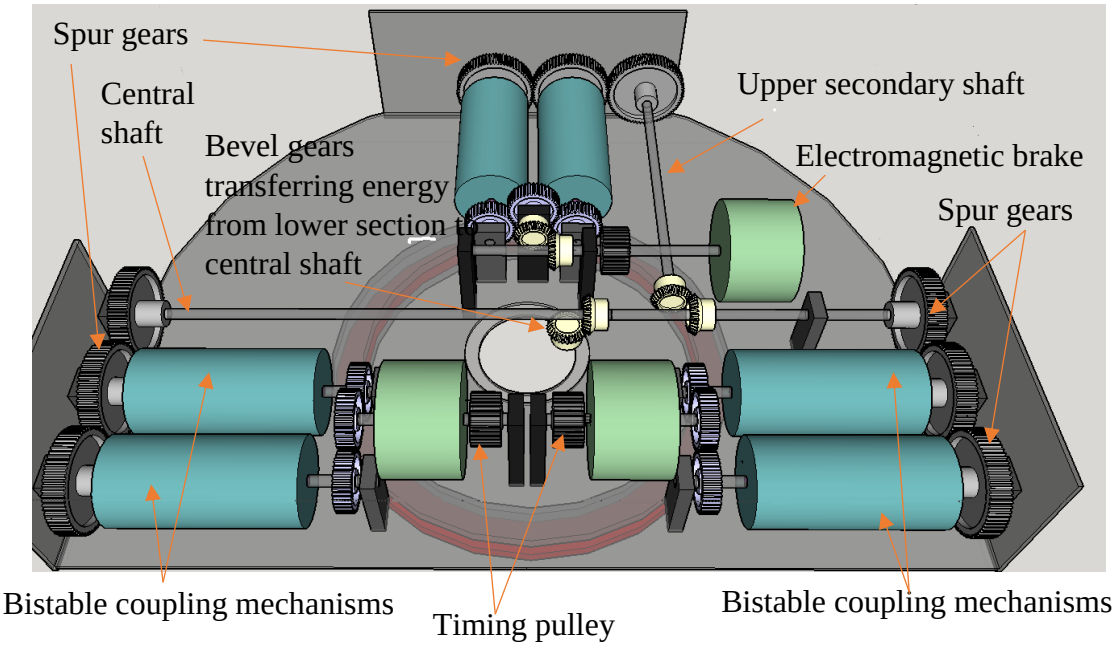

Figure 7.5: Upper section of the proposed manipulator design model.

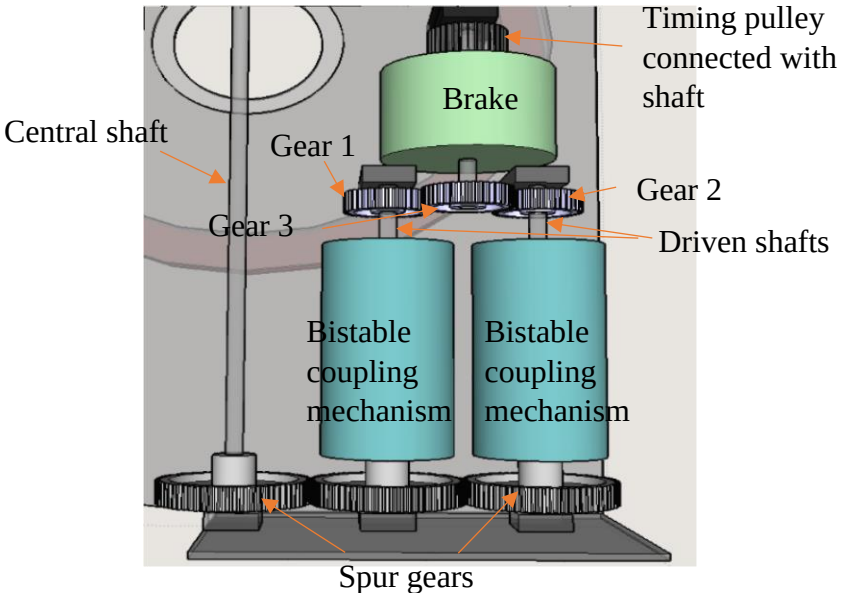

Figure 7.6: Mechanism used to transfer energy from the central shaft to each joint at upper section.

7.3 Kinematics and Dynamic Modelling of the Enhanced Manipulator Model Incorporated with Single Motor

The forward kinematics and the dynamic model development of the enhanced manipulator model incorporated with single motor are presented in this section. The computation of forward kinematics of the enhanced manipulator model is performed using Denavit-Hartenberg approach. The dynamic model of the manipulator model is developed following the Lagrange approach.

7.3.1 Forward Kinematics of the Enhanced Manipulator model Incorporated with Single Motor

In the process of computation of forward kinematics, identification of the DH parameters is essential as discussed in the previous Chapter 5. The computation of forward kinematics is discussed in detail under Chapter 5 in Section 5.3.1. Therefore, under this section main segments of the forward kinematic modelling are presented. The frames assigned for the proposed single motor tendon driven manipulator model are shown in Figure 7.7. Furthermore, the corresponding DH parameters are shown in Table 7.1 The links lengths of the manipulator link 1, link 2 and link 3 are represented by l_1, l_2 and l_3 respectively.

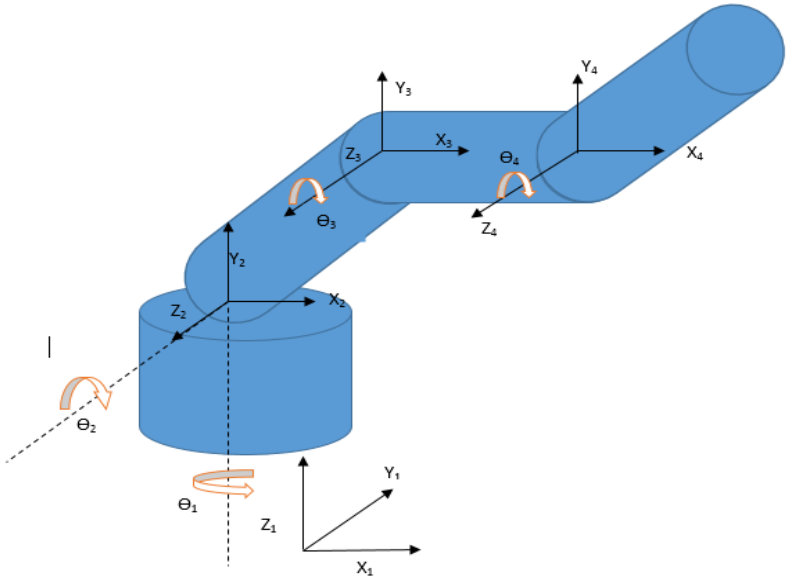

Figure 7.7: Enhanced manipulator model incorporated with single motor with DH frame assignment.

Table 7.1: The DH parameter table for the enhanced manipulator model incorporated with single motor.

i	α_i	a_i	d_i	Θ_i
1	90	0	0	Θ_1
2	0	l_1	0	Θ_2
3	0	l_2	0	Θ_3
4	0	l_3	0	Θ_4

$$ {}^{i-1}T_i = \begin{bmatrix} \cos\theta_i & -\sin\theta_i \cos\alpha_i & \sin\theta_i \sin\alpha_i & a_i \cos\theta_i \\ \sin\theta_i & \cos\theta_i \cos\alpha_i & -\cos\theta_i \sin\alpha_i & a_i \sin\theta_i \\ 0 & \sin\alpha_i & \cos\alpha_i & d_i \\ 0 & 0 & 0 & 1 \end{bmatrix} \quad (7.1) $$

The Equation (7.1) shows the Homogenous transformation matrix ${}^{i-1}T_i$ [200].The transformation matrices computed for each joint using the Homogenous transformation matrix shown in Equation (7.1) are as follows:

$$ {}^{0}T_{1} = \begin{bmatrix} \text{Cos}\,\theta_1 & 0 & \text{Sin}\,\theta_1 & 0 \\ \text{Sin}\,\theta_1 & 0 & -\text{Cos}\,\theta_1 & 0 \\ 0 & 1 & 0 & 0 \\ 0 & 0 & 0 & 1 \end{bmatrix} \tag{7.2} $$

$$ {}^{1}T_{2} = \begin{bmatrix} \text{Cos}\,\theta_2 & \text{Sin}\,\theta_2 & 0 & l_1\text{Cos}\,\theta_2 \\ \text{Sin}\,\theta_2 & \text{Cos}\,\theta_2 & 0 & l_1\text{Sin}\,\theta_2 \\ 0 & 0 & 1 & 0 \\ 0 & 0 & 0 & 1 \end{bmatrix} \tag{7.3} $$

$$ {}^{2}T_{3} = \begin{bmatrix} \text{Cos}\,\theta_3 & -\text{Sin}\,\theta_3 & 0 & l_2\text{Cos}\,\theta_3 \\ \text{Sin}\,\theta_3 & \text{Cos}\,\theta_3 & 0 & l_2\text{Sin}\,\theta_3 \\ 0 & 0 & 1 & 0 \\ 0 & 0 & 0 & 1 \end{bmatrix} \tag{7.4} $$

$$ {}^{3}T_{4} = \begin{bmatrix} \text{Cos}\,\theta_4 & -\text{Sin}\,\theta_4 & 0 & l_3\text{Cos}\,\theta_4 \\ \text{Sin}\,\theta_4 & \text{Cos}\,\theta_4 & 0 & l_3\text{Sin}\,\theta_4 \\ 0 & 0 & 1 & 0 \\ 0 & 0 & 0 & 1 \end{bmatrix} \tag{7.5} $$

The matrix which could be utilized to identify the end effector frame position with respective to the base frame of the proposed manipulator is written as :

$$ {}^{0}\text{T}_4 = {}^{0}T_1\ {}^{1}T_2\ {}^{2}T_3\ {}^{3}T_4 \tag{7.6} $$

Finally, the computed transformation matrix for forward kinematics model can be expressed as shown in Equation (7.7). As explained before in Section 5.2 P_y, P_x, P_z elements in the last column of the matrix (${}^{0}\text{T}_4$) provides the x, y, z

coordinates of the end effector position of the proposed single motor tendon driven manipulator model.

$$ {}^{0}\mathrm{T}_{4} = \begin{bmatrix} r_{11} & r_{12} & r_{13} & P_x \\ r_{21} & r_{22} & r_{23} & P_y \\ r_{31} & r_{32} & r_{34} & P_z \\ 0 & 0 & 0 & 1 \end{bmatrix} \quad (7.7) $$

x, y, z coordinates can be calculated separately by substituting respective joint angle values and link parameter values in to the Equation (7.8), Equation (7.9) and Equation (7.10) as given below.

$$ P_x = l_1 \cos\theta_1 \cos\theta_2 + l_3 \cos\theta_4 \cos\theta_1 (\cos\theta_2 \cos\theta_3 + \sin\theta_2 \sin\theta_3) - l_3 \sin\theta_4 \cos\theta_1 (\cos\theta_2 \sin\theta_3 - \sin\theta_2 \cos\theta_3) + l_2 \cos\theta_1 (\cos\theta_2 \cos\theta_3 + \sin\theta_2 \sin\theta_3) \quad (7.8) $$

$$ P_y = l_1 \cos\theta_2 \sin\theta_1 + l_3 \cos\theta_4 \sin\theta_1 (\cos\theta_2 \cos\theta_3 + \sin\theta_2 \sin\theta_3) - l_3 \sin\theta_4 \sin\theta_1 (\cos\theta_2 \sin\theta_3 - \sin\theta_2 \cos\theta_3) + l_2 \sin\theta_1 (\cos\theta_2 \cos\theta_3 + \sin\theta_2 \sin\theta_3) \quad (7.9) $$

$$ P_z = l_1 \sin\theta_2 + l_2 \cos\theta_2 \sin\theta_3 + l_2 \cos\theta_3 \sin\theta_2 + l_3 \cos\theta_4 \sin\theta_2 (\cos\theta_2 \sin\theta_3 + \cos\theta_3 \sin\theta_2) + l_3 \sin\theta_4 (\sin\theta_2 \sin\theta_3 + \cos\theta_2 \cos\theta_3) \quad (7.10) $$

7.3.2 Dynamic Modelling of the Enhanced Manipulator Model Incorporated with Single Motor

Lagrange dynamic modelling approach is followed in the development of dynamic model of the enhanced manipulator model. Thus, dynamic model equation of the enhanced manipulator model could be defined using Lagrange formulation as [102][205]:

$$ \mathrm{M}(q)\,\ddot{q} + \mathrm{V}(q, \dot{q}) + \mathrm{G}(q) = \tau \quad (7.11) $$

M(q), V(q, $\dot{q}$) and G (q) terms of the equation represent the mass matrix , Coriolis and centrifugal forces and the gravitational force respectively. Utilising the Equation (7.11), dynamic model equation for the enhanced manipulator model could be expressed as:

$$\begin{bmatrix}\tau_1\\ \tau_2\\ \tau_3\\ \tau_4\end{bmatrix} = \begin{bmatrix}M_{11} & M_{12} & M_{13} & M_{14}\\ M_{21} & M_{22} & M_{23} & M_{24}\\ M_{31} & M_{32} & M_{33} & M_{34}\\ M_{41} & M_{42} & M_{43} & M_{44}\end{bmatrix}\begin{bmatrix}\ddot{\theta}_1\\ \ddot{\theta}_2\\ \ddot{\theta}_3\\ \ddot{\theta}_4\end{bmatrix} + \begin{bmatrix}V_1(\theta & \dot{\theta})\\ V_2(\theta & \dot{\theta})\\ V_3(\theta & \dot{\theta})\\ V_4(\theta & \dot{\theta})\end{bmatrix}\begin{bmatrix}\dot{\theta}_1\\ \dot{\theta}_2\\ \dot{\theta}_3\\ \dot{\theta}_4\end{bmatrix} + \begin{bmatrix}G_1(\theta)\\ G_2(\theta)\\ G_3(\theta)\\ G_4(\theta)\end{bmatrix} \quad (7.12)$$

The enhanced single motor tendon driven manipulator model is with four degrees of freedom. Therefore, the mass matrix is 4x4 matrix. Where, mass matrix can be obtained from the Equation (7.13). Equation (7.14) is used for the computation of Coriolis and centrifugal forces. Finally, the gravitation force values are obtained from the Equation (7.15):

$$M(\theta) = \sum_{i=1}^{4} J_{vi}^{T} m_i J_{vi} + J_{\omega}^{T} I_i J_{\omega i} \quad (7.13)$$

$$\mathrm{V}(\theta, \dot{\theta}) = \sum_{j=1}^{n=4}\sum_{k=1}^{n=4}\left(\frac{\delta M_{ij}}{\delta \theta_k} - \frac{1}{2}\frac{\delta M_{jk}}{\delta \theta_i}\right)\dot{\theta}_j\dot{\theta}_k \quad (7.14)$$

$$\mathrm{G}(\theta) = \sum_{j=1}^{n=4} m_j g^T J_{vj}^{i} \quad (7.15)$$

Finally, derivation of the joint torque equations for individual joints are performed by compiling Equation (7.13), Equation (7.14) and Equation (7.15). The detail derivation of the dynamic model of proposed enhanced manipulator is

shown in the appendix section. The derived dynamic model joint torque equations for each joint are presented as follows:

$$\begin{aligned}\boldsymbol{\tau_1} &= 2(-3\text{Sin}[2\theta_1]\text{Sin}[2(\theta_2+\theta_3)](-1+\text{Cos}[\theta_2]l_1)l_2^2m_3 - 6\text{Cos}[\theta_2+\theta_3]\text{Sin}[2\theta_1](-1+\\ &\text{Cos}[\theta_2]l_1)l_2(2\text{Sin}[\theta_2]l_1+\text{Sin}[\theta_2+\theta_3]l_2)m_3 + 4(4\text{Cos}[\theta_2]^2l_1^2m_2 + \text{Cos}[\theta_2+\theta_3]^2l_2^2m_3 +\\ &12(\text{Sin}[\theta_1]^2\left(\text{Cos}[\theta_2]l_1+\frac{1}{2}\text{Cos}[\theta_2+\theta_3]l_2\right)^2 + \frac{1}{4}\text{Cos}[\theta_1]^2\text{Cos}[\theta_2]^2l_1^2(2+\text{Cos}[\theta_2+\theta_3]l_2)^2)m_3 +\\ &\text{Cos}[\theta_2+\theta_3+\theta_4]^2l_3^2m_4 + 3(2\text{Cos}[\theta_2]l_1+2\text{Cos}[\theta_2+\theta_3]l_2+\text{Cos}[\theta_2+\theta_3+\theta_4]l_3)^2m_4)) -\\ &2l_1^2(16\text{Sin}[2\theta_2](m_2+3(m_3+m_4))\dot{\theta}_1\dot{\theta}_2 + 6\text{Cos}[\theta_2]\text{Cos}[\theta_2+\theta_3]l_2^2m_3\dot{\theta}_1(\text{Cos}[\theta_2]\text{Cos}[\theta_2+\\ &\theta_3]\text{Sin}[2\theta_1]\dot{\theta}_1 + 4\text{Cos}[\theta_1]^2(\text{Sin}[2\theta_2+\theta_3]\dot{\theta}_2+\text{Cos}[\theta_2]\text{Sin}[\theta_2+\theta_3]\dot{\theta}_3)) + 3l_2m_3(8\text{Cos}[\theta_2]^2\text{Cos}[\theta_2+\\ &\theta_3]\text{Sin}[2\theta_1]\dot{\theta}_1^2 + 8\text{Cos}[\theta_1]^2\text{Cos}[\theta_2]\dot{\theta}_1((-\text{Sin}[\theta_3]+3\text{Sin}[2\theta_2+\theta_3])\dot{\theta}_2 + 2\text{Cos}[\theta_2]\text{Sin}[\theta_2+\theta_3]\dot{\theta}_3) +\\ &\text{Sin}[2\theta_1]\dot{\theta}_2((\text{Cos}[\theta_2-\theta_3]+3\text{Cos}[3\theta_2+\theta_3])\dot{\theta}_2 - 2\text{Sin}[2\theta_2]\text{Sin}[\theta_2+\theta_3]\dot{\theta}_3))) + 4(l_2^2(-24\text{Sin}[2(\theta_2+\\ &\theta_3)]m_4\dot{\theta}_1(\dot{\theta}_2+\dot{\theta}_3) + m_3(3\text{Cos}[\theta_2+\theta_3]^2\text{Sin}[2\theta_1]\dot{\theta}_1^2 + (-5+3\text{Cos}[2\theta_1])\text{Sin}[2(\theta_2+\theta_3)]\dot{\theta}_1(\dot{\theta}_2+\\ &\dot{\theta}_3) + 3\text{Cos}[2(\theta_2+\theta_3)]\text{Sin}[2\theta_1](\dot{\theta}_2+\dot{\theta}_3)^2)) - 8\text{Sin}[2(\theta_2+\theta_3+\theta_4)]l_3^2m_4\dot{\theta}_1(\dot{\theta}_2+\dot{\theta}_3+\dot{\theta}_4) -\\ &24l_2l_3m_4\dot{\theta}_1(\text{Sin}[2\theta_2+2\theta_3+\theta_4]\dot{\theta}_2+\text{Sin}[2\theta_2+2\theta_3+\theta_4]\dot{\theta}_3+\text{Cos}[\theta_2+\theta_3]\text{Sin}[\theta_2+\theta_3+\theta_4]\dot{\theta}_4)) +\\ &3l_1(-\text{Sin}[2\theta_1]l_2^2m_3(\dot{\theta}_2+\dot{\theta}_3)((\text{Cos}[\theta_2+2\theta_3]+3\text{Cos}[3\theta_2+2\theta_3])\dot{\theta}_2 + 4\text{Cos}[\theta_2]\text{Cos}[2(\theta_2+\\ &\theta_3)]\dot{\theta}_3) + 8l_2(-8m_4\dot{\theta}_1(\text{Sin}[2\theta_2+\theta_3]\dot{\theta}_2+\text{Cos}[\theta_2]\text{Sin}[\theta_2+\theta_3]\dot{\theta}_3) + m_3(2\text{Cos}[\theta_2]\text{Cos}[\theta_2+\\ &\theta_3]\text{Sin}[2\theta_1]\dot{\theta}_1^2 - 4\text{Sin}[\theta_1]^2\dot{\theta}_1(\text{Sin}[2\theta_2+\theta_3]\dot{\theta}_2+\text{Cos}[\theta_2]\text{Sin}[\theta_2+\theta_3]\dot{\theta}_3) + \text{Sin}[2\theta_1]\dot{\theta}_2(\text{Cos}[2\theta_2+\\ &\theta_3]\dot{\theta}_2 - \text{Sin}[\theta_2]\text{Sin}[\theta_2+\theta_3]\dot{\theta}_3))) - 32l_3m_4\dot{\theta}_1(\text{Sin}[2\theta_2+\theta_3+\theta_4]\dot{\theta}_2+\text{Cos}[\theta_2]\text{Sin}[\theta_2+\theta_3+\\ &\theta_4](\dot{\theta}_3+\dot{\theta}_4))))\end{aligned} \tag{7.16}$$

$$\begin{aligned}\boldsymbol{\tau_2} &= \frac{1}{48}(24g\text{Cos}[\theta_2+\theta_3+\theta_4]l_3m_4 + 120\text{Cos}[\theta_4]l_2l_3m_4 + 48l_3^2m_4 + 48l_1^2(\frac{m_2}{3} + (1-\frac{1}{8}\text{Cos}[\theta_2+\\ &\theta_3]\text{Sin}[2\theta_1]\text{Sin}[2\theta_2]l_2)m_3 + m_4) + 24g\text{Cos}[\theta_2+\theta_3]l_2(m_3+2m_4) + l_2^2((32+3\text{Sin}[2\theta_1]\text{Sin}[2(\theta_2+\\ &\theta_3)])m_3 + 96m_4) + 24g\text{Cos}[\theta_2]l_1(m_2+2(m_3+m_4)) + 3l_1(-\text{Cos}[\theta_2]\text{Sin}[2\theta_1]\text{Sin}[2(\theta_2+\theta_3)]l_2^2m_3 +\\ &32\text{Cos}[\theta_3+\theta_4]l_3m_4 + 4l_2((6\text{Cos}[\theta_3]+\text{Cos}[\theta_2+\theta_3]\text{Sin}[2\theta_1]\text{Sin}[\theta_2])m_3 + 12\text{Cos}[\theta_3]m_4)) +\\ &8\text{Sin}[2(\theta_2+\theta_3+\theta_4)]l_3^2m_4\dot{\theta}_1^2 + \text{Sin}[2(\theta_2+\theta_3)]l_2^2((5+3\text{Cos}[2\theta_1])m_3 + 24m_4)\dot{\theta}_1^2 +\\ &l_1^2\dot{\theta}_1(8\text{Sin}[2\theta_2]m_2\dot{\theta}_1 + 3(8\text{Sin}[2\theta_2]m_4\dot{\theta}_1 + m_3((8\text{Sin}[2\theta_2]+\text{Cos}[\theta_2](-\text{Sin}[2\theta_1-\theta_3]-\text{Sin}[2\theta_1-\\ &2\theta_2-\theta_3]-2\text{Sin}[\theta_3]+\text{Sin}[2\theta_1+\theta_3]+6\text{Sin}[2\theta_2+\theta_3]+\text{Sin}[2\theta_1+2\theta_2+\theta_3])l_2 +\\ &2\text{Cos}[\theta_1]^2\text{Cos}[\theta_2](\text{Sin}[\theta_2]+\text{Sin}[3\theta_2+2\theta_3])l_2^2)\dot{\theta}_1 + 2\text{Sin}[2\theta_1]\text{Sin}[2\theta_2]\text{Sin}[\theta_2+\theta_3]l_2\dot{\theta}_3))) +\\ &24l_2l_3m_4(\text{Sin}[2\theta_2+2\theta_3+\theta_4]\dot{\theta}_1^2 - \text{Sin}[\theta_4]\dot{\theta}_4(2\dot{\theta}_2+2\dot{\theta}_3+\dot{\theta}_4)) + 6l_1(-\text{Sin}[2(\theta_2+\\ &\theta_3)]l_2^2m_3\dot{\theta}_1(\text{Cos}[2\theta_1]\text{Cos}[\theta_2]\dot{\theta}_1 + \text{Cos}[\theta_1]\text{Sin}[\theta_1]\text{Sin}[\theta_2]\dot{\theta}_3) + l_2(m_3((\text{Sin}[2\theta_1-\theta_3]-\text{Sin}[2\theta_1+\theta_3]+\\ &2\text{Sin}[2\theta_2+\theta_3])\dot{\theta}_1^2 - 2\text{Sin}[2\theta_1]\text{Sin}[\theta_2]\text{Sin}[\theta_2+\theta_3]\dot{\theta}_1\dot{\theta}_3 - 4\text{Sin}[\theta_3]\dot{\theta}_3(2\dot{\theta}_2+\dot{\theta}_3)) + 8m_4(\text{Sin}[2\theta_2+\\ &\theta_3]\dot{\theta}_1^2 - \text{Sin}[\theta_3]\dot{\theta}_3(2\dot{\theta}_2+\dot{\theta}_3))) + 4l_3m_4(\text{Sin}[2\theta_2+\theta_3+\theta_4]\dot{\theta}_1^2 - \text{Sin}[\theta_3+\theta_4](\dot{\theta}_3+\dot{\theta}_4)(2\dot{\theta}_2+\dot{\theta}_3+\\ &\dot{\theta}_4))))\end{aligned} \tag{7.17}$$

$$\begin{aligned}\boldsymbol{\tau_3} &= \frac{1}{48}(8l_3m_4(3g\text{Cos}[\theta_2+\theta_3+\theta_4] + l_3(6+\text{Sin}[2(\theta_2+\theta_3+\theta_4)]\dot{\theta}_1^2) + 3l_1(\text{Cos}[\theta_3+\theta_4] +\\ &\text{Cos}[\theta_2]\text{Sin}[\theta_2+\theta_3+\theta_4]\dot{\theta}_1^2 + \text{Sin}[\theta_3+\theta_4]\dot{\theta}_2^2)) + l_2^2(24m_4(4+\text{Sin}[2(\theta_2+\theta_3)]\dot{\theta}_1^2) + m_3(32 +\\ &3\text{Sin}[2\theta_1]\text{Sin}[2(\theta_2+\theta_3)] + (5+3\text{Cos}[2\theta_1])\text{Sin}[2(\theta_2+\theta_3)]\dot{\theta}_1^2 + 6\text{Cos}[\theta_1]^2\text{Cos}[\theta_2]^2\text{Sin}[2(\theta_2+\\ &\theta_3)]l_1^2\dot{\theta}_1^2 - 3\text{Sin}[2(\theta_2+\theta_3)]l_1(\text{Cos}[\theta_2]\text{Sin}[2\theta_1] + 2\text{Cos}[2\theta_1]\text{Cos}[\theta_2]\dot{\theta}_1^2 - \text{Sin}[2\theta_1]\text{Sin}[\theta_2]\dot{\theta}_1\dot{\theta}_2))) +\\ &6l_2(m_3(4g\text{Cos}[\theta_2+\theta_3] + \text{Sin}[\theta_2+\theta_3]l_1^2\dot{\theta}_1(4\text{Cos}[\theta_1]^2\text{Cos}[\theta_2]^2\dot{\theta}_1 - \text{Sin}[2\theta_1]\text{Sin}[2\theta_2]\dot{\theta}_2) +\\ &2l_1(2\text{Cos}[\theta_2]\text{Sin}[\theta_1]^2\text{Sin}[\theta_2+\theta_3]\dot{\theta}_1^2 + \text{Sin}[2\theta_1]\text{Sin}[\theta_2]\text{Sin}[\theta_2+\theta_3]\dot{\theta}_1\dot{\theta}_2 + 2(\text{Cos}[\theta_3]+\text{Sin}[\theta_3]\dot{\theta}_2^2))) +\\ &4m_4(2g\text{Cos}[\theta_2+\theta_3] + 2l_1(\text{Cos}[\theta_3]+\text{Cos}[\theta_2]\text{Sin}[\theta_2+\theta_3]\dot{\theta}_1^2 + \text{Sin}[\theta_3]\dot{\theta}_2^2) + l_3(5\text{Cos}[\theta_4] + \text{Sin}[2\theta_2+\\ &2\theta_3+\theta_4]\dot{\theta}_1^2 - 2\text{Sin}[\theta_4]\dot{\theta}_2\dot{\theta}_4 - 2\text{Sin}[\theta_4]\dot{\theta}_3\dot{\theta}_4 - \text{Sin}[\theta_4]\dot{\theta}_4^2))))\end{aligned} \tag{7.18}$$

$$\boldsymbol{\tau_4} = \frac{1}{36} l_3 m_4 (18g\mathrm{Cos}[\theta_2+\theta_3+\theta_4] + 18(\mathrm{Cos}[\theta_3+\theta_4]l_1 + 2(\mathrm{Cos}[\theta_4]l_2 + l_3)) + \mathrm{Sin}[\theta_2+\theta_3+\theta_4]l_3(3\mathrm{Cos}[\theta_2]l_1 + 3\mathrm{Cos}[\theta_2+\theta_3]l_2 + 2\mathrm{Cos}[\theta_2+\theta_3+\theta_4]l_3)m_4\dot{\theta}_1^2(\mathrm{Sin}[2(\theta_2+\theta_3+\theta_4)]l_3\dot{\theta}_1^2 + 3l_1(\mathrm{Cos}[\theta_2]\mathrm{Sin}[\theta_2+\theta_3+\theta_4]\dot{\theta}_1^2 + \mathrm{Sin}[\theta_3+\theta_4]\dot{\theta}_2^2) + 3l_2(\mathrm{Cos}[\theta_2+\theta_3]\mathrm{Sin}[\theta_2+\theta_3+\theta_4]\dot{\theta}_1^2 + \mathrm{Sin}[\theta_4](\dot{\theta}_2+\dot{\theta}_3)^2)) + 9\dot{\theta}_3(\mathrm{Sin}[\theta_3+\theta_4]l_1\dot{\theta}_2 + \mathrm{Sin}[\theta_4]l_2(2\dot{\theta}_2+2\dot{\theta}_3-\dot{\theta}_4)) + 9\dot{\theta}_2(\mathrm{Sin}[\theta_3+\theta_4]l_1(2\dot{\theta}_2 - \dot{\theta}_3-\dot{\theta}_4) + \mathrm{Sin}[\theta_4]l_2(2\dot{\theta}_2+2\dot{\theta}_3-\dot{\theta}_4)) + 9(\mathrm{Sin}[\theta_3+\theta_4]l_1\dot{\theta}_2 + \mathrm{Sin}[\theta_4]l_2(\dot{\theta}_2+\dot{\theta}_3))\dot{\theta}_4)$$

(7.19)

As stated previously, the dynamic model enables to identify the required joint torques to perform a specified motion of the manipulator. Driving joint torque values are calculated for both conventional and for the proposed manipulator model. Mathematica software is employed for the computation of the driving joint torque results. The joint torque values obtained for both the conventional and for the proposed manipulator model are presented in Section 7.4 of this chapter. The obtained results are used to analyse the effectiveness of the proposed manipulator model. Link lengths of the proposed manipulator model from link 1 to link 3 are 0.30 m, 0.20 m and 0.1 m respectively. Similarly, mass of the links 1, 2 and 3 are 0.92 kg, 0.72 kg and 0.6 kg respectively. The dimensions, material properties, degrees of freedom and structure aspects of the conventional manipulator used for the comparison are also maintained equivalent to the proposed design in the simulation studies. However, conventional manipulator design contains a servo motor at each joint and the proposed model contains a single servo motor fixed at the base. As such conventional manipulator has an additional weight at each joint apart from its link weight. 2.6 kg, 8.6 kg, 5.5 kg and 2.6 kg are general mass specifications of servo motors installed at joint 1, joint 2, joint 3 and joint 4 of a conventional manipulator [216]. Hence total mass of the motors used for the actuation is about 19.3 kg. Similarly, in the proposed design the total mass of eight bistable coupling mechanism (5.360 kg), four brakes (2.26 kg) [217] and

the servo motor (5.5 kg) [216] used for actuation is 14.06 kg. The Table 2 shows the mass specification of both conventional and proposed manipulator design including the motors and the links.

Table 7.2: Mass specification of both proposed and conventional manipulators.

Joint	Conventional Manipulator Mass	Proposed Manipulator Mass
Joint 1 (Base)	Servo Motor 1 (2.6 kg)	Servo Motor (5.5 kg) + Eight bistable coupling mechanisms (5.36 kg) and Four Brakes (2.26 kg)
Joint 2	Link 1 (0.92 kg) + Servo Motor 2 (8.6 kg)	Link 1 (0.92 kg)
Joint 3	Link 2(0.72 kg) + Servo Motor 3 (5.5 kg)	Link 2 (0.72 kg)
Joint 4	Link 3 (0.6 kg) + Servo Motor 4 (2.6 kg)	Link 3 (0.6 kg)

7.4. Results and Discussion

In this section effectiveness of the proposed enhanced manipulator model in reducing driving joint torques when performing a desired motion with comparison to a conventional manipulator design (motors are installed at each degree of freedom for the actuation) is analysed. For the analysis, the torque values at each joint are computed for both proposed and for the conventional manipulator (motor fixed at each degree of freedom) while performing motion in a provided joint angle path. In addition, graphs are plotted for joint torque vs time as shown in Figure 7.8, 7.9, 7.10 and 7.11. The Figure 7.8 to 7.11 show the significance of the proposed manipulator model in minimising the joint torques. The joint angles of the path followed by the manipulator model is defined as:

$$\theta_1 = -0.4\cos 6t \quad (7.20) \qquad \theta_2 = -\cos 4t + 2 \quad (7.21)$$

$$\theta_3 = -2\cos(t) + 5 \quad (7.22) \qquad \theta_4 = -6\cos 2t + 4 \quad (7.23)$$

Figure 7.8 shows the values of the torques of the first joint using both manipulators. The proposed manipulator model (with single actuator) and the conventional manipulator (with four actuators, one actuator at each joint). Figure 7.9 shows the values of the torques vs time of the second joint for both manipulators. Similarly Figure 7.10 shows the joint torques for the third joint while Figure 7.11 shows the values of the torques of the fourth joint using both manipulators.

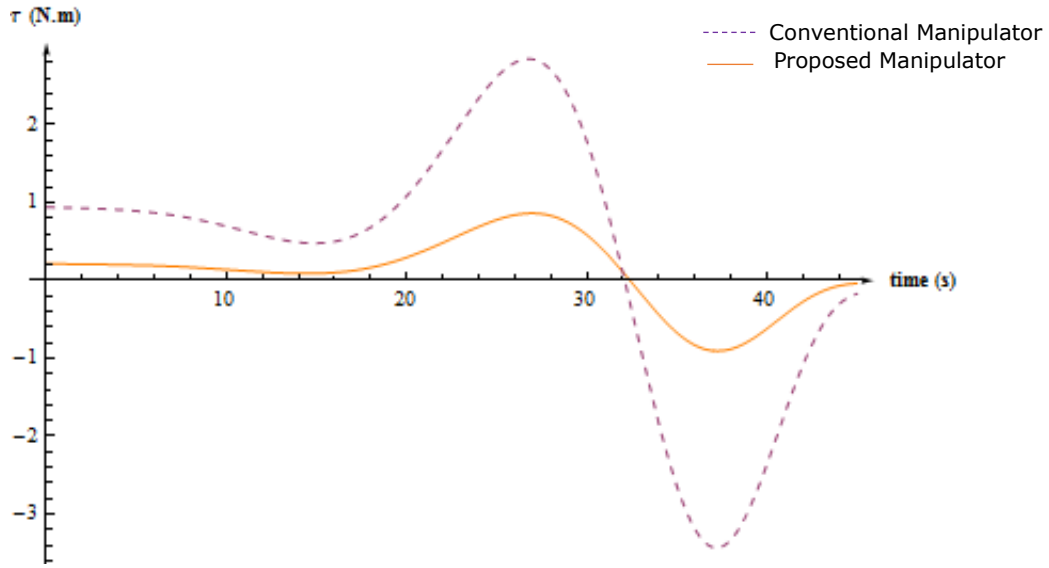

Figure 7.8: The torque values of the first joint using both manipulators.

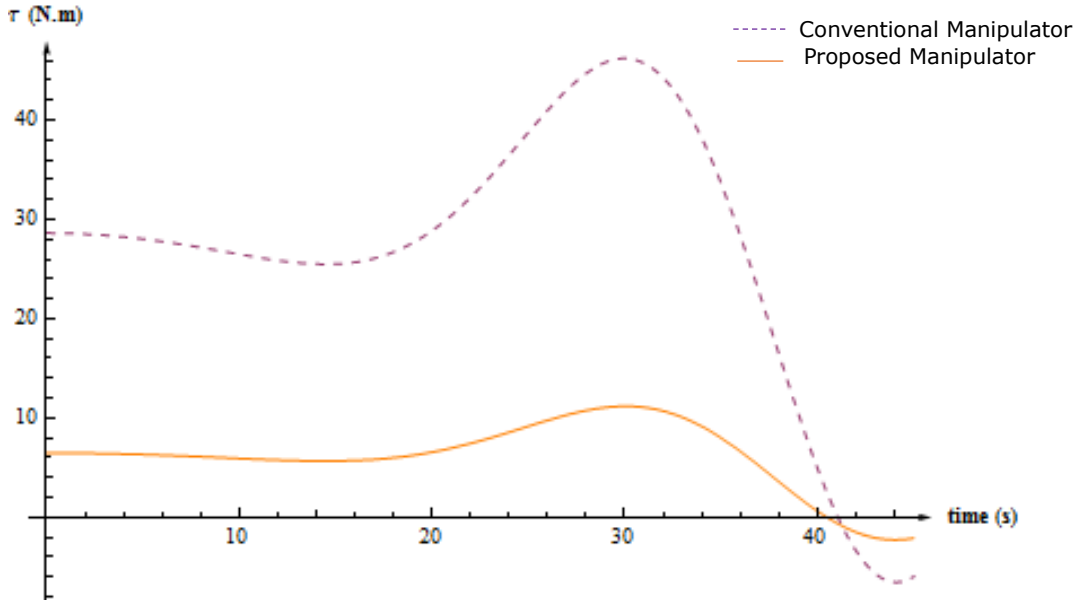

Figure 7.9: The torque values of the second joint using both manipulators.

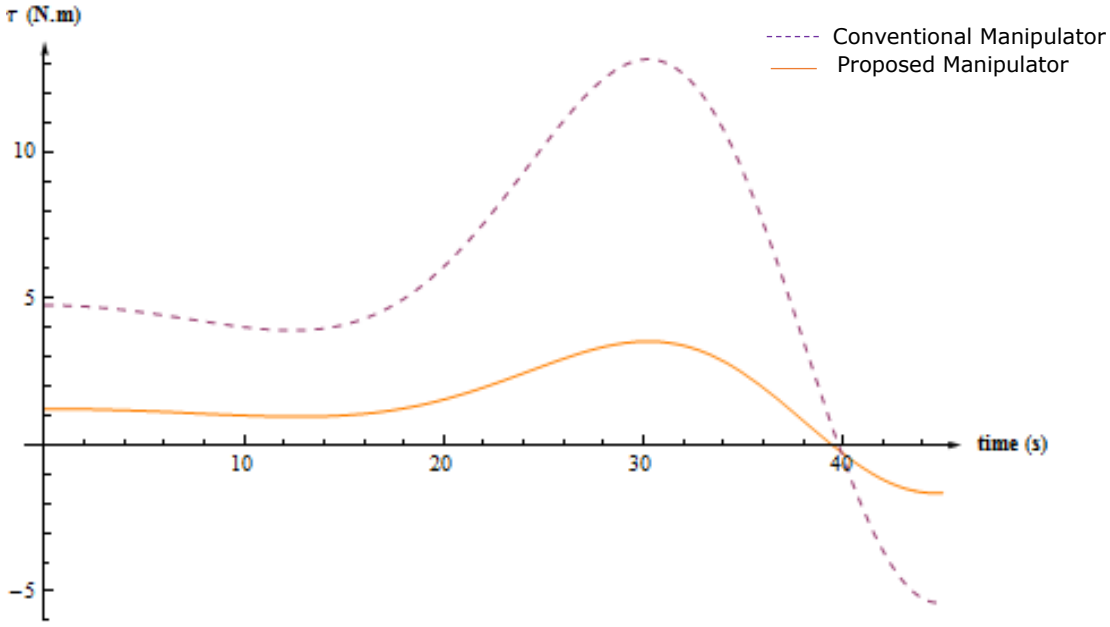

Figure 7.10: The torque values of the third joint using both manipulators.

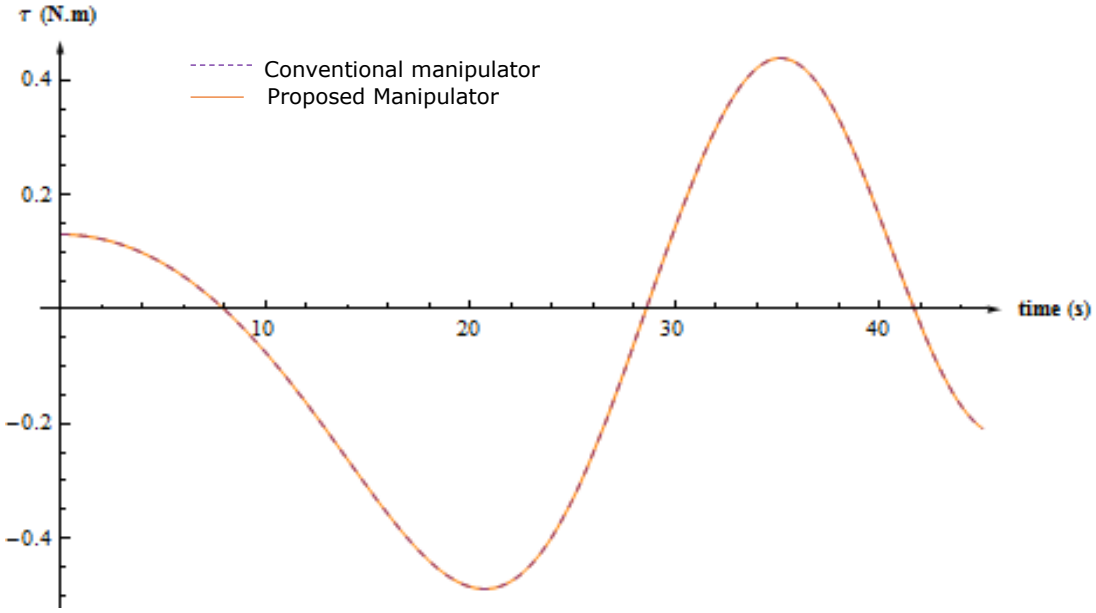

Figure 7.11: The torque values of the fourth joint using both manipulators.

It could be noted that from results the driving joint torque at each degree of freedom has a greater value for the conventional manipulator design in comparison to the proposed manipulator model. However, at the fourth joint equivalent torque values can be observed for both manipulators as shown in Figure 7.11. This result due to the manipulators contain equal amount of mass after the fourth joint that contributes for the joint torque. After the final joint there are no actuator installed to the manipulator. As such joint torque at the fourth joint is affected only by the mass of the third link, which is similar to the proposed manipulator model. Thus, same value is obtained for the joint torque in both manipulators at the fourth joint. Referring to the results it could be observed that the proposed manipulator model is effective in minimising the driving joint torque.

Movereover the proposed model also incoperate bistable coupling mechanisms for the joint actuation replacing the traditional actuation method similar to the developed manipulator prototype. Therefore the proposed model also incoperates the benefits of bistable coupling mechanism based actuation approach similar to the developed manipulator protoype. Furthermore, the

proposed design minimizes the cost due to the reduction of motors. Majority of the conventional manipulators utlizes AC servo motors for the actuation of the robot manipulators [212][216].The cost of a AC servo motor is relatively higer that ranges from 1000 – 2000 US dollar [216][218]. However the estimated cost of a bistable coupling mechanims is about 250 US dollar. Thus the proposed design apparoach that uses underactuation method (reduction of the motors) implimenting bistable coupling mechanism is also with the capability of reducing cost apart from other advantages.

7.5 Chapter Conclusion

In this chapter the possibility of enhancing the developed manipulator prototype presented in Chapter 5 is analysed by reducing the number of motors utilised. As an improvement to the developed manipulator prototype introduced in Chapter 5, a single motor tendon driven manipulator design is presented. The detailed design and the operation principle of the proposed model are explained in this chapter. Furthermore, dynamic model and the forward kinematics are also derived for the improved single motor tendon driven manipulator model. The derived dynamic model is utilised to highlight the significance of the enhanced single motor manipulator design in reducing driving joint torques with comparison to conventional manipulator design (motors are installed at each degree of freedom for the actuation). The significance of the proposed model in reducing driving joint torques was analysed via simulation studies. The simulation results have proven the effectiveness of the proposed model in minimising joint torques with comparison to conventional manipulator design.

Chapter 8

Conclusions and Future Work

8.1 Conclusions and Summary of Findings

This section depicts an outline of achievements and contributions of the work. The research work is focused on the development of underactuated manipulator with reduced driving joint torques incorporated with energy saving coupling mechanism. The proposed design is with the capability of reducing driving joint torques and reducing the number of motors utilised for the actuation. Furthermore, the bistable electromagnetic coupling mechanism employed in the manipulator is with the capability of providing an energy saving and safe coupling mechanism for underactuated lightweight manipulators. Findings from each chapter are summarised as follows:

Chapter 1

This chapter introduces background study of designing of lightweight manipulators. The chapter further presents general motivation, aims and objectives of the research study. It could be observed from the literature that the conventional actuation principle has been adopted in majority of the developed lightweight manipulator designs. In the conventional approach, a dedicated motor allocated for each joint for the actuation. Plurality of motors increase the mass of the

system. Reduced use of motors (underactuated) have significant benefits over the traditional actuation such cost reduction, compactness and reduced weight. Integration of underactuated concept with the lightweight manipulator design could merge advantages of underactuated concept with the lightweight manipulator that enhances the design. Furthermore, majority of the underactuated systems use electromagnetic clutches as coupling device. However electromagnetic clutches consume electric energy throughout the operation. Therefore, additional energy is required for electromagnetic clutches during joint actuation apart from the energy required for the motors. Thus, designing of energy saving coupling mechanism is also vital for the development of energy efficient underactuated lightweight manipulator. These factors have become the main drive for this research.

Chapter 2

This chapter presents a literature review conducted on lightweight manipulator designs. The literature study is performed on three main design approaches namely designs based on tendon driven mechanisms, gear driven mechanisms and modular mechatronic based designs. The design mechanism constrains and the significance of each design approach are reviewed in this chapter. Furthermore, the literature study presented in this chapter also illustrates the future research trends in the field of lightweight manipulator design.

Chapter 3

The research methodology utilised in the study is illustrated in this chapter. The chapter provides an overview of the research activities performed at different stages of the research study. To illustrate the sequence of the research activities, a flowchart of the research methodology is also presented.

Chapter 4

In this chapter, design of the bistable electromagnetic coupling mechanism for underactuated manipulator is presented. The bistable coupling mechanism is with the capability of reducing energy consumption during the actuation of the manipulator joints. The theoretical model is developed for two states of the mechanism namely engaging and disengaging. The model is verified through experimental tests. A good correlation was observed between the theoretical and experimental results with percentage error of 11.8% and 10.9%.

For the analysis of the electric energy consumption, current and voltage usage of the mechanism were measured experimentally. Results revealed that the current and voltage are consumed only for 12 ms during the engaging and disengaging of the mechanism. Furthermore, energy consumption of both the proposed mechanism and the conventional electromagnetic clutch were measured. The measured results revealed that the bistable coupling mechanism has utilised 270.336 J less electrical energy with comparison to the electromagnetic clutch. Experimental results have shown the significance of the proposed bistable

electromagnetic coupling mechanism in minimising the electric energy consumption with comparison to the traditional electromagnetic clutch.

Moreover, the proposed mechanism is with permanent magnetic bistable design. Thus, proposed design can sustain the state (engaged/disengaged) of the mechanism even without an electrical power supply. Therefore, the proposed mechanism could maintain its current state even during sudden power failure condition. As such the proposed bistable coupling mechanism is not only capable of saving energy but also provides a safe coupling mechanism.

Chapter 5

Design of a tendon driven manipulator with reduced number of motors incorporated with bistable coupling mechanisms is introduced in this chapter. The chapter presents mechanical design and the operation principle of the proposed manipulator. Development of kinematics and the dynamic model of the proposed manipulator design are also illustrated in the chapter. Denavit-Hartenberg convention is used for the computation of forward kinematics of the manipulator. DH parameters were identified for the proposed manipulator prior to the computation of forward kinematics. The computed DH parameters and the forward kinematics are shown in the chapter. Lagrange approach is utilised for the derivation of dynamic model of the manipulator. The developed dynamic model could predict the torque requirement of each joint for the actuation. The model is verified via experimental studies and the results are shown in Chapter 6. Good agreement was shown between the experimental and theoretical results as illustrated in the Chapter 6.

Chapter 6

This chapter investigates the significance of the proposed manipulator design in minimising driving joint torques and the energy consumption during joint actuation of the manipulator. Theoretical and experimental studies were performed to analyse the joint torques of the manipulator design. Good correlation was observed between the theoretical and experimental results. The results obtained have highlighted the significance of the proposed manipulator design in reducing driving joint torques with comparison to conventional manipulator design.

In addition, the energy consumption of the proposed design during the joint actuation is analysed experimentally in this chapter. Experimental studies were performed to investigate the energy consumption of both conventional actuation approach (electromagnetic clutch) and the bistable coupling mechanism based approach during the joint actuation. The results revealed that the bistable coupling mechanism based approach has reduced the energy consumption by 188 J and 144 J with comparison to the conventional (electromagnetic clutch) actuation method. Thus, the results have shown the significance of the bistable coupling mechanism based actuation approach in minimising energy consumption. The experimental results have highlighted the effectiveness of proposed manipulator design in reducing both driving joint torques and the energy consumption during joint actuation.

Chapter 7

In this chapter, further enhancement to the manipulator design presented in Chapter 5 is proposed by reducing the number of motors incorporated. Single motor tendon driven manipulator design is proposed as an improvement to the developed manipulator design. The chapter includes detail design and the working principle of the proposed enhanced manipulator design. Kinematics and the dynamic model are also developed for the enhanced manipulator model. The developed dynamic model is employed for the analysis of driving joint torque requirement of the proposed manipulator model. The simulation results have illustrated the significance of the enhanced single motor manipulator model in reducing driving joint torques with comparison to the conventional manipulator design (motors are installed at each degree of freedom for the actuation).

Conclusion

Manipulator design with reduced driving joint torques incorporated with energy saving bistable coupling mechanism based actuation approach is examined in this research study. The background study to the lightweight manipulator design is presented under Chapter 1 of the thesis. This chapter also illustrates the general motivation, aims and objectives of this research study. An in-depth literature review is performed on the lightweight manipulator designs as presented in Chapter 2. Future research direction and trends in lightweight manipulator design are analysed under the literature review. Design of an energy saving and fail-safe actuation mechanism is introduced for underactuated manipulators under the Chapter 4. To evaluate the performance of the proposed mechanism theoretical

and experimental analysis were performed. The theoretical model developed has shown a good correlation with the experimental results. The experimental results obtained for the current and voltage consumption illustrated that the bistable coupling mechanism has utilised 270.336 J less electrical energy with comparison to electromagnetic clutch. The experimental results have highlighted the significance of the proposed mechanism in reducing electric energy usage in comparison to the conventional electromagnetic clutch. Furthermore, the proposed bistable electromagnetic design is safe in operation compared to the traditional electromagnetic clutch due to the permanent magnetic bistable design. Hence the mechanism is unaffected due to sudden power failure. The reduced electric energy consumption and fail-safe design make the bistable electromagnetic mechanism a promising concept for underactuated lightweight manipulators. In the Chapter 5, design of a tendon driven manipulator with reduced number of motors incorporated with bistable coupling mechanisms is presented. This chapter also presents development of kinematic and dynamic model of the proposed manipulator design. Significance of the proposed manipulator in reducing driving joint torques and energy consumption is analysed under the Chapter 6. The manipulator design is with the capability of reducing driving joint torques as the proposed actuation approach positions all the components at the base of the manipulator. Experimental results have highlighted the potential of the manipulator design in reducing the joint torques. Furthermore, the energy consumption of the proposed bistable coupling mechanism based actuation approach and the electromagnetic clutch based conventional actuation method were analysed experimentally during the actuation. The experimental results illustrated that the bistable coupling mechanism based actuation approach has minimised the energy consumption by 188 J and 144 J with comparison to

traditional electromagnetic clutch based actuation approach. The results have proven the effectivness of the proposed actuation approach in minimizing energy consumption with comparison to the traditional electromagnetic clutch based actuation approach, which is widely implemented in underactuated manipulators. Therefore, the proposed actuation method could be a promising actuation approach for the reduction of energy consumption of underactuated manipulator designs. In addition, research study introduces a novel single motor tendon driven manipulator design with reduced driving joint torques in Chapter 7. The significance of the proposed single motor manipulator design is analysed through simulation studies. The results have highlighted the impact of the design in reducing driving joint torque. Reduction of cost is also a vital aspect in manipulator design. The single motor manipulator design offers additional benefits such as minimization of cost and space required. This is due to the usage of underactuated approach over traditional actuation method (motors are installed at each joint). Therefore, the proposed design can be used to reduce the cost and achieve a compact design apart from joint torque minimization.

8.2 Future Work

This section presents the potential future research directions based on the developments in the project. Chapter 4 presented the development of a bistable electromagnetic coupling mechanism. The time taken for the engagement and disengagement of the bistable mechanism are observed to be 11.3 ms and 10.1 ms. These values of the proposed mechanism approximate the engaging and disengaging time (12 ms - 20 ms) of the conventional electromagnetic clutches providing

similar operation condition [219-221]. Moreover, from the analysis performed on the current consumption of the mechanism in this chapter, it could be observed that the current is only consumed during the engaging and disengaging of the mechanism. Therefore, by considering further reduction of the engaging and disengaging time, the energy consumption of the design could be further minimised. As such, future research could be performed on the development of bistable coupling mechanism on reducing the engaging and disengaging time of the design. Moreover, future work can be conducted on the development of control system for the proposed underactuated manipulator. For the development of the control system significant study and extensive research have to be performed.

Furthermore, single motor manipulator design could be further improved by increasing the number of joints (degrees of freedom) of the design maintaining single motor actuation approach introduced. The increase of degrees of freedom enhance the manipulator dexterity. Thus, future research work could be also conducted on increasing the number of degrees of freedom of the single motor manipulator design presented in Chapter 7.

Bibliography

[1] J. Artigas and G. Hirzinger, "A brief history of DLR's space telerobotics and force-feedback teleoperation," *Acta Polytechnica Hungarica*, vol. 20, no. 1, pp. 239-249, 2016.

[2] K. Nanos and E. G. Papadopoulos, "On the dynamics and control of flexible joint space manipulators," *Control Engineering Practice*, vol. 45, pp. 230-243, 2015.

[3] G. Hirzinger, N. Sporer, M. Schedl, J. Butterfab and M. Grebenstein, "Torque-controlled lightweight arms and articulated hands: Do we reach technological limits now? ," *The International Journal of Robotics Research*, vol. 23, no. 4-5, pp. 331-340, 2004.

[4] L. Zhou and S. Bai, "A new approach to design of a lightweight anthropomorphic arm for service applications, " *Journal of Mechanisms and Robotics*, vol. 7, no. 3, pp. 031-041, 2015.

[5] P. Masinga, H. Campbell and J. A. Trimble, "A framework for human collaborative robots, operations in South African automotive industry, " *IEEE International Conference on Industrial Engineering and Engineering Management (IEEM)*, Singapore, 6-9 December, 2015.

[6] J. Smith, J. Jivraj, R. Wong and V. Yang, "30 years of neurosurgical robots: review and trends for manipulators and associated navigational systems," *Annals of biomedical engineering*, vol. 44, no. 4, pp. 836-846, 2016.

[7] T. Kanno, D. Haraguchi, M. Yamamoto, K. Tadano and K. Kawashima, "A forceps manipulator with flexible 4-DOF mechanism for laparoscopic surgery," *IEEE/ASME Transactions on Mechatronics*, vol. 20, no. 3, pp. 1170-1178, 2015.

[8] J. Galliott, *Commercial space exploration: ethics, policy and governance*, Routledge, 2016.

[9] T.S. Tadele, T. de Vries and S. Stramigioli, "The safety of domestic robotics: A survey of various safety-related publications," *IEEE Robotics & Automation Magazine*, vol. 21, no. 3, pp. 134-142, 2014.

[10] A. M. Djuric, R. J. Urbanic, and J. L., Rickli, "A framework for collaborative robot (CoBot) integration in advanced manufacturing systems," *SAE International Journal of Materials and Manufacturing*, vol. 9, pp. 457-464, 2016.

[11] S. Haddadin, A. Albu-Schäffer and G. Hirzinger, "Safety analysis for a human-friendly manipulator," *International Journal of Social Robotics*, vol. 2, no. 3, pp. 235-252, 2010.

[12] S. Haddadin and A. Albu-Schaffer, "The role of the robot mass and velocity in physical human-robot interaction - part II: constrained blunt impacts, " IEEE *International Conference on Robotics and Automation (ICRA 2008)*, Pasadena, USA, 19-23 May, 2008.

[13] A. Verl, A. Albu-Schäffer, O. Brock and A. Raatz, *Soft Robotics: Transferring Theory to Application*, Springer, 2015.

[14] M. Mratins, "Modelling, control and validation of flexible manipulators, " *Advances in Computational Multibody Systems Computational Methods in Applied Sciences*, vol. 2, Springer, 2005, pp. 239-269.

[15] A. Rodić, B. Miloradović, S. Popić and D. Urukalo, "On developing lightweight robot-arm of anthropomorphic characteristics," in *Proc. 3rd International Workshop New Trends in Medical and Service Robotics,* Lausanne, Switzerland, 2014, pp 34-36.

[16] A. Albu-Schäffer, S. Haddadin, C. Ott, A. Stemmer, T. Wimböck and G. Hirzinger, "The DLR lightweight robot: design and control concepts for robots in human environments," *Industrial Robot: An International Journal*, vol. 34, pp. 376-385, 2007.

[17] U. Hagn, M. Nickl, S. Jörg, G. Passig, T. Bahls, A. Nothhelfer, F. Hacker, L. Le-Tien, A. Albu-Schäffer and R. Konietschke, "The DLR MIRO: a versatile lightweight robot for surgical applications," *Industrial Robot: An International Journal*, vol. 35, no. 4, pp. 324-336, 2008.

[18] U. Culha, J. Hughes, A. Rosendo, F. Giardina and F. Iida, *Design principles for soft-rigid hybrid manipulators,* In Soft Robotics: Trends, Applications and Challenges, Springer International Publishing, 2017.

[19] S. Ma, S. Hirose and H. Yoshinada," Design and experiments for a coupled tendon-driven manipulator," *IEEE Control Systems Magazine*, vol. 13, no. 1, pp. 30-36, 1993.

[20] F. Londi, E. Pennestrì, P. P. Valentini and Vita, L.,"Control and virtual reality simulation of tendon driven mechanisms," *Multibody System Dynamics*, vol. 12, no. 2, pp. 133-145, 2004.

[21] Y. Gue and X. Yangsheng, "Under-actuated robot systems: dynamic interaction and adaptive control," *IEEE International Conference on Systems, Man, and Cybernetics,* San Antonio, 2-5 October, 1994.

[22] R.Balasubramanian and M. Dollar, "Performance of serial underactuated mechanisms: number of degrees of freedom and actuators," *IEEE/RSJ International Conference on Intelligent Robots and Systems*, San Francisco, CA,USA, September, 2011.

[23] T. Ende, S. Haddadin, S. Parusel, T. Wusthoff, M. Hassenzahl and A. AlbuSchaffer, "A human-centered approach to robot gesture based communication within collaborative working processes," *IEEE/RSJ International Conference on Intelligent Robots and Systems,* San Francisco, CA, USA, 25 - 30 September, 2011.

[24] J. A. Corrales, G. J. G. Gómez, F. Torres and V. Perdereau, "Cooperative tasks between humans and robots in industrial environments," *International Journal of Advanced Robotic Systems*, vol. 9, pp. 94-104, 2012.

[25] C. Heyer, "Human-robot interaction and future industrial robotics applications," *International Conference on Intelligent Robots and Systems*, Taipei, Taiwan, 18 - 22 October, 2010.

[26] S. Haddadin, M. Suppa, S. Fuchs, T. Bodenmüller, A. AlbuSchäffer and G. Hirzinger, " Towards the robotic co-worker, " in *Proc 14th International Symposium Robotics Research (ISRR)*, Lausanne, Switzerland, 2011, pp. 261-282.

[27] L. Probst, L. Frideres, B. Pedersen and C. Caputi, "Service innovation for smart industry human-robot collaboration report," *Business Innovation Observatory* European Union, February, 2015.

[28] V. Weistroffer, A. Paljic, P. Fuchs, O. Hugues and J.P. Chodacki, " Assessing the acceptability of human-robot co-Presence on assembly lines: A comparison between actual situations and their virtual reality counterparts, " *23rd IEEE International Symposium on Robot and Human Interactive Communication (ROMAN),* Edinburgh, United Kingdom, 25 - 29 August, 2014.

[29] A. Lasota, A. Przemyslaw and J.A. Shah, " Analyzing the effects of human-aware motion planning on close-proximity human–robot collaboration, " *Human Factors: The Journal of the Human Factors and Ergonomics Society*, vol. 57, no. 1, pp. 21–33, 2015.

[30] B. Matthias, "Industrial safety requirements for collaborative robots and applications, " *Workshop: Workspace Safety in Industrial Robotics: trends, integration and standards,* ABB Corporate Research, March, 2014.

[31] ISO 10218-1:2011 Robots and robotic devices safety requirements for industrial robots catalogue, 2011.

[32] C. Schuster, D. George and M. Winrich ,"Robotics safety," *Rockwell Automation, White Paper SAFETYWP009A-EN-P*, 2009.

[33] X. Xin, and Y. Liu, *Control design and analysis for underactuated robotic systems*, Springer Science & Business Media, 2014.

[34] S. Moussaoui, A. Boulkroune and S. Vaidyanathan, "Fuzzy adaptive sliding-mode control scheme for uncertain underactuated systems," *Advances and Applications in Nonlinear Control Systems*, Springer International Publishing, 2016, pp. 351-367.

[35] A. Choukchou-Braham, B. Cherki, M. Djemai and K. Busawon, *Analysis and control of underactuated mechanical systems*, Springer Science & Business Media, 2016.

[36] L. Wu and M. Ceccarelli, "A numerical simulation for design and operation of an underactuated finger mechanism for LARM hand," *Mechanics Based Design of Structures and Machines*, vol. 37, no. 1, pp 86-112, 2009.

[37] S. Ma, S. Hirose and H. Yoshinada," Design and experiments for a coupled tendon-driven manipulator," *IEEE Control Systems Magazine*, vol. 13, no. 1, pp. 30-36, 1993.

[38] F. Londi, E. Pennestrì, P. P. Valentini and L. Vita, "Control and virtual reality simulation of tendon driven mechanisms," *Multibody System Dynamics*, vol. 12, no. 2, pp. 133-145, 2004.

[39] M. Hägele, W. Schaaf and E. Helms, " Robot assistants at manual workplaces: effective co-operation and safety aspects, " *33rd International Symposium on Robotics*, Sweden, 7-11 October, 2002.

[40] L. Probst, L. Frideres, B. Pedersen and C. Caputi, "Service innovation for smart industry human-robot collaboration report," *Business Innovation Observatory* European Union, February, 2015.

[41] E. Rouse, L. Mooney and H. Herr, "Clutchable series-elastic actuator: implications for prosthetic knee design," *International Journal of robotics Research*, vol. 33, no. 13, pp. 1611-1625, 2014.

[42] X. Li, H. Zhou, H. Li and X. S. Li , "Nonlinear feedforward-feedback control of an electric clutch actuator, " *Advanced Materials Research*, vol. 1014, pp. 339-343, 2014.

[43] M. Canesi , M. Xiloyannis , A. Ajoudani , A. Biechi and L. Masia, "Modular one-to-many clutchable actuator for a soft elbow exosuit, " *International Conference on IEEE Rehabilitation Robotics (ICORR)*, London, UK, 17-20 July, 2017.

[44] W. J. Wu and P. C. Lin, "A switchable clutched parallel elasticity actuator ," *IEEE International Conference on* IEEE *Intelligent Mechatronics*, Munich, Germany, 3-7 July , 2017.

[45] M.Plooij, G. Mathijssen, P. Cherelle, D. Lefeber and B. Vanderborght, "Lock your robot: A review of locking devices in robotics, " *IEEE Robotics & Automation Magazine*, vol. 22, no. 1, pp. 106-117, 2015.

[46] S.P. Thompson, *The Electromagnet and electromagnetic mechanism*, BiblioLife, 2015.

[47] C. Own, A.S. Duffey and G. Wright, *Fundamentals of Mobile Heavy Equipment*, Jones & Bartlett Learning, 2017.

[48] A. Junji, "Development of third-generation electronically controlled AWD coupling with new high-performance electromagnetic clutch," *SAE International Journal of Passenger Cars-Mechanical Systems*, vol. 7, no. 2, pp. 882-887, 2014.

[49] J. Jenneson and B. Harper, *Electrical principles for the electrical trades vol 2*", McGraw-Hill Education, 2014.

[50] M. A. Laughton and M. G. Say, *Electrical Engineer's Reference Book*, Elsevier, 2013.

[51] Directive 2006/42/EC of the European Parliament and of the Council of 17 May 2006 on machinery and amending directive 95/16/EC report on journal of European union, May, 2006.

[52] S. Yahya , M. Moghavvemi and H. Abbas," Dexterity of underactuated six degrees of freedom three dimensional redundant manipulators," *ANZIAM Journal*, vol. 55, no. 1, pp. 416-436, 2014.

[53] D. Reintsema, K. Landzettel, and G. Hirzinger, "DLR's Advanced Telerobotic Concepts and Experiments for On-Orbit Servicing," *Advances in Telerobotics Springer Tracts in Advanced Robotics,* 2007, pp 323-345.

[54] K. Landzettel, G. Hirzinger, B. Brunner, N. Sporer, J. Butterfab and M. Schedl, "Space Robotics - DLR's Telerobotic Concepts, Lightweight Arms and Articulated Hands", *Autonomous Robots*, vol. 14, no. 2, pp. 127–145, 2003.

[55] A. Suarez, C. Jimenez, V.M. Vega, G. Heredia, C. A. Rodriguez and A. Ollero, "Design of a lightweight dual arm system for Aerial Manipulation," *Mechatronics*, vol. 50, pp. 30-44, 2018.

[56] Y. Zhang, P. Huang, Z. Meng and Z. Liu, " Precise angles-only navigation for noncooperative proximity operation with application to tethered space robot,*" IEEE Transactions on Control Systems Technology*, vol. 27*,* no. 3*,* pp. 1139-1150, 2019.

[57] A. Goswami and P. Vadakkepat , *Humanoid Robots : A Reference*, Springer, 2017.

[58] J. Heinzmann and A. Zelinsky, "The safe control of human–friendly robots," *IEEE/RSJ International Conference on Intelligent, Robots and System,* Kjongju, Korea, 17-21 October, 1999.

[59] C. Schlenk, T. Bahls, S. Tarassenko, J. Klodmann, M. Bihler, T. Wuesthoff, "Robot integrated user interface for physical interaction with the DLR MIRO in versatile medical procedures," *Journal of Medical Robotics Research*, vol. 3, no. 2, pp. 212-223, 2018.

[60] C. Quaglia, G. Petroni, M. Niccolini, S. Caccavaro, P. Dario and A. Menciassi, "Design of a compact robotic manipulator for single-port laparoscopy," *Journal of Mechanical Design*, vol. 136, no. 10, pp. 1050-1059, 2014.

[61] J. Mendes, J. Martins and S. D. Costa," Integrated design of lightweight robot manipulators," *in Proc Inter-Noise and Noise-Con Congress and Conference*, England, 2010, pp. 6295-6304.

[62] C. Daisuke and S. Yokota," Advances in the modelling and control of elastic parallel manipulators," *Introduction to Modern Robotics II*. 1st Edition**,** iConcept Press, 2012, pp. 1025-1044.

[63] W. J. Book, T.E. Alberts and G. G. Hastings , " Design strategies for high speed lightweight robots," *Computers in Mechanical Engineering,* vol. 5, no. 2, pp. 26–33, 1986**.**

[64] T. Lens, O.V. Stryk and A. Karguth, "Safety properties and collision behaviour of robotic arms with elastic tendon actuation," *7th German Conference on Robotics (ROBOTIK),* Berlin, German, 21-22 May*, 2012.*

[65] Y. She, H. J. Su, D. Meng, S. Song and J. Wang," Design and modelling of a compliant link for inherently safe co-robots, " *Journal of Mechanisms and Robotics*, vol. 10, no. 1, pp. 2020-1030, 2018.

[66] Z. J. Li, H. B. Wu, J. M. Yang, M. H. Wang and J. H. Ye, " A position and torque switching control method for robot collision safety, " *International Journal of Automation and Computing*. Vol. 15, no. 2, pp. 156-68, 2018.

[67] S. Haddadin, A. Albu-Schaffer and G. Hirzinger, "Safe physical human-robot interaction: measurements, analysis & new insights, "*Springer Tracts in Advanced Robotics* ,vol. 66, 2011.

[68] A. Bicchi and G. Tonietti, " Fast and soft arm tactics: dealing with the safety-performance trade-off in robot arms design and control," *IEEE Robotics & Automation Magazine.* vol. 11, pp. 22–33, 2004.

[69] S. Haddadin, A. Albu-Schaffer and G. Hirzinger, "The role of the robot mass and velocity in physical human-robot interaction - part I: unconstrained blunt impacts," IEEE *International Conference on Robotics and Automation (ICRA 2008)*, Pasadena, USA, 19-23 May, 2008.

[70] N. Mansfeld, M. Hamad, M. Becker, A. G. Marin and S. Haddadin, " Safety map: A unified representation for biomechanics impact data and robot instantaneous dynamic properties," *IEEE Robotics and Automation Letters,* vol. 3, no. 3, pp. 1880-1887, 2018.

[71] A. Ozer and S. E. Semercigil," Effective vibration Suppression of a manoeuvring two link flexible arm with an even base stiffness controller, " *in Proc International Modal Analysis Conference (IMAC*), Florida, USA, 1-4 February, 2011, pp. 323-330.

[72] C. W. De Silva, *Model predictive control of flexible robot, mechatronic systems: devices, design, control, operation and monitoring*, CRC press, 2008.

[73] Z. Tao, T. Zhang, M. Qi and J. Ji ," Research and implementation of a new 6-DOF light-weight robot*", 3rd International Conference on Advances in Energy, Environment and Chemical Engineering*, Chengdu, China,26–28 May, 2017.

[74] A. Rodić, B. Miloradović, S. Popić and D. Urukalo ," On developing lightweight robot-arm of anthropomorphic characteristics, " *3rd International Workshop New Trends in Medical and Service Robotics*, Lausanne, Switzerland, 10-14 July, 2014.

[75] A. Morecki, Z. Busko, H. Gasztold and K. Jaworek, " Synthesis and control of the anthropomorphic two handed manipulator, " *International Symposium on Industrial Robots*, Milan, Italy,1980.

[76] S. C. Jacobsen, J. E. Wood and D.F Knutti, " The Utah/MIT dexterous hand: work in progress, " *International Journal of Robotics Research ,*vol. 3, no. 4, pp. 21-50, 1984.

[77] K. Salisbury, W. Townsend, B. Eberman and D. DiPietro, "Preliminary design of a whole-arm manipulation system (WAMS), " *IEEE International Conference in Robotics and Automation,* Philadelphia, USA, 24-29 April, 1988.

[78] K. Yokoi, K. Komoriya and K. Tanie, "Development of a coupled tendon drive manipulator with seven degrees-of-freedom,*" RoManSy 9. Lecture Notes in Control and Information Sciences,*vol. 187, pp. 339–346, 1993

[79] T. Lens, J. Kirchhoff and V.O. Stryk," Dynamic modeling of elastic tendon actuators with tendon slackening," *12th IEEE-RAS International Conference on Humanoid Robots (Humanoids)*, Osaka, Japan, 29-30 November, 2012.

[80] Barrett Technology company, "Whole arm manipulator datasheet", Barrett Technology company, USA, 2009.

[81] H. Karbasi, J. P. Huissoon and A. Khajepour, "Uni-drive modular robots: theory, design and experiments," *Mechanism and Machine theory*, vol. 39,no 1, pp. 183-200, 2004.

[82] A. Shafer and M. Kermani, "Design and validation of a magnetorheological clutch for practical control applications in human-friendly manipulation", *IEEE International Conference on Robotics and Automation*, Shanghai, China, 9-13 May, 2011.

[83] T. R. Hunt, C. J. Berthelette and M. B. Popovic," Linear one-to-many (otm) system," *IEEE International Conference on Technologies for Practical Robot Applications (TePR*A), Woburn, USA, 22-23 April, 2013.

[84] G. Hirzinger, K. Landzettel, and C. Fagerer, "Telerobotics with large time delays-the ROTEX experience," in *Proceedings of IEEE/RSJ International Conference on Intelligent Robots and Systems (IROS'94)*, 1994, vol. 1, pp. 571–578.

[85] G. Hirzinger, A. Albu-Schaffer, M. Hahnle, I. Schaefer, and N. Sporer, "On a new generation of torque controlled light-weight robots," in *Proceedings 2001 ICRA. IEEE International Conference on Robotics and Automation (Cat. No. 01CH37164)*, 2001, vol. 4, pp. 3356–3363.

[86] M. Manz, J. Hilljegerdes, A. Dettmann, and F. Kirchner, "Development of a lightweight manipulator arm using heterogeneous materials and manufacturing technologies," in *Proceedings of the International Symposium on Artificial Intelligence, Robotics and Automation in Space (i-SAIRAS 2012)*, 2012, pp. 4–6.

[87] G. Hirzinger, "Mechatronics for a new robot generation," *IEEE/ASME Transactions on Mechatronics*, vol. 1, no. 2, pp. 149–157, 1996.

[88] G. Hirzinger, N. Sporer, A. Albu-Schaffer, M. Krenn, A. Pascucci and M. Schedl ,"DLR's torque-controlled light weight robot III-are we reaching the technological limits now?," in *Proceedings 2002 IEEE International Conference on Robotics and Automation (Cat. No. 02CH37292)*, 2002, vol. 2, pp. 1710–1716.

[89] DLR Micro robot specification, DLR company Germany, 2016

[90] KUKA lightweight robot GMBH 3 specification, Kuka Robotics Germany, 2017.

[91] M. T. Mason and J. K. Salisbury Jr, "Robot hands and the mechanics of manipulation," The MIT Press, 1985.

[92] M. Grebenstein, M. Chalon, G. Hirzinger, and R. Siegwart," Antagonistically driven finger design for the anthropomorphic DLR hand arm system," *IEEE International Conference on Intelligent Robots and Systems*, Nashville, USA, 6-8 December, 2010.

[93] S. Hirose and Y. Umetani, "The development of soft gripper for the versatile robot hand," *Mechanism and Machine Theory*, vol. 13, no. 1, pp.351–359, 1978.

[94] W. T. Townsend. "*The effect of transmission design on force-controlled manipulator performance,*" PhD thesis, Massachusetts Institute Of Technology, 1988.

[95] H. Kobayashi and R. Ozawa, "Adaptive neural network control of tendon-driven mechanisms with elastic tendons," *Automatica*, vol. 39, no. 9, pp. 1509–1519, 2003.

[96] A. Horigome, H. Yamada, G. Endo, S. Sen, S. Hirose and E. F. Fukushima, **"** Development of a coupled tendon-driven 3D multi-joint manipulator," *IEEE International Conference on Robotics & Automation (ICRA),* Hong Kong, China, 30-31 May, 2014.

[97] H. Kino, N. Okamura and S. Yabe, "Basic characteristics of tendon-driven manipulator using belt pulleys," *IEEE/RSJ International Conference on Intelligent Robots and Systems,* Sendai, Japan, 28-30 September, 2004.

[98] R. Beira, A. Sengul, M. Hara, P. Schoeneich and H. Bleuler, "Tendon-based transmission for surgical robotics: systematic experimental friction modeling," *International Conference on Applied Bionics and Biomechanics,* Venice, Italy, 14-16 October,2010.

[99] L.Ludvig, "Analysis and synthesis of open ended tendon structures,"*Periodica Polytechnica Mechanical Engineering Journal*, vol. 42, no. 1, pp. 69-88, 1998.

[100] M. Uros and M. Munih, "Force control of cable-driven robotic segment," *10th International Conference on Advanced Robotics*, Budapest, Hungary,22-25 August, 2001.

[101] Y.H. Lee and J. J. Lee, "Modelling of the dynamics of tendon-driven robotic mechanisms with flexible tendons," *Mechanism and Machine Theory*, vol. 38, no. 1, pp. 1431–1447, 2003.

[102]L. W. Tsai, *Robot analysis: the mechanics of serial and parallel manipulators,* John Wiley & Sons, 1999.

[103] S. Jacobsen, H. Ko, E. Iversen and C. Davis, "Control strategies for tendon-driven manipulators," *IEEE Control Systems Magazine*, vol. 10, no. 2, pp.23-28, 1990.

[104] S. Jacobsen, H. Ko, E. K. Iversen and C. Davis**, "**Antagonistic control of a tendon driven manipulator," *IEEE International Conference on Robotics and Automation*, Scottsdale, USA, 14-19 May, 1989.

[105] H. M. Do, C. Park and D. H. Kim, "Design and control of tendon-driven mechanism with 2N configuration: A feasibility study," *International Journal of Engineering and Innovative Technology (IJEIT*), vol. 4, no. 5, pp.32-36, 2014.

[106] W. Khalil and A. Liegeois," The dynamics of a class of electrically-actuated and cable-driven manipulators," *ICITAM Symposium,* Munich, Germany, 29-30 August, 1977.

[107] T. Okada, " On a versatile finger system," *7thInternational Symposium on Industrial Robots*, Tokyo, Japan, 19-21 October, 1977.

[108] A. Morecki, H. Gasztold and K. Jaworek, "Synthesis and control of the anthropomorphic two-handed manipulator," *10th International Symposium in Industrial Robots,* Milan, Italy, 5-7 March, 1980.

[109] J. K. Salisbury and J. J. Craig, "Articulated hands: force control and kinematic issues," *International Journal of Robotics Research, v*ol. 1, no. 1, pp. 4-17, 1982.

[110]S. Haddadin, *Towards safe robots: approaching Asimov's 1st law,* Springer, 2013.

[111] W. J. Book, S. L. Dickerson, G. Hastings, S. Cetinkunt and T. Alberts, " Combined approaches to lightweight arm utilisation," *ASME Winter Annual Meet*, Miami, USA, 17-22 November, 1985.

[112] R. Ozawa, H. Kobayashi and K. Hashiri, "Analysis, classification, and design of tendon-driven mechanisms," *IEEE Transactions on Robotics*, vol. 30, no. 2, pp. 396-410, 2014.

[113] G. Palli, G. Borghesan and C. Melchiorri," Modeling, identification, and control of tendon-based actuation systems," *IEEE Transactions on Robotics*, vol. 28, no. 2, pp.277-290, 2012.

[114] M.M Kaluarachchi, J.H Ho, and S. Yahya," Design of a single motor, tendon driven redundant manipulator with reduced driving joint torques," *Mechanics Based Design of Structures and Machines*, vol. 46, no. 5, pp. 591-614, 2018.

[115] L. Wen, Y. Li, M. Cong, H. Lang and Y. Du," Design and optimization of a tendon-driven robotic hand," *IEEE International Conference on Industrial Technology (ICIT),* Toronto, Canada, 22-25 March, 2017.

[116] I. Mizuuchi, T. Yoshikai, Y. Sodeyama, Y. Nakanishi, A. Miyadera,T. Yamamoto, T. Niemela, M. Hayashi, J. Urata, T. Nishino and M. Inaba, "Development of musculoskeletal humanoid Kotaro," *IEEE Conference on Robotics and Automation*, Orlando, USA, 15-19 May, 2006.

[117] E. Nazma and S. Mohd, "Tendon driven robotic hands a review," *International Journal of Mechanical Engineering and Robotics Research*, vol. 1,no. 3, pp. 350-357, 2012.

[118] S. Hirose and M. Shugen, "Coupled tendon driven multijoint manipulator," *IEEE International Conference on Robotics and Automation*, California, USA, 9-11 April, 1991.

[119] M Shugen, S Hirose and H Yoshinada, "CT ARM-I: coupled tendon-driven manipulator model I-design and basic experiments, " *International Conference on Robotics Automation*, France, 12-14 May, 1992.

[120] S. Hirose and M. Shugen, "Development of coupled tendon-driven multijoint manipulator," *IEEE/RSJ International Workshop on Intelligent Robots and Systems lROS*, Osaka, Japan, 3-5 November, 1991.

[121] K. Yokoi, K. Tanie, N. Imamura, T. Kawai and K. Agou, "Design and control of a seven-degrees-of-freedom manipulator actuated by a coupled tendon-driven system," *IEEE/RSJ International Workshop on Intelligent Robots and Systems IROS*, Osaka, Japan, 3-5 November, 1991.

[122] T. Lens, J. Kunz, O. Von Stryk, C. Trommer and A. Karguth, " BioRob-arm: a quickly deployable and intrinsically safe, lightweight robot arm for service robotics applications," *International Symposium on and 2010 6th German Conference on Robotics (ROBOTIK)*, Berlin, Germany, 7-9 June, 2010.

[123] T. Lens and O.V. Stryk, "Investigation of safety in human-robot-interaction for a series elastic tendon-driven robot arm," *IEEE/RSJ International Conference on Intelligent Robots and Systems,* Vilamoura, Portugal, 7-12 October, 2012.

[124] J. K. Lee, C .H. Choi, K. H. Yoon, H. J. Lee, B. S. Park and J. S.Yoon, "Design and evaluation of cable-driven manipulator with motion-decoupled joints," *International Conference on Smart Manufacturing Application*, Gyeonggi-do, Korea, 9-11 April, 2008.

[125] J. K. Lee, C .H. Choi, K. H. Yoon, H. J. Lee, B. S. Park and J. S. Yoon , "Cable-driven manipulator," United States patent, Pub. N0.2 US 2009/0148263 A1, July, 2009.

[126] J. K. Lee, H. J. Lee, K. H. Yoon, B. S. Park and J. S. Yoon, "A servo manipulator for remote handling of ACP equipment," *International Conference on Advanced Robotics,* Jeju Island, Korea, 21-24 August, 2007.

[127] Y. Maeda, "Wire guide apparatus for wire-driven mechanism," United State patent 5,020,388, June, 1991.

[128] K. Salisbury, W. Townsend, B. Eberman and D. DiPietro, "Preliminary design of a whole-arm manipulation system (WAMS)," IEEE International Conference in Robotics and Automation, Philadelphia, USA, 24-29 April, 1988.

[129] B. Rooks, "The harmonious robot, "*Industrial Robot: An International Journal*, vol. 33, no. 2, pp. 125 – 130, 2006.

[130] W. T. Townsend and J. A. Guertin, "Tele operator slave - WAM design methodology," *Industrial Robot: An International Journa*l, vol. 26, no. 3, pp. 167 – 177, 1999.

[131] D. Z. Chen, Y. C. Huang and D. W. Duh, "Geared robot manipulators with a jointed unit: topological synthesis and its application, "*International Journal of Robotics Research*, vol. 19, no. 2, pp. 183-194, 2000.

[132] D. Z. Chen, C. P. Liu and D. W. Duh, "A modular approach for the topological synthesis of geared robot manipulators," *Mechanism and Machine Theory*, vol. 38, no. 1, pp 53–69, 2003.

[133] S. L. Chang and L. W. Tsai, "Topological synthesis of articulated gear mechanisms, " *IEEE/ASME Transactions on Robotics and Automation*, vol. 6, no. 1, pp 97-103, 1990.

[134] B. Siciliano and O. Khatib, *Springer handbook of robotics*, Springer Science & Business Media, 2008.

[135] S. Li, Y. Liu and M. Xie, "Implementation of a single motor driven manipulator with multiple joints," *Industrial Robot: An International Journal*, vol. 38, no. 1, pp. 48 – 57, 2011.

[136] M. Xie, *Fundamentals of robotics: linking perception to action*, *World Scientific*, Singapore, 2003.

[137] H. Karbasi, J. P. Huissoon, A. Khajepour and S. J. Park, "A new modular robot: uni-drive with pulse width modulation control," *IEEE International Conference Mechatronics and Automation*, Ontario, Canada, 29-30 July, 2005.

[138] S. Yahya, M. Moghavvemi and H. Abbas, "Joint torque reduction of a three dimensional redundant planar manipulator," *Sensors*, vol. 12, no. 6, pp. 6869-6892, 2012.

[139] S. Yahya, M. Moghavvemi and H. Abbas, "Artificial neural networks aided solution to the problem of geometrically bounded singularities and joint limits prevention of a three dimensional planar redundant manipulator," *Neuro Computing*, vol. 137, no. 1, pp.34-46, 2014.

[140] S. Yahya, M. Moghavvemi and H. Abbas," Singularity avoidance of a six degree of freedom three-dimensional redundant planar manipulator," *Computers and Mathematics with Applications,* vol. *64*, no. 5, pp. 856–868, 2012.

[141] A. Shafer and M. Kermani, "Development of high performance intrinsically safe 3-DOF Robot," *IEEE International Conference on Robotics & Automation (ICRA),* Hong Kong, China, 1-7 June, 2014.

[142] A. Shafer and M. Kermani, "On the feasibility and suitability of MR fluid clutches in human-friendly manipulators," *IEEE/ASME Transactions on Mechatronics*, vol. 16, no. 6, pp.1073-1082, 2011.

[143] A. Shafer and M. Kermani, "On the feasibility and suitability of MR and ER based actuators in human friendly manipulators," *IEEE/RSJ International Conference on Intelligent Robots and Systems*, St.Louis, USA, 10-15 October, 2009.

[144] H. Böse, T. Gerlach and J. Ehrlich, "Magnetorheological torque transmission devices with permanent magnets," *Journal of Physics: Conference Series*, vol. 412, no. 1, pp 012-022, 2013.

[145] A. Shafer and M. Kermani, "Magneto and electro- rheological based actuators for human friendly manipulators," U.S. Patent 61/272 597, November, 2009.

[146] P. Yadmellat, A. Shafer and M. Kermani, "Design and development of a single-motor two-DOF, safe manipulator," *IEEE/ASME Transactions on Mechatronics*, vol. 19, no. 2, pp. 1384-1391, 2014.

[147] P. Yadmellat, A. Shafer and M. Kermani, "Design and development of a safe robot manipulator using a new actuation concept," *IEEE International Conference on Robotics and Automation (ICRA)*, Karlsruhe, Germany, 6-10 May, 2013.

[148] A. Shafer and M. Kermani, "Magneto-rheological clutch with sensors measuring electromagnetic field strength," WO Patent 2 011 041 890, April, 2011.

[149] B. Gombert, G. Hirzinger, G Plank and M. Schedl, " Modular concepts for a new generation of light weight robots," *20th International Conference on Industrial Electronics, Control and Instrumentation*, Bologna, Italy, 5-9 September, 1994.

[150] B. Schäfer, B. Rebele, M. Schedl, M. Görner, A. Wedler, R. Krenn and G. Hirzinger, "Lightweight mechatronics and sensorics for robotic exploration: a DLR perspective," *DLR Research publication, 2008.*

[151] S. Haddadin, S. Parusel, R. Belder, A. Albu-Schaffer and G. Hirzinger, "Safe acting and manipulation in human environments :A key concept for robots in our society," *IEEE Workshop on Advanced Robotics and its Social Impacts (ARSO),* 2-4 October, 2011

[152] A. AlbuSchaffer, O. Eiberger, M. Grebenstein, S. Haddadin, C. Ott, T. Wimbock, S. Wolf and G. Hirzinger, "Soft robotics: from torque feedback controlled lightweight robots to intrinsically compliant systems," *IEEE Robotics & Automation Magazine,* vol. 15, pp. 20–30, 2008.

[153] S. Rolf and K. Hans, "Lightweight harmonic drive® gears for next-generation robots," *Robotics Today (Online Newsletter)* Society of Manufacturing Engineers, 2004.

[154] R. Slatter and H. Koenen, "Lightweight harmonic drive gears for service robots. A technical paper," Harmonic Drive AG Germany, 2007.

[155] G. Hirzinger, M. Fischer, B. Brunner, R. Koeppe, M. Otter, M. Grebenstein and I. Schafer, "Advances in robotics: DLR experience," *International Journal of Robotics Research*, vol. 18, no. 11, pp. 1064-1087, 1999.

[156] DLR Lightweight robot I datasheet, DLR Germany, 2010.

[157] G. Hirzinger, J. Butterfafl, M. Fischer, M. Grcbenstein, M. Hiihnle, H. Liu, I. Schafer and N. Sporer, "A mechatronics approach to the design of lightweight arms and muitifingered hands Approach," *IEEE International Conference on Robotics & Automation*, San Francisco, USA, 24-28 April, 2000.

[158] G. Hirzinger, M. Grebenstein and N. Sporer, "Robonauts need lightweight arms and articulated hands, " *6th ESA Workshop on Advanced Space Technologies for Robotics and Automation (ASTRA)*, Noordwijk, Netherland, 5-7 December, 2000.

[159] G. Hirzinger, N. Sporer, M. Schedl, J. Butterfab and M. Grebenstein, "Torque-controlled lightweight arms and articulated hands - do we reach technological limits now," *International Journal of Robotics Research*, vol. 23, no. 4, pp. 331-340, 2004.

[160] G. Hirzinger, B. Brunner, J. Butterfab, M. Fischer, M. Grebenstein, K. Landzettel and M. Schedl, "Space robotics – towards advanced mechatronic components and powerful telerobotic systems," *6th International Symposium on Artificial Intelligence and Robotics & Automation in Space*, Quebec, Canada, 18-22 June, 2001.

[161] DLR Lightweight robot II datasheet, DLR Germany, 2016.

[162] G. Hirzinger, N. Sporer, M. Schedl, J. Butterfab and M. Grebenstein," Robotics and mechatronics in aerospace," *7th International Workshop on Advanced Motion Control,* Maribor, Slovenia,3-5 July 2002.

[163] A. Wedler, M. Chalon, K. Landzettel, M. Görner, E. Krämer, R. Gruber, A. Beyer, H. Sedlmayr, B. Willberg, W. Bertleff, J. Reill, M. Grebenstein, M. Schedl, A. AlbuSchäffer and G. Hirzinger, "DLR's dynamic actuator modules for robotic space applications," *Aerospace Mechanisms Symposium (AMS)*, Pasadena, USA, 16-18 May, 2012.

[164] Lightweight robots: construction, DLR robotics and mechatronic centre article, 2014.

[165] R. Krenn, B. Schäfer and G. Hirzinger, "Dynamics simulation and assembly environment for rapid manipulator design," *7th ESA Workshop on Advanced Space Technologies for Robotics and Automation,* Noordwijk, Netherland, 19-21 November, 2002.

[166] DLR Lightweight robot III datasheet, DLR Germany, 2011.

[167] R. Bischoff, J. Kurth and G. Schreiber, "The KUKA-DLR lightweight robot arm – a new reference platform for robotics research and manufacturing," *ISR 2010 (41st International Symposium on Robotics) and ROBOTIK 2010 (6th German Conference on Robotics),* Munich, Germany, 7-9 June, 2010.

[168] U. Hagen, R. Konietschke, A. Tobergte, M. Nickle, S. Jörg, B. Kübler, G. Passig, M. Gröger, F. Fröhlich, U. Seibold, L. Letien, A. AlbuSchäffer, A. Nothhelfer, F. Hacker, M. Grebenstein and G. Hirzinger, "DLR MiroSurge: a versatile system for research in endoscopic telesurgery," *International Journal of Computer Assisted Radiology and Surgery*, vol. 5, no. 2, pp. 183-193,2010.

[169] R Konietschke, U. Hagn, M. Nickl, S. Jorg, A. Tobergte, G. Passig, U. Seibold, L. Letien, B. Kubler, M. Groger, F. Frohlich, C. Rink, A. AlbuSchaffer, M. Grebenstein, T. Ortmaier and G. Hirzinger , "The DLR Mirosurge – A robotic system for surgery," *IEEE International Conference on Robotics and Automation,* Kobe, Japan, 12-17 May, 2009.

[170] DLR Miro robot datasheet, DLR Germany, 2013.

[171] K. Oonishi, N. Oonishi and K. Shimoyama, "Producing and the latest development programs of the portable general purpose intelligent arm 'Mitsubishi PA-10' ," *Advanced Robotics*, vol. 15, no. 3, pp. 333– 337, 2001.

[172] C. W. Kennedy and J. P. Desai, "Modelling and control of the Mitsubishi PA-10 robot arm harmonic drive system, " *IEEE/ASME Transactions on Mechatronics*, vol. 10, no. 3, pp. 263-274, 2005.

[173] Mitsubishi PA-10 LWA robot datasheet, Mitsubishi Electric Corporation, 2015.

[174] M. Higuchi, T. Kawamura, T. Kaikogi, T. Murata and M.Kawaguchi, "Mitsubishi clean room robot clean material handling originated from plant equipment inspection," *Mitsubishi heavy industries Ltd technical review*, vol. 40, no. 5, pp. 25-30, 2003

[175] S. Brellcokcan and J. Braumann, *Robotic fabrication in architecture, art and design*, Springer Science & Business Media Technology & Engineering, 2013.

[176] Schunk Powerball robot datasheet, Schunk GmbH & Co. KG, 2016.

[177] M. Chen, *Modular Robots handbook of manufacturing engineering and technology*, Springer London, 2014.

[178] S. Li, Y. Liu and M. Xie, "Design and implementation of a new single-motor driven arm manipulator," *IEEE International Conference on Mechatronics and Automation*, Harbin, China, 5-8 August, 2007.

[179] J. M. Valenzuela and A. C. Avelar, *Motion control of underactuated mechanical systems*, Springer International Publishing, 2018.

[180] T. Vorobyeva, and O. Blunn, *Electromagnetic clutches and couplings, international series of monographs on electronics and instrumentation*, Elsevier Press, 2013.

[181] T. S. Phillips, *The electromagnet and electromagnetic mechanism*, E & FN Spon, 1991.

[182] W.C. Orthwein, *Clutches and brakes: design and selection,* CRC Press, 2004.

[183] S.P. Thompson, "*The electromagnet, and electromagnetic mechanism*", BiblioLife, 2015.

[184] C. Own, A.S. Duffey, and G. Wright, *Fundamentals of mobile heavy equipment*", Jones & Bartlett Learning, Massachusetts, United States, 2017.

[185] A. Junji, "Development of third-generation electronically controlled AWD coupling with new high-performance electromagnetic clutch.," *SAE International Journal of Passenger Cars-Mechanical Systems*, vol. 7,no. 1, pp 882-887, 2014.

[186] P. Flores and V.Fernando, *New trends in mechanism and machine science: from fundamentals to industrial applications,* Springer, 2014.

[187] E. Kiel, "*Drive solutions. mechatronics for production and logistics"*, Springer Berlin, 2008.

[188] W. Cai, G. Chenglin and W. Chenhui, "Novel bistable PM electromagnetic clutch unit for wheel EV drive." *17th International Conference on Electrical Machines and Systems (ICEMS),* pp. 1164-1167, 22 October 2014.

[189] W. Cai, C. Gu and X. Hu, "Analysis and design of a permanent magnet bi-stable electro-magnetic clutch unit for in-wheel electric vehicle drives", *Energies*, vol. *8*, Issue 6, pp 5598-5612, 2015.

[190] W. Yu and C. Gu, "Design and implementation of an electromagnetic clutch system for hub motors", *17th International Conference on* Electrical *Machines and Systems (ICEMS),* pp. 1183-1186, 22 October 2014.

[191] F. Yang, C. Gu and C. Wang, "Magnetic field analysis and optimal design of a novel bistable permanent electromagnetic clutch", *17th International Conference on* Electrical *Machines and Systems (ICEMS),* pp. 1667-1670, 22 October 2014.

[192] Maschinenfabrik Mönninghoff GmbH & Co. KG, *Mönninghoff Bistable electromagnet - tooth coupling type 556 M1 Datasheet*, August 2017.

[193] KEB Automation KG, *KEB Product Portfolio Automotive Catalogue,* November 2017.

[194] Electroid Company, *BSB Series Pulse Operated Bistable Brake Datasheet*, June 2015.

[195] EIDE Company (2018), *EIDE Company Website Article on Bistable Brake*, Retrieved from: http://www.eide.net/en/bistable-brake/, [Accessed 26th October 2019]

[196] C. B. Rajanathan, Z. W. Shi, A. T. Sapeluk, and N. G. Taylor, "Design and control of an electromagnetic actuator without mechanical springs", *IEEE Transactions on Energy Conversion*, vol. *14*,pp 643-648, 1999

[197] Al Otaibi, Zaid. "Spring-less buried magnet linear-resonant motor." U.S. Patent 8,692,422, 8 April, 2014.

[198] M. E. Brumbach and J. A. Clade, "*Industrial Maintenance*", Cengage Learning, Boston, United States, 2013.

[199] P. Chan, J. Kim, S.J. Kim, and J. Yoo, "Development of a permanent magnet type micro-robot actuated by external electromagnetic system," Microsystem *Technologies*, vol. 21, no. 6, pp. 1257-1265, 2015.

[200] J. Sutanto, A. D. Papania, Y. H. Berthelot and P. J. Hesketh, "Dynamic characteristics of membrane displacement of a bidirectional electromagnetic micro actuator with micro coil fabricated on a single wafer," *Microelectronic Engineering*, vol. 82, no. 1, pp. 12-27, 2005.

[201] L. Arcese, M. Fruchard and A. Ferreira, "Endovascular magnetically guided robots: navigation modeling and optimization," IEEE *Transactions on Biomedical Engineering*, vol. 59, no. 4, pp. 977-987, 2012.

[202] D. J. Huang, L. G. Yao, W. J. Li and J. Zhang, "Design and realization of a novel magnetic nutation drive for industry robotic wrist reducer," *Industrial Robot: An International Journal,* vol. 44, no. 1, pp. 58–63, 2017.

[203] D. Jiles, *Introduction to magnetism and magnetic materials,* CRC press, 2015.

[204] N. Ida and J. P. Bastos, *Electromagnetics and calculation of fields,* Springer Science & Business Media, 2013.

[205] N. A. Spaldin, *Magnetic materials: fundamentals and applications*, Cambridge University Press, 2010.

[206] H. Fang, L. Guo and S. Bai, In *Recent Advances in Mechanism Design for Robotics*, Springer International Publishing, 2015.

[207] Z. Wang, Y. Tian and Y. A. Yao, "A novel underactuated tetrahedral mobile robot," *Journal of Mechanisms and Robotics*, vol. 10, no. 4, pp. 044506-044513, 2018.

[208] C. R. Rocha, C. P. Tonetto and A. Dias, "A comparison between the Denavit–Hartenberg and the screw-based methods used in kinematic modeling of robot manipulators", *Robotics and Computer-Integrated Manufacturing,* vol. 27, no. 4, pp 723-728, 2011.

[209] S. K. Saha, *"Introduction to robotics", Tata McGraw-Hill Education*, 2008.

[210] W. Khalil and E.Dombre, *Modelling, identification and control of robots,* Butterworth-Heinemann, 2004.

[211] J. Angeles, *Fundamentals of robotic mechanical systems: theory, methods, and algorithms*, Springer Science & Business Media, 2013.

[212] B. Siciliano, L. Sciavicco, L. Villani and G. Oriolo, *Robotics: modelling, planning and control*, Springer Science & Business Media, 2010.

[213] R. M. Murray, Z. Li and S. S. Sastry, *A mathematical introduction to robotic manipulation,* CRC press, 1994.

[214] Z. Li and S. S. Ge, *Fundamentals in modelling and control of mobile manipulators*, CRC Press, 2013.

[215] P. Corke, *Robotics, vision and control: fundamental algorithms in MATLAB,* Springer, 2017.

[216] Yaskawa AC servo motor catalogue, Yaskawa Drives and Motion, 2018.

[217] BSB Series electromagnetic brake datasheet, Electroid Company Springfield, 2018

[218] Schneider AC servo motor catalogue, Schneider Servo Drives and Motors, 2018.

[219] 102 Series electromagnetic clutches datasheet, Miki Pulley Company Japan, 2018.

[220] CSZ Series electromagnetic clutches datasheet, Miki Pulley Company Japan, 2018.

[221] AMC Series electromagnetic clutches datasheet, Ogura Industrial Cooperation New Jersey, 2018.

Appendix

The following section explains the dynamic model calculations of the further enhanced manipulator model. The inertia matrix is 4x4 matrix. The inertia matrix is obtained using the given below Equation (A.1).

$$M = \sum_{i=1}^{4} J_{vi}^{T} m_i J_{vi} + J_{\omega}^{T} I_i J_{\omega i} \tag{A.1}$$

Where J_i is the link Jacobian matrix and J_{vi} and $J_{\omega i}$ are the link Jacobian submatrices. J_{vi} represents Jacobian submatrix of the linear velocity and the $J_{\omega i}$ represents Jacobian submatrix of the angular velocity.

The l_1, l_2, l_3 are the link length of link 1, link 2 and link 3 of the manipulator. θ_1, θ_2, θ_3 and θ_4 represents the angle value of joint 1, joint 2, joint 3 and joint 4 respectively. The computed Jacobian submatrices J_{vi} *are as* given below:

$$J_{v1} = \begin{bmatrix} 0 & 0 & 0 & 0 \\ 0 & 0 & 0 & 0 \\ 0 & 0 & 0 & 0 \end{bmatrix} \tag{A.2}$$

J_{v1} is a zero matrix. Referring to the DH parameters table of the manipulator Table 1, it could be observed that a_1 is zero because base joint and the base frame are on the same frame.

$$J_{v2} = \begin{bmatrix} -\frac{1}{2}\mathrm{C}_2\mathrm{S}_1 l_1 & -\frac{1}{2}\mathrm{C}_1\mathrm{S}_2 l_1 & 0 & 0 \\ \frac{1}{2}\mathrm{C}_1\mathrm{C}_2 l_1 & -\frac{1}{2}\mathrm{S}_1\mathrm{S}_2 l_1 & 0 & 0 \\ 0 & -\frac{1}{2}\mathrm{C}_2 l_1 & 0 & 0 \end{bmatrix} \tag{A.3}$$

$$J_{v3} = \begin{bmatrix} -\frac{1}{2}\mathrm{S}_1(2\mathrm{C}_2 l_1 + \mathrm{C}_{23} l_2) & -\frac{1}{2}\mathrm{C}_1(2\mathrm{S}_1 l_1 + \mathrm{S}_{23} l_2) & -\frac{1}{2}\mathrm{C}_1\mathrm{S}_{23} l_2 & 0 \\ \frac{1}{2}\mathrm{C}_1\mathrm{C}_2 l_1(2 + \mathrm{C}_{23} l_2) & -\frac{1}{2}\mathrm{S}_1(2\mathrm{S}_2 l_1 + \mathrm{S}_{23} l_2) & -\frac{1}{2}\mathrm{S}_1\mathrm{S}_{23} l_2 & 0 \\ 0 & \mathrm{C}_2 l_1 + \frac{1}{2}\mathrm{C}_{23} l_2 & \frac{1}{2}\mathrm{C}_{23} l_2 & 0 \end{bmatrix} \quad \text{(A.4)}$$

$$J_{v4} =$$

$$\begin{bmatrix} -\mathrm{S}_1\left(\mathrm{C}_2 l_1 + \mathrm{C}_{23} l_2 + \frac{1}{2}\mathrm{C}_{234} l_3\right) & -\mathrm{C}_1(\mathrm{S}_2 l_1 + \mathrm{S}_1 l_2 + \frac{1}{2}\mathrm{S}_{234} l_3) & -\frac{1}{2}\mathrm{C}_1(2\mathrm{S}_{23} l_2 + \mathrm{S}_{234} l_3) & -\frac{1}{2}\mathrm{C}_1\mathrm{S}_{234} l_3 \\ \mathrm{C}_1\left(\mathrm{C}_2 l_1 + \mathrm{C}_{23} l_2 + \frac{1}{2}\mathrm{C}_{234} l_3\right) & -\mathrm{S}_1\left(\mathrm{S}_2 l_1 + \mathrm{S}_{23} l_2 + \frac{1}{2}\mathrm{S}_{234} l_3\right) & -\frac{1}{2}\mathrm{S}_1(2\mathrm{S}_{23} l_2 + \mathrm{S}_{234} l_3) & -\frac{1}{2}\mathrm{S}_1\mathrm{S}_{234} l_3 \\ 0 & \mathrm{C}_2 l_1 + \mathrm{C}_{23} l_2 + \frac{1}{2}\mathrm{C}_2 l_3 & \mathrm{C}_{23} l_2 + \frac{1}{2}\mathrm{C}_{234} l_3 & \frac{1}{2}\mathrm{C}_{234} l_3 \end{bmatrix} \quad \text{(A.5)}$$

$J_{\omega i}$ Jacobian submatrices of angular velocity are computed for the proposed manipulator as follows:

$$J_{\omega 1} = \begin{bmatrix} 0 & 0 & 0 & 0 \\ 0 & 0 & 0 & 0 \\ 1 & 0 & 0 & 0 \end{bmatrix} \quad \text{(A.6)} \qquad J_{\omega 2} = \begin{bmatrix} 0 & \mathrm{S}_1 & 0 & 0 \\ 0 & -C_1 & 0 & 0 \\ 1 & 0 & 0 & 0 \end{bmatrix} \quad \text{(A.7)}$$

$$J_{\omega 3} = \begin{bmatrix} 0 & \mathrm{S}_1 & \mathrm{S}_1 & 0 \\ 0 & -\mathrm{C}_1 & -\mathrm{C}_1 & 0 \\ 1 & 0 & 0 & 0 \end{bmatrix} \quad \text{(A.8)} \qquad J_{\omega 4} = \begin{bmatrix} 0 & \mathrm{S}_1 & \mathrm{S}_1 & \mathrm{S}_1 \\ 0 & -C_1 & -\mathrm{C}_1 & -\mathrm{C}_1 \\ 1 & 0 & 0 & 0 \end{bmatrix} \quad \text{(A.9)}$$

The link *i* inertia matrix about the link's center of mass with respect to the link frames is computed using the Equation (A.10). The link *i* inertia matrix about the link's center of mass with respect to base frame is calculated using the Equation (A.11).

$$I_i^i = \frac{1}{12} m_i a_i^2 \begin{bmatrix} 0 & 0 & 0 \\ 0 & 1 & 0 \\ 0 & 0 & 1 \end{bmatrix} \quad \text{(A.10)}$$

$$I_i = R_i^0 \, I_i^i \, (R_i^0)^T \quad \text{(A.11)}$$

m_2, m_3 and m_4 corresponds to the mass of link 1 ,link 2 and link 3 respectively. The inertia matrices of the links 1, link 2 and link 3 about the centre

of mass of the links with respect to the base frame are calculated using Equation (A.10) and Equation (A.11) as following:

$$I_1 = \begin{bmatrix} 0 & 0 & 0 & 0 \\ 0 & 0 & 0 & 0 \\ 0 & 0 & 0 & 0 \end{bmatrix} \tag{A.12}$$

$$I_2 = \begin{bmatrix} \frac{1}{12}(S_1{}^2 + C_1{}^2 S_2{}^2) l_1^2 m_2 & \frac{1}{12}(-C_1 S_1 + C_1 S_1 S_1^2) l_1^2 m_2 & -\frac{1}{12} C_1 C_2 S_2 l_1^2 m_2 \\ \frac{1}{12}(-C_1 S_1 + C_1 S_1 S_2{}^2) l_1^2 m_2 & \frac{1}{12}(C_1^2 + S_1{}^2 S_2{}^2) l_1^2 m_2 & -\frac{1}{12} C_2 S_1 S_2 l_1^2 m_2 \\ -\frac{1}{12} C_1 C_2 S_2 l_1^2 m_2 & -\frac{1}{12} C_2 S_1 S_2 l_1^2 m_2 & \frac{1}{12} C_2{}^2 l_1^2 m_2 \end{bmatrix} \tag{A.13}$$

$$I_3 = \begin{bmatrix} \frac{1}{12}(S_1{}^2 + C_1{}^2 (C_3 S_2 + C_2 S_3)^2) l_2^2 m_3 & \frac{1}{12}(-C_1 S_1 + C_1 S_1 (C_3 S_2 + C_2 S_3)^2) l_2^2 m_3 & -\frac{1}{12} C_1 (C_3 S_2 + C_2 S_3)(C_2 C_3 - S_2 S_3) l_2^2 m_3 \\ \frac{1}{12}(-C_1 S_1 + C_1 S_1 (C_3 S_2 + C_2 S_3)^2) l_2^2 m_3 & \frac{1}{12}(C_1{}^2 + S_1{}^2 (C_3 S_2 + C_2 S_3)^2) l_2^2 m_3 & -\frac{1}{12} S_1 (C_3 S_2 + C_2 S_3)(C_2 C_3 - S_2 S_3) l_2^2 m_3 \\ -\frac{1}{12} C_1 (C_3 S_2 + C_2 S_3)(C_2 C_3 - S_2 S_3) l_2^2 m_3 & -\frac{1}{12} S_1 (C_3 S_2 + C_2 S_3)(C_2 C_3 - S_2 S_3) l_2^2 m_3 & \frac{1}{12}(C_2 C_3 - S_2 S_3)^2 l_2^2 m_3 \end{bmatrix} \tag{A.14}$$

$$I_4 = \begin{bmatrix} \frac{1}{12}\left(s_1{}^2 + (-c_1 c_4 (c_3 s_2 + c_2 s_3) - c_1 (c_2 c_3 - s_2 s_3) s_4)^2\right) l_3^2 m_4 & \frac{1}{12}(-c_1 s_1 + (-c_1 c_4 (c_3 s_2 + c_2 s_3) - c_1 (c_2 c_3 - s_2 s_3) s_4)(-c_4 s_1 (c_3 s_2 + c_2 s_3) - s_1 (c_2 c_3 - s_2 s_3) s_4)) l_3^2 m_4 & \frac{1}{12}(c_4 (c_2 c_3 - s_2 s_3) - (c_3 s_2 + c_2 s_3) s_4)(-c_1 c_4 (c_3 s_2 + c_2 s_3) - c_1 (c_2 c_3 - s_2 s_3) s_4)) l_3^2 m_4 \\ \frac{1}{12}(-c_1 s_1 + (-c_1 c_4 (c_3 s_2 + c_2 s_3) - c_1 (c_2 c_3 - s_2 s_3) s_4)(-c_4 s_1 (c_3 s_2 + c_2 s_3) - s_1 (c_2 c_3 - s_2 s_3) s_4)) l_3^2 m_4 & \frac{1}{12}\left(c_1{}^2 + (-c_4 s_1 (c_3 s_2 + c_2 s_3) - s_1 (c_2 c_3 - s_2 s_3) s_4)^2\right) l_3^2 m_4 & \frac{1}{12}(c_4 (c_2 c_3 - s_2 s_3) - (c_3 s_2 + c_2 s_3) s_4)(-c_4 s_1 (c_3 s_2 + c_2 s_3) - s_1 (c_2 c_3 - s_2 s_3) s_4)) l_3^2 m_4 \\ \frac{1}{12}(c_4 (c_2 c_3 - s_2 s_3) - (c_3 s_2 + c_2 s_3) s_4)(-c_1 c_4 (c_3 s_2 + c_2 s_3) - c_1 (c_2 c_3 - s_2 s_3) s_4)) l_3^2 m_4 & \frac{1}{12}(c_4 (c_2 c_3 - s_2 s_3) - (c_3 s_2 + c_2 s_3) s_4)(-c_4 s_1 (c_3 s_2 + c_2 s_3) - s_1 (c_2 c_3 - s_2 s_3) s_4)) l_3^2 m_4 & \frac{1}{12}(c_4 (c_2 c_3 - s_2 s_3) - (c_3 s_2 + c_2 s_3) s_4)^2 l_3^2 m_4 \end{bmatrix} \tag{A.15}$$

The complete 4x 4 inertia matrix of the proposed manipulator is computed by substituting the Equations (A.2) through (A.9) and Equations (A.12) to (A.15) into the above mentioned Equation (A.1):

$$\mathrm{M} = \begin{bmatrix} M_{11} & M_{12} & M_{13} & M_{14} \\ M_{21} & M_{22} & M_{23} & M_{24} \\ M_{31} & M_{32} & M_{33} & M_{34} \\ M_{41} & M_{42} & M_{43} & M_{44} \end{bmatrix} \tag{A.16}$$

$$\begin{aligned} \mathrm{M}_{11} = \; & \frac{1}{12}\Big(4\mathrm{Cos}[\theta_2]^2 l_1^2 m_2 + \mathrm{Cos}[\theta_2 + \theta_3]^2 l_2^2 m_3 + 12\Big(\mathrm{Sin}[\theta_1]^2 \Big(\mathrm{Cos}[\theta_2] l_1 + \frac{1}{2}\mathrm{Cos}[\theta_2 + \theta_3] l_2\Big)^2 + \\ & \frac{1}{4}\mathrm{Cos}[\theta_1]^2 \mathrm{Cos}[\theta_2]^2 l_1^2 (2 + \mathrm{Cos}[\theta_2 + \theta_3] l_2)^2\Big) m_3 + \mathrm{Cos}[\theta_2 + \theta_3 + \theta_4]^2 l_3^2 m_4 + 3(2\mathrm{Cos}[\theta_2] l_1 + 2\mathrm{Cos}[\theta_2 + \theta_3] l_2 + \\ & \mathrm{Cos}[\theta_2 + \theta_3 + \theta_4] l_3)^2 m_4\Big) \end{aligned} \tag{A.17}$$

$$M_{12} = -\frac{1}{8}\text{Cos}[\theta_2+\theta_3]\text{Sin}[2\theta_1](-1+\text{Cos}[\theta_2]l_1)l_2(2\text{Sin}[\theta_2]l_1+\text{Sin}[\theta_2+\theta_3]l_2)m_3 \quad \text{(A.18)}$$

$$M_{13} = -\frac{1}{16}\text{Sin}[2\theta_1]\text{Sin}[2(\theta_2+\theta_3)](-1+\text{Cos}[\theta_2]l_1)l_2^2m_3 \quad \text{(A.19)}$$

$$M_{14} = 0 \quad \text{(A.20)}$$

$$M_{21} = -\frac{1}{8}\text{Cos}[\theta_2+\theta_3]\text{Sin}[2\theta_1](-1+\text{Cos}[\theta_2]l_1)l_2(2\text{Sin}[\theta_2]l_1+\text{Sin}[\theta_2+\theta_3]l_2)m_3 \quad \text{(A.21)}$$

$$M_{22} = \frac{1}{6}\Big(3l_1\big(\text{Cos}[\theta_3+\theta_4]l_3m_4+\text{Cos}[\theta_3]l_2(m_3+2m_4)\big)+2\Big(3\text{Cos}[\theta_4]m_2l_3m_4+l_3^2m_4+l_2^2(m_3+3m_4)\Big)\Big) \quad \text{(A.22)}$$

$$M_{23} = \frac{1}{6}(3l_1(\text{Cos}[\theta_3+\theta_4]l_3m_4+\text{Cos}[\theta_3]l_2(m_3+2m_4))+2(3\text{Cos}[\theta_4]l_2l_3m_4+l_3^2m_4+l_2^2(m_3+3m_4))) \quad \text{(A.23)}$$

$$M_{24} = \frac{1}{6}l_3(3\text{Cos}[\theta_3+\theta_4]l_1+3\text{Cos}[\theta_4]l_2+2l_3)m_4 \quad \text{(A.24)}$$

$$M_{31} = -\frac{1}{16}\text{Sin}[2\theta_1]\text{Sin}[2(\theta_2+\theta_3)](-1+\text{Cos}[\theta_2]l_1)l_2^2m_3 \quad \text{(A.25)}$$

$$M_{32} = \frac{1}{6}(3l_1(\text{Cos}[\theta_3+\theta_4]l_3m_4+\text{Cos}[\theta_3]l_2(m_3+2m_4))+2(3\text{Cos}[\theta_4]l_2l_3m_4+l_3^2m_4+l_2^2(m_3+3m_4))) \quad \text{(A.26)}$$

$$M_{33} = \frac{1}{3}(3\text{Cos}[\theta_4]l_2l_3m_4+l_3^2m_4+l_2^2(m_3+3m_4)) \quad \text{(A.27)}$$

$$M_{34} = \frac{1}{6}l_3(3\text{Cos}[\theta_4]l_2+2l_3)m_4 \quad \text{(A.28)}$$

$$M_{41} = 0 \quad \text{(A.29)}$$

$$M_{42} = \frac{1}{6}l_3(3\text{Cos}[\theta_3+\theta_4]l_1+3\text{Cos}[\theta_4]l_2+2l_3)m_4 \quad \text{(A.30)}$$

$$M_{43} = \frac{1}{6}l_3(3\text{Cos}[\theta_4]l_2+2l_3)m_4 \quad \text{(A.31)}$$

$$M_{44} = \frac{1}{3}l_3^2m_4 \quad \text{(A.32)}$$

The velocity coupling vector is computed using the Equation (7.14). The partial derivatives of the manipulator inertia matrix given in Equation (A.16) is computed to obtain the velocity coupling vector. The computed velocity coupling vector terms are given from Equation (A.33) to Equation (A.36).

$$V_1 = \frac{1}{96}(-2l_1^2(16\text{Sin}[2\theta_2](m_2+3(m_3+m_4))\dot{\theta}_1\dot{\theta}_2+6\text{Cos}[\theta_2]\text{Cos}[\theta_2+\theta_3]l_2^2m_3\dot{\theta}_1(\text{Cos}[\theta_2]\text{Cos}[\theta_2+\theta_3]\text{Sin}[2\theta_1]\dot{\theta}_1+$$
$$4\text{Cos}[\theta_1]^2(\text{Sin}[2\theta_2+\theta_3]\dot{\theta}_2+\text{Cos}[\theta_2]\text{Sin}[\theta_2+\theta_3]\dot{\theta}_3))+3l_2m_3(8\text{Cos}[\theta_2]^2\text{Cos}[\theta_2+\theta_3]\text{Sin}[2\theta_1]\dot{\theta}_1^2+$$
$$8\text{Cos}[\theta_1]^2\text{Cos}[\theta_2]\dot{\theta}_1((-\text{Sin}[\theta_3]+3\text{Sin}[2\theta_2+\theta_3])\dot{\theta}_2+2\text{Cos}[\theta_2]\text{Sin}[\theta_2+\theta_3]\dot{\theta}_3)+\text{Sin}[2\theta_1]\dot{\theta}_2((\text{Cos}[\theta_2-\theta_3]+3\text{Cos}[3\theta_2+$$
$$\theta_3])\dot{\theta}_2-2\text{Sin}[2\theta_2]\text{Sin}[\theta_2+\theta_3]\dot{\theta}_3)))+4(l_2^2(-24\text{Sin}[2(\theta_2+\theta_3)]m_4\dot{\theta}_1(\dot{\theta}_2+\dot{\theta}_3)+m_3(3\text{Cos}[\theta_2+\theta_3]^2\text{Sin}[2\theta_1]\dot{\theta}_1^2+(-5+$$

$3\text{Cos}[2\theta_1])\text{Sin}[2(\theta_2+\theta_3)]\dot{\theta}_1(\dot{\theta}_2+\dot{\theta}_3)+3\text{Cos}[2(\theta_2+\theta_3)]\text{Sin}[2\theta_1](\dot{\theta}_2+\dot{\theta}_3)^2))-8\text{Sin}[2(\theta_2+\theta_3+\theta_4)]l_3^2m_4\dot{\theta}_1(\dot{\theta}_2+\dot{\theta}_3+\dot{\theta}_4)-24l_2l_3m_4\dot{\theta}_1(\text{Sin}[2\theta_2+2\theta_3+\theta_4]\dot{\theta}_2+\text{Sin}[2\theta_2+2\theta_3+\theta_4]\dot{\theta}_3+\text{Cos}[\theta_2+\theta_3]\text{Sin}[\theta_2+\theta_3+\theta_4]\dot{\theta}_4))+3l_1(-\text{Sin}[2\theta_1]l_2^2m_3(\dot{\theta}_2+\dot{\theta}_3)((\text{Cos}[\theta_2+2\theta_3]+3\text{Cos}[3\theta_2+2\theta_3])\dot{\theta}_2+4\text{Cos}[\theta_2]\text{Cos}[2(\theta_2+\theta_3)]\dot{\theta}_3)+8l_2(-8m_4\dot{\theta}_1(\text{Sin}[2\theta_2+\theta_3]\dot{\theta}_2+\text{Cos}[\theta_2]\text{Sin}[\theta_2+\theta_3]\dot{\theta}_3)+m_3(2\text{Cos}[\theta_2]\text{Cos}[\theta_2+\theta_3]\text{Sin}[2\theta_1]\dot{\theta}_1^2-4\text{Sin}[\theta_1]^2\dot{\theta}_1(\text{Sin}[2\theta_2+\theta_3]\dot{\theta}_2+\text{Cos}[\theta_2]\text{Sin}[\theta_2+\theta_3]\dot{\theta}_3)+\text{Sin}[2\theta_1]\dot{\theta}_2(\text{Cos}[2\theta_2+\theta_3]\dot{\theta}_2-\text{Sin}[\theta_2]\text{Sin}[\theta_2+\theta_3]\dot{\theta}_3)))-32l_3m_4\dot{\theta}_1(\text{Sin}[2\theta_2+\theta_3+\theta_4]\dot{\theta}_2+\text{Cos}[\theta_2]\text{Sin}[\theta_2+\theta_3+\theta_4](\dot{\theta}_3+\dot{\theta}_4))))$ (A.33)

$V_2 = \frac{1}{48}(8\text{Sin}[2(\theta_2+\theta_3+\theta_4)]l_3^2m_4\dot{\theta}_1^2+\text{Sin}[2(\theta_2+\theta_3)]l_2^2((5+3\text{Cos}[2\theta_1])m_3+24m_4)\dot{\theta}_1^2+a_1^2\dot{\theta}_1(8\text{Sin}[2\theta_2]m_2\dot{\theta}_1+3(8\text{Sin}[2\theta_2]m_4\dot{\theta}_1+m_3((8\text{Sin}[2\theta_2]+\text{Cos}[\theta_2](-\text{Sin}[2\theta_1-\theta_3]-\text{Sin}[2\theta_1-2\theta_2-\theta_3]-2\text{Sin}[\theta_3]+\text{Sin}[2\theta_1+\theta_3]+6\text{Sin}[2\theta_2+\theta_3]+\text{Sin}[2\theta_1+2\theta_2+\theta_3])l_2+2\text{Cos}[\theta_1]^2\text{Cos}[\theta_2](\text{Sin}[\theta_2]+\text{Sin}[3\theta_2+2\theta_3])l_2^2)\dot{\theta}_1+2\text{Sin}[2\theta_1]\text{Sin}[2\theta_2]\text{Sin}[\theta_2+\theta_3]a_2\dot{\theta}_3)))+24l_2l_3m_4(\text{Sin}[2\theta_2+2\theta_3+\theta_4]\dot{\theta}_1^2-\text{Sin}[\theta_4]\dot{\theta}_4(2\dot{\theta}_2+2\dot{\theta}_3+\dot{\theta}_4))+6a_1(-\text{Sin}[2(\theta_2+\theta_3)]l_2^2m_3\dot{\theta}_1(\text{Cos}[2\theta_1]\text{Cos}[\theta_2]\dot{\theta}_1+\text{Cos}[\theta_1]\text{Sin}[\theta_1]\text{Sin}[\theta_2]\dot{\theta}_3)+l_2(m_3((\text{Sin}[2\theta_1-\theta_3]-\text{Sin}[2\theta_1+\theta_3]+2\text{Sin}[2\theta_2+\theta_3])\dot{\theta}_1^2-2\text{Sin}[2\theta_1]\text{Sin}[\theta_2]\text{Sin}[\theta_2+\theta_3]\dot{\theta}_1\dot{\theta}_3-4\text{Sin}[\theta_3]\dot{\theta}_3(2\dot{\theta}_2+\dot{\theta}_3))+8m_4(\text{Sin}[2\theta_2+\theta_3]\dot{\theta}_1^2-\text{Sin}[\theta_3]\dot{\theta}_3(2\dot{\theta}_2+\dot{\theta}_3)))+4l_3m_4(\text{Sin}[2\theta_2+\theta_3+\theta_4]\dot{\theta}_1^2-\text{Sin}[\theta_3+\theta_4](\dot{\theta}_3+\dot{\theta}_4)(2\dot{\theta}_2+\dot{\theta}_3+\dot{\theta}_4))))$ (A.34)

$V_3 = m_4\dot{\theta}_1^2+\text{Sin}[2(\theta_2+\theta_3)]l_2^2((5+3\text{Cos}[2\theta_1])m_3+24m_4)\dot{\theta}_1^2+6\text{Sin}[\theta_2+\theta_3]l_1^2l_2m_3\dot{\theta}_1(2\text{Cos}[\theta_1]^2\text{Cos}[\theta_2]^2(2+\text{Cos}[\theta_2+\theta_3]l_2)\dot{\theta}_1-\text{Sin}[2\theta_1]\text{Sin}[2\theta_2]\dot{\theta}_2)+3l_1(\text{Sin}[2(\theta_2+\theta_3)]l_2^2m_3\dot{\theta}_1(-2\text{Cos}[2\theta_1]\text{Cos}[\theta_2]\dot{\theta}_1+\text{Sin}[2\theta_1]\text{Sin}[\theta_2]\dot{\theta}_2)+8l_3m_4(\text{Cos}[\theta_2]\text{Sin}[\theta_2+\theta_3+\theta_4]\dot{\theta}_1^2+\text{Sin}[\theta_3+\theta_4]\dot{\theta}_2^2)+4l_2(4m_4(\text{Cos}[\theta_2]\text{Sin}[\theta_2+\theta_3]\dot{\theta}_1^2+\text{Sin}[\theta_3]\dot{\theta}_2^2)+m_3(2\text{Cos}[\theta_2]\text{Sin}[\theta_1]^2\text{Sin}[\theta_2+\theta_3]\dot{\theta}_1^2+\text{Sin}[2\theta_1]\text{Sin}[\theta_2]\text{Sin}[\theta_2+\theta_3]\dot{\theta}_1\dot{\theta}_2+2\text{Sin}[\theta_3]\dot{\theta}_2^2)))+24l_2l_3m_4(\text{Sin}[2\theta_2+2\theta_3+\theta_4]\dot{\theta}_1^2-\text{Sin}[\theta_4]\dot{\theta}_4(2\dot{\theta}_2+2\dot{\theta}_3+\dot{\theta}_4)))$ (A.35)

$V_4 = \frac{1}{6}l_3m_4(\text{Sin}[2(\theta_2+\theta_3+\theta_4)]l_3\dot{\theta}_1^2+3l_1(\text{Cos}[\theta_2]\text{Sin}[\theta_2+\theta_3+\theta_4]\dot{\theta}_1^2+\text{Sin}[\theta_3+\theta_4]\dot{\theta}_2^2)+3l_2(\text{Cos}[\theta_2+\theta_3]\text{Sin}[\theta_2+\theta_3+\theta_4]\dot{\theta}_1^2+\text{Sin}[\theta_4](\dot{\theta}_2+\dot{\theta}_3)^2))\ (\frac{1}{6}\text{Sin}[\theta_2+\theta_3+\theta_4]l_3(3\text{Cos}[\theta_2]l_1+3\text{Cos}[\theta_2+\theta_3]l_2+2\text{Cos}[\theta_2+\theta_3+\theta_4]l_3)m_4\dot{\theta}_1^2)+(\frac{1}{4}l_3m_4\dot{\theta}_2(\text{Sin}[\theta_3+\theta_4]l_1(2\dot{\theta}_2-\dot{\theta}_3-\dot{\theta}_4)+\text{Sin}[\theta_4]l_2(2\dot{\theta}_2+2\dot{\theta}_3-\dot{\theta}_4)))+(\frac{1}{4}l_3m_4\dot{\theta}_3(\text{Sin}[\theta_3+\theta_4]l_1\dot{\theta}_2+\text{Sin}[\theta_4]l_2(2\dot{\theta}_2+2\dot{\theta}_3-\dot{\theta}_4)))+(\frac{1}{4}l_3m_4(\text{Sin}[\theta_3+\theta_4]l_1\dot{\theta}_2+\text{Sin}[\theta_4]l_2(\dot{\theta}_2+\dot{\theta}_3))\dot{\theta}_4$ (A.36)

The respective gravitational vector is computed using Equation (7.15) and the computed gravitational vector are expressed as:

$$G_1 = 0 \quad \text{(A.37)}$$

$$G_2 = 1/2\, gm_4l_3\text{Cos}[\theta_2+\theta_3+\theta_4]+g(m_4+1/2\, m_3)l_2\text{Cos}[\theta_2+\theta_3]+g(m_4+m_3+1/2\, m_2)l_1\text{Cos}[\theta_2] \quad \text{(A.38)}$$

$$G_3 = 1/2\, gm_4l_3\text{Cos}[\theta_2+\theta_3+\theta_4]+g(m_4+1/2\, m_3)l_2*\text{Cos}[\theta_2+\theta_3] \quad \text{(A.39)}$$

$$G_4 = 1/2\, gm_4l_3\text{Cos}[\theta_2+\theta_3+\theta_4] \quad \text{(A.40)}$$

Finally, the torque equations for the each joint are obtained by compiling computed manipulator inertia matrix, velocity coupling vector and the gravitational vector.

The obtained final torque equations are shown in Chapter 7 from Equation (7.16) to Equation (7.19).